

AN ABSTRACT OF THE THESIS OF

Travis J Kraupa for the degree of Master of Science in Civil Engineering presented on November 22, 2013.

Title: Static and Cyclic Response of Ecoroof Soil.

Abstract approved: _____

H. Benjamin Mason

Armin W. Stuedlein

Green technology in the United States has been on the rise over the past few decades in the United States. However, certain green technologies have been developed in the absence of design standards. Ecoroofs, which are vegetated soil masses placed on the top of a building's roof structure, present several engineering concerns. Several important engineering concerns include overstressing of the roof structure due to ponding or excessive saturated soil dead loads during storm events, sliding of the ecoroof material causing overtopping or complete failure of the parapet walls during a seismic event, and the increase of inertial load at the top of the building. Standardization of ecoroof soil and the development of design codes for ecoroof systems in the United States would minimize the possibility of structural failure. Accordingly, this study presents the quantification of the geotechnical index properties and their variability, static stress-strain and volumetric response, and dynamic soil response and properties for ecoroof soil.

A field exploration program, which included gathering undisturbed Shelby tube samples of ecoroof soil, was conducted in Portland, Oregon. The field exploration

provided the basis for the geotechnical characterization of ecoroof soil. Sample statistics of the geotechnical index properties showed significant variability. Sieve testing showed that field samples of ecoroof soils tended to cluster; therefore, three target gradations were selected to serve as representative ecoroof gradations, which varied in the amount of fines present (i.e. material passing No. 200 sieve), median grain sizes, and uniformity of the gradation. Drained static simple shear tests were conducted on specimens reconstituted from each of the target gradations. The tests were performed to investigate the effect of relative density, applied vertical stress, and gradation on static shear strength, each of which contribute to variations in ecoroof strength. To understand the effect of organic matter on the strength parameters, three undisturbed specimens were sheared and the test results indicated that the organic content has significant influence on the volumetric and stress-strain response of ecoroof soil. Preliminary dynamic soil properties, such as the modulus reduction and damping characteristics, and the liquefaction susceptibility of ecoroof soil was determined from a series of undrained cyclic simple shear tests on reconstituted and undisturbed tube specimens. Many reconstituted ecoroof soil specimens exhibited liquefaction under undrained cyclic strain controlled conditions, and variations in liquefaction susceptibility, were attributed to the type of soil gradation. Cyclic simple shear tests on undisturbed tube specimen specimens indicated that the organic content influences the dynamic response of ecoroof soil. Accordingly, this study provides a baseline with which practicing engineers can begin to assess the loading associated with ecoroof soil, and may be used to guide future studies and code development.

©Copyright by Travis J Kraupa
November 22, 2013
All Rights Reserved

Static and Cyclic Response of Ecoroof Soil

by
Travis J Kraupa

A THESIS

submitted to

Oregon State University

in partial fulfillment of
the requirements for the
degree of

Master of Science

Presented November 22, 2013
Commencement June 2014

Master of Science thesis of Travis J Kraupa presented on November 22, 2013

APPROVED:

Co-Major Professor, representing Civil Engineering

Co-Major Professor, representing Civil Engineering

Head of the School of Civil and Construction Engineering

Dean of the Graduate School

I understand that my thesis will become part of the permanent collection of Oregon State University libraries. My signature below authorizes release of my thesis to any reader upon request.

Travis J Kraupa, Author

ACKNOWLEDGEMENTS

I would like to profess my upmost gratitude to both of my advisors, Dr. Ben Mason and Dr. Armin Stuedlein. I am grateful to both of them for their knowledge and critical advice they provided throughout this research program. Without the support and guidance of both Dr. Mason and Dr. Stuedlein, the work presented herein could not have been possible.

I would like to thank the National Science Foundation for providing the financial support required for completion of this research.

I would like to thank Dr. John Lambrinos for his willingness to allow access of his ecoroof test plots. The knowledge gained during this process aided in the development of the sampling equipment presented herein. I would also like to thank Dr. Cann and his graduate students for allowing access to their laboratory, and use of equipment.

I would also like to thank the City of Portland Environmental Services employees who assisted during the field exploration program. Specifically, I want to thank Tom Liptan for his willingness to assist during the initial stages of the field exploration program. I would also like to thank all of the building owners and agencies who allowed access during the field exploration. Also, the assistance of Mr. Li Zheng during the field exploration and setup of cyclic simple shear device is greatly appreciated, and Mary Ann Triska for her assistance at the beginning of the project.

I would like to thank James Batti for his assistance during the setup and installation of the new direct simple shear device, and Michel Dyson for his effort during installation of the new de-aired water system.

My wife has supported me since the beginning, and without her I could not have finished this research program. I would also like to thank all of my fellow graduate students and CCE faculty and administration, for their moral support throughout my time at Oregon State University.

CONTRIBUTION OF AUTHORS

I would like to thank Dr. Chris Higgins for his assistance throughout this research program, and his knowledge about the structural performance of ecoroofs. Specifically, in the development of estimated roof drifts necessary for conducting the cyclic simple shear tests.

TABLE OF CONTENTS

	<u>Page</u>
Chapter 1: Introduction	1
1.1 Background	1
1.2 Outline of Work Completed.....	3
1.3 Figures	6
Chapter 2: Literature Review	10
2.1 Direct Shear Box	10
2.2 Simple Shear Device	11
2.3 Cyclic Simple Shear Device.....	18
2.4 Figures	23
Chapter 3: Characterization of Ecoroofs and Ecoroof Materials.....	29
3.1 Abstract	30
3.2 Introduction	30
3.3 Field Sampling	32
3.4 Field Sites.....	33
3.5 Soil Characterization.....	35
3.6 Strength Tests.....	38
3.7 Conclusion	40
3.8 Acknowledgements	40
3.9 References	41
3.10 Tables	42
3.11 Figures.....	44

TABLE OF CONTENTS (Continued)

	<u>Page</u>
Chapter 4: Geotechnical Characterization and Drained Shear Strength of Ecoroof Soil.....	47
4.1 Abstract	48
4.1.1 Subject Headings	48
4.2 Introduction	49
4.3 Ecoroof Soil Characterization	51
4.3.1 Index Properties of Field Samples.....	51
4.3.2 Variability of Index Properties	52
4.4 Simple Shear Response of Ecoroof Soils.....	53
4.4.1 Background.....	53
4.4.2 Experimental Setup	55
4.4.3 Shear Response of Reconstituted Specimens	57
4.4.4 Shear Response of Relatively Undisturbed Specimens.....	59
4.4.5 Discussion.....	61
4.5 Conclusions	62
4.6 Acknowledgements	64
4.7 References	64
4.8 Tables	67
4.9 Figures	70
Chapter 5: Undrained Cyclic Simple Shear Response of Ecoroof Soil	77
5.1 Introduction	78
5.2 Background	80

TABLE OF CONTENTS (Continued)

	<u>Page</u>
5.2.1 Ecoroof Soil.....	80
5.2.2 Cyclic Simple Shear Testing and Soil Liquefaction.....	81
5.2.3 Modulus Reduction and Damping Curves	83
5.3 Experimental Program	84
5.4 Cyclic Response of Ecoroof Soil	88
5.4.1 Reconstituted Specimens.....	88
5.4.2 Excess Pore Water Pressure Distribution	90
5.4.3 Modulus Reduction and Damping Values.....	91
5.4.4 Response of Shelby Tube Specimens Retrieved From the Field	92
5.5 Discussion	93
5.6 Conclusions	96
5.7 Acknowledgements	97
5.8 References	97
5.9 Tables	101
5.10 Figures.....	102
Chapter 6: Summary and Conclusions.....	112
6.1 Summary	112
6.2 Summary and Conclusions.....	112
6.2.1 Field Exploration and Geotechnical Characterization Properties	112
6.2.2 Drained Static Simple Shear Response	113
6.3.3 Preliminary Undrained Cyclic Simple Shear Properties	114
6.3 Future Work	115

TABLE OF CONTENTS (Continued)

	<u>Page</u>
Bibliography	117
Appendix A: Sampling Program and Ecoroof Soil Characterization	125
Appendix B: Static Simple Shear Procedure	161
Appendix C: Static Simple Shear Test Data	177
Appendix D: Cyclic Simple Shear Test Data	188

LIST OF FIGURES

<u>Figure</u>	<u>Page</u>
Figure 1.1: Typical cross-section of an ecoroof (after Wark and Wark 2003).....	6
Figure 1.2: Typical encountered ecoroofs: (a, b) monolithic extensive ecoroofs (c, d) intensive ecoroofs	7
Figure 1.3: Various encountered interior and exterior ecoroof drains.....	8
Figure 1.4: Developed Shelby tube sampler used throughout the field exploration at various encountered ecoroofs. Note the variation in vegetation and soil gradation	9
Figure 2.1: Typical setup and boundary stress conditions for a direct shear test (after Matthews 1988)	23
Figure 2.2: Simple shear device developed at (a) NGI (b) Cambridge (after Matthews 1988)	23
Figure 2.3: (a) Typical simple shear device showing applied forces (b) device showing actual stresses at the center of the specimen (after Airey et al. 1985)	23
Figure 2.4: Plane strain conditions for (a) pure shear (b) simple shear (after Saada and Townsend 1981).....	24
Figure 2.5: Boundary conditions and shear stress distribution of circular beam for the St. Venant solution (after Saada and Townsend 1981)	24
Figure 2.6: Images from simple shear photoelastic studies for (a) circular specimen and (b) square specimen (after Wright et al. 1978)	25
Figure 2.7: Stress distributions in typical simple shear devices (a) non-uniform shear stresses (b) non-uniform normal stresses (after Wood et al. 1979)	25
Figure 2.8: Shear stress field within a circular simple shear specimen at failure (after Doherty and Fayey 2011).....	26
Figure 2.9: Schematic of a cyclic simple shear device and specimen (a) plan view (b) elevation view (after Peacock and Seed 1968)	27
Figure 2.10: Comparison between the generated cyclic shear stress during cyclic triaxial and cyclic simple shear (after Peacock and Seed 1968)	27

LIST OF FIGURES (Continued)

<u>Figure</u>	<u>Page</u>
Figure 2.11: Cyclic simple shear stress-strain response for (a) stress control (after Boulanger et al. 1993) (b) strain control (after Hazirbaba and Rathje 2009)	28
Figure 3.1: Sampling equipment (a) sampler side and profile view (b) assembled plunger (c) profile view of cap. Note- Figures are exaggerated for detail and are not to scale.....	44
Figure 3.2: Ecoroof variation (a) intensive tray system (b) monolithic-extensive	44
Figure 3.3: Measured and respective targeted grain size distributions.....	45
Figure 3.4: Stress-strain response for (a) the fine, (b) intermediate, and (c) coarse gradations; and volumetric strain response of (d) the fine, (e) intermediate, and (f) coarse gradations. Contraction is plotted as positive	45
Figure 3.5: Variation of mobilized friction angle at 10 percent shear strain with the coefficient of uniformity, C_u	46
Figure 4.1: Measured and target grain size distributions.....	70
Figure 4.2: Histogram and probability distribution functions for various geotechnical index properties: (a) D_{10} (b) Median grain size, D_{50} , (c) C_u , and (d) O_c	71
Figure 4.3: Conventions assumed for the simple shear test: (a) cross-section showing applied stresses and strains, and (b) Mohr's circle of strain and dilation angle, based on major and minor principal strains	72
Figure 4.4: Simple shear stress-strain response and volumetric response for specimens reconstituted using the fine target gradation (a, b) $D_r = 30$ percent (c, d) $D_r = 50$ percent.....	72
Figure 4.5: Simple shear stress-strain response and volumetric response for specimens reconstituted using the intermediate target gradation (a, b) $D_r = 30$ percent (c, d) $D_r = 50$ percent.....	73
Figure 4.6: Simple shear stress-strain response and volumetric response for specimens reconstituted using the coarse target gradation (a, b) $D_r = 30$ percent (c, d) $D_r = 50$ percent.....	73

LIST OF FIGURES (Continued)

<u>Figure</u>	<u>Page</u>
Figure 4.7: Secant shear modulus at $\gamma_{zx} = 1$ percent versus σ_{zz} at varying C_u for specimens with (a) $D_r = 30$ percent, and (b) $D_r = 50$ percent, and mobilized friction angle at $\gamma_{zx} = 15$ percent versus coefficient of uniformity at varying applied vertical stresses for specimens with (c) $D_r = 30$ percent (d) $D_r = 50$ percent.....	74
Figure 4.8: Comparison of particles size distributions for the tube specimens and the three idealized target gradations	74
Figure 4.9: Stress-strain response (a) and volumetric response (b) for the tube specimens.....	75
Figure 4.10: Friction angle mobilized throughout shearing for the tube specimens	75
Figure 4.11: Comparison of stress-strain response of tube and reconstituted specimens for: (a) fine gradations and $\sigma_{zz} = 30$ kPa, (b) intermediate gradations and $\sigma_{zz} = 10$ kPa, and (c) coarse gradations and $\sigma_{zz} = 20$ kPa.....	76
Figure 5.1: Targeted grain size distributions	102
Figure 5.2: Typical results from the fine gradation specimen reconstituted to $D_r = 30$ percent, with $\gamma_c = 4\%$ CSS test for the first 40 cycles where: (a) cyclic stress-strain loops (b) cyclic shear strain induced excess pore pressure (c) specimen normal strain (d) excess pore pressure ratio. Note: $f = 2$ Hz.....	102
Figure 5.3: Typical results from the intermediate gradation specimen reconstituted to $D_r = 30$ percent, with $\gamma_c = 4\%$ CSS test for the first 40 cycles where: (a) cyclic stress-strain loops (b) cyclic shear strain induced excess pore pressure (c) specimen normal strain (d) excess pore pressure ratio. Note: $f = 2$ Hz.....	103
Figure 5.4: Typical results from the coarse gradation specimen reconstituted to $D_r = 30$ percent, with $\gamma_c = 4\%$ CSS test for the first 40 cycles where: (a) cyclic stress-strain loops (b) cyclic shear strain induced excess pore pressure (c) specimen normal strain (d) excess pore pressure ratio. Note: $f = 2$ Hz.....	103
Figure 5.5: One hertz cyclic shear stress response at both relative densities for the fine (a, d), intermediate (b, e), and coarse (c, f) reconstituted specimens with $\gamma_c = 1.5$ and 4 percent, respectively	104

LIST OF FIGURES (Continued)

<u>Figure</u>	<u>Page</u>
Figure 5.6: Two hertz cyclic shear stress response at both relative densities for the fine (a, d), intermediate (b, e), and coarse (c, f) reconstituted specimens with $\gamma_c = 1.5$ and 4 percent, respectively	105
Figure 5.7: Excess pore pressure ratio versus number of cycles for specimens reconstituted to $D_r = 30$ percent: (a,b) $\gamma_c = 1.5\%$ and $f = 1, 2$ Hz respectively (c,d) $\gamma_c = 4\%$ and $f = 1, 2$ Hz respectively	106
Figure 5.8: Excess pore pressure ratio versus number of cycles for specimens reconstituted to $D_r = 50$ percent: (a,b) $\gamma_c = 1.5\%$ and $f = 1, 2$ Hz respectively (c,d) $\gamma_c = 4\%$ and $f = 1, 2$ Hz respectively	107
Figure 5.9: Specimens reconstituted to $D_r = 50$ percent and $\sigma'_v = 100$ kPa, excess pore pressure ratio versus number of cycles.	108
Figure 5.10: (a) Median and $\pm 1 \sigma$ modulus reduction curves for all $\sigma'_v = 30$ kPa reconstituted specimens; (b) Median modulus reduction curves for the target gradations compared to the modulus reduction curves for: peat soil (Boulanger et al. 1998 and Kramer 2000-upper bound), upper bound clean sand (Seed and Idriss 1970), PI = 0 and 200 fine grained soils (Vucetic and Dobry 1991) and PI = 0 soil (Darendeli 2001).....	109
Figure 5.11: (a) Tube and targeted reconstituted specimen grain size distributions and (b) tube specimen excess pore pressure ratio versus number of cycles.....	110
Figure 5.12: Comparison between the undisturbed tube and reconstituted specimens (a) excess pore pressure response, and (b) modulus reduction curves. The colored line types represent the associated specimen reconstituted to $D_r = 30$ percent and tested under similar parameters (i.e. γ_c, f , and σ'_v) to its respective tube specimen	110
Figure 5.13: Comparison of generated excess pore pressure ratio to previous studies for all tests (a) N= 10 cycles (b) N= 30 cycles	111

LIST OF TABLES

<u>Table</u>	<u>Page</u>
Table 3.1: Ecoroof Characteristics from Field Exploration.....	42
Table 3.2: Descriptive statistics for the ecoroof material characterization.....	42
Table 3.3: C_u and the Max and Minimum Void Ratios for the Reconstituted Gradations.....	43
Table 4.1: Ecoroof soil properties used to reconstitute specimens.....	67
Table 4.2: Index properties for the target gradations and reconstituted specimens.....	67
Table 4.3: Descriptive statistics for the ecoroof material characterization (after Kraupa et al. 2014).....	68
Table 4.4: Secant shear modulus, in MPa, for the reconstituted specimens at one percent γ_{zx}	68
Table 4.5: Summary of (ψ_p) for the reconstituted specimens, σ_{zz} in kPa.....	69
Table 5.1: Gradational properties for targeted gradations.....	101
Table 5.2: Damping ratios in percent for reconstituted specimens sheared with $\sigma'_v = 30$ kPa.....	101

LIST OF APPENDIX FIGURES

<u>Figure</u>	<u>Page</u>
Figure A.1: Grain size distribution for Wastewater Treatment Plant-S1.....	127
Figure A.2: Grain size distribution for the Portland Building-S1, S4	127
Figure A.3: Grain size distribution for the Hamilton-S1, S4.....	128
Figure A.4: Grain size distribution for the Buchman Terrace-S1.....	128
Figure A.5: Grain size distribution for Swan Island Pumphouse-S1, S3.....	129
Figure A.6: Grain size distribution for the Village Home Apartments-S1, S4.....	129
Figure A.7: Grain size distribution for Riva at the Park-S1, S4	130
Figure A.8: Grain size distribution for the Atwater-S3, S4	130
Figure A.9: Grain size distribution for Riva at the Ardea-S5, S6.....	131
Figure A.10: Grain size distribution for Fields Hall-S1	131
Figure A.11: Grain size distribution for Riva at Ramona Apartments-S3, S4	132
Figure A.12: Grain size distribution for Jean Vollum-S1	132
Figure A.13: Grain size distribution for John Ross-S1, S3.....	133
Figure A.14: Grain size distribution for International Harvester-S1, S4.....	133
Figure A.15: Grain size distribution for Broadway Housing-S3	134
Figure A.16: Grain size distribution for Multnomah County-S3.....	134
Figure A.17: Grain size distribution for 911 Federal Building-S2, S3.....	135
Figure A.18: Grain size distribution for BPA Building-S1, S4	135
Figure A.19: Grain size distribution for Wastewater Treatment Plant-S1, no organics..	136
Figure A.20: Grain size distribution for the Portland Building-S1, S4, no organics.....	136
Figure A.21: Grain size distribution for the Hamilton-S1, S4, no organics	137

LIST OF APPENDIX FIGURES (Continued)

<u>Figure</u>	<u>Page</u>
Figure A.22: Grain size distribution for the Buchman Terrace-S1, no organics	137
Figure A.23: Grain size distribution for Swan Island Pumphouse-S1, S3, no organics ..	138
Figure A.24: Grain size distribution for the Village Home Apartments-S1, S4, no organics.....	138
Figure A.25: Grain size distribution for Riva at the Park-S1, S4, no organics.....	139
Figure A.26: Grain size distribution for the Atwater-S3, S4, no organics.....	139
Figure A.27: Grain size distribution for Riva at the Ardea-S5, S6, no organics	140
Figure A.28: Grain size distribution for Fields Hall-S1, no organics.....	140
Figure A.29: Grain size distribution for Riva at Ramona Apartments-S3, S4, no organics.....	141
Figure A.30: Grain size distribution for Jean Vollum-S1, no organics	141
Figure A.31: Grain size distribution for John Ross-S1, S3, no organics	142
Figure A.32: Grain size distribution for International Harvester-S1, S4, no organics	142
Figure A.33: Grain size distribution for Broadway Housing-S3, no organics.....	143
Figure A.34: Grain size distribution for Multnomah County-S3, no organics	143
Figure A.35: Grain size distribution for 911 Federal Building-S3, no organics.....	144
Figure A.36: Grain size distribution for BPA Building-S1, S4, no organics.....	144
Figure A.37: Complete grain size distribution for Wastewater Treatment Plant-S1	145
Figure A.38: Complete grain size distribution for the Portland Building-S1, S4.....	145
Figure A.39: Complete grain size distribution for the Hamilton-S1, S4	146
Figure A.40: Complete grain size distribution for the Buchman Terrace-S1	146
Figure A.41: Complete grain size distribution for Swan Island Pumphouse-S1, S3.....	147

LIST OF APPENDIX FIGURES (Continued)

<u>Figure</u>	<u>Page</u>
Figure A.42: Complete grain size distribution for the Village Home Apartments-S1, S4.....	147
Figure A.43: Complete grain size distribution for Riva at the Park-S1, S4.....	148
Figure A.44: Complete grain size distribution for the Atwater-S3, S4	148
Figure A.45: Complete grain size distribution for Riva at the Ardea-S5, S6	149
Figure A.46: Complete grain size distribution for Fields Hall-S1	149
Figure A.47: Complete grain size distribution for Riva at Ramona Apartments-S3, S4.....	150
Figure A.48: Complete grain size distribution for Jean Vollum-S1	150
Figure A.49: Complete grain size distribution for John Ross-S1, S3.....	151
Figure A.50: Complete grain size distribution for International Harvester-S1, S4	151
Figure A.51: Complete grain size distribution for Broadway Housing-S3	152
Figure A.52: Complete grain size distribution for Multnomah County-S3	152
Figure A.53: Complete grain size distribution for 911 Federal Building-S3	153
Figure A.54: Complete grain size distribution for BPA Building-S1, S4	153
Figure A.55: Flow curve for the Hamilton-S4.....	154
Figure A.56: Flow curve for Buchman Terrace-S1	154
Figure A.57: Flow curve for the Swan Island-S1	155
Figure A.58: Flow curve for Swan Island-S3	155
Figure A.59: Flow curve for Jean Vollum-S1	156
Figure A.60: Flow curve for John Ross-S3	156
Figure A.61: Target Gradations.....	157

LIST OF APPENDIX FIGURES (Continued)

<u>Figure</u>	<u>Page</u>
Figure A.62: Schematic of sampling tube.....	158
Figure A.63: Schematic of plunger and cap.....	158
Figure A.64: Side view of transport box.....	159
Figure A.65: Cross-section of sampler box.. ..	159
Figure A.66: Top view of sampler box.....	160
Figure B.1: Assembly of specimen membrane, O-rings, and bottom platen.....	162
Figure B.2: Confining rings stacked onto steel rods.....	163
Figure B.3: Membrane stretched around confining rings	163
Figure B.4: Micrometer used to determine diameter of specimen.....	164
Figure B.5: (a) Membrane around top platen (b) O-rings around top platen.....	165
Figure B.6: Built specimen placed into shear box	166
Figure B.7: Set screws on base of shear box	166
Figure B.8: Circular plate slid around stainless steel rod	167
Figure B.9: Raised swing arm.....	167
Figure B.10: Assembly of stainless steel rod and circular plate	168
Figure B.11: Simple Shear unit and specimen fully assembled.....	169
Figure B.12: Zeroing of load cells.. ..	171
Figure B.13: Windows displaying front panel information	172
Figure C.1: Stress-strain response for specimens reconstituted to $D_r= 30\%$ for the (a) fine (b) intermediate (c) coarse gradations, respectively.	178
Figure C.2: Stress-strain response for specimens reconstituted to $D_r= 50\%$ for the (a) fine (b) intermediate (c) coarse gradations, respectively.	179

LIST OF APPENDIX FIGURES (Continued)

<u>Figure</u>	<u>Page</u>
Figure C.3: Volumetric response for specimens reconstituted to $D_r = 30\%$ for the (a) fine (b) intermediate (c) coarse gradations, respectively.	180
Figure C.4: Volumetric response for specimens reconstituted to $D_r = 50\%$ for the (a) fine (b) intermediate (c) coarse gradations, respectively.	181
Figure C.5: Secant shear modulus at one percent shear strain with $\sigma_{zz} = 10$ kPa and $D_r = 30\%$ for: (a) fine, (b) intermediate, and (c) coarse gradations.	182
Figure C.6: Secant shear modulus at one percent shear strain with $\sigma_{zz} = 20$ kPa and $D_r = 30\%$ for: (a) fine, (b) intermediate, and (c) coarse gradations.	183
Figure C.7: Secant shear modulus at one percent shear strain with $\sigma_{zz} = 30$ kPa and $D_r = 30\%$ for: (a) fine, (b) intermediate, and (c) coarse gradations.	184
Figure C.8: Secant shear modulus at one percent shear strain with $\sigma_{zz} = 10$ kPa and $D_r = 50\%$ for: (a) fine, (b) intermediate, and (c) coarse gradations.	185
Figure C.9: Secant shear modulus at one percent shear strain with $\sigma_{zz} = 20$ kPa and $D_r = 50\%$ for: (a) fine, (b) intermediate, and (c) coarse gradations.	186
Figure C.10: Secant shear modulus at one percent shear strain with $\sigma_{zz} = 30$ kPa and $D_r = 50\%$ for: (a) fine, (b) intermediate, and (c) coarse gradations.	187
Figure D.1: Results from the fine gradation CSS test through 1000 cycles where: (a) constant magnitude sinusoidal $\gamma_c = 1.5\%$ (b) cyclic shear stress response (c) specimen normal strain. Results for the first 50 cycles: (d), (e), and (f), respectively. Note: $f = 1$ Hz.	189
Figure D.2: Results from the fine gradation CSS test through 1000 cycles where: (a) cyclic stress-strain loops (b) cyclic shear strain induced excess pore pressure (c) excess pore pressure ratio. Results for the first 50 cycles: (d), (e), and (f), respectively. Note: $f = 1$ Hz.	190
Figure D.3: Results from the fine gradation CSS test through 1000 cycles where: (a) constant magnitude sinusoidal $\gamma_c = 4\%$ (b) cyclic shear stress response (c) specimen normal strain. Results for the first 50 cycles: (d), (e), and (f), respectively. Note: $f = 1$ Hz.	191

LIST OF APPENDIX FIGURES (Continued)

<u>Figure</u>	<u>Page</u>
Figure D.4: Results from the fine gradation CSS test through 1000 cycles where: (a) cyclic stress-strain loops (b) cyclic shear strain induced excess pore pressure (c) excess pore pressure ratio. Results for the first 50 cycles: (d), (e), and (f), respectively. Note: $f = 1$ Hz.	192
Figure D.5: Results from the fine gradation CSS test through 1000 cycles where: (a) constant magnitude sinusoidal $\gamma_c = 1.5\%$ (b) cyclic shear stress response (c) specimen normal strain. Results for the first 50 cycles: (d), (e), and (f), respectively. Note: $f = 2$ Hz.	193
Figure D.6: Results from the fine gradation CSS test through 1000 cycles where: (a) cyclic stress-strain loops (b) cyclic shear strain induced excess pore pressure (c) excess pore pressure ratio. Results for the first 50 cycles: (d), (e), and (f), respectively. Note: $f = 2$ Hz.	194
Figure D.7: Results from the fine gradation CSS test through 1000 cycles where: (a) constant magnitude sinusoidal $\gamma_c = 4\%$ (b) cyclic shear stress response (c) specimen normal strain. Results for the first 50 cycles: (d), (e), and (f), respectively. Note: $f = 2$ Hz.	195
Figure D.8: Results from the fine gradation CSS test through 1000 cycles where: (a) cyclic stress-strain loops (b) cyclic shear strain induced excess pore pressure (c) excess pore pressure ratio. Results for the first 50 cycles: (d), (e), and (f), respectively. Note: $f = 2$ Hz.	196
Figure D.9: Results from the intermediate gradation CSS test through 1000 cycles where: (a) constant magnitude sinusoidal $\gamma_c = 1.5\%$ (b) cyclic shear stress response (c) specimen normal strain. Results for the first 50 cycles: (d), (e), and (f), respectively. Note: $f = 1$ Hz.	197
Figure D.10: Results from the intermediate gradation CSS test through 1000 cycles where: (a) cyclic stress-strain loops (b) cyclic shear strain induced excess pore pressure (c) excess pore pressure ratio. Results for the first 50 cycles: (d), (e), and (f), respectively. Note: $f = 1$ Hz.	198
Figure D.11: Results from the intermediate gradation CSS test through 1000 cycles where: (a) constant magnitude sinusoidal $\gamma_c = 4\%$ (b) cyclic shear stress response (c) specimen normal strain. Results for the first 50 cycles: (d), (e), and (f), respectively. Note: $f = 1$ Hz.	199

LIST OF APPENDIX FIGURES (Continued)

<u>Figure</u>	<u>Page</u>
Figure D.12: Results from the intermediate gradation CSS test through 1000 cycles where: (a) cyclic stress-strain loops (b) cyclic shear strain induced excess pore pressure (c) excess pore pressure ratio. Results for the first 50 cycles: (d), (e), and (f), respectively. Note: $f = 1$ Hz...	200
Figure D.13: Results from the intermediate gradation CSS test through 1000 cycles where: (a) constant magnitude sinusoidal $\gamma_c = 1.5\%$ (b) cyclic shear stress response (c) specimen normal strain. Results for the first 50 cycles: (d), (e), and (f), respectively. Note: $f = 2$ Hz.....	201
Figure D.14: Results from the intermediate gradation CSS test through 1000 cycles where: (a) cyclic stress-strain loops (b) cyclic shear strain induced excess pore pressure (c) excess pore pressure ratio. Results for the first 50 cycles: (d), (e), and (f), respectively. Note: $f = 2$ Hz.	202
Figure D.15: Results from the intermediate gradation CSS test through 1000 cycles where: (a) constant magnitude sinusoidal $\gamma_c = 4\%$ (b) cyclic shear stress response (c) specimen normal strain. Results for the first 50 cycles: (d), (e), and (f), respectively. Note: $f = 2$ Hz.....	203
Figure D.16: Results from the intermediate gradation CSS test through 1000 cycles where: (a) cyclic stress-strain loops (b) cyclic shear strain induced excess pore pressure (c) excess pore pressure ratio. Results for the first 50 cycles: (d), (e), and (f), respectively. Note: $f = 2$ Hz..	204
Figure D.17: Results from the coarse gradation CSS test through 1000 cycles where: (a) constant magnitude sinusoidal $\gamma_c = 1.5\%$ (b) cyclic shear stress response (c) specimen normal strain. Results for the first 50 cycles: (d), (e), and (f), respectively. Note: $f = 1$ Hz.....	205
Figure D.18: Results from the coarse gradation CSS test through 1000 cycles where: (a) cyclic stress-strain loops (b) cyclic shear strain induced excess pore pressure (c) excess pore pressure ratio. Results for the first 50 cycles: (d), (e), and (f), respectively. Note: $f = 1$ Hz..	206
Figure D.19: Results from the coarse gradation CSS test through 1000 cycles where: (a) constant magnitude sinusoidal $\gamma_c = 4\%$ (b) cyclic shear stress response (c) specimen normal strain. Results for the first 50 cycles: (d), (e), and (f), respectively. Note: $f = 1$ Hz.....	207

LIST OF APPENDIX FIGURES (Continued)

<u>Figure</u>	<u>Page</u>
Figure D.20: Results from the coarse gradation CSS test through 1000 cycles where: (a) cyclic stress-strain loops (b) cyclic shear strain induced excess pore pressure (c) excess pore pressure ratio. Results for the first 50 cycles: (d), (e), and (f), respectively. Note: $f = 1$ Hz	208
Figure D.21: Results from the coarse gradation CSS test through 1000 cycles where: (a) constant magnitude sinusoidal $\gamma_c = 1.5\%$ (b) cyclic shear stress response (c) specimen normal strain. Results for the first 50 cycles: (d), (e), and (f), respectively. Note: $f = 2$ Hz.....	209
Figure D.22: Results from the coarse gradation CSS test through 1000 cycles where: (a) cyclic stress-strain loops (b) cyclic shear strain induced excess pore pressure (c) excess pore pressure ratio. Results for the first 50 cycles: (d), (e), and (f), respectively. Note: $f = 2$ Hz... ..	210
Figure D.23: Results from the coarse gradation CSS test through 1000 cycles where: (a) constant magnitude sinusoidal $\gamma_c = 4\%$ (b) cyclic shear stress response (c) specimen normal strain. Results for the first 50 cycles: (d), (e), and (f), respectively. Note: $f = 2$ Hz.....	211
Figure D.24: Results from the coarse gradation CSS test through 1000 cycles where: (a) cyclic stress-strain loops (b) cyclic shear strain induced excess pore pressure (c) excess pore pressure ratio. Results for the first 50 cycles: (d), (e), and (f), respectively. Note: $f = 2$ Hz... ..	212
Figure D.25: Results from the fine gradation CSS test through 1000 cycles where: (a) constant magnitude sinusoidal $\gamma_c = 1.5\%$ (b) cyclic shear stress response (c) specimen normal strain. Results for the first 50 cycles: (d), (e), and (f), respectively. Note: $f = 1$ Hz.....	213
Figure D.26: Results from the fine gradation CSS test through 1000 cycles where: (a) cyclic stress-strain loops (b) cyclic shear strain induced excess pore pressure (c) excess pore pressure ratio. Results for the first 50 cycles: (d), (e), and (f), respectively. Note: $f = 1$ Hz.... ..	214
Figure D.27: Results from the fine gradation CSS test through 1000 cycles where: (a) constant magnitude sinusoidal $\gamma_c = 4\%$ (b) cyclic shear stress response (c) specimen normal strain. Results for the first 50 cycles: (d), (e), and (f), respectively. Note: $f = 1$ Hz.....	215

LIST OF APPENDIX FIGURES (Continued)

<u>Figure</u>	<u>Page</u>
Figure D.28: Results from the fine gradation CSS test through 1000 cycles where: (a) cyclic stress-strain loops (b) cyclic shear strain induced excess pore pressure (c) excess pore pressure ratio. Results for the first 50 cycles: (d), (e), and (f), respectively. Note: $f = 1$ Hz	216
Figure D.29: Results from the fine gradation CSS test through 1000 cycles where: (a) constant magnitude sinusoidal $\gamma_c = 1.5\%$ (b) cyclic shear stress response (c) specimen normal strain. Results for the first 50 cycles: (d), (e), and (f), respectively. Note: $f = 2$ Hz.....	217
Figure D.30: Results from the fine gradation CSS test through 1000 cycles where: (a) cyclic stress-strain loops (b) cyclic shear strain induced excess pore pressure (c) excess pore pressure ratio. Results for the first 50 cycles: (d), (e), and (f), respectively. Note: $f = 2$ Hz....	218
Figure D.31: Results from the fine gradation CSS test through 1000 cycles where: (a) constant magnitude sinusoidal $\gamma_c = 4\%$ (b) cyclic shear stress response (c) specimen normal strain. Results for the first 50 cycles: (d), (e), and (f), respectively. Note: $f = 2$ Hz.....	219
Figure D.32: Results from the fine gradation CSS test through 1000 cycles where: (a) cyclic stress-strain loops (b) cyclic shear strain induced excess pore pressure (c) excess pore pressure ratio. Results for the first 50 cycles: (d), (e), and (f), respectively. Note: $f = 2$ Hz....	220
Figure D.33: Results from the intermediate gradation CSS test through 1000 cycles where: (a) constant magnitude sinusoidal $\gamma_c = 1.5\%$ (b) cyclic shear stress response (c) specimen normal strain. Results for the first 50 cycles: (d), (e), and (f), respectively. Note: $f = 1$ Hz.....	221
Figure D.34: Results from the intermediate gradation CSS test through 1000 cycles where: (a) cyclic stress-strain loops (b) cyclic shear strain induced excess pore pressure (c) excess pore pressure ratio. Results for the first 50 cycles: (d), (e), and (f), respectively. Note: $f = 1$ Hz....	222
Figure D.35: Results from the intermediate gradation CSS test through 1000 cycles where: (a) constant magnitude sinusoidal $\gamma_c = 4\%$ (b) cyclic shear stress response (c) specimen normal strain. Results for the first 50 cycles: (d), (e), and (f), respectively. Note: $f = 1$ Hz.....	223

LIST OF APPENDIX FIGURES (Continued)

<u>Figure</u>	<u>Page</u>
Figure D.36: Results from the intermediate gradation CSS test through 1000 cycles where: (a) cyclic stress-strain loops (b) cyclic shear strain induced excess pore pressure (c) excess pore pressure ratio. Results for the first 50 cycles: (d), (e), and (f), respectively. Note: $f = 1$ Hz	224
Figure D.37: Results from the intermediate gradation CSS test through 1000 cycles where: (a) constant magnitude sinusoidal $\gamma_c = 1.5\%$ (b) cyclic shear stress response (c) specimen normal strain. Results for the first 50 cycles: (d), (e), and (f), respectively. Note: $f = 2$ Hz.....	225
Figure D.38: Results from the intermediate gradation CSS test through 1000 cycles where: (a) cyclic stress-strain loops (b) cyclic shear strain induced excess pore pressure (c) excess pore pressure ratio. Results for the first 50 cycles: (d), (e), and (f), respectively. Note: $f = 2$ Hz.	226
Figure D.39: Results from the intermediate gradation CSS test through 1000 cycles where: (a) constant magnitude sinusoidal $\gamma_c = 4\%$ (b) cyclic shear stress response (c) specimen normal strain. Results for the first 50 cycles: (d), (e), and (f), respectively. Note: $f = 2$ Hz.....	227
Figure D.40: Results from the intermediate gradation CSS test through 1000 cycles where: (a) cyclic stress-strain loops (b) cyclic shear strain induced excess pore pressure (c) excess pore pressure ratio. Results for the first 50 cycles: (d), (e), and (f), respectively. Note: $f = 2$ Hz.	228
Figure D.41: Results from the coarse gradation CSS test through 1000 cycles where: (a) constant magnitude sinusoidal $\gamma_c = 1.5\%$ (b) cyclic shear stress response (c) specimen normal strain. Results for the first 50 cycles: (d), (e), and (f), respectively. Note: $f = 1$ Hz.....	229
Figure D.42: Results from the coarse gradation CSS test through 1000 cycles where: (a) cyclic stress-strain loops (b) cyclic shear strain induced excess pore pressure (c) excess pore pressure ratio. Results for the first 50 cycles: (d), (e), and (f), respectively. Note: $f = 1$ Hz.	230
Figure D.43: Results from the coarse gradation CSS test through 1000 cycles where: (a) constant magnitude sinusoidal $\gamma_c = 4\%$ (b) cyclic shear stress response (c) specimen normal strain. Results for the first 50 cycles: (d), (e), and (f), respectively. Note: $f = 1$ Hz.....	231

LIST OF APPENDIX FIGURES (Continued)

<u>Figure</u>	<u>Page</u>
Figure D.44: Results from the coarse gradation CSS test through 1000 cycles where: (a) cyclic stress-strain loops (b) cyclic shear strain induced excess pore pressure (c) excess pore pressure ratio. Results for the first 50 cycles: (d), (e), and (f), respectively. Note: $f = 1$ Hz.	232
Figure D.45: Results from the coarse gradation CSS test through 1000 cycles where: (a) constant magnitude sinusoidal $\gamma_c = 1.5\%$ (b) cyclic shear stress response (c) specimen normal strain. Results for the first 50 cycles: (d), (e), and (f), respectively. Note: $f = 2$ Hz.	233
Figure D.46: Results from the coarse gradation CSS test through 1000 cycles where: (a) cyclic stress-strain loops (b) cyclic shear strain induced excess pore pressure (c) excess pore pressure ratio. Results for the first 50 cycles: (d), (e), and (f), respectively. Note: $f = 2$ Hz.	234
Figure D.47: Results from the coarse gradation CSS test through 1000 cycles where: (a) constant magnitude sinusoidal $\gamma_c = 4\%$ (b) cyclic shear stress response (c) specimen normal strain. Results for the first 50 cycles: (d), (e), and (f), respectively. Note: $f = 2$ Hz.	235
Figure D.48: Results from the coarse gradation CSS test through 1000 cycles where: (a) cyclic stress-strain loops (b) cyclic shear strain induced excess pore pressure (c) excess pore pressure ratio. Results for the first 50 cycles: (d), (e), and (f), respectively. Note: $f = 2$ Hz.	236
Figure D.49: Results from the fine gradation CSS test through 1000 cycles where: (a) constant magnitude sinusoidal $\gamma_c = 4\%$ (b) cyclic shear stress response (c) specimen normal strain. Results for the first 50 cycles: (d), (e), and (f), respectively. Note: $f = 1$ Hz.	237
Figure D.50: Results from the fine gradation CSS test through 1000 cycles where: (a) cyclic stress-strain loops (b) cyclic shear strain induced excess pore pressure (c) excess pore pressure ratio. Results for the first 50 cycles: (d), (e), and (f), respectively. Note: $f = 1$ Hz.	238
Figure D.51: Results from the intermediate gradation CSS test through 1000 cycles where: (a) constant magnitude sinusoidal $\gamma_c = 4\%$ (b) cyclic shear stress response (c) specimen normal strain. Results for the first 50 cycles: (d), (e), and (f), respectively. Note: $f = 1$ Hz.	239

LIST OF APPENDIX FIGURES (Continued)

<u>Figure</u>	<u>Page</u>
Figure D.52: Results from the intermediate gradation CSS test through 1000 cycles where: (a) cyclic stress-strain loops (b) cyclic shear strain induced excess pore pressure (c) excess pore pressure ratio. Results for the first 50 cycles: (d), (e), and (f), respectively. Note: $f = 1$ Hz.	240
Figure D.53: Results from the intermediate gradation CSS test through 1000 cycles where: (a) constant magnitude sinusoidal $\gamma_c = 4\%$ (b) cyclic shear stress response (c) specimen normal strain. Results for the first 50 cycles: (d), (e), and (f), respectively. Note: $f = 1$ Hz.....	241
Figure D.54: Results from the intermediate gradation CSS test through 1000 cycles where: (a) cyclic stress-strain loops (b) cyclic shear strain induced excess pore pressure (c) excess pore pressure ratio. Results for the first 50 cycles: (d), (e), and (f), respectively. Note: $f = 1$ Hz..	242
Figure D.55: Results from John Ross tube specimen CSS test with 1000 cycles where: (a) constant magnitude sinusoidal $\gamma_c = 1.5\%$ (b) cyclic shear stress response (c) specimen normal strain. Results for the first 50 cycles: (d), (e), and (f), respectively. Note: $f = 1$ Hz.....	243
Figure D.56: Results from John Ross tube specimen CSS test with 1000 cycles where: (a) cyclic stress-strain loops (b) cyclic shear strain induced excess pore pressure (c) excess pore pressure ratio. Results for the first 50 cycles: (d), (e), and (f), respectively. Note: $f = 1$ Hz..	244
Figure D.57: Results from Portland Building tube specimen CSS test with 1000 cycles where: (a) constant magnitude sinusoidal $\gamma_c = 4\%$ (b) cyclic shear stress response (c) specimen normal strain. Results for the first 50 cycles: (d), (e), and (f), respectively. Note: $f = 1$ Hz.....	245
Figure D.58: Results from Portland Building tube specimen CSS test with 1000 cycles where: (a) cyclic stress-strain loops (b) cyclic shear strain induced excess pore pressure (c) excess pore pressure ratio. Results for the first 50 cycles: (d), (e), and (f), respectively. Note: $f = 1$ Hz	246
Figure D.59: Results from Swan Island tube specimen CSS test with 1000 cycles where: (a) constant magnitude sinusoidal $\gamma_c = 4\%$ (b) cyclic shear stress response (c) specimen normal strain. Results for the first 50 cycles: (d), (e), and (f), respectively. Note: $f = 1$ Hz.....	247

LIST OF APPENDIX FIGURES (Continued)

<u>Figure</u>	<u>Page</u>
Figure D.60: Results from Swan Island tube specimen CSS test with 1000 cycles where: (a) cyclic stress-strain loops (b) cyclic shear strain induced excess pore pressure (c) excess pore pressure ratio. Results for the first 50 cycles: (d), (e), and (f), respectively. Note: $f = 1$ Hz..	248
Figure D.61: Modulus reduction curves fine gradation reconstituted to $D_r = 30\%$ specimens..	249
Figure D.62: Modulus reduction curves intermediate gradation reconstituted to $D_r = 30\%$ specimens..	250
Figure D.63: Modulus reduction curves coarse gradation reconstituted to $D_r = 30\%$ specimens..	251
Figure D.64: Modulus reduction curves fine gradation reconstituted to $D_r = 50\%$ specimens..	252
Figure D.65: Modulus reduction curves intermediate gradation reconstituted to $D_r = 50\%$ specimens..	253
Figure D.66: Modulus reduction curves coarse gradation reconstituted to $D_r = 50\%$ specimens..	254
Figure D.67: Modulus reduction curves for $\sigma'_v = 100$ kPa specimens reconstituted to $D_r = 50\%$	255
Figure D.68: Modulus reduction curves for tube specimens with $\sigma'_v = 30$ kPa... ..	256

NOTATION

Acronyms

ASTM	American Society for Testing Materials
COV	Coefficient of Variation
CSS	Cyclic Simple Shear
CTNI	Cumulative Trapezoidal Numerical Integration
CTX	Cyclic Triaxial
DEM	Discrete Element Modeling
DL	Dead Load
DSS	Direct Simple Shear
FC	Fines Content
FLL	Forschungsgesellschaft Landschaftsentwicklung Landschaftsbau
GCTS	Geotechnical Consultants and Testing Systems
LVDT	Linear Variable Differential Transformer
NGI	Norwegian Geotechnical Institute
PDF	Probability Density Function
PI	Plastic Index
SIG	Swedish Geotechnical Institute
SM	Silty Sand
USACE	United States Army Corps of Engineers
USCS	United States Soil Classification System

NOTATION (Continued)

Symbols

A_s	Area of the specimen on the x-y plane
C_c	Coefficient of curvature
C_u	Coefficient of uniformity
D_i	Inside diameter of sampling tube
D_o	Outside diameter of sampling tube
D_x	Grain size threshold corresponding to percent finer by mass (mm)
D_{10}	Grain size threshold corresponding to 10 percent finer by mass (mm)
D_{50}	Grain size threshold corresponding to 50 percent finer by mass (mm)
D_r	Relative density (%)
e	Void ratio
e_{min}	Minimum void ratio
e_{max}	Maximum void ratio
f	Frequency (Hz)
F_x	Applied horizontal force to vertical plane (kN)
F_z	Applied horizontal force to horizontal plane (kN)
G	Secant shear modulus (MPa)
G_{max}	Maximum secant shear modulus (MPa)
G_{max}^*	Estimated maximum secant shear modulus (MPa)
G_s	Specific gravity of solids
G_{sec}	Secant shear modulus (MPa)
H_o	Initial height of specimen
Δh	Change in height of specimen

NOTATION (Continued)

Symbols

K_0	At rest earth pressure coefficient
N	Number of cycles
N_L	Number of cycles to liquefaction
O_c	Organic content (%)
P	Normal force
Q	Shear force
r_u	Excess pore pressure ratio (%)
r_u^*	Normalized excess pore pressure ratio
w	Water content (%)
u	Pore pressure (kPa)
Δu	Excess pore pressure (kPa)
Δx	Horizontal displacement of the specimen along the x-axis
Δz	Change in height of specimen
ε_1	Major principal strain (%)
$\Delta \varepsilon_1$	Incremental change in major principal strain (%)
ε_3	Minor principal strain (%)
$\Delta \varepsilon_3$	Incremental change in minor principal strain (%)
ε_n	Normal strain (%)
ε_z	Vertical strain (volumetric strain)
γ_m	Moist unit weight of ecoroof soil (kN/m ³)
γ_d	Dry unit weight of ecoroof soil (kN/m ³)

NOTATION (Continued)

Symbols

γ_c	Cyclic shear strain amplitude (%)
$\Delta\gamma_c$	Range in cyclic shear strain (%)
$\gamma_{d,max}$	Maximum dry unit weight (kN/m ³)
$\gamma_{d,min}$	Minimum dry unit weight (kN/m ³)
γ_{zx}	Shear strain on x-z plane (%)
ϕ_m	Mobilized friction angle
σ	Standard deviation
σ'_n	Normal stress
σ'_v	Effective vertical stress (kPa)
σ'_{v0}	Effective vertical consolidation stress (kPa)
σ_{yy}	Normal stress on horizontal plane
σ_{zz}, σ_z	Normal stress on horizontal plane (kPa)
ψ	Dilation angle
ψ_p	Peak dilation angle
τ	Shear stress on horizontal plane (kPa)
τ_c	Cyclic shear stress (kPa)
$\Delta\tau_c$	Range in cyclic shear stress (kPa)
τ_{xy}	Shear stress on horizontal plane
τ_{yx}	Shear stress on the y-plane in the x-direction
τ_{yz}	Shear stress on the y-plane in the z-direction
ζ	Damping ratio (%)
$\oint \tau_c d\gamma_c$	Area of the stress-strain loop from CSS test

For my wife, Kelsey

Chapter 1: Introduction

1.1 Background

The recent proliferation of green technology in the United States has led to a variety of sustainable economic, building, and construction material alternatives. However, certain green technologies have outpaced the engineering and construction community in terms of design standards and codes. Specifically, ecoroofs, or green roofs have no enforced building or design standards in the United States. The lack of building or design standards is concerning because ecoroofs are becoming a popular alternative to traditional roofing options. Ecoroofs are gaining popularity, because they provide benefits to building owners and city municipalities. Examples of ecoroof benefits include aesthetics, storm water control, extended roof membrane life, reduction of urban heat island effects, and increased building insulation (e.g. Hutchinson et al. 2003; Liptan and Strecker 2003; Getter and Rowe 2006; MacMullan et al. 2008; Spolek 2008). Benefits do not outweigh the potential for catastrophic failure from the lack of ecoroof standardization.

Ecoroofs are a layered system (e.g. Figure 1.1) consisting of an uppermost vegetative layer followed by the soil column, drainage mat, and protective barrier, respectively. The exact composition of layers defines the type of ecoroof system as either an extensive or intensive ecoroof. Typical extensive ecoroofs are designed to be monolithic (i.e. uniform) across the roof or tray-based systems, are located on the uppermost floor, and have minimal public access (e.g. Figure 1.2a and 1.2b). Monolithic systems provide a uniform contact between the ecoroof soil and the layers beneath; whereas, tray systems are

typically proprietary in design and vary by manufacturer. The soil depth of an extensive ecoroof is typically 40 to 150 mm (Friedrich 2008, Getter and Rowe 2006, Wark and Wark 2008). The shallow soil depth is intended to support self-sustaining vegetation such as sedums, mosses, and short grasses. These plants are typically chosen because of their ability to grow in shallow soil depths and their resistance to extended dry periods (FLL 2008, Friedrich 2008, Getter and Rowe 2006). Additionally, irrigation and maintenance of extensive ecoroofs is conducted on a limited basis, and is dependent on the climate or owner preference.

Intensive ecoroofs (e.g. Figure 1.2c and 1.2d) have soil depths greater than extensive roofs and are sometimes referred to as rooftop gardens. Correspondingly, intensive ecoroofs are capable of sustaining larger species of plants such as thick mature grasses, small bushes and trees. Frequent irrigation and maintenance is required for intensive ecoroofs due to the water requirements and growth cycle associated with larger plant species. Intensive ecoroofs are typically located at intermediate rooftop elevations, where public access is possible.

The lack in standardization for ecoroof technology has become a leading concern among engineers and insurance firms, particularly for those buildings with ecoroofs located in seismically active areas (e.g. Pacific Northwest), where the probability of a significant earthquake is expected in the next 50 years is as high as 45 percent (Mazzotti and Adams 2004; Goldfinger et al. 2012). Seismic forces may cause the ecoroof soil to slide horizontally along the interface of the roof membrane and ecoroof material, and subsequently, the ecoroof soil laterally loads the parapet walls. This scenario has potential to cause overtopping of the parapet walls or complete failure of the roof system

if the roof structure becomes overloaded due to the non-uniform inertial forces from the ecoroof material. Accordingly, the work documented in this thesis was conducted to understand and quantify the geotechnical soil indices, drained static strength, and dynamic soil properties for ecoroof soil. Additionally, an ecoroof soil sampling procedure and equipment were developed for use during a sampling program conducted on ecoroofs in Portland, Oregon. For reference, various encountered drainage types and conditions, and the employed sampler at various ecoroofs can be seen in Figures 1.3 and 1.4, respectively.

1.2 Outline of Work Completed

The investigation presented herein provides an initial geotechnical characterization data set, which was determined by sampling soils from eighteen ecoroofs in Portland, Oregon. In addition, the static and dynamic response of ecoroof soil subjected to simple shear boundary conditions is presented. Chapter 2 contains a literature review of static simple shear testing devices, boundary conditions, assumptions, and failure definitions as well as a brief literature review of cyclic simple shear devices. Supplementary details regarding analytical procedures, definition of liquefaction potential and data reduction methods for cyclic simple shear tests are presented in Chapter 5.

Chapter 3 presents the first manuscript entitled: “Characterization of Ecoroofs and Ecoroof Materials”. This manuscript was submitted and accepted for the Proceedings of the American Society of Civil Engineers (ASCE) 2014 GeoCongress conference in Atlanta, Georgia. Presented within the manuscript is the ecoroof sampling program and sampling equipment developed specifically for this research, a literature review on

ecorooofs, the geotechnical characterization and statistical description of index properties, and preliminary drained simple shear response of two reconstituted ecoroof soil specimens.

Chapter 4 presents the second manuscript entitled: “Geotechnical Characterization and Drained Shear Strength of Ecoroof Soil”, which was submitted to ASCE’s *Journal of Geotechnical and Geoenvironmental Engineering* for possible publication. The second manuscript presents a brief overview of the variability determined for the geotechnical index properties, but focuses on the detailed exploration of drained static simple shear testing. Specifically, the second manuscript describes: the simple shear equipment used, the theoretical considerations for interpreting simple shear tests, and the stress-strain and volumetric strain response of reconstituted and undisturbed tube samples. Additionally, the static shear modulus, mobilized friction angles, and mobilized dilation characteristics of ecorooofs soils are described.

The third manuscript constitutes Chapter 5 and is entitled: “Undrained Cyclic Simple Shear Response of Ecoroof Soil”. The third manuscript will be submitted to *Earthquake Spectra* for possible publication. The third manuscript focuses on the undrained dynamic response of ecoroof soil. Specifically, the pore pressure response, modulus reduction, and damping characteristics for the three target ecoroof soil gradations subjected to various testing conditions are presented. Additionally, the cyclic response of ecoroof soil is compared to previously reported dynamic soil responses. Specifically, a roof displacement model was developed, which allows engineers to obtain an estimate for the liquefaction susceptibility of ecoroof soil for a given roof displacement.

The overall research program, which is described within the three manuscripts, is summarized in Chapter 6. Additionally, recommendations for future work and possible guidelines are described in Chapter 6. A full bibliography that encompasses the literature review and the three manuscripts is listed immediately following Chapter 6. Appendices A through D are listed at the end of the document. Appendix A provides details on the design of the sampling equipment, grain size distributions for various stages of the characterization program, and the targeted grain size distributions. Summary tables for all the characterization data for each of the sampled buildings are also provide in Appendix A. Appendix B provides a manual for the static simple shear equipment used. Appendix C provides the stress-strain and volumetric strain plots for each of the reconstituted and tube specimens and provides details on the determination of the secant shear modulus. Appendix D outlines the results from the undrained cyclic simple shear tests. The fitted and extrapolated modulus reduction curves are also presented.

1.3 Figures

Cross section of basic elements

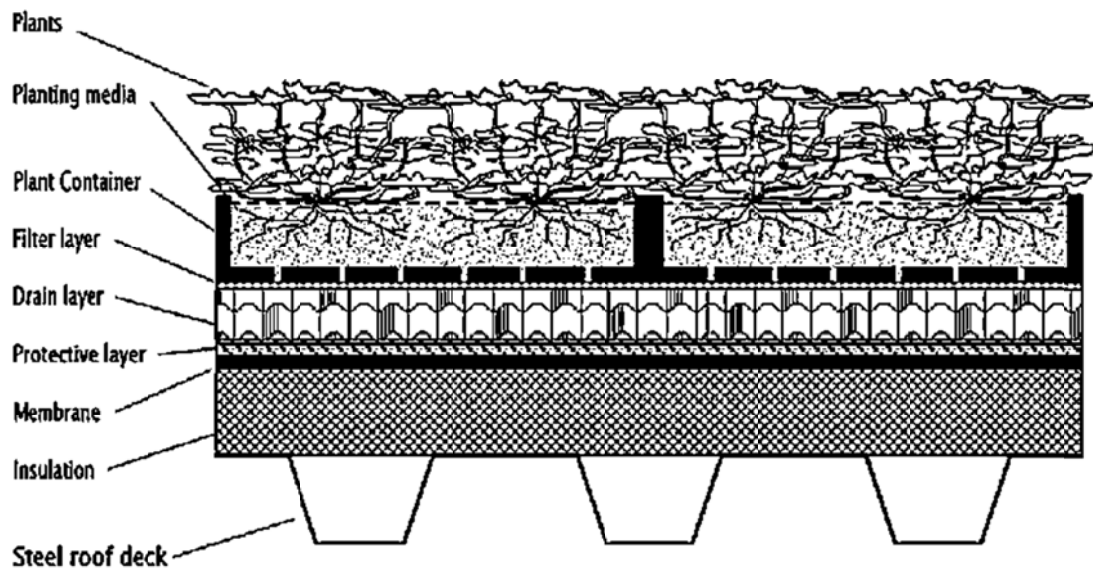


Figure 1.1: Typical cross-section of an ecoroof (after Wark and Wark 2003).



(a)



(b)



(c)



(d)

Figure 1.2: Typical encountered ecoroofs: (a, b) monolithic extensive ecoroofs (c, d) intensive ecoroofs.



Figure 1.3: Various encountered interior and exterior ecoroof drains.



Figure 1.4: Developed Shelby tube sampler used throughout the field exploration at various encountered ecoroofs. Note the variation in vegetation, soil depth and soil gradation.

Chapter 2: Literature Review

Ecoroofs are typically employed on flat horizontal roof structures. Accordingly, a reasonable assumption for the critical failure surface is the horizontal plane at the interface of the ecoroof materials and roof structure. Due to both the relatively shallow depths of ecoroof soil columns and the inability to model the aforementioned horizontal failure plane, conventional triaxial compression tests are not ideal for determining the strength properties of ecoroof soils. In contrast, the direct shear box and simple shear device are capable of modeling this assumed horizontal plane. The direct shear box predates the simple shear device and was not used. However, a brief documentation of the direct shear device is presented herein for completeness, and is followed by a more detailed description of the static and cyclic simple shear devices, respectively.

2.1 Direct Shear Box

The shear strength of soils is widely used for stability analyses (e.g. slopes, settlement, etc.) in geotechnical engineering design. One of the earliest testing devices used to determine the strength properties is a direct shear box. The direct shear box setup requires the soil specimen to be confined within a rigid box split in two, and the specimen is typically either circular or square in shape (Figure 2.1). Normal stresses (σ'_n) are applied vertically to the specimen and a horizontal actuator applies the shear stress (τ) that results from the horizontal displacement. The dashed line at the interface of the split box indicates the horizontal failure surface that develops following significant horizontal displacement. By forcing the failure surface onto the horizontal plane, and allowing the area of the specimen underneath the normal stress to constantly change throughout the

test, the stress state within the specimen becomes unknown (Matthews 1988). Specifically, the principal stresses are unknown unless assumptions are made, and stress concentrations develop on the specimen boundary, causing non-uniform strain fields within the specimen (Holtz et al. 2011). An external vertical displacement gauge measures the volumetric response (i.e. contraction or dilation) of the specimen. Additional information on the stress-strain and volumetric response of granular soils in a direct shear box and testing procedure are given by: Rowe 1969; USACE 1970; Saada and Townsend 1981; Jewel and Wroth 1987; Wu et al. 2007; among others.

2.2 Simple Shear Device

To alleviate the stress-strain and boundary condition deficiencies observed in the direct shear box, researchers in the early 1950s began to develop simple shear devices to determine the shear strength of clay (Kjellman 1951, Roscoe 1953). The original Kjellman (1951) simple shear device was developed at the Swedish Geotechnical Institutes (SGI), and was designed to test a cylindrical specimen constrained by an unreinforced membrane enclosed by a stack of thin rings (Figure 2.2a). The thin rings provide the presumed lateral restraint needed to maintain a constant diameter throughout shearing (i.e. create a plane strain condition) and allow free rotation of principal stresses and strains. Bjerrum and Landva (1966) made improvements to the Kjellman (1951) device. The Bjerrum and Landva (1966) simple shear device is often referred to as the “NGI simple shear device,” because it was developed at the Norwegian Geotechnical Institute. The NGI simple shear device requires specimens to be laterally restrained with a wire-reinforced membrane. The simple shear device developed at Cambridge (Roscoe 1953) was designed to test a square specimen laterally confined with two rigid hinged

flaps. The rigid hinged flaps are allowed to rotate when the shear stress is applied (e.g. Figure 2.2b). Various researchers (Franke et al. 1979 and Budhu 1988) have since made advancements to the two original simple shear devices.

Airey et al. (1985) describes the differences of measured normal and shear stresses for two simple shear testing devices, which are representative of the SGI/NGI and the Cambridge device. One device, herein referred to as the “un-instrumented device,” has external load cells capable of determining the average normal force on the horizontal plane (P) and average shear force (Q) (Figure 2.3a). The other device, herein referred to as the “instrumented device” has a load cell located directly on the specimen (Figure 2.3b), which is capable of determining the normal stress (σ_{yy}) and shear stress (τ_{xy}) in the center of the specimen. The instrumented device is less common in industry, because it is considered impractical and expensive. The simple shear device used for this research was similar had similar boundary conditions to the un-instrumented device shown in Figure 2.3a. The shear stress (τ) and vertical stress (σ_{zz}) were determined by dividing the vertical (P) and shear (Q) loads by the cross-sectional area of the specimen. Chapter 5 and Appendix B contain further discussions of the simple shear device used for the research presented in this thesis.

Researchers (e.g. Airey and Wood 1987, Budhu 1985, Prevost and Høeg 1976 and Wood et al. 1979) have compared the varying measured stress states within the simplified and sophisticated simple shear devices to determine the applicability of both devices. Airey and Wood (1987) and Wood et al. (1979) have shown that the simplified device

typically underestimates the magnitude of the normal force and shear force within the specimen during simple shear.

The term *pure shear* implies plane strain boundary condition where the specimen displaces in two directions (e.g. X and Y) while maintaining a constant volume (Saada and Townsend 1981). Constant volume is maintained through equivalent specimen extension in one direction (e.g. X-direction) and compression in the other (e.g. Y-direction). The term *simple shear* implies a plane strain boundary condition where the specimen displaces in only one direction (e.g. X-direction) while maintaining a constant height (e.g. volume) (Saada and Townsend 1981). Both pure shear and simple shear require no change in the third direction (e.g. Z-direction). Figure 2.4 shows a comparison of pure shear and simple shear.

Researchers (e.g. Airey et al. 1985, Atkinson and Lau 1991, Rossato and Simonini 1991, Shibuya and Hight 1987, and Wood et al. 1979) have found that maintaining plane strain (constant volume) conditions during simple shear testing is difficult. Roscoe (1953) showed analytically, using the Cambridge simple shear device, that maintaining plane strain conditions during simple shear testing is difficult, because the stress distribution applied to the boundary of the specimen is non-uniform.

With the observed difficulties of maintaining plane strain conditions, Saada and Townsend (1981) provided a critical review of the plane strain assumption for both the Cambridge (i.e. square specimen) and NGI (i.e. circular specimen) simple shear devices. Their review describes the comparison of the assumed plane strain conditions to the elastic theory solution of the St. Venant problem. The St. Venant problem consists of a

point load being placed on the end of fixed beam, either square or circular in shape. The associated stresses and strains at the fixed end may then be determined using elasticity theory. Saada and Townsend (1981) noted that the stresses determined from the St. Venant solution vary significantly from the stresses measured during simple shear testing, because soils rarely remain elastic during shearing. Notwithstanding the shortcomings of using the St. Venant solution, Saada and Townsend (1981) suggested that it provides an adequate verification to the validity of the assumed plane strain conditions in the simple shear device. Figure 2.5 shows the axis system and the shear stress distribution for the circular fixed end beam. In Figure 2.5, τ_{yx} is the shear stress on the horizontal plane in the direction of the applied end load (e.g. the y-plane in the x-direction), and τ_{yz} is the shear stress on the horizontal plane in the z-direction. For plane strain conditions to exist two things are required: 1) zero deformation in the z-direction and 2) the magnitude of τ_{yz} must be zero. Examination of the St. Venant solution (Figure 2.5) clearly shows that this is not true. Figures 2.5a and 2.5b show the τ_{yx} shear stress distribution for various lines of action. Saada and Townsend (1981) noted that the magnitude of τ_{yx} (e.g. Figure 2.5a and b) and τ_{yz} (e.g. Figure 2.5c) are the same. Because the magnitude of τ_{yz} is not equal to zero, the solution does not conform to the requirements of plane strain. Only the solution for the circular fixed beam is presented herein, because the simple shear devices (both static and cyclic) used throughout this research program were similar to the simple shear devices described by Kjellman (1951) and Bjerrum and Landva (1966).

Furthermore, a series of photoelastic experiments were conducted to study the assumed plane strain conditions in simple shear devices (Wright et al. 1978). The results

of the photoelastic experiments concluded that the simple shear device is incapable of maintaining plane strain conditions throughout shearing, due to the stress-strain non-uniformities developed on the boundary of the specimen. Figure 2.6 shows the results of this study for both a circular and square simple shear specimen. Further explanation of the testing program and parameters can be found in Wright et al. (1978).

Observations on the stress non-uniformities present within simple shear devices have been documented since the development of the device. To match the assumed plane strain condition, shear stresses must develop along all four sides of a test specimen, and the associated normal stresses must be equal on the top and bottom of the specimen. However, this stress state cannot be accomplished due to the configuration of the device. Wood et al. (1979) describe the development of non-uniform boundary shear stresses caused by the lack of shear stresses on the sides of the specimen. The dashed lines in Figure 2.7a show the location of the non-existent side shear stresses. The absence of side shear stresses induces a moment within the specimen. The induced moment must be balanced by a second moment, which is produced from the non-uniform distribution of normal stresses applied to the top and bottom of the specimen (e.g. Figure 2.7b). Accordingly, simple shear specimens are subjected to eccentric shear and normal stresses. The fully instrumented Cambridge simple shear device (e.g., Wood et al. 1979 and Shibuya and Hight 1987) is capable of determining the magnitude of the eccentric shear and normal stresses. Therefore, the fully instrumented Cambridge simple shear device can determine the true stress distribution at the center of the specimen. The NGI device cannot the true stress distribution, unless it is fully instrumented like the Cambridge device, as described by Budhu (1985).

Various researchers have conducted numerical simulations (e.g., Lucks et al. 1973, Budhu and Britto 1987, Dounias and Potts 1993, Doherty and Fayey 2011, and Wijewickreme et al. 2013) to determine the validity of the various interpretations and boundary conditions of the different simple shear devices. The researchers consistently show that non-uniform stresses develop in specimens during simple shear testing; thus, assumptions must be made when interpreting test results. However, these simulations have also shown that the state of stress within the central portion of the specimen is relatively uniform. An example of the stress state within a simple shear specimen at failure can be seen in Figure 2.8.

To interpret simple shear test results, when the stress state within a specimen is not completely known, a failure criterion must be assumed (Airey et al. 1985). If the maximum shear stress is assumed to lie on the horizontal plane, then the mobilized friction angle (ϕ_m) may be determined by

$$\phi_m = \sin^{-1} \left(\frac{\tau}{\sigma_{zz}} \right), \quad (2.1)$$

where τ and σ_{zz} are the shear stress and vertical stress on the horizontal plane, respectively. If the failure plane is assumed to occur on a plane of maximum stress obliquity, then the mobilized friction angle (ϕ_m) may be determined with:

$$\phi_m = \tan^{-1} \left(\frac{\tau}{\sigma_{zz}} \right). \quad (2.2)$$

Additionally, through the use of a simple shear analogy involving a stack of books subjected to horizontal deformation, De Josselin De Jong (1971) determined that ϕ_m can be determined by

$$\frac{\sin(\phi_m) \cos(\phi_m)}{1 + \sin^2(\phi_m)} = \frac{\tau}{\sigma_{zz}}. \quad (2.3)$$

Additionally, De Josselin De Jong (1971) noted that the failure criterion for a given soil specimen may be any of the three described (i.e., Equations 2.1, 2.2, or 2.3), but it is directly dependent on the path of least resistance for a given soil type and testing parameters. In this research, the failure criteria shown in Equations 2.1 and 2.2 were used, and further details and justification of their usage is given in Chapter 5.

The determination of the volumetric response from simple shear test results, and notably the determination of the dilation angle, is typically performed graphically by constructing the Mohr's circle of strain, or analytically, by using incremental changes in principal strains ($\Delta\varepsilon_1$ and $\Delta\varepsilon_3$). For an assumed plane strain condition, the determination of the major (ε_1) and minor (ε_3) principal strains can be determined from the measured volumetric (ε_z) and shear (γ_{zx}) strains (Rossato and Simonini 1991). Accordingly, the major and minor principal strains can be determined with:

$$\varepsilon_1 = \frac{1}{2} \left(\varepsilon_z + \sqrt{\varepsilon_z^2 + \gamma_{zx}^2} \right) \quad (2.5)$$

$$\varepsilon_3 = \frac{1}{2} \left(\varepsilon_z - \sqrt{\varepsilon_z^2 + \gamma_{zx}^2} \right). \quad (2.6)$$

As noted, the change in major and minor principal strain allow for the determination of the peak dilation angle during simple shear. Houlsby (1991), among others, provide the following relationship for determination of the peak dilation angle:

$$\psi_p = \sin^{-1} \left[-\frac{\Delta\varepsilon_1 + \Delta\varepsilon_3}{\Delta\varepsilon_1 - \Delta\varepsilon_3} \right]. \quad (2.7)$$

Owing to the conventional geotechnical approach to volumetric response of soils, compressive strains are taken as being positive. Accordingly, a positive dilation angle indicates that the specimen expanding in volume and a negative dilation angle indicates compression of the specimen.

2.3 Cyclic Simple Shear Device

The 1964 earthquakes in Niigata, Japan and Prince William Sound, Alaska provided the motivation for understanding the fundamentals of soil liquefaction, and dynamic soil response during cyclic loading in the laboratory (Seed and Lee 1966; Seed and Idriss 1967). Following this, Peacock and Seed (1968) describe the development of a cyclic simple shear device, which was modeled after the original Roscoe (1953) simple shear device. Figure 2.9 shows the physical characteristics of the device during cyclic loading. A square specimen is contained within a rigid box. The box is allowed to rotate at

predefined hinge points, which allows the specimen to maintain simple shear deformation throughout cyclic loading. Additionally, in the 1960s, cyclic triaxial compression test data was much more abundant than cyclic simple shear data. Therefore, Peacock and Seed (1968) made comparisons between the stress controlled cyclic simple shear results and cyclic triaxial test results (Peacock and Seed 1968).

The overall findings of the cyclic simple shear indicated that the measured liquefaction potential of saturated sand in cyclic simple shear was relative to that of cyclic triaxial compression. Furthermore, the authors concluded the most significant finding in the new cyclic simple shear device was that the required cyclic shear stress required to initiate liquefaction was approximately 65 percent less than in the cyclic triaxial compression test. A comparison plot of the generated cyclic shear stresses for both devices can be seen in Figure 2.10.

The stress conditions of the cyclic simple shear device are non-uniform, and this must be taken into account when comparing to in-situ soil conditions and interpreting cyclic simple shear test results. If the boundary issues of the cyclic simple shear device are ignored, then the required cyclic shear stresses to cause liquefaction would likely be 40 to 50 percent than the experimentally determined values (Peacock and Seed 1968).

Silver et al. (1980) performed an investigation with a series of cyclic simple shear and cyclic triaxial compression tests on saturated sand. The main objectives were to study the variation of the results between the two devices for the same type of sand under similar loading conditions, and to understand the effect of relative density, specimen preparation, and number of loading cycles on the dynamic soil response. Silver et al. (1980) found

that the similarities between the two devices' undrained cyclic strength varied in a more complex manner than that previously described by: Peacock and Seed (1968), Finn et al. (1971), and Seed and Peacock (1971), among others. The observed variation depended on, but was not limited to the specimen preparation method, the specimen density, the failure definition, and the number of cyclic cycles.

Furthermore, due to the lack of plane strain boundary conditions and associated stress non-uniformities of the simple shear device, various studies were conducted to determine how specimen size effects the stress state during cyclic simple shear (e.g. Franke et al. 1979; Vucetic and Lacasse 1982; Amer et al. 1987). Specifically, the device developed by Franke et al. (1979), uses a circular specimen with one diameter (i.e. 75 mm) and two heights (i.e. 10 and 20 mm). Franke et al. (1979) concluded that the diameter to height ratios (D/H) used in their device had little influence on the stress condition of the specimen. Amer et al. (1987) followed with the development of a simple shear device capable of testing a much wider range in both specimen diameters and heights. Specifically, specimen heights and diameters ranged from 6.35 to 101.6 mm and 76.2 to 304.8 mm, respectively. Amer et al. (1987) concluded that for specimens with large diameters or large D/H ratios the stress state within the specimen was relatively uniform. Amer et al. (1987) also concluded that the dynamic soil properties (i.e. shear modulus and damping values) indicated little variation for specimens with minimum dimensions of 203.2 and 25.4 mm, for the diameter and height, respectively. For reference, the cyclic simple shear device used for the research presented in this thesis had a D/H of 2.55 with specimen dimensions of 102 and 40 mm, for the diameter and height, respectively.

The determination of dynamic soil properties (i.e. shear modulus and damping) with a cyclic simple shear device has been investigated by researchers (e.g. Lanzo et al. 1997; Vucetic et al. 1998; Matesic and Vucetic 2003; Mortezaie and Vucetic 2012). All of the studies listed used simple shear devices that were capable of determining the small strain shear modulus (G_{\max}). This is a critical parameter needed for the determination of modulus reduction curves. Modulus reduction curves are developed from normalizing the small strain shear modulus by the secant shear modulus (G) at various levels of cyclic shear strain. This process generates a series of data points. Accordingly, curves are generally fit to the data points. Specifically, a methodology developed by Borden et al. (1996) using the least squares method:

$$\frac{G}{G_{\max}} = \frac{1}{[1 + a(\gamma_c)^b]^c} \quad (2.8)$$

where a , b , and c are fitting coefficients, and γ_c is the cyclic shear strain amplitude.

The material damping ratio (ζ) or quantification of the dissipation of energy during cyclic loading cycles is determined from the stress-strain response of cyclically loaded soil. The stress-strain response of soils subjected to cyclic loading resembles a hysteretic loop. Accordingly, the conventional approach assumes elastic soil conditions, and only considers the first quarter of the hysteretic stress-strain loop. The conventional approach uses the single degree-of-freedom model developed by Jacobsen (1930). Brennan et al. (2004) developed a modified model that considers the entire area of the stress-strain loop. The damping ration from the modified model is determined with:

$$\zeta = \frac{1}{2\pi} \frac{\oint \tau_c d\gamma_c}{\frac{1}{4} \Delta\tau_c \Delta\gamma_c} \quad (2.8)$$

where $\oint \tau_c d\gamma_c$ is the area of the stress-strain loop, $\Delta\tau_c$ and $\Delta\gamma_c$ are the range in cyclic shear stress and strain. Figure 2.11 shows typical stress-strain responses for both stress and strain controlled tests. In a cyclic stress controlled test, the cyclic shear stress (τ_c) is typically applied with a sinusoidal waveform, and allows for the generation of cyclic shear strains (γ_c) (e.g. Figure 2.11a). Typical strain controlled cyclic tests apply cyclic shear strains with a sinusoidal waveform, and the cyclic shear stress response is measured (e.g. Figure 2.11b).

2.4 Figures

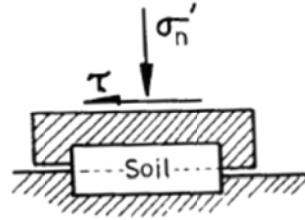


Figure 2.1: Typical setup and boundary stress conditions for a direct shear test (after Matthews 1988).



Figure 2.2: Simple shear device developed at (a) NGI (b) Cambridge (after Matthews 1988).

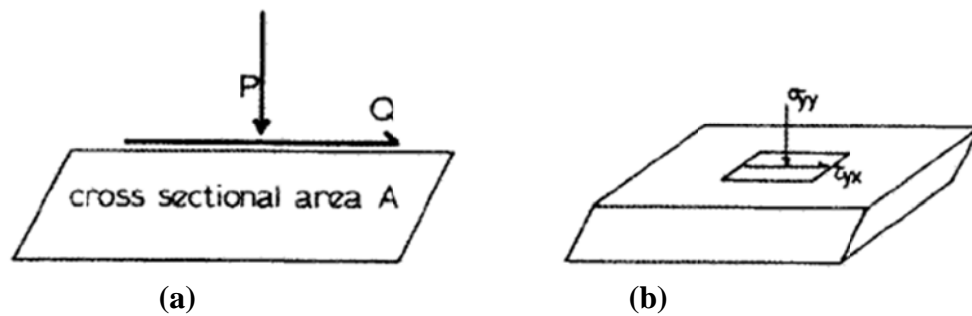


Figure 2.3:(a) Typical simple shear device showing applied forces (b) device showing actual stresses at the center of the specimen (after Airey et al. 1985).

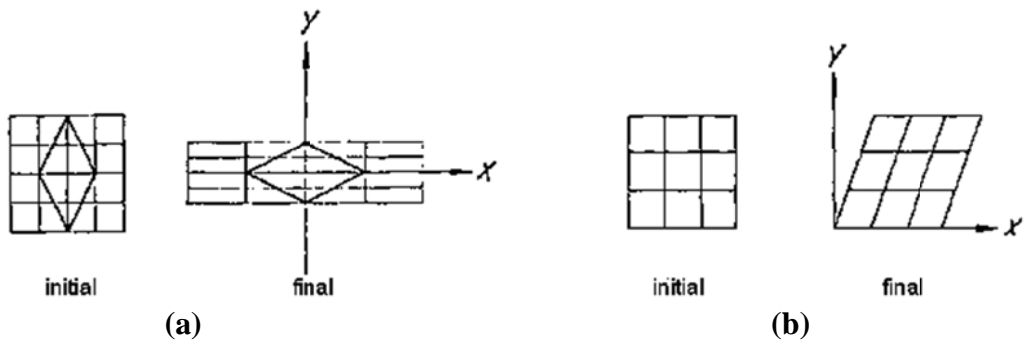


Figure 2.4: Plane strain conditions for (a) pure shear (b) simple shear (after Saada and Townsend 1981).

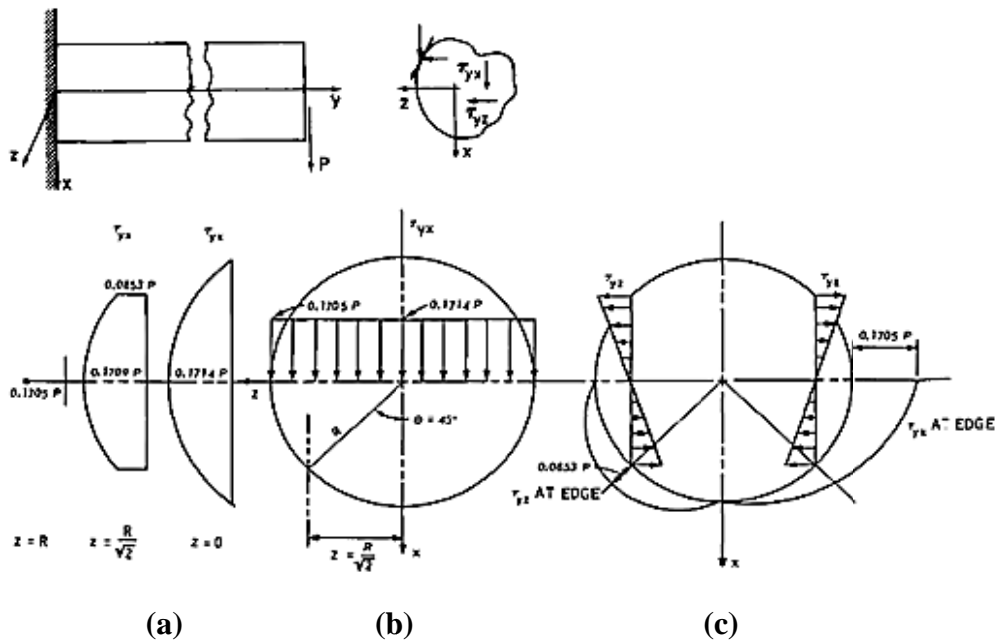


Figure 2.5: Boundary conditions and shear stress distribution of circular beam for the St. Venant solution (after Saada and Townsend 1981).

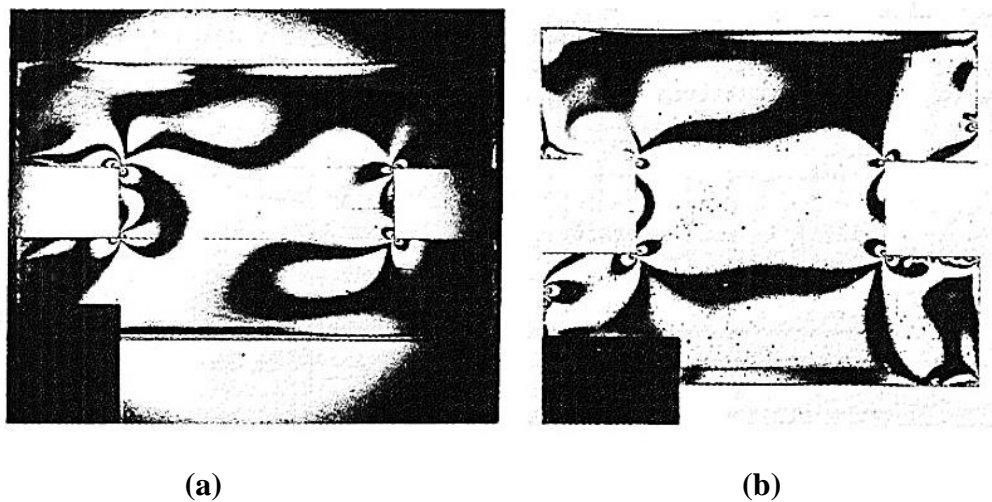


Figure 2.6: Images from simple shear photoelastic studies for (a) circular specimen and (b) square specimen (after Wright et al. 1978).

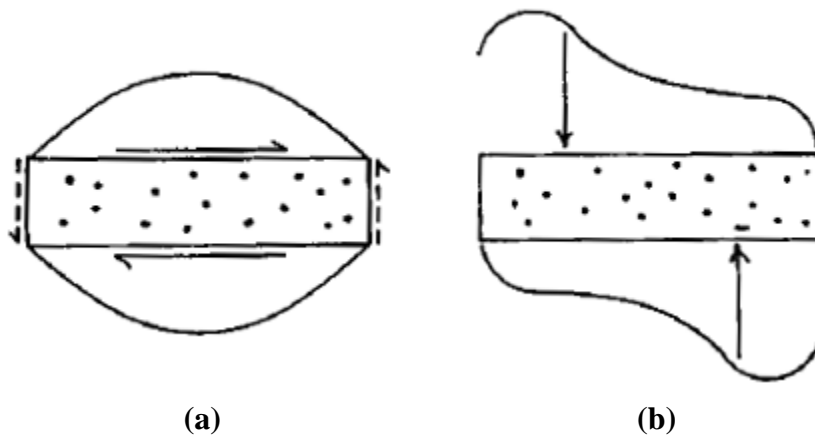


Figure 2.7: Stress distributions in typical simple shear devices (a) non-uniform shear stresses (b) non-uniform normal stresses (after Wood et al. 1979).

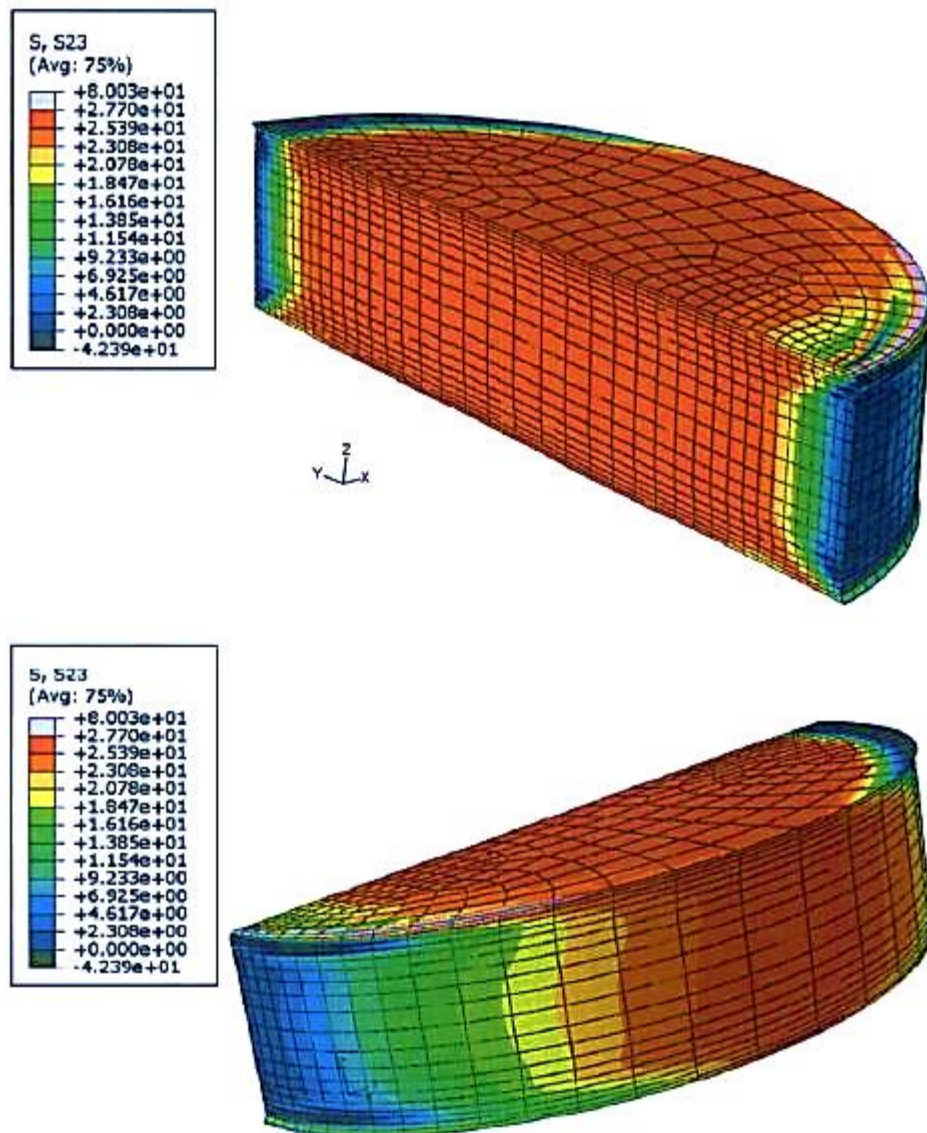


Figure 2.8: Shear stress field within a circular simple shear specimen at failure (after Doherty and Fayey 2011).

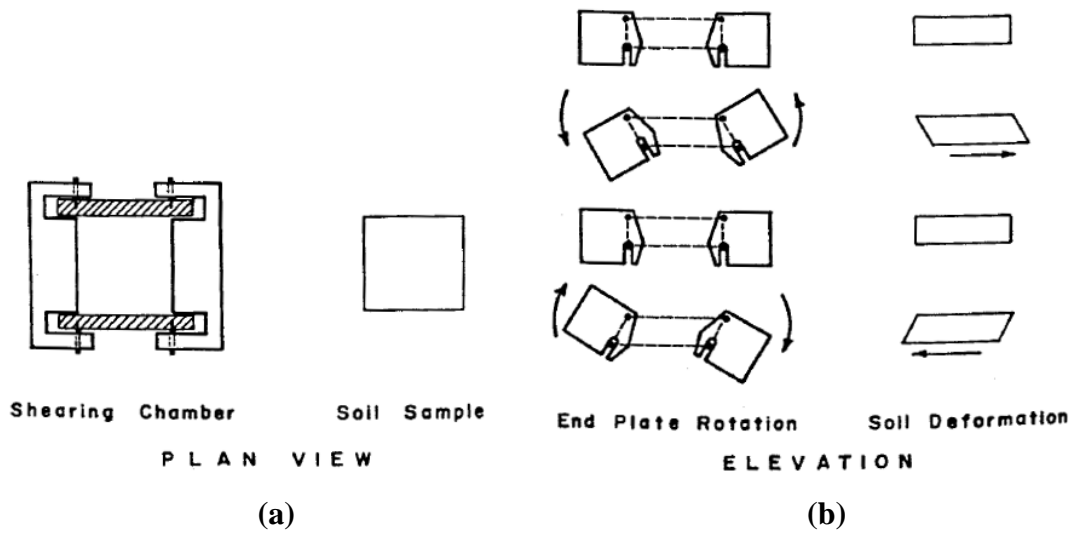


Figure 2.9: Schematic of a cyclic simple shear device and specimen (a) plan view (b) elevation view (after Peacock and Seed 1968).

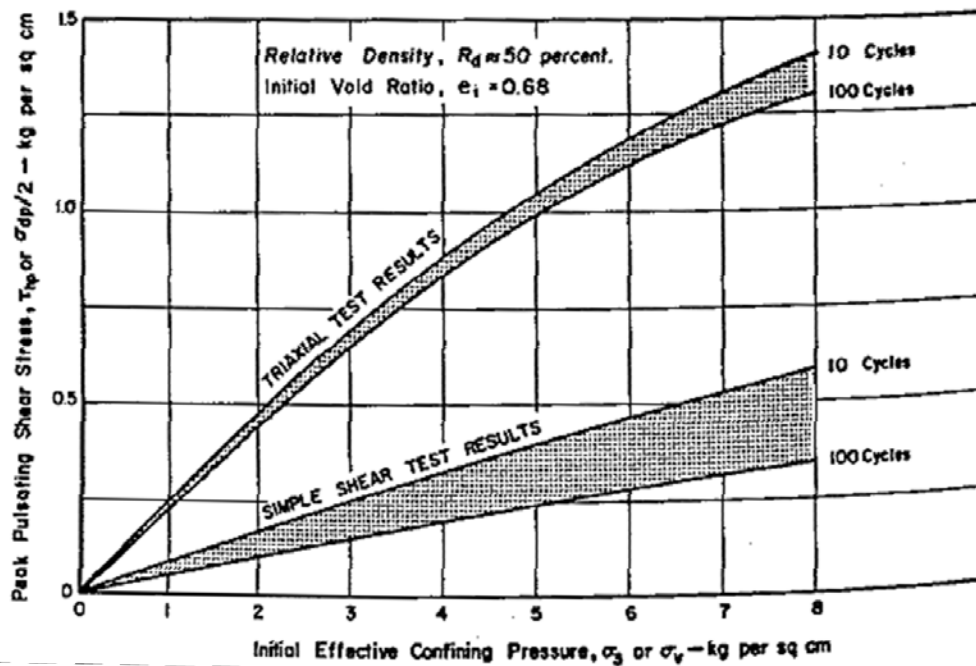


Figure 2.10: Comparison between the generated cyclic shear stress during cyclic triaxial and cyclic simple shear (after Peacock and Seed 1968).

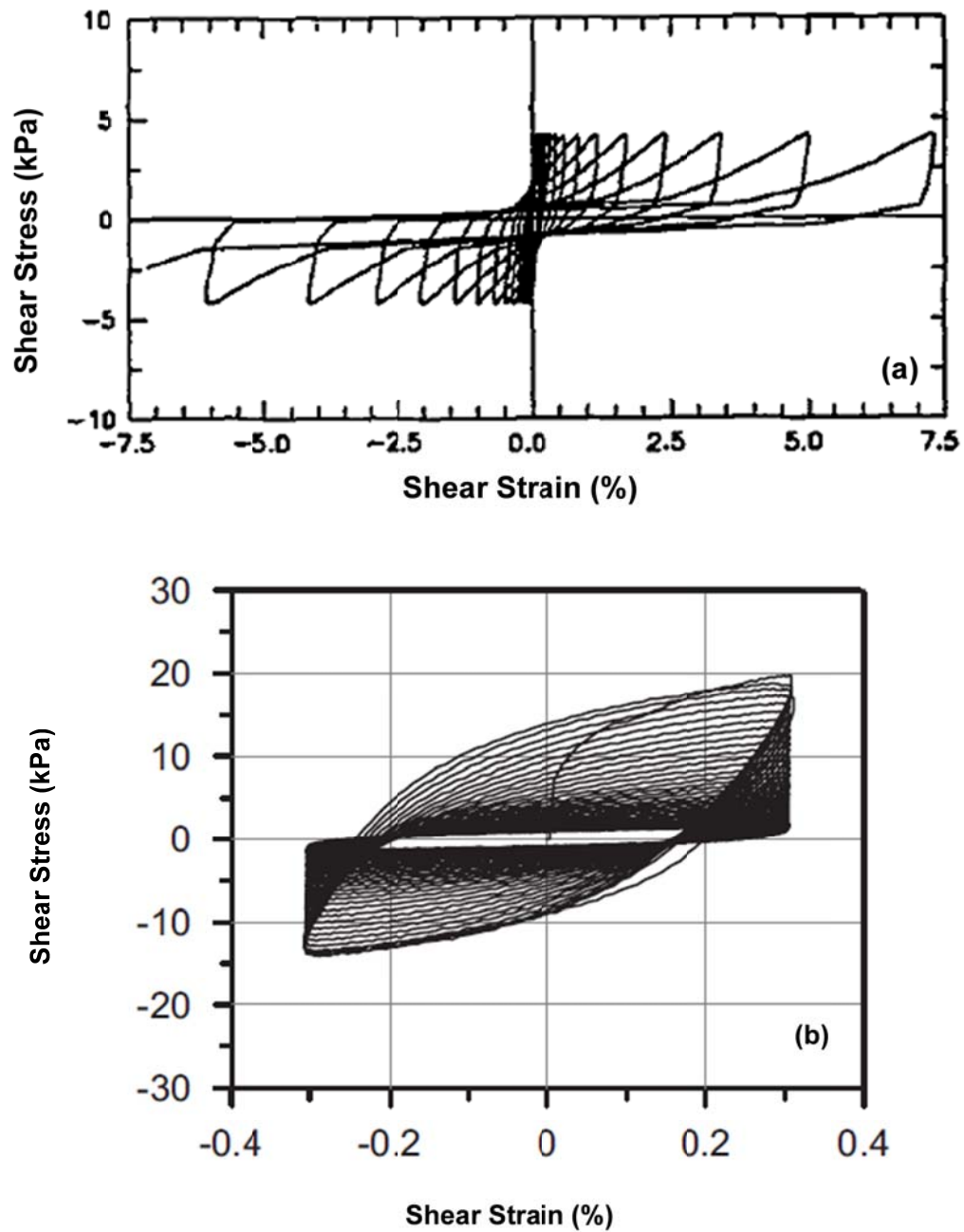


Figure 2.11: Cyclic simple shear stress-strain response for (a) stress control (after Boulanger et al. 1993) (b) strain control (after Hazirbaba and Rathje 2009).

Chapter 3: Characterization of Ecoroofs and Ecoroof Materials

Authors:

Travis J. Kraupa, H. Benjamin Mason, Ph.D., Armin W. Stuedlein, Ph.D., and
Christopher C. Higgins, Ph.D.

Proceedings for: Geo-Characterization and Modeling for Sustainability, GeoCongress
2014

Accepted for Publication: October 25th, 2013

3.1 Abstract

Ecoroofs are increasingly being used to provide sustainable thermal, hydrological, and aesthetic improvements to urban buildings. However, there is a lack of familiarity with the geotechnical engineering properties of ecoroof materials. To address this gap in knowledge, a comprehensive soil characterization program was performed with soil samples taken from ecoroofs in the Portland, Oregon metropolitan area. The selected ecoroofs differed primarily in terms of location, age, soil constitution, organic content, areal extent, drainage system, and plant material. A comprehensive geotechnical soil characterization program was performed on the samples. The results show that the soil characteristics and soil strength vary widely from roof-to-roof and with age of the roof. In addition, simple shear tests were performed on reconstituted specimens to provide a basis for static and dynamic parapet wall loading. These results strengthen the argument for developing unified design and construction guidance for ecoroofs in the United States.

3.2 Introduction

Ecoroofs provide both sustainable economic and environmental benefits to urban communities that include: controlling of the heat island effect, longevity to the life of rubber roof membranes, and opportunities for specialized consultants, landscape architects, and contractors (Liptan and Strecker 2003, Getter and Rowe 2006). Ecoroofs are used to store stormwater at the top of residential and commercial structures, because they can delay the storm flow contribution to municipal storm sewer networks, and ecoroofs are becoming a popular roofing option for residential and commercial developers in the United States (Getter and Rowe 2006). However, implementation of

ecoroofs has outpaced the geotechnical and structural engineering standards (e.g., building codes) in the United States, including those that dictate minimum structural loads. International guidelines for ecoroof design, construction, and maintenance exist, such as the German Society of Landscape Development and Landscape Design (FLL 2008); however, there is a need to develop guidelines and codes more relevant for engineering and construction practices in the United States. Engineering concerns that remain to be addressed include the appropriate calculation of the unsaturated and saturated dead weight of the ecoroof material, the static and dynamic (e.g., seismic) loading of parapet walls, and the uncertainty of these ecoroof-source loads on structural building elements.

To improve the understanding of the possible loads ecoroofs can provide, field samples from ecoroofs in Portland, Oregon, were collected and their geotechnical properties characterized. Ecoroof systems on commercial buildings were targeted for this investigation, because they have employed the largest systems in depth, extent and consequence. This paper describes a new sampling procedure appropriate for ecoroofs, geotechnical characterization properties, and simple shear strength test results. Fundamental geotechnical indices representative of the ecoroof samples were characterized, including their in-situ water content, moist and dry unit weight, void ratio, and other indicial parameters. The stress-strain strength characteristics of reconstituted samples were evaluated as part of a greater research program, aimed to provide a basis for the application of traditional design analyses to ecoroof materials.

3.3 Field Sampling

Initial efforts determined that the sampling of ecoroof materials was problematic. Suitable sampling procedures and equipment were therefore developed to minimize sample disturbance. The sampling equipment consisted of thin walled steel tubes, a plunger, and a stainless steel cutting spatula. Thin-walled sampling tubes are generally characterized using the area ratio, which is typically specified to be less than 10 percent (USACE 1972). Using this guidance, a custom sampler was constructed from cold drawn seamless steel with an outer diameter, $D_o = 107.9$ mm, and an inner diameter, $D_i = 103.1$ mm, which yielded an acceptable area ratio of 9.5%. To improve cutting of roots and other organic materials expected during sampling, a sharp, 5° bevel was machined at the leading edge of the sampler as shown in Figure 3.1a. Samplers were fabricated with lengths of 254 and 457 mm, because ecoroofs have variable soil thicknesses.

The plunger and stainless steel spatula were used to ensure that the sample remained stable while the tube was extracted from the ecoroof soil. The plunger was fabricated using a 51 mm tall circular wooden plug attached to a 12.7 mm thick steel rod that slides through the center of a two-tiered machined plastic cap (Figure 3.1b). The outside and inside diameters of the lower tier were 132 and 108 mm, respectively (Figure 3.1c). A 23 mm recessed edge allowed the cap to rest on top of the sampling tube. Four set screws secure the plunger and cap to the sampling tube, and provide lateral and vertical stability for the sample once tightened. The uppermost screw secures the rod to the smaller top-tier of the cap and prohibits the plug and rod from moving vertically. The remaining three screws were located on the outside of the lower tier and secured the cap to the sampling tube. Similarly, the stainless steel cutting spatula provided vertical stability for the sample

throughout the soil removal process. Spring-loaded storage boxes capable of carrying between 9 and 12 samples were used during the field-sampling program to minimize disturbance during transportation. The boxes were designed with sample templates that restricted horizontal translation of the samples but allowed the sample to move vertically. Sharp vertical inertial loads and subsequent displacement of the samples were limited by coil springs at the base and cushioning polyurethane foam attached to the lid of the box.

3.4 Field Sites

Samples were obtained from 18 different ecoroofs in Portland, Oregon, and are summarized in Table 3.1. Multiple samples were taken from each roof. Sampling locations were chosen based on proximity to roof drains and parapet walls. Two primary types of ecoroofs were encountered: (1) monolithic extensive and (2) intensive ecoroofs (shown in Figure 3.2). Additionally, ecoroofs with flexible wooden or rigid concrete tray systems were encountered. The pitch of the sampled ecoroofs was relatively flat, with the exception of small grade changes needed for drainage.

Monolithic-extensive ecoroof systems are the predominant ecoroof type for commercial applications in Portland, Oregon, based on the sampling conducted. Monolithic systems provide a uniform continuous bond between the waterproof membrane and roof of the building. The membrane is typically overlain with a root barrier, drainage mat, and ecoroof soil (FLL 2008, Getter and Rowe 2006). These overlying layers provide an extended working life for the waterproof membrane (Getter and Rowe 2006, Liptan and Strecker 2003). The depth of ecoroof soil sampled from extensive ecoroofs during this investigation ranged from 76 to 152 mm, which conformed

to the typical standard of practice in the United States (Friedrich 2008, Getter and Rowe 2006, Wark and Wark 2008). Encountered vegetation capable of thriving in relatively shallow soil depths consisted of sedums (flowering succulents), mosses, and short grasses. Additionally, these plants are typically chosen for extensive ecoroof purposes because of their resistance to extended dry periods and low amount of required routine maintenance (FLL 2008, Friedrich 2008, Getter and Rowe 2006). Observations made during the sampling program showed that irrigation of extensive ecoroofs depended on the age of the ecoroof (e.g., new ecoroofs require more irrigation to establish growing media), owner preference, and desired aesthetic purposes. Interior drains typically accompanied these systems and consisted of a boxed-in gravel filter encompassing a primary and overflow pipe. Although less common, exterior scupper drains were also observed. Both well-functioning and marginally-functioning drain pipe inlets were encountered. Marginally-functioning drains were restricted with vegetation and sediments. Restricted drain pipes may limit flow and may result in ponding of stormwater, causing differential and potentially unanticipated magnitudes of ponding load, which is a serious concern.

The second encountered ecoroof systems were intensive ecoroofs. Intensive ecoroofs are typically constructed with soil depths that are greater than extensive ecoroofs (Friedrich 2008, Wark and Wark 2008). Correspondingly, the variety of suitable vegetation, applied soil dead loads, and maintenance requirements are larger than extensive ecoroofs (Getter and Rowe 2006). Intensive ecoroofs appear as aesthetic rooftop gardens rather than an engineered vegetative layer associated with extensive ecoroofs. The typical intensive ecoroof vegetation encountered throughout this

investigation consisted of tall mature grasses, shrubs, small bushes, and trees. During the sampling program, the interface of the soil and drainage mat was never encountered for any of the intensive roofs. Therefore, the depth of the soil column was then determined by a depth probe or by knowledge of the depth at placement of the ecoroof soil. In order to sample more deeply from these ecoroofs, the longer 457 mm samplers were used. Irrigation and drainage characteristics were similar to those observed on the extensive ecoroofs and are displayed in Table 3.1.

A less encountered subset of ecoroof systems were the modular or tray systems. These systems were observed to house both intensive and ecoroof soils and plants. The design and functionality of these systems are typically proprietary and therefore varied based on developer and contractor preference for the sampled ecoroofs. Fundamentally, these systems are similar to monolithic ecoroofs, and provide similar economic, environmental, and aesthetic benefits. The exception is that, unlike monolithic systems, the ecoroof soil is contained within a “tray” unconnected from the roof (Wark and Wark 2003). Typical modular systems consisted of concrete and wooden planter boxes and stainless steel trays. The lateral extent of these systems was observed to cover most or all of the rooftop. The dead loads applied by the trays depended on the size, depth, and volume of rock comprising maintenance pathways. Similar drainage characteristics, as compared to the monolithic systems, were observed.

3.5 Soil Characterization

Currently, there is a paucity of geotechnical index property data for ecoroof soils. Therefore, a soil characterization study was conducted on the obtained ecoroof soil

samples and the following soil characteristics were experimentally determined: water content (w), wet and dry sieve analyses, sedimentation analysis, specific gravity (G_s), Atterberg limits, and organic content (O_c). Analytically determined soil properties included moist and dry unit weight (γ_m, γ_d), and the in-situ void ratio (e).

Sedimentation (hydrometer) analyses were generally conducted in accordance with ASTM D422-63 after the organic content was removed. However, Lu et al. (2000) showed that, when Stokes' Law is assumed valid, the hydrometer analyses should be performed on only the material passing the No. 200 sieve (0.075 mm), which is contrary to the ASTM D422-63 guidance. The Lu et al. (2000) guidance was followed in this study.

Pumice was present in all of the obtained samples. The vesicular nature of pumice particles allows them to float in water. Accordingly, determining the specific gravity in accordance with ASTM D854-10 was problematic. Visual inspection of the samples demonstrated that material retained on the No. 30 sieve was primarily pumice. Material passing the No. 30 sieve was assumed to be small enough such that no internal air voids were present. Therefore, vacuum extraction was used on material passing the No. 30 sieve. The pumice particles retained on the No. 30 sieve were pulverized and subsequently subjected to vacuum extraction. The samples' specific gravity of solids was then determined by using a weighted average by mass of both the material retained and passing the No. 30 sieve respectively.

Figure 3.3 shows the 29 measured grain size distributions for ecoroof soil after the organic material had been removed. It was found that the grain size distribution curves

varied as a function of organic content, ecoroof type, and drainage conditions. Three design gradations were developed from all the grain size distribution curves, and are shown as bold lines in Figure 3.3. The design gradations were used to reconstitute representative samples for strength testing.

Descriptive statistics for each of the soil parameters investigated are summarized in Table 3.2. In addition to the index properties previously described above, particle thresholds D_{10} and D_{50} , shape parameters C_u and C_c , and applied soil dead load (DL), are listed within Table 3.2. The unit soil dead load was estimated by multiplying the depth of the soil column by its moist unit weight at the time of sampling. The dispersion in measured parameters was characterized using the coefficient of variation (i.e. COV), which is defined as the ratio of standard deviation to the mean. The variability observed in the ecoroof materials was significantly higher than natural soils. For example, the typical COV in unit weight is 9 percent for natural soils (Jones et al. 2002); however, for the ecoroof soil, the observed COV in moist and dry unit weight was 21 and 24 percent, respectively. The high variation in moist unit weight is partially responsible for the COV in dead load, which is equal to 106 percent. Much of the variability in DL arises from the pooling of data from disparate ecoroofs. Nonetheless, the ecoroof materials sampled in a narrow geographic region range widely in composition, with COV s ranging from 82 to 119 percent for typical gradational indices, which justifies further engineering investigations.

3.6 Strength Tests

Simple shear tests were performed on six reconstituted ecoroof specimens. Gradations for the reconstituted specimens were targeted to fit one of the three distributions plotted in Figure 3.3 (i.e. fine, intermediate, and coarse). Specimens were placed in membranes lining a series of thin stacked rings, which provided lateral confinement during testing. The fine and intermediate reconstituted specimens were tested in rings with a 64 mm diameter. The coarse reconstituted specimens were tested in rings with a 100 mm diameter. The C_u and maximum and minimum void ratios (e_{min} , e_{max}) were determined for each of the three gradations shown (and are shown in Table 3.3), so specific relative densities (D_r) could be targeted. For initial testing, specimens were reconstituted to relative densities of 30% and 50%. Constant vertical stress (i.e. drained) tests were conducted, which allowed the specimens to contract or dilate throughout shearing. The vertical stress chosen for these initial tests was 30 kPa.

The stress-strain and volumetric strain response for six selected samples are shown in Figure 3.4. A similar stress-strain response was observed for the fine and intermediate gradations for both relative densities of 30 and 50% up to five percent shear strain, followed by a larger increase in shear stress for the 50% relative density specimens.

Conversely, the stress-strain response of the loose and medium dense coarse specimens (e.g. Figure 3.4c) exhibited markedly different responses throughout the range of strains imposed. The variation in response between the three distributions is hypothesized to originate from the amount of fines (i.e. passing No. 200) present within the reconstituted specimens.

Mobilized friction angles, ϕ_m , were determined at shear strains of 10% for the six sheared specimens. Wijewickreme et al. (2013) showed that for high shear strains, ϕ_m is best represented by the inverse tangent of the ratio of applied shear stress to vertical stress. This approach was therefore used to interpret the strength of the reconstituted ecoroof material specimens. Figure 3.5 shows the variation in ϕ_m versus the C_u and D_r of the reconstituted specimens. The observed trends indicate that higher ϕ_m are achieved with increases in both C_u and D_r of the specimens.

The volumetric strains shown in Figure 3.4(d-f) were assumed to be equal to the measured axial strain of the specimen. Specimens reconstituted from fine and medium gradations generally contracted throughout the range in shear strain imposed; however, the coarse gradation exhibited dilation after 6 to 7% shear strain as the coarser pumice material climbed up and over neighboring particles in response to shear. These results indicate that the amount of fines influenced the strength of the ecoroof materials.

3.7 Conclusion

Owing to their good performance in delaying contributions to storm flow, ecoroofs are becoming a popular alternative to other engineered hydrologic storm flow mitigation applications. However, little is known about the geotechnical properties of the materials soil that comprise the ecoroof itself. This paper presented a first step towards improving the understanding of ecoroof materials through a field investigation and inventory of a number of production ecoroofs samples. New sampling equipment and procedures used to obtain ecoroofs were described. Fundamental geotechnical characteristics of ecoroofs soil were determined and their variability presented. In general, these field observations

and laboratory investigations found a high degree of variability of the ecoroof soils used in the Portland, Oregon metropolitan area.

Initial observations, which will be expanded on in future work, indicate that the age of the ecoroof is a major source of variability, because the soils' hydrologic properties change as a function of time. Ultimately, this can lead to undesired water ponding and increases in dead loads. This implies that standardized codes for ecoroof design and construction in the United States should be developed and implemented. The stress-strain response of reconstituted ecoroof soil specimens, generated based on the observed variation in sampled soils, was determined to be directly dependent on the grain size distribution and relative density. Similar response was observed for the fine and intermediate specimens with a stiffer soil response occurring for the coarse specimens.

In addition to the reconstituted static simple shear specimens, a series of reconstituted undrained cyclic simple shear tests will be conducted on ecoroof soil in the near future. The cyclically-tested specimens will be fit to each of the three design gradations, and observations will be made about the dynamic strength properties and pore pressure generation of ecoroof soil. The results of the cyclic testing will allow the investigators to provide baseline dynamic characteristics for ecoroof soil, and eventually, will help with the development of ecoroof standards.

3.8 Acknowledgements

This material is based upon work supported by the National Science Foundation under Grant No. CMMI-1162616. Additionally, we gratefully acknowledge the help of John Lambrinos for his willingness to allow the investigators to sample ecoroof test plots

at Oregon State University, Tom Liptan for obtaining access to the sampled ecoroofs in Portland Oregon, and Zheng Li for his assistance throughout the field exploration.

3.9 References

- ASTM Standard D422, 1963 (2007). "Standard Test Method for Particle-Size Analysis of Soils." ASTM International, West Conshohocken, PA.
- ASTM Standard D854, (2010). "Standard Test Methods for Specific Gravity of Soil Solids by Water Pycnometer." ASTM International, West Conshohocken, PA.
- Forschungsgesellschaft Landschaftsentwicklung Landschaftsbau (FLL), (2008). "Guidelines for the Planning, Construction and Maintenance of Green Roofing – Green Roofing Guideline," Germany.
- Friedrich, C. (2008). "Selecting the Proper Components for a Green Roof Growing Media." *2nd National Low Impact Development Conference*, Wilmington, NC, 240-251.
- Getter, K. L., and Rowe, D. B. (2006). "The Role of Extensive Green Roofs in Sustainable Development." *HORTSCIENCE*, 41 (5), 1276-1285.
- Jones, A.L., Kramer, S.L., and Arduino, P. (2000). "Estimation of Uncertainty in Geotechnical Properties for Performance-Based Earthquake Engineering." *Pacific Earthquake Engineering Research Center, Report PEER 2002/16*, 114.
- Liptan, T., and Strecker, E. (2003). "EcoRoofs (Greenroofs)—a more sustainable infrastructure." *Proceedings National Conference on Urban Stormwater: Enhancing Programs at the Local Level*, Chicago, IL, 198-214.
- Lu, N., Ristow, G. H., and Likos, W. J. (2000). "The Accuracy of Hydrometer Analysis for Fine-Grained Clay Particles." *Geotechnical Testing Journal*, 23 (4), 487-495.
- U.S. Army Corps of Engineers (1972). "Soil Sampling." *Engineer Manual EM 1110-2-1907*, U.S. Government Printing Office, Washington, D.C.
- Wark, C. G., and Wark, W. W. (2003). "Green Roof Specifications and Standards." *The Construction Specifier*, 56(8), 1-12.
- Wijewickreme, D., Dabeet, A., and Byrne, P. (2013). "Some Observations on the State of Stress in the Direct Simple Shear Test Using 3D Discrete Element Analysis," *Geotechnical Testing Journal*, 36 (2), 1–8.

3.10 Tables

Table 3.1: Ecoroof Characteristics from Field Exploration.

Building	Ecoroof Type	Year Constructed	Irrigated	Area (m²)	Depth (cm)
B1	Monolithic/Extensive	2011	No	576	12.7
B2	Monolithic/Extensive	2006	Yes	279	7.6
B3	Monolithic/Extensive	1999	No	543	10.2
B4	Monolithic/Extensive	2000	No	139	10.2
B5	Monolithic/Extensive	2005	No	604	10.2
B6	Monolithic/Extensive	2007	Yes	1301	8.9
B7	Monolithic/Extensive	2007	Yes	674	7.6
B8	Monolithic/Extensive	2005	Yes	2165	9.5
B9	Monolithic/Extensive Tray/Intensive	2007	Yes	437	Ext.= 12.7 Int.= 26.6
B10	Monolithic/Intensive	2009	No	167	33.0
B11	Monolithic/Extensive	2010	Yes	2973	10.2
B12	Tray/Extensive	2010	No	557	7.6
B13	Monolithic/Extensive Tray/Intensive	2004	Yes	474	Ext.= 15.2 Int.= 45.7
B14	Monolithic/Extensive	2010	Yes	576	12.7
B15	Monolithic/Extensive	2004	No	1691	15.2
B16	Monolithic/Extensive	2003	Yes	1105	15.2
B17	Monolithic/Extensive	2011	No	1606	15.2
B18	Intensive	2011	Yes	1226	91 to 152

Table 3.2: Descriptive statistics for the ecoroof material characterization.

Soil Property	No. of Samples	Mean (μ)	COV (%)
w (%)	30	62	40
O_c (%)	29	12	56
D_{10} (mm)	29	0.021	82
D_{50} (mm)	29	1.64	79
C_u	29	150	94
C_c	29	14	119
G_s	29	2.10	13
e	29	1.30	39
γ_m (kN/m ³)	30	7.55	21
γ_d (kN/m ³)	30	4.76	24
DL (kPa)	30	1.27	106

Table 3.3: C_u and the Max and Minimum Void Ratios for the Reconstituted Gradations.

Gradation	C_u	e_{min}	e_{max}
Fine	19.6	1.37	2.20
Intermediate	59.8	1.41	2.03
Coarse	74.6	2.09	2.54

3.11 Figures

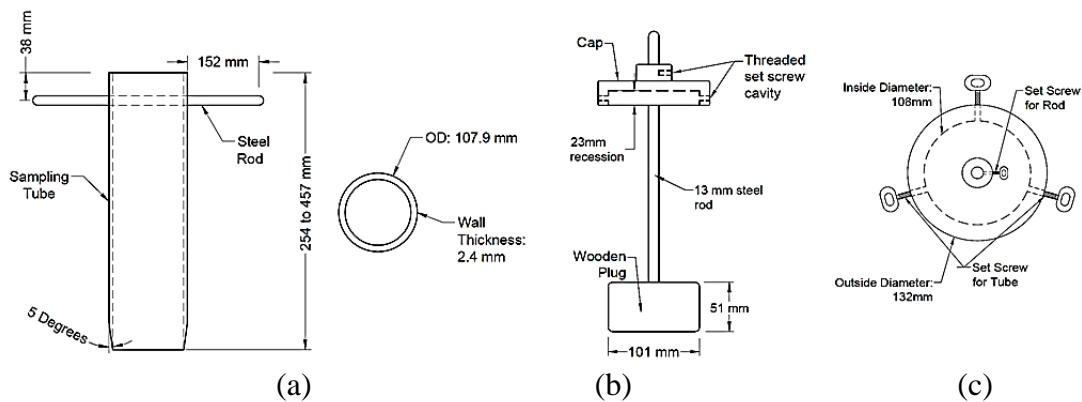


Figure 3.1: Sampling equipment (a) sampler side and profile view (b) assembled plunger (c) profile view of cap. Note- Figures are exaggerated for detail and are not to scale.



(a)



(b)

Figure 3.2: Ecoroof variation (a) intensive tray system (b) monolithic-extensive.

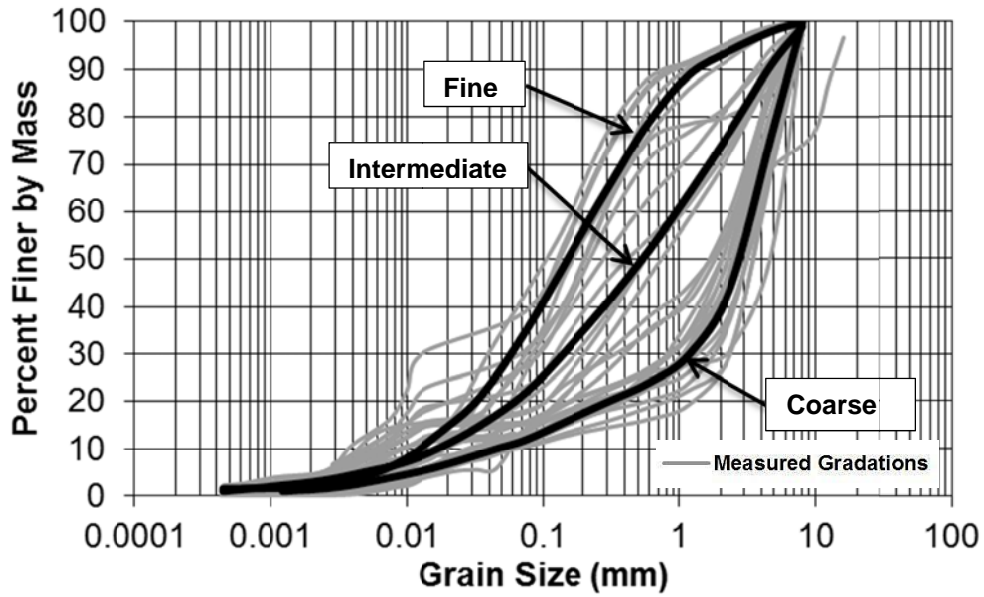


Figure 3.3: Measured and respective targeted grain size distributions.

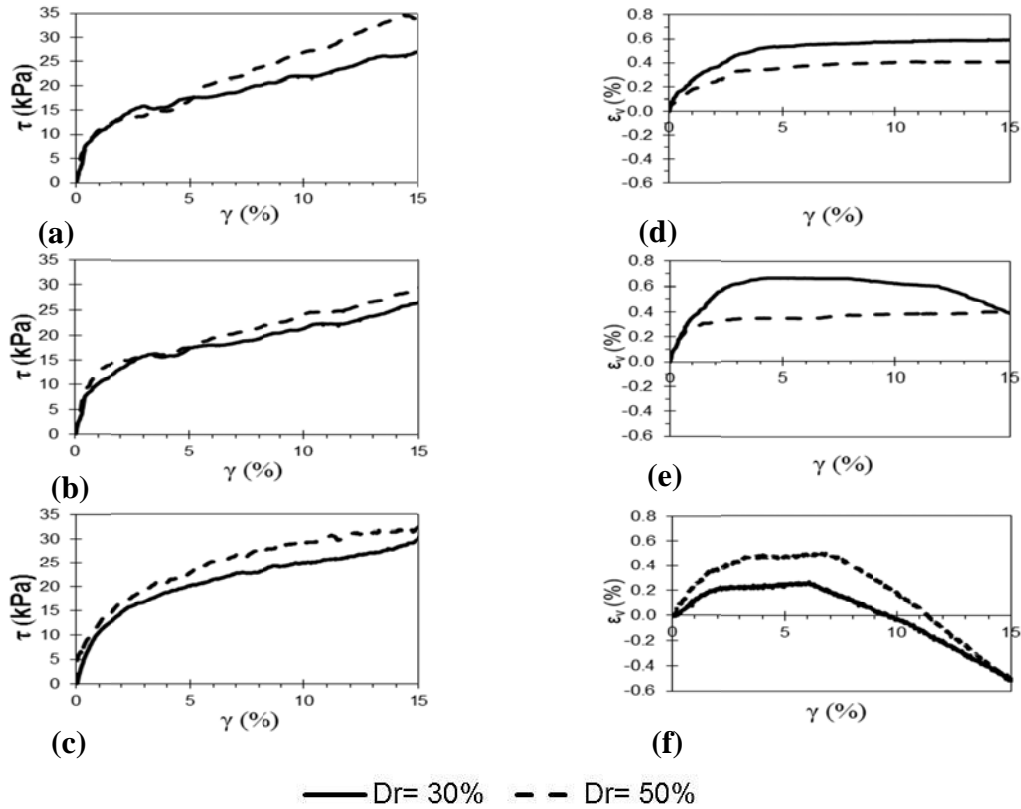


Figure 3.4: Stress-strain response for (a) the fine, (b) intermediate, and (c) coarse gradations; and volumetric strain response of (d) the fine, (e) intermediate, and (f) coarse gradations. Contraction is plotted as positive.

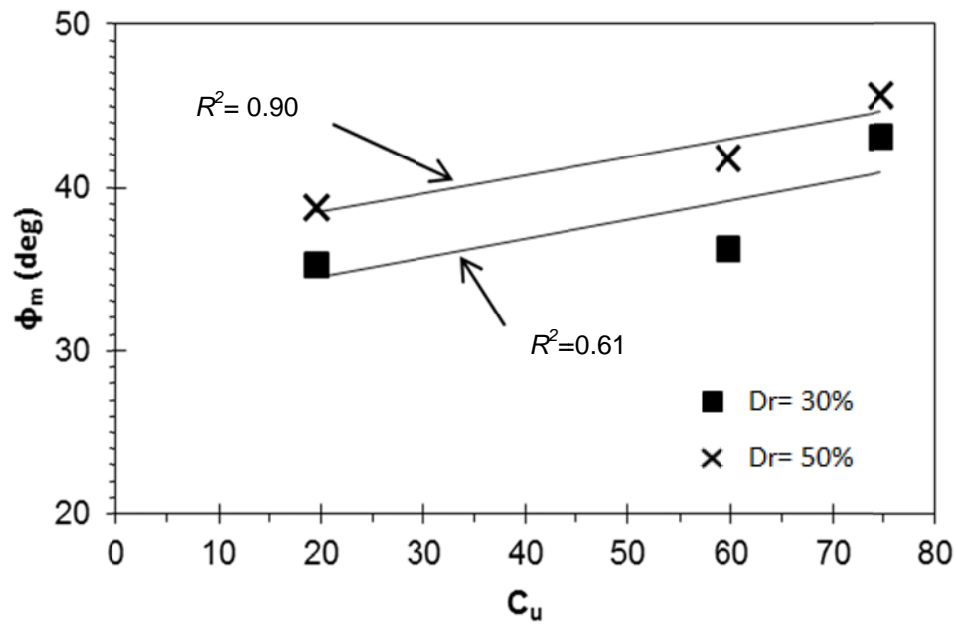


Figure 3.5: Variation of mobilized friction angle at 10 percent shear strain with the coefficient of uniformity, C_u .

Chapter 4: Geotechnical Characterization and Drained Shear Strength of Ecoroof Soil

Authors:

Travis J. Kraupa, Armin W. Stuedlein, Ph.D., H. Benjamin Mason, Ph.D., and
Christopher C. Higgins, Ph.D.

Journal:

Journal of Geotechnical and Geoenvironmental Engineering
1801 Alexander Bell Dr.
Reston, VA 20191

Submitted on October 9th, 2013

4.1 Abstract

Ecoroofs are becoming a more common sustainable roofing alternative, but currently, there are no ecoroof design codes or standards in the United States. A field exploration and laboratory characterization program was conducted to develop a geotechnical baseline for ecoroof soil. The laboratory investigation indicated that the ecoroof soil currently used in production was highly variable, with a wide range in index properties such as the effective and mean grain size, organic content, water content, and gradation shape parameters. A series of relatively low-stress static drained simple shear tests were conducted on both reconstituted and relatively undisturbed specimens. Simple shear tests were performed on specimens reconstituted from three target gradations. The volumetric response of the reconstituted ecoroof soil ranged from fully contractive, to somewhat dilative following the accumulation of large strains. In comparison, the relatively undisturbed specimens with organic material had a purely contractive response and developed significantly larger magnitudes of volumetric strain during simple shear testing. The mobilized friction angle of the ecoroof materials ranged from approximately 37 to 65 degrees, and varied as a function of normal stress, gradation, and relative density. The results show that the organic content has a significant effect on the stress-strain and volumetric responses of ecoroof soil in the field, which indicates that ecoroof design codes and standards are needed.

4.1.1 Subject Headings

Ecoroofs, simple shear, statistics, granular soil, soil properties, drained tests.

4.2 Introduction

Ecoroofs are becoming a popular structural roofing alternative in the United States. Ecoroofs detain rainwater, and subsequently, the rainwater is partially transpired into the atmosphere via the ecoroof vegetation (FLL 2008, Getter and Rowe 2006, Hutchinson et al. 2003, Liptan and Strecker 2003, Spolek 2008). The detention and transpiration of rainwater can result in a significant reduction in the peak storm flow to municipal sewers, which is the fundamental engineering benefit of ecoroofs. Accordingly, well-maintained ecoroofs are a sustainable and aesthetically pleasing roofing alternative. The interested reader is referred to Dunnet et al. (2008a), Hutchinson et al. (2003), MacMullan et al. (2008) and Stovin et al. (2007), for information regarding the aesthetic performance of ecoroofs.

Optimal ecoroof soils should reduce ponding loads on the roof while effectively retaining and transpiring rainwater. Accordingly, typical ecoroof soils are relatively lightweight, coarse-grained soils; however, some organic content is required to allow the support of healthy vegetation. Drought-resistant sedums are typical ecoroof vegetation, but larger vegetation, including decorative shrubs and trees, can be planted. Irrigation is usually required, especially when larger vegetation is planted. The ecoroof soils and their vegetation lie within monolithic arrangements or within discrete modular units, as described by Kraupa et al. (2014). Monolithic ecoroofs are the focus of this investigation.

Recent catastrophic failures of ecoroof systems (e.g., Weiler and Scholz-Barth 2009, Fountain 2011) have raised concerns about the absence of ecoroof design and

construction codes in the United States. Accordingly, it is critical to improve our understanding of the static and seismic response of ecoroof soils, as well as their hydrologic properties, to evaluate standard building codes and suggest revisions, if necessary. With this motivation, Kraupa et al. (2014) reported a first attempt to characterize the geotechnical index properties of typical ecoroof materials derived from a sampling program from 18 ecoroofs in Portland, Oregon. As part of the characterization, a laboratory program was undertaken to understand the fundamental soil properties and the results of an initial investigation of the static strength of ecoroof soils. Kraupa et al. (2014) focused particular attention on a sampling procedure developed specifically for ecoroof soil, the variability of the ecoroof soil types, and the geotechnical properties encountered during the testing program. In this paper, the results of a series of constant vertical stress simple shear tests, which were conducted on reconstituted and relatively undisturbed ecoroof specimens, are reported. The results further our understanding of the static constitutive response of ecoroof soils. The effect of ecoroof soil gradation on the static strength was evaluated using specimens reconstituted from three idealized gradations, which were selected based on the clustering of gradations observed in the field. The response of the ecoroof materials is characterized by a summary of the mobilized friction angle (ϕ_m) and peak dilation angle (ψ_p) at large shear strain (γ_{zx}), and the secant shear modulus (G_{sec}) at one percent shear strain. Existing ecoroof soils exhibit pore structures representative of production techniques and include organic matter, such as plant roots and compost. The effect of the in-situ pore structure and organic content on constitutive response was evaluated with simple shear tests on relatively undisturbed

samples. The results of this work should provide a baseline for designers interested in providing geotechnical recommendations for ecoroof designers.

4.3 Ecoroof Soil Characterization

4.3.1 Index Properties of Field Samples

Geotechnical laboratory tests performed to determine the fundamental soil properties for the sampled ecoroof soil included the water content testing (w), wet and dry sieving, sedimentation testing (i.e., hydrometer testing), specific gravity testing (G_s), Atterberg limits, and organic content determination (O_c). In addition, the moist (γ_m) and dry unit (γ_d) weights as well as the in-situ void ratios (e) were determined analytically. More details about the laboratory index tests are given in Kraupa et al. (2014).

A wide range of grain size distributions was observed for the sampled ecoroof soils, as shown in Figure 4.1. From the observed gradations, three “target” gradations were assessed for the purposes of strength characterization of reconstituted samples: a fine, intermediate, and coarse gradation (indicated using heavy lineweight in Figure 4.1). The ecoroof soil used to reconstitute test specimens was derived from Philips Soil Products, and the relevant properties for this soil are given in Table 4.1. The organic content of the ecoroof soil used for reconstitution was minimal, because the soil was never used in the field.

The three target gradations were selected to understand the static strength response of the ecoroof soil across the range of observed grain size distributions. The coefficient of uniformity, C_u , of the reconstituted specimens (Table 4.2) was determined and used as a reference parameter, which allowed the quantification of the response of ecoroof soil

based on specimen gradation. Relative densities (D_r) of 30 and 50 percent were targeted, because these relative densities bound the conditions encountered throughout the field investigation. The maximum and minimum void ratios (e_{max} and e_{min}) for the three design gradations are listed in Table 4.2 and range from 2.54 to 1.37, respectively. Common ecoroof soils contain a relatively high quantity of pumice; accordingly, void ratios, and therefore dry unit weights, are higher and lower, respectively, than typical soils with similar gradations.

4.3.2 Variability of Index Properties

Sample statistics of soil index properties were determined for the ecoroof soil sampled in the field investigation. The mean (μ) and coefficient of variation (COV) for each ecoroof soil property are reported in Table 4.3. The coefficient of variation, defined as the ratio of the sample standard deviation over the sample mean, was used as a convenient dimensionless quantification of dispersion. As shown in Table 4.3, significant dispersion (i.e. large COV s) was encountered for all of the soil parameters and samples investigated. For example, the gradational indices (i.e. D_{10} , D_{50} , C_c , and C_u) had measured COV s nearly equal to or greater than 100 percent.

Histograms and fitted probability distribution functions (PDFs) for D_{10} , D_{50} , C_u and O_c are plotted in Figure 4.2 to assist in the visual interpretation of the test data. Figure 4.2 indicates that D_{10} , C_u and O_c of the in-situ samples were approximately lognormally distributed. The range in D_{50} encountered was large (i.e., from 0.10 to 4.55 mm) and was not well described by the fitted distributions. The soils sampled were well-graded, as indicated by the coefficient of uniformity (Figure 4.2c), and the D_{10} for most of the

specimens was near the No. 200 sieve (0.074 mm), which indicates that the hydraulic conductivity of ecoroof materials, though not evaluated herein, would have likely been on the lower end of typical values for sandy soils. The lower hydraulic conductivity is contrary to the ecoroof design goal of providing rapid drainage to roof drains; however, it meets the design goals of delaying stormwater discharge and providing water to the ecoroof vegetation. Figure 4.2d indicates that the organic content of the ecoroof samples was predominantly between 5 and 12 percent. The effect of the variable ecoroof soil index properties on the static shear strength of ecoroof material is explored in the remainder of the paper.

4.4 Simple Shear Response of Ecoroof Soils

4.4.1 Background

The first documented simple shear testing device was developed by Kjellman (1951) to determine the shear strength of clays, which had been difficult to achieve using the conventional direct shear test. Since this initial effort, Wood et al. (1979), Airey et al. (1985), Shibuya and Hight (1987), Atkinson and Lau (1991), among others, have studied the stress states that develop within a specimen during simple shear. Findings from these efforts have consistently highlighted the difficulties associated with determining the true state of stress within the specimen, and maintaining zero lateral expansion (i.e. plain strain conditions) throughout the test. Without significant instrumentation along the boundaries of the specimen, the principal stresses and corresponding shear stresses within the specimen cannot be readily determined (Airey et al. 1985). Accordingly, a state of pure simple shear cannot be achieved during simple shear testing, and simplifying

assumptions must be made about the stress state within the specimen and failure plane to determine strength parameters.

Two common approaches for estimating the mobilized friction angle (ϕ_m) can be used in consideration of the assumed horizontal failure plane (Airey et al. 1985). By considering the plane of maximum shear stress to coincide with a horizontal plane, ϕ_m can be computed as:

$$\phi_m = \sin^{-1} \left(\frac{\tau}{\sigma_{zz}} \right) \quad (4.1)$$

where τ is the shear stress acting on the horizontal plane, and σ_{zz} is the normal stress acting on the horizontal plane. Conversely, if failure is assumed to occur where the plane of maximum stress obliquity coincides with the horizontal plane, then ϕ_m can be calculated as:

$$\phi_m = \tan^{-1} \left(\frac{\tau}{\sigma_{zz}} \right) \quad (4.2)$$

Discrete element model (DEM) simulations of drained simple shear tests reported by Wijewickreme et al. (2013) showed that Equation 4.1 is valid for shear strains (γ_{zx}) of approximately 2 to 5 percent, whereas Equation 4.2 is valid for larger shear strains. Therefore, ϕ_m was computed for $\gamma_{zx} = 15$ percent using Eq. 2.

In this study, γ_{zx} was determined using the ratio of horizontal displacement (Δx) to the initial specimen height (H_o). The vertical strain (ε_z) was determined using the ratio of vertical displacement (Δh) to H_o and assuming that the specimen did not extend laterally

during testing (Figure 4.3a). Rossato and Simonini (1991) showed that if a plane strain condition is assumed, then ε_z and γ_{zx} can be used to determine the major principal strain:

$$\varepsilon_1 = \frac{1}{2} \left(\varepsilon_z + \sqrt{\varepsilon_z^2 + \gamma_{zx}^2} \right) \quad (4.3)$$

and minor principal strain:

$$\varepsilon_3 = \frac{1}{2} \left(\varepsilon_z - \sqrt{\varepsilon_z^2 + \gamma_{zx}^2} \right) \quad (4.4)$$

during simple shear testing in consideration of the Mohr circle of strain. The Mohr circle of strain (Figure 4.3b) was also used to determine the peak dilation angle (ψ_p) for drained simple shear tests following the methodologies of Atkinson and Lau (1991) and Rossato and Simonini (1991). Additionally, ψ_p can be analytically determined by

$$\psi_p = \sin^{-1} \left[\frac{\Delta\varepsilon_1 + \Delta\varepsilon_3}{\Delta\varepsilon_1 - \Delta\varepsilon_3} \right] \quad (4.5)$$

with an assumed plane strain condition (Houlsby 1991) and where compressive strains are positive. Therefore, ψ_p is positive for a dilating specimen in Eq. 4.5.

4.4.2 Experimental Setup

Simple shear testing was performed using two simple shear devices: a GEOCOMP ShearTrac II-DSS for 64 mm diameter specimens and a GCTS SSH-100 for 102 mm diameter specimens. The two devices are herein referred to as the small and large simple shear devices, respectively. Both devices have external vertical and horizontal LVDTs and load cells, but they do not have circumferential load cells on the boundary of the

specimen. Therefore, the applied normal stress (σ_{zz}) on the horizontal plane was determined by the ratio of applied normal force along the z-axis (F_z) by the area of the specimen (A_s), and the shear stress (τ) on the horizontal plane was determined by dividing the applied horizontal force along the x-axis (F_x) by A_s , as shown in Figure 3a.

Simple shear tests were performed under drained conditions. Drainage was accomplished using porous stones located on the top and bottom of the specimen. The ecoroof soils sampled in the field investigation had thicknesses ranging from 70 to 1520 mm (Kraupa et al. 2014), and correspondingly small magnitudes of in-service vertical stresses. Accordingly, $\sigma_{zz} = 10, 20$ and 30 kPa were selected for the test program, and these vertical stresses were maintained throughout shearing. All specimens were sheared under normally consolidated conditions. The reconstituted specimens were prepared, saturated, and sheared within an unreinforced rubber membrane enclosed by a stack of twenty-nine 0.85 mm thick coated steel rings and a stack of twelve 2.75 mm thick brass rings for the small and large devices, respectively. The rigid stack of rings ensured that the specimens were laterally confined and thus, maintained a constant diameter throughout shearing. The specimens reconstituted to match the fine and intermediate gradations were sheared in the small device, and the specimens reconstituted to match the coarse gradation were sheared in the large device, which accommodated the larger maximum particle sizes. Specimens were sheared using strain control at a strain rate of 0.5 percent per minute, which prohibited the generation of excess pore pressure throughout shearing. All tests were terminated when the shear strain reached 15 percent.

4.4.3 Shear Response of Reconstituted Specimens

Eighteen simple shear tests were performed on specimens reconstituted using the three target gradations (fine, intermediate and coarse), at three different vertical stress levels (10, 20 and 30 kPa), and at two different relative densities (30 and 50 percent). The stress-strain and volumetric response of six specimens reconstituted using the fine target gradations are shown in Figure 4.4. The shear response for all specimens, initially stiff and associated with contraction, transitioned to a less stiff strain hardening response following yielding, which occurred at about 0.5 to 1 percent shear strain. The strain hardening response largely occurred during constant volume shear, as indicated in Figures 4.4b and 4.4d. However, specimens sheared at $\sigma_{zz} = 10$ kPa exhibited dilation at shear strains of approximately 11 and 6 percent for $D_r = 30$ and 50 percent, respectively, following significant constant volume shear. The secant shear modulus (G_{sec}) at one percent shear strain is tabulated in Table 4.4. The observed secant shear moduli increased with relative density and vertical stress, which is consistent with the typical mechanical response of soils.

The simple shear test results of the specimens reconstituted at the target intermediate gradation are shown in Figure 4.5. Similar to specimens reconstituted to the target fine gradation, the initial shear and volumetric response was initially stiff and contractive up to a shear strain of approximately 0.5 to 1 percent. Thereafter, constant volume shearing occurred to various levels of shear strain prior to transitioning to the tertiary response (e.g. Figure 4.4b and 4.4d). For example, the specimens with $D_r = 30$ percent transitioned to a dilative response at shear strains of approximately 4, 11, and 12 percent

at $\sigma_{zz} = 10, 20,$ and 30 kPa, respectively. The specimens with $D_r = 50$ percent exhibited a dilative response at shear strains of approximately 6 and 12 percent at $\sigma_{zz} = 10$ and 20 kPa, respectively. The volumetric response remained contractive throughout shearing for the specimen sheared at $\sigma_{zz} = 30$ kPa.

The stress-strain and volumetric response of the coarse gradation specimens are shown in Figure 4.6. The response is similar to the response of the target intermediate gradation specimens. Specifically, all of the specimens yielded and contracted at shear strains of 0.5 to 1 percent. Constant volume shearing was observed for increasing shear strains and again transitioned to a tertiary dilative response. For the specimens with $D_r = 30$ percent, dilation initiated at shear strains of approximately 7, 4, and 6 percent at $\sigma_{zz} = 10, 20,$ and 30 kPa, respectively. The specimens with $D_r = 50$ percent showed a similar volumetric response, with dilation initiating at shear strains of approximately 5, 6, and 7 percent at $\sigma_{zz} = 10, 20,$ and 30 kPa, respectively. In comparison to the specimens reconstituted using fine and intermediate gradations, the observed dilative response for the coarse gradation specimens occurred at lower shear strains, which is expected, because the coarse target gradation is more well-graded (i.e., high C_u) than the other two target gradations.

As observed in Figures 4.4 through 4.6, the specimens typically yielded at a γ_{zx} of about one percent, which marks the transition to a softer constitutive response. To compare the stiffness and strength of the reconstituted specimens as a function of gradation, the secant shear modulus, G_{sec} , and mobilized friction angles, ϕ_m , were plotted as a function of σ_{zz} and C_u for shear strains of one and 15 percent, respectively (e.g.

Figure 4.7). Figure 4.7 shows that G_{sec} increased with σ_{zz} and D_r , although G_{sec} was more sensitive to changes in vertical stress than changes in relative density. Additionally, the sensitivity of G_{sec} to gradation type was minimal, which is likely a function of the relatively high strain level. The variation in the stiffness of ecoroof materials at very small strains would likely be more sensitive to gradation than shown herein, but further small-strain soil testing is needed to confirm this hypothesis. The mobilized friction angle was sensitive to both vertical stress and gradation (linear increases in ϕ_m with both σ_{zz} and C_u are observed in Figure 4.7). In contrast, ϕ_m was not sensitive to the relative density. However, the effect of relative density is likely muted, because of the small range of D_r investigated. Nonetheless, ϕ_m had a maximum value of 65 degrees and differed by more than 20 degrees over the small range in the variables investigated. In summary, Figure 4.7 demonstrates the importance of characterizing the governing variables when estimating the strength of ecoroof materials.

Table 4.5 summarizes the observed peak dilation angles (ψ_p) for the reconstituted specimens. The dilation angle generally reduced with increasing vertical stress, in accordance with well-known soil mechanics principles. However, considerable variability was observed when comparing ψ_p with relative density. The highly angular pumice was characterized with numerous weak asperities, and the variability in the frequency of local asperities likely contributed to the variable volumetric response of the ecoroof material.

4.4.4 Shear Response of Relatively Undisturbed Specimens

An investigation into the shearing response of relatively undisturbed specimens was undertaken to determine the in-situ constitutive response of the ecoroof material and to

determine the effect of organic content on the static strength. Observations made during the field exploration indicated that the organic root structure did not penetrate the full depth of ecoroof. Therefore, the tensile strength of the root system would be limited the near surface soil column. The relatively undisturbed samples were retrieved from the ecoroofs using specially made sampling equipment (Kraupa et al. 2014). A limited number of relatively undisturbed field samples were available; therefore, three test specimens were selected for static strength evaluation based on their gradational characteristics. The three test specimens were carefully extracted from the sampling tubes following precision metal cutting along the longitudinal axis of the tube using a very slow, automated machining saw to minimize vibration and other disturbance of the sample. This technique minimized compression of the sample during extraction. Figure 4.8 presents the gradations of the relatively undisturbed tube specimens in comparison to the representative target gradations for materials larger than the No. 200 sieve. Figure 4.8 shows that the tube specimens were relatively similar in gradational characteristics to the representative target gradations of the reconstituted specimens. Although each tube specimen was sampled from a different roof, the organic content was remarkably similar across samples, equal to 7.7, 7.8, and 7.7 percent, for the fine, intermediate and coarse tube specimens, respectively.

Determination of the relative density for the tube specimens proved difficult due to the high amounts of fine-grained particles and organic matter. Therefore, the dry unit weight, γ_d , of the tube specimens was used to make comparisons to the specimens reconstituted using the targeted gradations. The dry unit weights measured for the tube specimens were 7.9, 6.4, and 4.9 kN/m³ for the fine, intermediate, and coarse gradations

respectively. Thus, these tube specimens were can be inferred to be relatively loose in their in-situ state as compared to the range in $\gamma_{d,min}$ and $\gamma_{d,max}$ reported in Table 4.2.

The stress-strain and volumetric response for the tube specimens is presented in Figures 4.9a and 4.9b, respectively. The stress-strain response shows that the stiffness of the tube specimens is much larger than the stiffness of the reconstituted specimens; additionally, the yield shear strain was smaller for the tube specimens than for the reconstituted specimens. The tube specimens contracted continuously throughout shearing, and reached magnitudes of ε_z that were significantly larger than the magnitudes of ε_z reached during simple shear testing of the reconstituted specimens (e.g., Figures 4.4 through 4.6). The larger ε_z observed for the tube specimens indicates the relatively loose state of the tube specimens and the compressibility of the organic material. Figure 4.10 shows the transition of ϕ_m for the tube specimens throughout shearing. As seen in Figure 4.10, ϕ_m at 15 percent shear strain is 50, 42, and 38 degrees for the intermediate gradation specimen at $\sigma_{zz}= 10$ kPa, coarse gradation specimen at $\sigma_{zz}= 20$ kPa, and fine gradation specimen at $\sigma_{zz}= 30$ kPa, respectively. Although less than 8 percent by mass, the organic content of these tube specimens produced a noticeable reduction in the mobilized friction angle, when compared to the reconstituted specimens.

4.4.5 Discussion

The reconstituted specimens allowed the quantification of the static strength properties in a controlled environment. In general, the reconstituted specimens did not reach a critical state in terms of shear strength and continued to harden at termination of the tests. In contrast, the rate of hardening, if any, was markedly reduced for the tube

specimens. The variation in the stress-strain response for the three tube specimens are compared to similar reconstituted specimens (i.e. gradation, σ_{zz}) in Figure 4.11. The intermediate ($\sigma_{zz}= 10$ kPa) and coarse ($\sigma_{zz}= 20$ kPa) reconstituted specimens had significantly more shear strength mobilized throughout shearing compared to the corresponding tube specimens. Contrastingly, the fine-grained ($\sigma_{zz}= 30$ kPa) reconstituted specimens exhibited relatively similar stress-strain responses as that of the fine-grained tube specimen throughout shearing. The response shown in Figure 4.11 could indicate that the amount of organic content present has a greater effect on the static shear strength of more well-graded ecoroof soils, but additional studies are required to confirm this hypothesis.

Similarly, the volumetric response of the reconstituted specimens varied significantly from the tube specimens. Relatively significant contractive response was observed for the tube specimens, whereas dilative response was observed for the reconstituted specimens. The dilative tendencies of the reconstituted specimens depended to various extents on the D_r , C_u , and magnitude of σ_{zz} . It appears that the amount of organic matter present within the specimen contributes significantly to the volumetric response of the ecoroof materials.

4.5 Conclusions

The emerging use of ecoroofs as a sustainable roof alternative has raised concerns regarding the lack of geotechnical information for ecoroof soil as well as the lack of formal building codes and standards. This study attempts to provide a geotechnical baseline for designers considering various ecoroof soils, so they can make informed

selections of design loads. Sample statistics, determined from a large field exploration program, indicated that the soil properties used in production roofs are highly variable. Specifically, critical geotechnical index properties, such as the effective and mean grain size, the coefficient of uniformity, and the organic content, exhibited relative dispersions of up to 100 percent. Therefore, the ecoroof soil mix design (i.e., gradation) and ecoroof vegetation vary widely between ecoroof soil manufacturers, landscape architects, and contractors. A first step towards standardization and generation of building codes is to evaluate the effect of the geotechnical index properties on the mechanical response of ecoroof soil.

Drained simple shear tests on reconstituted and relatively undisturbed, tube specimens were conducted to evaluate the static strength of ecoroof soil. The results of the simple shear tests on reconstituted specimens lead to the following four observations.

1. A transition in the stiffness of the ecoroof soil occurred at a shear strain of about one percent.
2. The amount of contraction and dilation depended on the gradation of the specimen.
3. The mobilized friction angle increased with an increase in the coefficient of uniformity, but was relatively similar for specimens sharing the same normal stress and relative density.
4. No critical state or peak shear strength was observed. The observed trends in the constitutive response indicate that strength mobilization and volumetric response

of the reconstituted ecoroof soil specimens is most dependent on the gradation (i.e. C_u).

The stress-strain and volumetric response of the tube specimens retrieved from the field differed from the corresponding responses of the reconstituted specimens. The shear strength mobilized at large strains for the tube specimens was less than that of the reconstituted specimens and appeared to approach a critical state at the end of shearing, and these specimens exhibited only contractive responses. Both of these observations indicate that the static strength response of the in-situ ecoroof soil depends on the organic content of the soil. Thus, the determination of the organic content, as well as the potential for the increase in organic content with the age of the roof, is critical for assessing the loads possible for existing and future ecoroofs. Additional studies on the effect of organic content on the constitutive response of ecoroof soils are required to support the development of ecoroof design and construction standards.

4.6 Acknowledgments

This material is based upon work supported by the National Science Foundation under Grant No. CMMI-1162616. We gratefully acknowledge the help of John Lambrinos for his willingness to allow the investigators to sample ecoroof test plots at Oregon State University, Tom Liptan for obtaining access to the sampled ecoroofs in Portland Oregon, Zheng Li for assistance throughout the field exploration, and Mary Ann Triska for assistance at the beginning of the project.

4.7 References

- Airey, D. W., Budhu, M., and Wood, D. M. (1985). "Some Aspects of the Behavior of Soils in Simple Shear." *Developments of Soil Mechanics and Foundation Engineering*, Vol. 2, 185-213.
- Atkinson, J. H., and Lau, W. H. W. (1991). "Measurement of soil strength in simple shear tests." *Canadian Geotechnical Journal*, Vol. 28, 255-262.
- Bjerrum, L., and Landva, A. (1966). "Direct Simple-Shear Tests on A Norwegian Quick Clay." *Geotechnique*, 16 (1), 1-20.
- Dunnett, N., Nagase, A., and Hallam, A. (2008a). "The dynamics of planted and colonizing species on a green roof over six growing seasons 2001–2006: influence of substrate depth" *Urban Ecosyst*, Vol. 11, 373–384.
- Forschungsgesellschaft Landschaftsentwicklung Landschaftsbau (FLL), (2008). "Guidelines for the Planning, Construction and Maintenance of Green Roofing – Green Roofing Guideline," Germany.
- Fountain, H. (2011). "Green Roof Collapses in Illinois." *The New York Times*. <http://green.blogs.nytimes.com/2011/02/18/greenroocollapsesin-illinois/>
- Getter, K. L., and Rowe, D. B. (2006). "The Role of Extensive Green Roofs in Sustainable Development." *HORTSCIENCE*, 41 (5), 1276-1285.
- Houlsby, G. T. (1991). "How the Dilatancy of Soils Affects Their Behavior." *Written version from invited lecture at: Tenth European Conference on Soil Mechanics and Foundation Engineering*, Florence, Italy, 1-15.
- Hutchinson, D., Abrams, P., Retzlaff, R., and Liptan, T. (2003). "STORMWATER MONITORING TWO ECOROOFES IN PORTLAND, OREGON, USA" *Greening Rooftops for Sustainable Communities*, Chicago, IL.
- Liptan, T., and Strecker, E. (2003) "EcoRoofs (Greenroofs)—a more sustainable infrastructure." *Proceedings National Conference on Urban Stormwater: Enhancing Programs at the Local Level*, Chicago, IL, 198-214.
- Kjellman, W. (1951). "Testing the Shear Strength of Clay in Sweden" *Geotechnique*, 2 (3), 225-232.
- Kraupa, T. J., Mason, H. B., Stuedlein, A. W., and Higgins, C. C. (2014). "Characterization of Ecoroofs and Ecoroof Materials," *Geo-Characterization and Modeling for Sustainability, GeoCongress 2014*, ASCE, Atlanta, GA, February 23-26, 2014, 10 pp.
- MacMullan, E., Reich, S., Puttman, T., and Rodgers, K. (2008). "Cost- Benefit Evaluation of Ecoroofs." *Proceedings of the 2008 International LID Conference (CD-ROM)*, ASCE, Seattle, WA.
- Rossato, G., and Simonini, P. (1991). "Stress-strain behavior of sands in triaxial and direct simple shear tests." *Canadian Geotechnical Journal*, 28: 276-281.

- Shibuya, S. and Hight, D. W. (1987). "On the stress path in simple shear." *Geotechnique*, 34 (4), 511-515.
- Spolek, G. (2008). "Performance monitoring of three ecoroofs in Portland, Oregon" *Urban Ecosyst*, Vol. 11, 349-259.
- Stovin, V., Dunnett, N., and Hallam, A. (2007). "Green Roofs- Getting Sustainable Drainage off the Ground." *Proceedings of the 6th NOVATECH International Conference of Sustainable Techniques and Strategies in Urban Water Management*, Lyon, France, Vol. 1, 11-18.
- Weiler, S. K., and Scholz-Barth, K. (2009). *Green Roof Systems; A Guide to the Planning, Design, and Construction of Landscapes over Structure*. John Wiley & Sons: Hoboken, NJ.
- Wijewickreme, D., Dabeet, A., and Byrne, P. (2013). "Some Observations on the State of Stress in the Direct Simple Shear Test Using 3D Discrete Element Analysis." *Geotechnical Testing Journal*, 36 (2), 1-8.
- Wood, D. M., Drescher, A., and Budhu, M. (1979). "On the Determination of Stress State in the Simple Shear Apparatus." *Geotechnical Testing Journal*, 2 (4), 211-221.

4.8 Tables

Table 4.1: Ecoroof soil properties used to reconstitute specimens.

Index Property	Measured Value
e_{max}	2.54
e_{min}	1.33
$\gamma_{d,max}$ (kN/m ³)	7.97
$\gamma_{d,min}$ (kN/m ³)	5.22
G_s	1.89
D_{10} (mm)	0.22
D_{30} (mm)	0.87
D_{60} (mm)	2.46
C_u	11.29
C_c	1.42

Table 4.2: Index properties for the target gradations and reconstituted specimens.

Gradation	C_u	e_{min}	e_{max}	$\gamma_{d,min}$ (kN/m ³)	$\gamma_{d,max}$ (kN/m ³)
Fine	19.6	1.37	2.20	6.8	9.2
Intermediate	59.8	1.41	2.03	6.7	8.4
Coarse	74.6	2.09	2.54	5.3	6.1

Table 4.3: Descriptive statistics for the ecoroof material characterization (after Kraupa et al. 2014).

Soil Property	No. of Samples	Mean (μ)	COV (%)
w (%)	30	62	40
O_c (%)	29	12	56
D_{10} (mm)	29	0.021	82
D_{50} (mm)	29	1.64	79
C_u	29	150	94
C_c	29	14	119
G_s	29	2.10	13
E	29	1.30	39
γ_m (kN/m ³)	30	7.55	21
γ_d (kN/m ³)	30	4.76	24
DL (kPa)	30	1.27	106

Table 4.4: Secant shear modulus, in MPa, for the reconstituted specimens at one percent γ_{zx} .

Gradation	σ_{zz} (kPa)	$D_r=30\%$	$D_r=50\%$
Fine	10	0.56	0.74
	20	0.82	0.88
	30	1.03	1.27
Intermediate	10	0.73	0.61
	20	0.97	0.81
	30	1.05	1.10
Coarse	10	0.69	0.73
	20	0.80	1.00
	30	1.07	1.25

Table 4.5: Summary of (ψ_p) for the reconstituted specimens, σ_{zz} in kPa.

<i>D_r</i> = 30%				<i>D_r</i> = 50%			
σ_{zz} (kPa)	Fine	Intermediate	Coarse	σ_{zz} (kPa)	Fine	Intermediate	Coarse
10	2.5	10.9	6.4	10	2.5	7.6	4.7
20	-	17.0	9.1	20	-	14.7	5.9
30	-	4.3	4.9	30	-	-	7.5

4.9 Figures

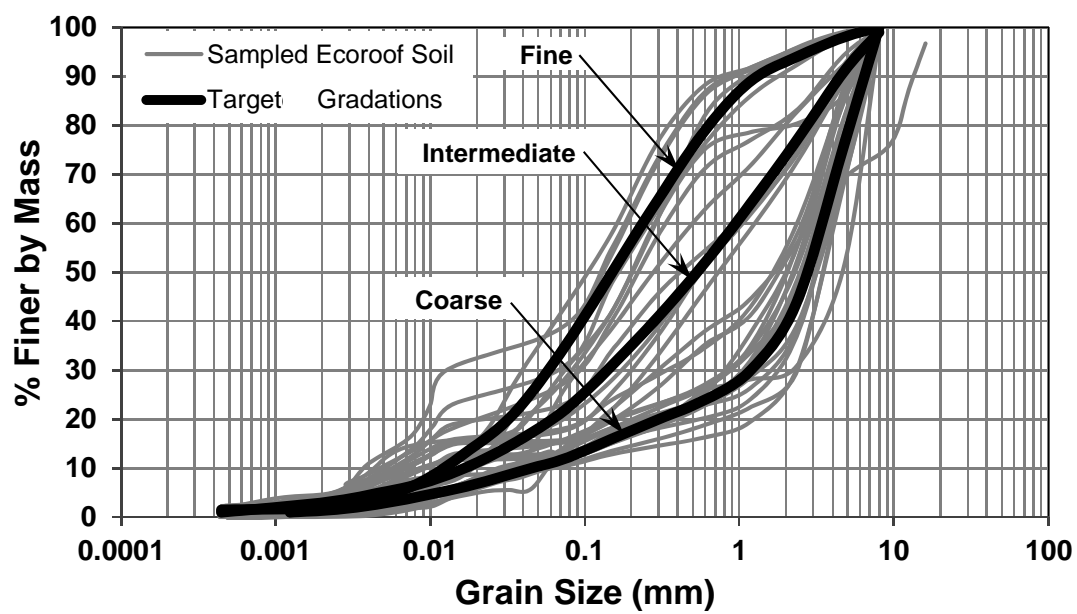


Figure 4.1: Measured and target grain size distributions.

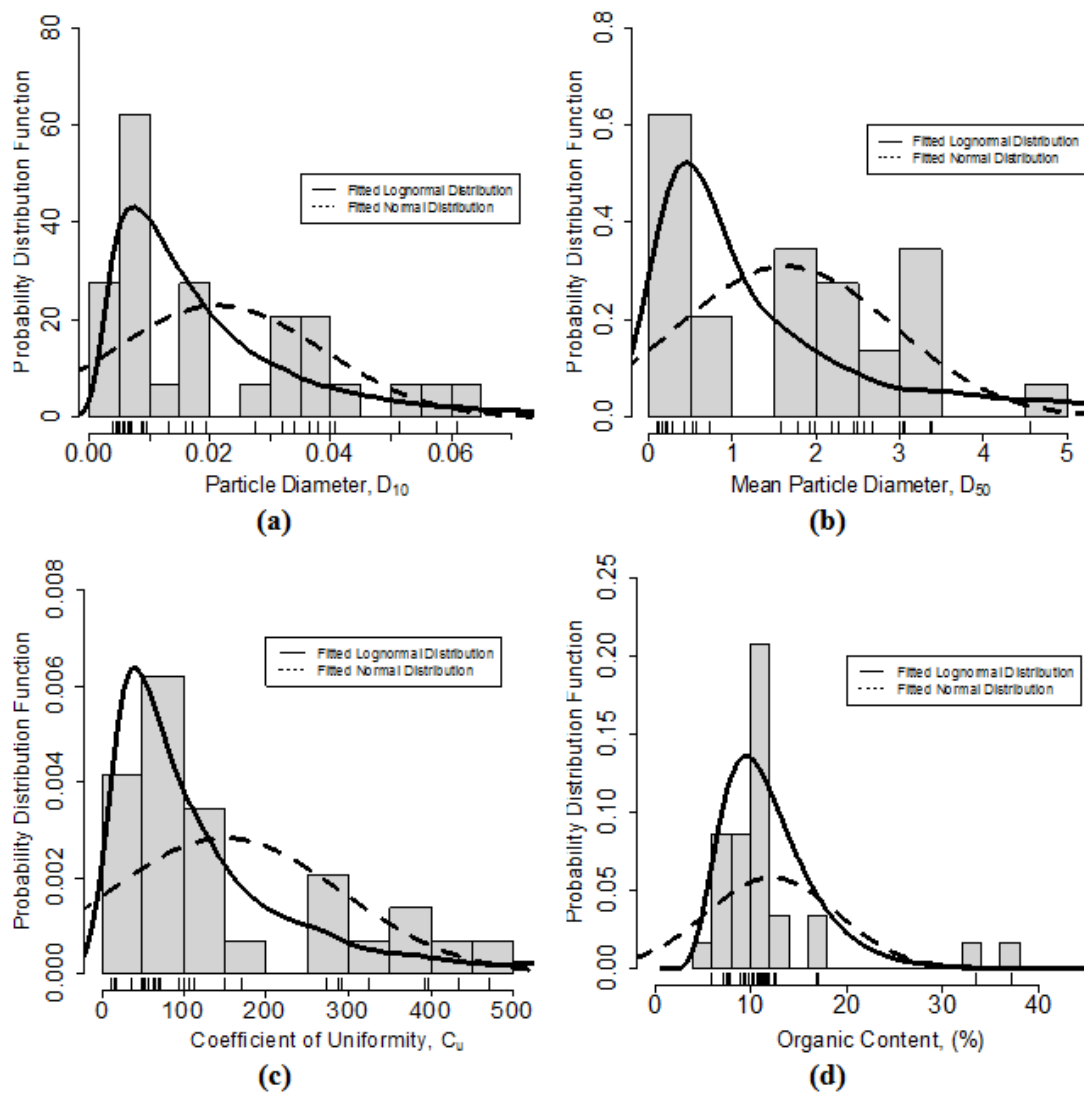


Figure 4.2: Histogram and probability distribution functions for various geotechnical index properties: (a) D_{10} (b) Median grain size, D_{50} , (c) C_u , and (d) O_c .

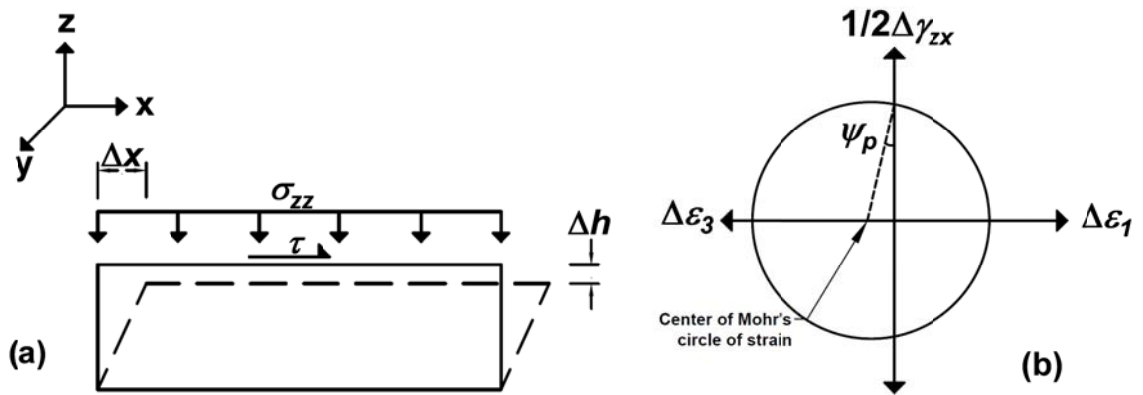


Figure 4.3: Conventions assumed for the simple shear test: (a) cross-section showing applied stresses and strains, and (b) Mohr's circle of strain and dilation angle, based on major and minor principal strains.

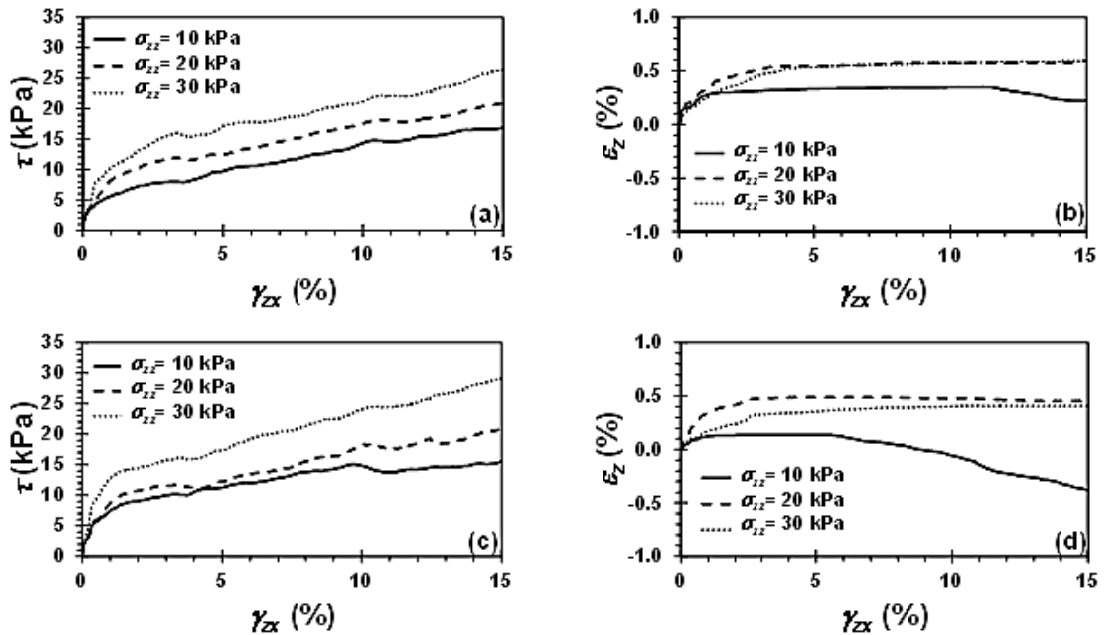


Figure 4.4: Simple shear stress-strain response and volumetric response for specimens reconstituted using the fine target gradation (a, b) $D_r = 30$ percent (c, d) $D_r = 50$ percent.

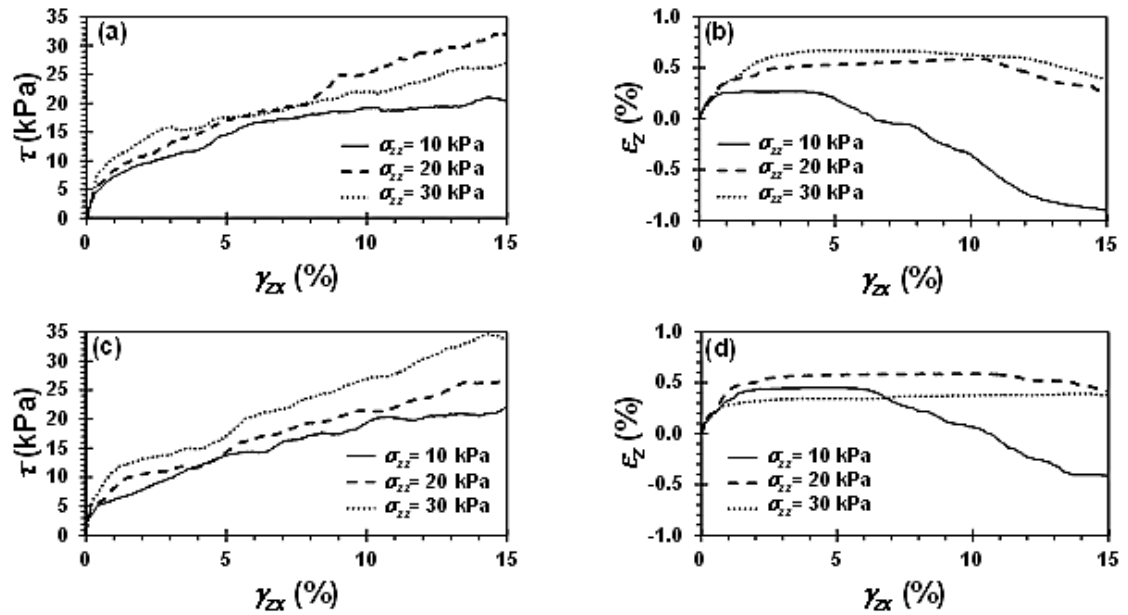


Figure 4.5: Simple shear stress-strain response and volumetric response for specimens reconstituted using the intermediate target gradation (a, b) $D_r = 30$ percent (c, d) $D_r = 50$ percent.

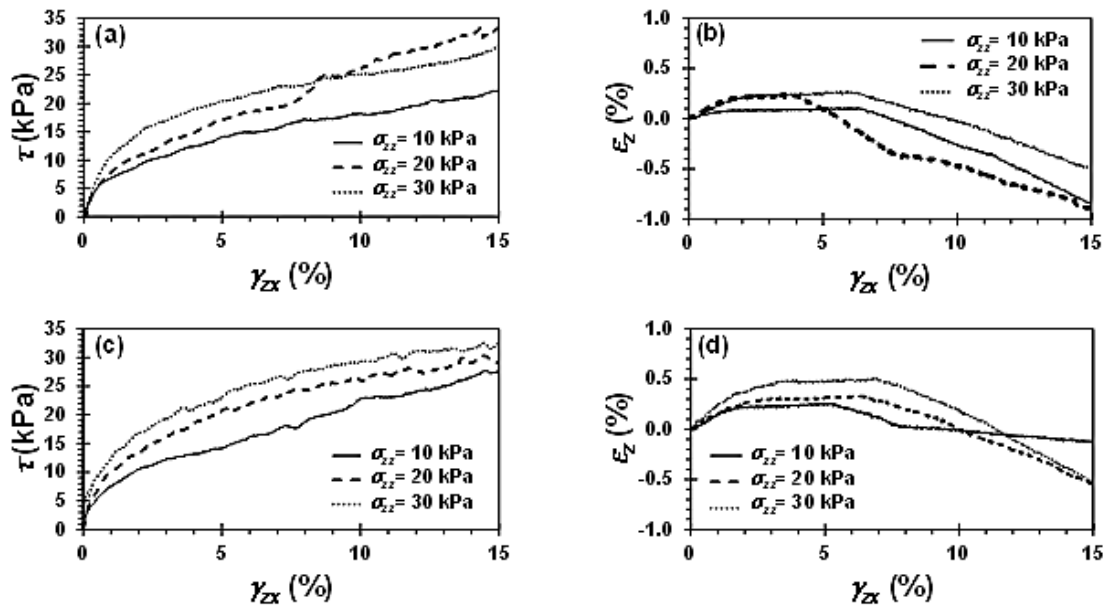


Figure 4.6: Simple shear stress-strain response and volumetric response for specimens reconstituted using the coarse target gradation (a, b) $D_r = 30$ percent (c, d) $D_r = 50$ percent.

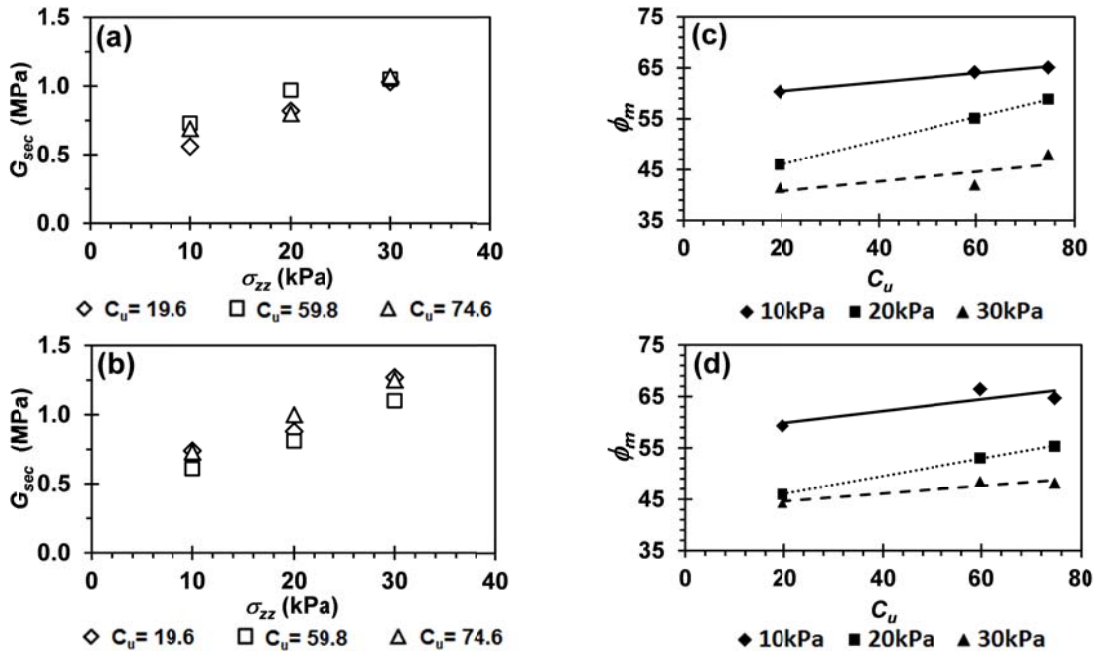


Figure 4.7: Secant shear modulus at $\gamma_{zx} = 1$ percent versus σ_{zz} at varying C_u for specimens with (a) $D_r = 30$ percent, and (b) $D_r = 50$ percent, and mobilized friction angle at $\gamma_{zx} = 15$ percent versus coefficient of uniformity at varying applied vertical stresses for specimens with (c) $D_r = 30$ percent (d) $D_r = 50$ percent.

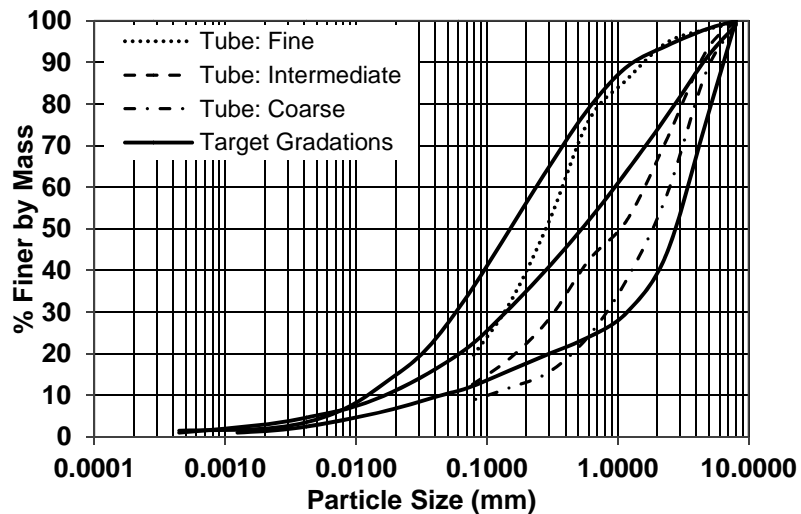


Figure 4.8: Comparison of particles size distributions for the tube specimens and the three idealized target gradations.

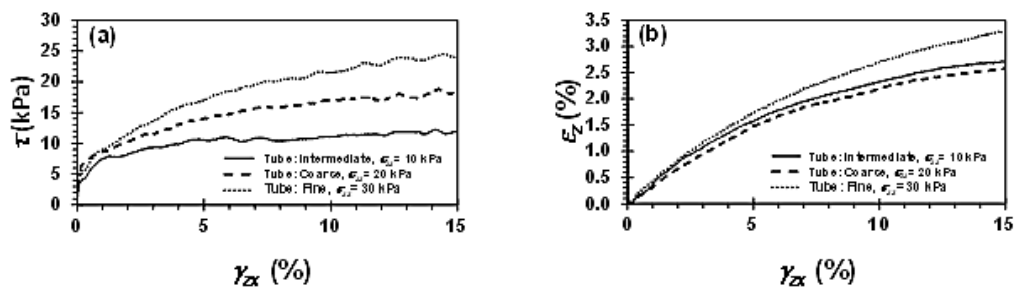


Figure 4.9: Stress-strain response (a) and volumetric response (b) for the tube specimens.

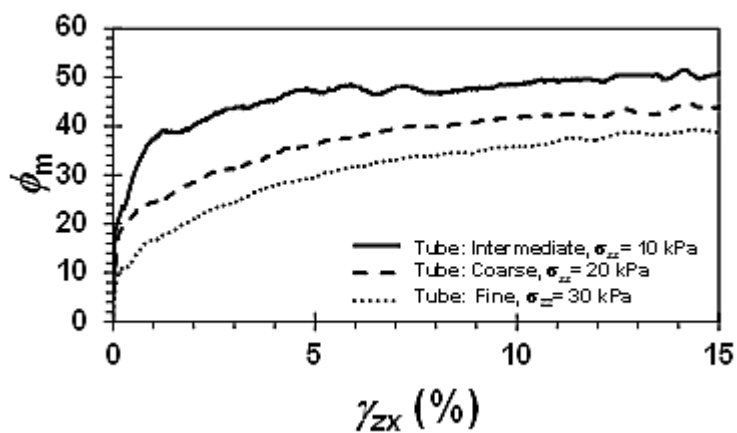


Figure 4.10: Friction angle mobilized throughout shearing for the tube specimens.

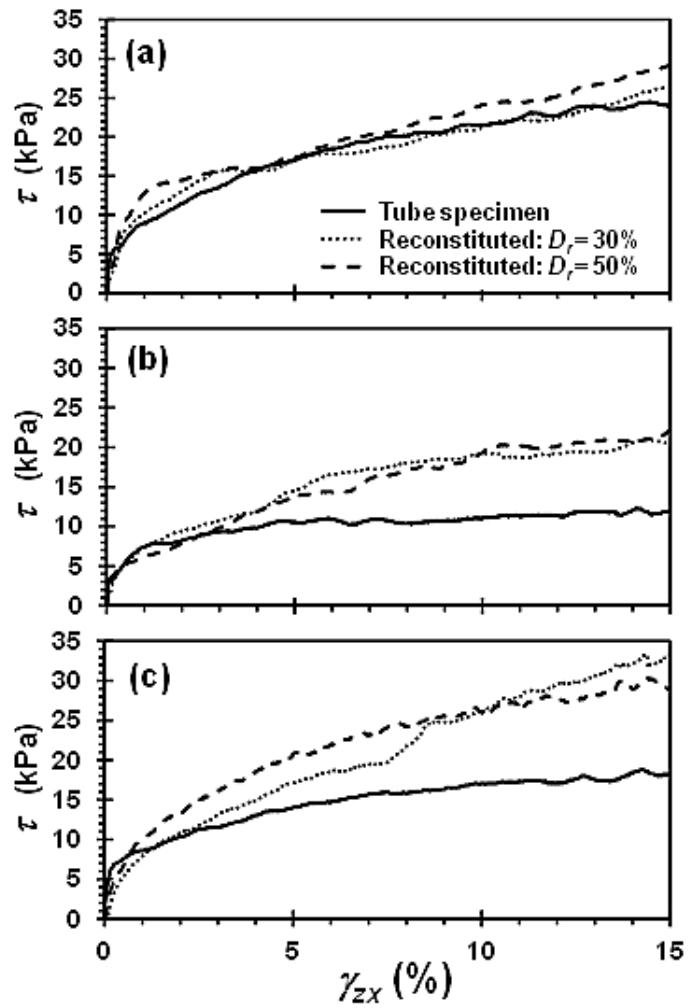


Figure 4.11: Comparison of stress-strain response of tube and reconstituted specimens for: (a) fine gradations and $\sigma_{zz} = 30$ kPa, (b) intermediate gradations and $\sigma_{zz} = 10$ kPa, and (c) coarse gradations and $\sigma_{zz} = 20$ kPa.

Chapter 5: Undrained Cyclic Simple Shear Response of Ecoroof Soil

Authors:

Travis J. Kraupa, H. Benjamin Mason, Ph.D., Armin W. Stuedlein, Ph.D., and
Christopher C. Higgins, Ph.D.

Journal to be submitted:

Earthquake Spectra

Ecoroofs are becoming a popular sustainable roofing alternative; however there is a dearth of information regarding the cyclic response of ecoroof soils, which inhibits the creation of needed ecoroof design guidelines. The pore pressure response, modulus degradation and damping ratios are experimentally determined for reconstituted ecoroof specimens as well as specimens prepared from Shelby tube samples retrieved from the field. Strain-controlled cyclic simple shear testing was employed. The ecoroof specimens were prepared and tested using realistic initial field conditions (i.e., low confining stresses and relative densities) and subjected to realistic cyclic frequencies. The results indicate that specimen gradation and organic content have the largest effect on the cyclic response of ecoroof soil. The results suggest that, when developing ecoroof design standards, attention needs to be given to specifying the gradation of ecoroof soils and tracking the temporal change in organic content.

5.1 Introduction

Ecoroofs are becoming prolific in the United States, because they can sustainably manage stormwater, reduce heat island effects, and provide leisure space for building occupants (Getter and Rowe 2006; Spolek 2008). Currently, there are no official building codes in the United States regulating the design, construction, and maintenance of ecoroofs. Some architects and contractors use German ecoroof standards (FLL 2008) as a guideline, but the German standards are not enforced in the United States and are developed for Germany, where ecoroof technology is more mature and seismic concerns are less significant. Accordingly, there is a need to develop codified guidance for the design, construction and maintenance of ecoroofs in the United States

In the United States, the examination of concerns associated with the design, construction, and maintenance of ecoroofs has been focused on the biological systems and the architectural benefits of ecoroofs (Liptan and Strecker 2003; Getter and Rowe 2006). Engineering concerns, such as the likelihood and effects of rainwater ponding, parapet wall loading during earthquakes, and cyclic ecoroof soil-roof interaction, have not been satisfactorily addressed, and these gaps in knowledge present an obstacle for the standardization of ecoroof guidelines. Fundamental studies of ecoroof soil response are required as a first step towards codified guidance that addresses engineering concerns while also incorporating biological, ecological, and architectural concerns.

Previous studies by Kraupa et al. (2014a and 2014b) have focused on characterizing the geotechnical index properties, static strength response, and volumetric strain response of ecoroof soil sampled from ecoroofs in Portland, Oregon. In this study, we attempt to further the fundamental understanding of ecoroof soils by investigating their undrained cyclic simple shear response. From a practical standpoint, we focus our study on the Pacific Northwest of the United States, where ecoroofs are becoming increasingly popular. In the Pacific Northwest, rainfall and ecoroof soil saturation can persist for periods extending nine months, and the probability of a large-magnitude, long-duration earthquake occurring within the next 50 years is estimated to be as high as 45 percent (Mazzotti and Adams 2004; Goldfinger et al. 2012). Therefore, a basic understanding of the seismic response of ecoroof soils is needed to provide baseline recommendations for ecoroof design standards and codes. To address the need for baseline recommendations, strain-controlled cyclic simple shear (CSS) tests were performed to investigate the pore-

pressure response, shear modulus degradation, and material damping ratios for reconstituted ecoroof soil specimens and Shelby tube field samples of ecoroof soil.

5.2 Background

5.2.1 Ecoroof Soil

Ecoroof soil is designed to support vegetation, which allows for the uptake and transpiration of stormwater, and it is simultaneously designed to ensure proper drainage, which decreases the probability of large roof dead loads caused by ponding. In addition, the ecoroof soil is designed to be light, so that it does not excessively increase the roof's dead load. Typical ecoroof soil constituents include lightweight vesicular volcanic soils (i.e. pumice), fine sands, non-plastic silts, and organic matter.

Kraupa et al. (2014a) described a specially designed sampler and sampling protocol, as well as the geotechnical index properties of ecoroof soils sampled from 18 roofs in Portland, Oregon. Kraupa et al. (2014b) examined the static strength of ecoroof soil using simple shear testing of manufactured ecoroof soil, which was reconstituted to match three target gradations selected from the predominant gradations observed during the field program, as well as undisturbed tube samples. Findings from Kraupa et al. (2014a and 2014b), which inform the present study, include:

1. The in-situ geotechnical properties (e.g. organic content, gradation) of ecoroof soil found in Portland, Oregon are highly variable, which demonstrates the need for further study and standardization;
2. The mobilization of the static strength depends on the relative density, the coefficient of uniformity, the organic content, and the applied normal stress; and,

3. The field specimens (i.e. tube samples), showed a fully contractive volumetric strain response as compared to the contractive-dilative response of the reconstituted laboratory specimens, which indicates that the organic content has an effect volumetric strain response of ecoroof soils.

5.2.2 Cyclic Simple Shear Testing and Soil Liquefaction

Two devices, among others, are commonly used to investigate the cyclic properties of soils: the cyclic triaxial (CTX) device and the cyclic simple shear (CSS) device. The CTX device is more popular, because of its widespread use and ease of interpretation. However, the CTX device produces the cyclic load via the vertical piston, which may not simulate realistic cyclic stress paths, depending on the scenario under investigation. On the other hand, the CSS device replicates the scenario of a level-ground soil specimen being subjected to vertically-propagating shear waves (Idriss and Boulanger 2008). Accordingly, the CSS device is more appropriate for the seismic loading conditions experienced by an ecoroof, and it is the device used for this research.

An early soil liquefaction study on clean uniform sand compared results for both the CTX and CSS devices (e.g. Peacock and Seed 1968). This study indicated that the CSS device produced level-ground boundary conditions, similar to those expected in the field. Accordingly, various researchers followed, and focused on seismically-induced pore pressure generation, shear modulus degradation, and material damping of clean sands (e.g. Seed and Peacock 1971; Finn et al. 1971; De Alba et al. 1976). More recently, researchers have employed the CSS device, as well as the CTX device, to understand the seismic response of fine-grained soils and silty sands (e.g. Yasuda et al. 1994; Yamamuro

and Covert 2001; Boulanger and Idriss 2006; Bray and Sancio 2006; Hazirbaba and Rathje 2009; Monkul and Yamamuro 2011). Additionally, researchers have quantified the seismic response of peat soils to understand the effect of organic content on liquefaction resistance, shear modulus reduction, and material damping (Boulanger et al. 1998; Kramer 2000; Wehling et al. 2003; Kishida et al. 2009). Given the presence of organic matter in ecoroof soil, and its demonstrated effect on the static volumetric strain response (Kraupa et al. 2014b), the aforementioned studies of the cyclic response of peat are shown to be relevant for the present study.

The definition of seismically-induced soil liquefaction is generally accepted to be the complete loss of soil strength caused by a rapid increase in excess pore water pressure and a corresponding decrease in the effective stress (Seed 1979; Jeffries and Been 2006; Idriss and Boulanger 2008). Following this general definition, there are several quantitative ways to define soil liquefaction. Often, the excess pore-water pressure ratio ($r_u = \Delta u / \sigma'_{v0}$) is used to define liquefaction and interpret CSS test results. When the excess pore-water pressure generated by the earthquake shaking (Δu) equals the vertical effective consolidation stress on the specimen (σ'_{v0}), then full liquefaction has occurred within the specimen. The excess pore-water pressure ratio, r_u , is often plotted with the number of cycles of loading, N , which shows when the onset of liquefaction occurs (i.e. the number of cycles to liquefaction, $N_L = N|_{r_u=1.0}$). Excessive soil deformation, which is important for ecoroof soil-roof interaction and parapet wall loading considerations, can occur when r_u is less than 100 percent; for this research, “onset of liquefaction” is defined as $r_u \geq 0.9$, used by Hazirbaba and Rathje (2009) and others.

5.2.3 Modulus Reduction and Damping Curves

During an earthquake, shear strains accumulate cyclically, resulting in a decrease in soil's shear modulus and increase in the material (i.e., hysteretic) damping. Accordingly, it is useful to plot the normalized shear modulus, G/G_{max} , and the material damping ratio, ζ , versus the cyclic shear strain, γ_c for understanding the seismic soil response and performing seismic site response analysis. The small-strain shear modulus, G_{max} , is usually measured experimentally using resonant column testing or bender elements, estimated in-situ using shear wave velocity measurements, or estimated based on correlations.

The secant shear modulus, G , was determined at various shear-strain levels, and shear modulus degradation curves were developed by normalizing G by the maximum measured secant shear modulus (G_{max}^*). The symbol, G_{max}^* , is used herein to indicate that it was not experimentally determined via a small-strain testing method. Instead, G_{max}^* was determined as the initial slope of the shear stress-shear strain curve produced by CSS testing. Using the least squares method, a best fit curve developed by Borden et al. (1996) was fit to the G/G_{max}^* data:

$$\frac{G}{G_{max}^*} = \frac{1}{[1 + a(\gamma_c)^b]^c} \quad (5.1)$$

where γ_c is the shear strain in percent and a , b , and c are curve fitting coefficients. Equation 1 was used to fit curves to $\gamma_c = 0.0001$ percent. Given that the lowest

experimentally investigated shear strain was 0.1 percent, which is in the strain range for CSS testing (Boulanger et al. 1993), the modulus degradation curves estimated using Equation 1 represent extrapolations for shear strains smaller than 0.1 percent.

The material damping ratio, ζ , is commonly used as a measure of the energy dissipated during loading cycle. Determination of the amount of energy dissipated is typically conducted with an idealized single degree-of-freedom model (Jacobsen 1930; Ishihara 1996), which only considers the first “quarter” of the shear stress-shear strain curve. A slightly modified method by Brennan et al. (2004) calculates the material damping ratio from the area of the entire stress strain loop, as follows:

$$\zeta = \frac{1}{2\pi} \frac{\oint \tau_c d\gamma_c}{\frac{1}{4} \Delta\tau_c \Delta\gamma_c} \quad (5.2)$$

where $\oint \tau_c d\gamma_c$ is the area of the stress-strain loop, and $\Delta\tau_c$ and $\Delta\gamma_c$ are the range in cyclic shear stress and strain, respectively. Given the non-linear shape of the stress-strain loops, a cumulative trapezoidal numerical integration (*CTNI*) was used to determine $\oint \tau_c d\gamma_c$ (Brennan et al. 2004).

5.3 Experimental Program

Kraupa et al. (2014a and 2014b) concluded that ecoroof soil’s geotechnical index properties, static strength, and volumetric strain response vary significantly over the wide range of observed field soil gradations. Accordingly, Kraupa et al. (2014a) determined

three target gradations that represented the observed grain size distributions of the field specimens. Figure 5.1 shows the three target gradations used for reconstituting laboratory specimens, and are termed the fine, intermediate, and coarse gradations, based on their respective particle size distributions. According to the Unified Soil Classification System (USCS), all three target gradations are classified as silty sands (SM). The percent of material passing the number 200 sieve (the fines content, FC), median grain size (D_{50}), coefficient of uniformity (C_u), and the maximum and minimum void ratio (e_{max} and e_{min}) for each of the target gradation are shown in Table 5.1.

The CSS tests were conducted with the hydraulically servo-controlled SSH-100 device manufactured by GCTS Testing Systems. The CSS device is capable of exerting a cell pressure and a vertical stress to the top of the specimen as well as a backpressure to the bottom of the specimen. The CSS device inputs cyclic motions, which in this study are sinusoids, by a servo-controlled tangential piston. The tangential piston can be controlled by the tangential load cell (i.e. stress control) or by the tangential displacement gauge (i.e. strain-control) via an active feedback control. Strain control was used for this study. All of cyclic loading reported herein was performed with the drainage valve closed to permit undrained loading.

Specimens were prepared by first flushing carbon dioxide through the ecoroof porespace for one hour, followed by permeation of de-aired water from the bottom to the top via gravity-induced flow. The in-flow of the de-aired water during saturation was restricted by a valve to reduce the development of seepage forces and subsequent flow channels. Backpressure was used to aid saturation, which was confirmed using the B-

value ($\Delta u/\Delta\sigma'_v$), check, which follows typical geotechnical testing procedures (Bardet 1997). However, ecoroof soil contains vesicular pumice with internal void spaces, which complicates the B-value calculation. The internal void space within the pumice particles increases as the pumice particle size increases (Kikkawa et al. 2013); therefore, the total internal void space for a specimen is, on average, largest for the coarse target gradation and smallest for the fine target gradation. To aid with saturation of the difficult ecoroof soils, minimum backpressures of 235 kPa were used. Acceptable B-values were chosen, based on our experiences, as 0.91 for the coarse and intermediate target gradations and 0.97 for the fine target gradation. We hypothesized that the low B-values for the coarse and intermediate target gradations were acceptable due to the difficulty with eliminating air entrapped within the internal vesicular void spaces

Specimens were prepared in an unreinforced membrane enclosed by a stack of rigid rings. The rigid rings provided lateral restraint (e.g. constant diameter) of the specimen. Kraupa et al. (2014b) found that ecoroof soils are relatively loose, with an average in-situ moist unit weight equal to 7.55 kN/m^3 . Accordingly, targeted relative densities used for reconstitution purposes were 30 and 50 percent. The reconstitution method used was similar to the moist undercompaction method (Ladd 1978). The moist undercompaction method was deemed the most appropriate reconstitution method, because the target gradations of the ecoroof soils were well-graded, have mean particle diameters ranging from 0.15 to 2.70, and contain brittle pumice particles. Specifically, to avoid segregation of the fine material during reconstitution, a small amount of de-aired water was added to the dry soil. The amount of water to add was predetermined for a given relative density. The specimen was prepared by first placing approximately half of the material into the

unreinforced membrane stretched around the rings. The material was then tamped to a uniform height. Thereafter, subsequent lifts were required until the required specimen volume was achieved. The in-situ tube specimens were prepared using the method described in Kraupa et al. (2014b). The rigid stack of confining rings allowed for 1-D vertical consolidation of the specimen with the final stress state being K_0 conditions (i.e. in situ conditions).

The ecoroofs investigated in Portland, Oregon had relatively shallow soil depths (70 to 1,520 mm; Kraupa et al. 2014a); therefore, a confining stress of 30 kPa was targeted for cyclic testing. To make comparisons with previous CSS test results and to account for future deeper ecoroofs, three additional CSS tests were performed with confining pressures of 100 kPa. The field exploration by Kraupa et al. (2014a) indicated that ecoroofs in Portland, Oregon were predominantly constructed on small-to-midsize commercial buildings (e.g. 5 to 10 stories). Accordingly, the period range-of-interest was targeted as 0.5 to 1 seconds. The vibration of the building, and thus the building's fundamental period, is expected to have a large impact on the seismic soil response at the roof level. Therefore, for this investigation, the frequencies of the sinusoidal loading cycles were chosen as 1 and 2 Hz. Constant sinusoidal amplitudes, or shear strains, γ_c , of 1.5 and 4 percent were chosen (i.e. peak-to-peak strains of 3 and 8 percent, respectively). The strain range was chosen to model the large horizontal roof displacements that can be caused by an intense, long duration earthquake. CSS tests were terminated after 1,000 cycles of loading.

In summary, CSS tests were performed on reconstituted specimens confined to 30 kPa with three varying target gradations, two varying relative densities, two varying cyclic loading frequencies, and two varying cyclic strain amplitudes. In addition, three CSS tests were performed on reconstituted specimens at a confining pressure of 100 kPa for each of the three target gradations with $D_r = 50$ percent, $\gamma_c = 4$ percent, and $f = 1$ Hz, and three CSS tests were performed on tube specimens, as explained below. In total, 30 CSS tests were performed to initially characterize the cyclic response of ecoroof soil.

5.4 Cyclic Response of Ecoroof Soil

5.4.1 Reconstituted Specimens

Specimen gradation was determined to be an influential factor on the dynamic response of the reconstituted ecoroof specimens. Typical results from a reconstituted fine gradation specimen with $D_r = 30$ percent, $\sigma'_v = 30$ kPa, $\gamma_c = 4$ percent, and $f = 2$ Hz are presented in Figure 5.2. The stress-strain loops are shown in Figure 5.2a, and the generation of the excess pore pressure as a function of cyclic strain is plotted in Figure 5.2b. The initially loose state of the specimen was confirmed by the large normal strain (ε_n) observed during the first 40 cycles (Figure 5.2c). Liquefaction, defined as $r_u = 0.90$, occurred at 30 cycles, followed thereafter by a moderate increase in r_u with additional shearing cycles, as shown in Figure 5.2d.

Figure 5.3 is similar to Figure 5.2, except the results are plotted for a reconstituted intermediate gradation specimen (other testing conditions i.e., D_r , γ_c , σ'_v and f , are the same). The stress-strain loops (Figure 5.3a), exhibited a significantly smaller maximum cyclic shear stress response than the stress-strain loops observed for the fine gradation.

After approximately 25 loading cycles the excess pore pressure remained constant (Figure 5.3b). The generation of excess pore pressure approached a steady state in fewer cycles than the fine gradation (Figure 5.3b), and the normal strain at the end of 40 cycles was approximately 4 percent. The intermediate specimen liquefied at approximately 25 cycles, and thereafter the excess pore pressure remained relatively constant.

Figure 5.4 shows the results shown in Figure 5.2 and 5.3 for the reconstituted coarse gradation specimen (with the other testing conditions held constant). Figure 5.4a shows a hysteretic response that was more comparable to the fine gradation than the intermediate gradation. However, the coarse specimen exhibited the largest generation of excess pore pressures and normal strain (Figures 5.4c and 5.4d) of the three gradations. Based on observations from CSS testing of the ecoroof soils reconstituted to the three target gradations, it appears that the most significant factors controlling the cyclic response of ecoroof soil under the loading conditions investigated are the gradation and the amount of fines.

Figures 5.5 and 5.6 shows the cyclic shear stress response for each of the gradations tested at cyclic frequencies of 1 and 2 Hz. Figures 5.5 and 5.6 further suggest that the gradation of the specimens has a significant influence on the dynamic response of ecoroof soil. Generally, it was observed that the coarse and fine gradations exhibited higher cyclic shear stresses than the intermediate gradations for a given test parameter. With the exception of the coarse specimen loaded at $f = 2$ Hz and $\gamma_c = 4$ percent, it was observed that both the frequency of loading and the relative density had a relatively insignificant influence on the cyclic shear stress response of ecoroof soil reconstituted to

each of the three target gradations. Other researchers (e.g. Boulanger et al. 1991) have observed that cyclic loading frequency has a negligible effect on the response of fully saturated soils. Relatively density, however, is known to have a more significant effect on liquefaction response (Seed and Idriss 1970). We hypothesize that the relatively insignificant effect of relative density on the liquefaction response of cyclic shear stress response of ecoroof soils arises from the low initial effective stress and narrow range in relative densities tested.

5.4.2 Excess Pore Water Pressure Distribution

The excess pore pressure generation for the specimens reconstituted with $D_r = 30$ percent, is shown in Figure 5.7. Liquefaction was observed for fine gradation specimens subjected to $\gamma_c = 1.5$ and $f = 2$ Hz as well as $\gamma_c = 4$ percent and $f = 1$ Hz (Figures 5.7b and 5.7c). Liquefaction was also observed for coarse gradation specimens subjected to $\gamma_c = 1.5$ percent and $f = 2$ Hz as well as $\gamma_c = 4$ percent and $f = 2$ Hz (Figures 5.7b and 5.7d). With the exception of Figure 5.7d, it was observed that the increase in r_u during the first 10 loading cycles was the fastest for the intermediate, fine, and coarse gradations, respectively. The excess pore pressure generation response for the specimens reconstituted to $D_r = 50$ percent is shown in Figure 5.8, and liquefaction was observed for the coarse and intermediate specimens subjected to $\gamma_c = 4$ percent and $f = 1$ Hz. Excess pore pressures developed more quickly during the initial loading cycles of the intermediate gradation and slowest for the coarse gradation for the $D_r = 50$ percent reconstituted specimens. Therefore, reconstituted specimens with different relative densities exhibited similar excess pore pressure development trends during cyclic

loading. Based on this observation, the gradation appears to be the most a significant factor in the generation of excess pore pressure in loosely reconstituted ecoroof soil specimens.

One reconstituted ecoroof specimen from each of the three gradations was tested with $D_r = 50$ percent, $\gamma_c = 4$ percent, and $f = 1$ Hz under a larger vertical effective stress (i.e., $\sigma'_v = 100$ kPa) to make comparisons to previously reported CSS and CTX results. The excess pore pressure responses for specimens with $\sigma'_v = 100$ kPa are shown in Figure 5.9. Liquefaction was observed for all of these specimens, which indicates that liquefaction can occur in deep saturated ecoroof materials. Similar to the previous results reported for $\sigma'_v = 100$ kPa specimens, the pore pressures in the intermediate specimen accumulated most rapidly and the coarse gradation most slowly.

5.4.3 Modulus Reduction and Damping Values

Figure 5.10 shows modulus reduction curves (G/G_{\max}^*) for the reconstituted ecoroof specimens. The experimentally determined modulus reduction data and median modulus reduction curves as well as plus and minus one standard deviation modulus reduction curves are shown in Figure 5.10a. For the data presented herein, the standard deviation was relatively semi-logarithmically uniform. The variation between the median modulus reduction response for each gradation (i.e. Figure 5.10b) indicates that the intermediate gradation exhibited the most rapid rate of softening, followed by the coarse and the fine gradations, respectively. The response shown in Figure 5.10b, with respect to the importance of ecoroof soil gradation, is consistent with the excess pore pressure observations described previously. The median modulus reduction curves for each of the

targeted gradations were compared to previously published data (Seed and Idriss 1970; Vucetic and Dobry 1991; Boulanger et al. 1998; Kramer 2000; Darendeli 2001). It was determined that the extrapolated portions of the modulus reduction curves (i.e. $\gamma_c < 0.1$ percent) followed relatively similar trends to peats (e.g. Boulanger et al. 1998 and the upper-bound 11 to 30 kPa region of the curves presented by Kramer 2000), and fine grained soils with a plastic index (PI) equal to 200 (Vucetic and Dobry 1991).

The damping ratio (ζ) was determined for the initial stress-strain loop determined during each CSS test. The calculated damping ratios are summarized in Table 2. Generally, the $D_r = 50$ percent specimens resulted in larger ζ magnitudes, and the reconstituted intermediate gradation specimens had the largest ζ . Recall that the intermediate gradation also exhibited the fastest rate of excess pore pressure generation (Figures 5.5 and 5.6).

5.4.4 Response of Shelby Tube Specimens Retrieved From the Field

Specimens from Shelby tube samples retrieved from ecoroofs in Portland, Oregon, were tested to understand the effect of organic content on the cyclic response of representative ecoroof materials. The sampling procedure used was developed specifically for ecoroof soils as described in Kraupa et al. (2014a) and resulted in relatively undisturbed specimens. Three tube specimens were tested: one for each representative target gradation. The specimen representing the intermediate gradation was tested with $\sigma'_v = 30$ kPa, $f = 1$ Hz and $\gamma_c = 1.5$ percent. Observations from this initial test indicated that the specimen did not exhibit liquefaction (Figure 5.11b). Therefore, to

determine if the two other tube specimens would liquefy, each were tested similarly but with $\gamma_c = 4$ percent.

Figure 5.11b shows the excess pore pressure generation of the field specimens. Liquefaction ($r_u \geq 0.9$) did not occur for any of the in-situ tube specimens. Kraupa et al. (2014b) showed that the presence of organic matter in ecoroof soil had a significant influence on the static stress-strain and volumetric response during simple shear testing. The organic content for the tube specimens were 6.7, 6.1, and 8.1 percent for the fine, intermediate, and coarse specimens, respectively. The initial observations of the dynamic response of the tube specimens indicated that the resistance to liquefaction, as defined for this investigation, increases with the presence of organic matter. However, cyclic mobility, or significant soil strength loss during dynamic loading, which causes excessive horizontal soil displacements, is possible for ecoroof soil with organic content. The damping ratios determined for the tube specimens were 36, 36, and 38 percent for the fine, intermediate, and coarse tube specimens, respectively, consistent with those observed from the reconstituted specimens.

5.5 Discussion

Figure 5.12a shows the excess pore pressure ratio versus the number of cycles for the tube specimens and reconstituted specimens. The reconstituted specimens were tested under similar conditions (i.e. undrained strain-controlled) as the respective tube specimens with similar gradations. Figure 5.12a shows that the tube specimens have a higher resistance to liquefaction. The intermediate tube specimen, tested with $\gamma_c = 1.5$ percent and $f = 1$ Hz, reached a peak r_u of approximately 0.67 at the end of 200 cycles. In

contrast, the intermediate gradation reconstituted specimen reached a peak r_u of 0.90. Evidently, organic content affects the liquefaction resistance of ecoroof soil, which is an observation in line with the studies of peats. With regards to the design, construction, and maintenance of ecoroofs, it is important to determine the temporal increase in organic content associated with vegetative renewal to estimate the temporal increase in liquefaction resistance. The temporal increase in organic content, however, has a negatively competing effect on ecoroof design. The increased organics can retain more moisture and reduce the hydraulic conductivity, thus increasing the roof's dead load and reducing its ability to maintain rapid discharge to roof drains. In summary, the amount of organic content required to support vegetation, its change with time, and its competing effects of increasing liquefaction resistance while also increasing dead loads, must be considered carefully during the development of ecoroof design guidelines.

Figure 5.12b shows the modulus reduction curves for the three Shelby tube specimens. The specimens reconstituted using the fine and coarse tubes have relatively similar modulus reduction curves. Figure 5.12b compares the modulus reduction response of the tube specimens to the median targeted gradation modulus reduction curves. Figure 5.12b shows that the fine and intermediate tube specimens exhibit relatively similar modulus reduction response to the corresponding gradation reconstituted specimens. However, the median response for the coarse specimens diverged from that of the respective tube specimens. Figure 5.12b indicates that organic content influences the modulus reduction response of ecoroof soil gradations with lower fines contents and higher coefficients of uniformity. Specifying proper ecoroof soil gradation and estimating

how the temporal change in gradation will affect the cyclic response of ecoroof soils is an important consideration when developing ecoroof design guidelines.

The generation of excess pore pressure versus the cyclic shear strain amplitude for all tests can be seen in Figure 5.13. The dashed line (Dobry 1985) in Figure 5.13a represents the results from strain controlled CTX tests on clean sand for the first ten loading cycles. Additionally, data from strain controlled CSS tests on sand with varying fine content is plotted (Hazirbaba and Rathje 2009). Comparison of the results for the first ten loading cycles indicates that the CTX (Dobry 1985) has larger measured values of r_u , for similar CSS cyclic strain amplitudes. Additionally, the results from this study indicate that the r_u increases with an increase in γ_c . This trend can also be seen from Hazirbaba and Rathje (2009) CSS results. Figure 5.13b is for the first 30 loading cycles, and discerns the effect that the number of loading cycles has on the generation of excess pore pressure, and generally indicates an increase in r_u for additional loading cycles.

Additionally, a roof displacement model was developed by using the median (i.e. bold line) and plus and minus one standard deviations (i.e. dotted line types) of the strain-controlled CSS data from this study and data from the Hazirbaba and Rathje (2009) study. The developed roof displacement model attempts to provide an estimate for the liquefaction potential of ecoroof soil given an estimated roof drift during a seismic event. The two loading cycles (i.e. 10 and 30 cycles) are representative of a shallow crustal and larger subduction zone earthquake event and can be used independently. The roof displacement model indicates that for 10 loading cycles (Figure 5.13a) liquefaction as defined by this study ($r_u = 0.9$) was not achieved within the bound of one standard

deviation, whereas for 30 loading cycles (Figure 5.13b) liquefaction was observed with this model for shear strain amplitudes of 1.5 and 4 percent.

5.6 Conclusions

The generation of excess pore water pressure and number of cycles to liquefaction for three targeted gradations and Shelby tube specimens are presented herein. Generally, it was observed that the intermediate gradation exhibited the fastest rate of excess pore pressure generation during the first 10 loading cycles, followed by the fine and coarse gradations, respectively. Liquefaction, as defined by an excess pore pressure ratio of 0.90 or greater, was observed for numerous specimens. Liquefaction potential of ecoroof soil depends on gradation, applied cyclic shear strain, density, and organic content. The intermediate gradation required the lowest number of cycles to liquefaction, followed by the coarse and the fine gradations, respectively. Ecoroof design standards would decrease the variability between gradations, which would allow engineers to quantify the expected liquefaction potential for the ecoroof soil more exactly. As noted, the organic content increases with time as the ecoroof matures; creating ecoroof design standards for changing organic contents is challenging and will require more investigation.

Modulus reduction curves and damping ratios were presented herein for the investigated ecoroof soils. Modulus reduction of ecoroof soil is dependent on cyclic loading frequency and maximum cyclic shear strain amplitude. Relatively large damping ratios were observed for ecoroof soil as compared to similar USCS silty sand soils. The modulus reduction curves and damping ratios were determined from experiments performed with a CSS device (i.e. large-strain experiments); however, the modulus

reduction curves and damping ratios provide an initial estimate for dynamic ecoroof soil response over realistic ranges of ecoroof soil gradations and seismic roof displacement amplitudes.

5.7 Acknowledgements

This material is based upon work supported by the National Science Foundation under Grant No. CMMI-1162616. Additionally, we gratefully acknowledge the assistance of Mr. Zheng Li for his work in setting up and calibrating the CSS device used during the initial phase of this investigation.

5.8 References

- Bardet, J. P., (1997). *Experimental Soil Mechanics*, 1st Edition, Prentice Hall, Upper Saddle River, NJ, 582pp.
- Borden, R. H., Shao, L., and A. Gupta, (1996). “Dynamic Properties of Piedmont Residual Soils.” *Journal of Geotechnical Engineering*, Vol. 122, 813-821.
- Boulanger, R. W., Seed, R. B., Chan, C. K., Seed, H. B., and J. Sousa, (1991). “Evaluation Behavior of Saturated Sands Under Uni-directional and Bi-directional Monotonic and Cyclic Simple Shear Loading,” *Report No. UCB/GT/91-08*, Berkeley, CA.
- Boulanger, R. W., Chan, C. K., Seed, H. B., Seed, R. B., and Sousa, J. B., (1993). “A low-compliance bi-directional cyclic simple shear apparatus.” *ASTM Geotechnical Testing Journal*, Vol. 16, 36-45.
- Boulanger, R. W., Arulnathan, R., Harder Jr., L. F., Torres, R. A., and M. W. Driller, (1998). “Dynamic Properties of Sherman Island Peat.” *Journal of Geotechnical and Geoenvironmental Engineering*, Vol. 12, 12-20.
- Boulanger, R. W. and I. M. Idriss, (2006). “Liquefaction Susceptibility Criteria for Silts and Clays.” *Journal of Geotechnical and Geoenvironmental Engineering*, Vol. 132, 1413-1426.
- Bray, J. D., and R. B. Sancio, (2006). “Assessment of the Liquefaction Susceptibility of Fine-Grained Soils.” *Journal of Geotechnical and Geoenvironmental Engineering*, Vol. 132, 1165-1177.

- Brennan, A.J., Thusyanthan, N. I., Madabhushi, S. P. G. (2004). "Evaluation of Shear Modulus and Damping in Dynamic Centrifuge Test." *Cambridge University Engineering Department Technical Report*, CUED/D-SOILS/TR-336: pp. 36.
- Darendeli, M. B., (2001). "Development of a New Family of Normalized Modulus Reduction and Material Damping Curves." *Ph.D. Dissertation*, University of Texas, Austin, Texas, 362 pp.
- De Alba, P., Seed, H. B., and C. K. Chan, (1976). "Sand Liquefaction in Large-Scale Simple Shear Tests." *Journal of the Geotechnical Engineering Division*, Vol. 102, 909-927.
- Dobry, R., Ladd, R. S., Yokel, F. Y., Chung, R. M., and D. Powell, (1982). "Prediction of pore water pressure buildup and liquefaction of sands during earthquakes by the cyclic strain method." *National Bureau of Standards Building Sciences*, Rep. No. 138.
- Figueroa, J., Saada, A., Liang, L., and N. Dahisaria, (1994). "Evaluation of Soil Liquefaction by Energy Principles." *Journal of Geotechnical Engineering*, Vol. 120, 1554–1569.
- Finn, W. D. L., Pickering, D. J., and P. L. Bransby, (1971). "Sand liquefaction in triaxial and simple shear tests." *Journal of Soil Mechanics and Foundation Division*, Vol. 97, 639–659.
- Forschungsgesellschaft Landschaftsentwicklung Landschaftsbau (FLL), (2008). "Guidelines for the Planning, Construction and Maintenance of Green Roofing – Green Roofing Guideline," Germany.
- Getter, K. L., and D. B. Rowe, (2006). "The Role of Extensive Green Roofs in Sustainable Development." *HORTSCIENCE*, Vol. 41, 1276-1285.
- Goldfinger, C., Nelson, C. H., Morey, A., Johnson, J. E., Gutierrez-Pastor, J., Eriksson, A. T., Karabanov, E., Patton, J., Gracia, E., Enkin, R., Dallimore, A., Dunhill, G., and T. Vallier, (2012). "Turbidite Event History: Methods and Implications for Holocene Paleoseismicity of the Cascadia Subduction Zone." *USGS Professional Paper 1661-F*, Reston, VA, U.S. Geological Survey, pp. 184.
- Hazirbaba, K., and E. M. Rathje, (2009). "Pore Pressure Generation of Silty Sands due to Induced Cyclic Shear Strains." *Journal of Geotechnical and Geoenvironmental Engineering*, Vol. 135, 1892-1905.
- Idriss, I. M., and Boulanger, R. W., (2008). "Soil Liquefaction during Earthquakes." Monograph MNO-12, Earthquake Engineering Research Institute, Oakland, CA, 261 pp.

- Jacobsen, L. S., (1930). "Steady Forced Vibrations as Influenced by Damping." *Transactions of the American Society of Mechanical Engineers*, Vol. 52, 169-181.
- Jefferies, M.G. and K. Been, (2006). *Soil Liquefaction – A critical state approach*. 1st Edition, Taylor & Francis, 478 pp.
- Kikkawa, N., Orense, R. P., and M. J. Pender, (2013). "Observations on microstructure of pumice particles using computed topography." *Canadian Geotechnical Journal*, Vol. 50, 1109-1117.
- Kishida, T., Wehling, T. M., Boulanger, R. W., Driller, M. W., and Stokoe, K. H. (2009). "Dynamic properties of highly organic soils from Montezuma Slough and Clifton Court," *Journal of Geotechnical and Geoenvironmental Engineering*, Vol. 135, 525-532.
- Kramer, S. L., (2000). "Dynamic Response of Mercer Slough Peat." *Journal of Geotechnical and Geoenvironmental Engineering*, Vol. 126, 504-510.
- Kraupa, T. J., Mason. H. B., Stuedlein, A. W., and C. C. Higgins, (2014a). "Characterization of Ecoroofs and Ecoroof Materials," *Geo-Characterization and Modeling for Sustainability, GeoCongress 2014*, ASCE, Atlanta, GA, 10 pp.
- Kraupa, T. J., Stuedlein, A. W., Mason. H. B., and Higgins, C. C. (2014b). "Geotechnical Characterization and Drained Shear Strength of Ecoroof Soil." *Journal of Geotechnical and Geoenvironmental Engineering*, submitted.
- Ladd, R. S., (1978). "Preparing Test Specimens Using Undercompaction." *Geotechnical Testing Journal*, Vol. 1, 16-23.
- Liptan, T., and E. Strecker, (2003). "EcoRoofs (Greenroofs)—a more sustainable infrastructure." *Proceedings National Conference on Urban Stormwater: Enhancing Programs at the Local Level*, Chicago, IL, 198-214.
- Mazzotti, S. and J. Adams, (2004). "Variability of near-term probability for the next great earthquake on the Cascadia subduction zone." *Bulletin of the Seismological Society of America*, Vol. 94, 1954-1959.
- Monkul, M. M. and J. A. Yamamuro, (2011). "Influence of silt size and content on liquefaction behavior of sands." *Canadian Geotechnical Journal*, Vol. 48, 931-942.
- Mulilis, J.P., Seed, H.B., Chan, C.K., Mitchell, J.K., and K. Arulanandan, (1977). "Effects of sample preparation on sand liquefaction." *Journal of Geotechnical Engineering*, Vol. 103, 91-108.
- Peacock, W. H. and H. B. Seed, (1968). "Sand liquefaction under cyclic loading simple shear conditions." *Journal of the Soil Mechanics and Foundation Division*, Vol. 94, 689-703.

- Polito, C. P., and J. R. Martin, (2001). "Effects of non-plastic fines on the liquefaction resistance of sands," *Journal of Geotechnical and Geoenvironmental Engineering*, Vol. 127, 408–415.
- Seed, H. B., and I. M. Idriss, (1967). "Analysis of Soil Liquefaction: Niigata Earthquake." *Journal of the Soil Mechanics and Foundations Division*, Vol. 93, 83-108.
- Seed, H. B., and I. M. Idriss, (1970). "Soil Moduli and Damping Factors for Dynamic Response Analyses." *Report No. EERC 70-10*, Berkeley, CA.
- Seed, H. B. and W. H. Peacock, (1971). "Test Procedures for Measuring Soil Liquefaction Characteristics." *Journal of the Soil Mechanics and Foundation Division*, Vol. 97, 1099-1119.
- Seed, H. B., (1979). "Soil Liquefaction and Cyclic Mobility Evaluation for Level Ground During Earthquakes." *Journal of the Geotechnical Engineering Division*, Vol. 105, 201-255.
- Spolek, G., (2008). "Performance monitoring of three ecoroofs in Portland, Oregon." *Urban Ecosyst*, Vol. 11, 249-259.
- Vucetic, M., and R. Dobry, (1991). "Effect of Soil Plasticity on Cyclic Response." *Journal of Geotechnical Engineering*, Vol. 117, 89-107.
- Wehling, T. M., Boulanger, R. W., Arulnathan, R., Harder, L. F., and M. W. Driller, (2003). "Nonlinear Dynamic Properties of a Fibrous Organic Soil." *Journal of Geotechnical and Geoenvironmental Engineering*, Vol. 129, 929-939.
- Yamamuro J. A., and K.M. Covert, (2001). "Monotonic and cyclic liquefaction of very loose sands with high silt content." *Journal of Geotechnical and Geoenvironmental Engineering*, Vol. 127, 314-324.
- Yasuda, S., Wakamatsu, K., and H. Nagase, (1994). "Liquefaction of artificially filled silty sands." *Geotechnical Special Publication*, Vol. 44, 91–104.

5.9 Tables

Table 5.1: Gradational properties for targeted gradations.

Gradation	FC (%)	D_{50} (mm)	C_u	e_{min}	e_{max}
Fine	35	0.15	19.6	1.37	2.20
Intermediate	22	0.53	59.8	1.41	2.03
Coarse	12	2.70	74.6	2.09	2.54

Table 5.1: Damping ratios in percent for reconstituted specimens sheared with $\sigma'_v = 30$ kPa.

$D_r = 30\%$				
Gradation	$\gamma_c = 1.5\%$ $f = 1$ Hz	$\gamma_c = 1.5\%$ $f = 2$ Hz	$\gamma_c = 4\%$ $f = 1$ Hz	$\gamma_c = 4\%$ $f = 2$ Hz
Fine	32	36	33	36
Intermediate	32	42	39	40
Coarse	32	29	29	35
$D_r = 50\%$				
Gradation	$\gamma_c = 1.5\%$ $f = 1$ Hz	$\gamma_c = 1.5\%$ $f = 2$ Hz	$\gamma_c = 4\%$ $f = 1$ Hz	$\gamma_c = 4\%$ $f = 2$ Hz
Fine	33	38	34	33
Intermediate	29	39	39	39
Coarse	31	30	31	31

5.10 Figures

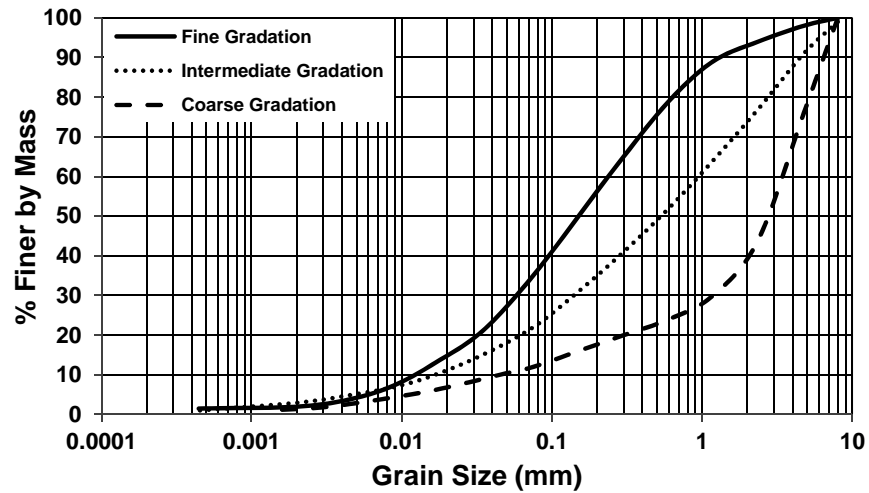


Figure 5.1: Targeted grain size distributions.

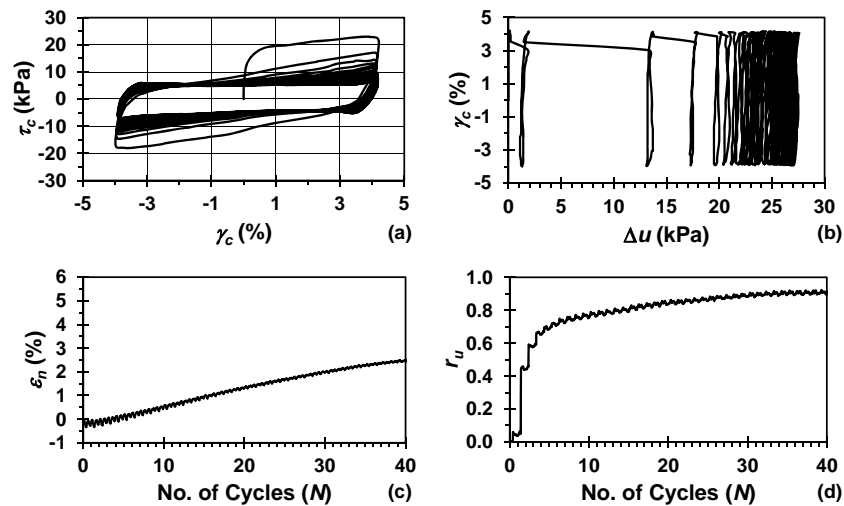


Figure 5.2: Typical results from the fine gradation specimen reconstituted to $D_r = 30$ percent, with $\gamma_c = 4\%$ CSS test for the first 40 cycles where: (a) cyclic stress-strain loops (b) cyclic shear strain induced excess pore pressure (c) specimen normal strain (d) excess pore pressure ratio. Note: $f = 2$ Hz.

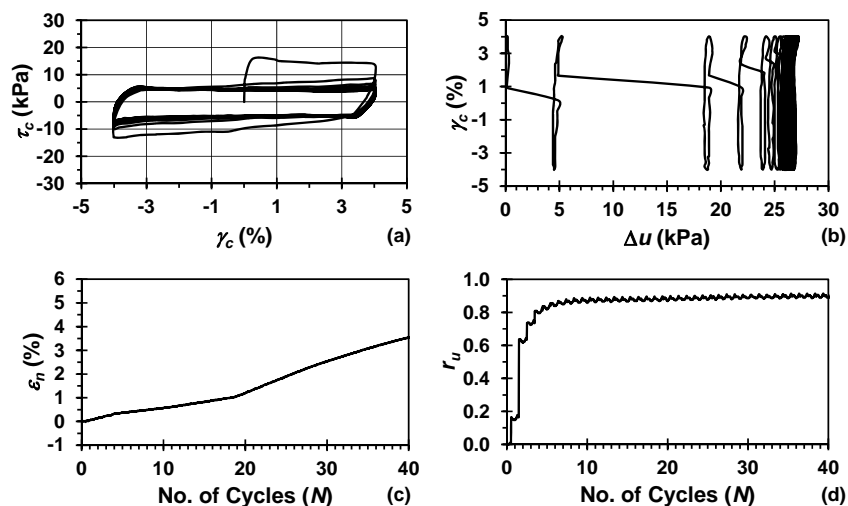


Figure 5.3: Typical results from the intermediate gradation specimen reconstituted to $D_r = 30$ percent, with $\gamma_c = 4\%$ CSS test for the first 40 cycles where: (a) cyclic stress-strain loops (b) cyclic shear strain induced excess pore pressure (c) specimen normal strain (d) excess pore pressure ratio. Note: $f = 2$ Hz.

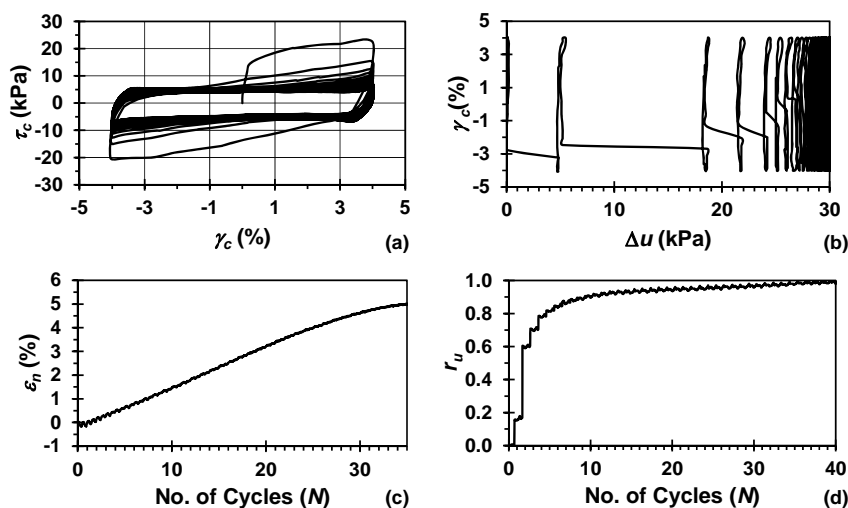


Figure 5.4: Typical results from the coarse gradation specimen reconstituted to $D_r = 30$ percent, with $\gamma_c = 4\%$ CSS test for the first 40 cycles where: (a) cyclic stress-strain loops (b) cyclic shear strain induced excess pore pressure (c) specimen normal strain (d) excess pore pressure ratio. Note: $f = 2$ Hz.

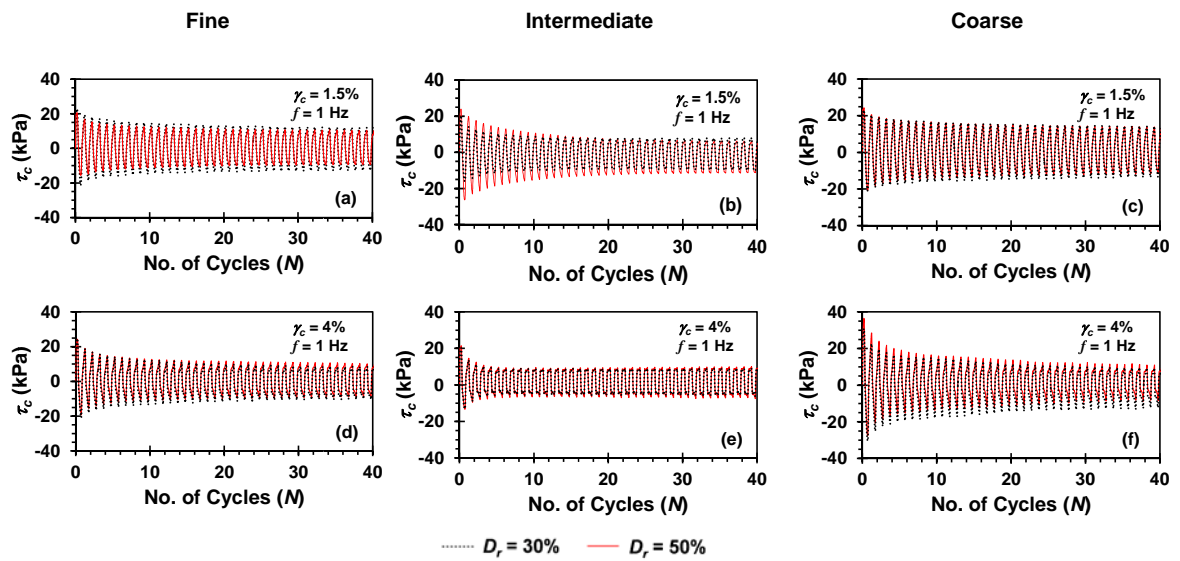


Figure 5.5: One hertz cyclic shear stress response at both relative densities for the fine (a, d), intermediate (b, e), and coarse (c, f) reconstituted specimens with $\gamma_c = 1.5$ and 4 percent, respectively.

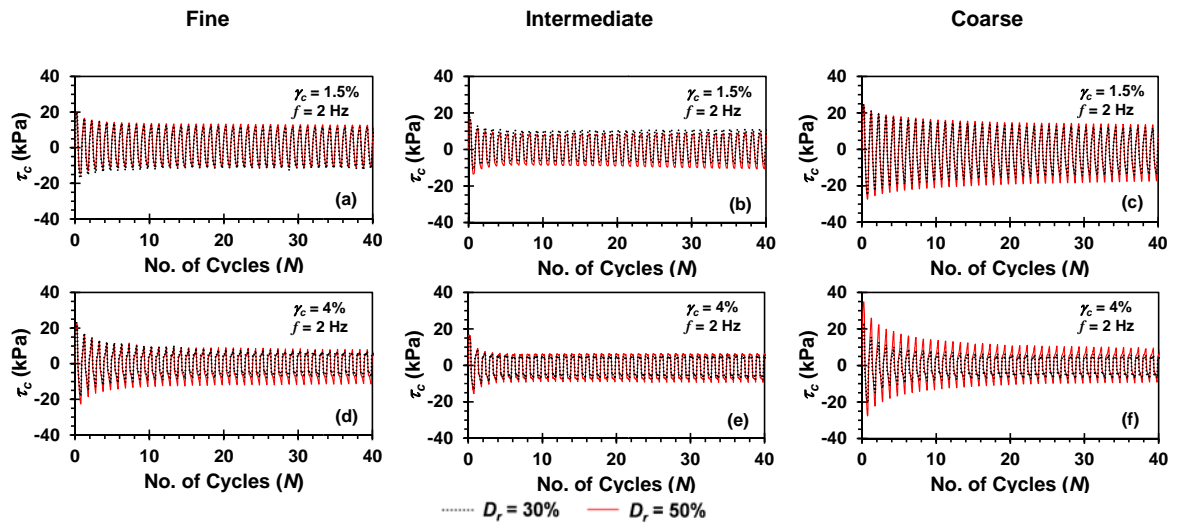


Figure 5.6: Two hertz cyclic shear stress response at both relative densities for the fine (a, d), intermediate (b, e), and coarse (c, f) reconstituted specimens with $\gamma_c = 1.5$ and 4 percent, respectively.

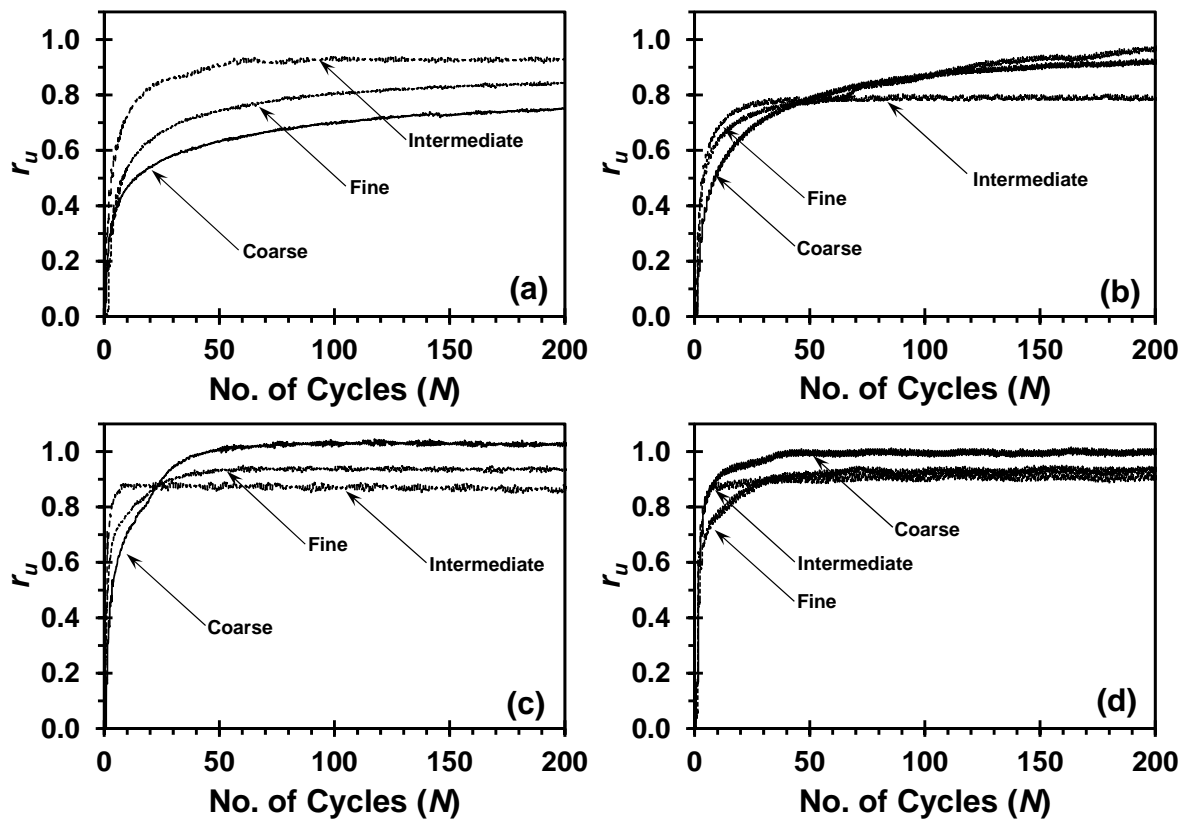


Figure 5.7: Excess pore pressure ratio versus number of cycles for specimens reconstituted to $D_r=30$ percent: (a,b) $\gamma_c = 1.5\%$ and $f = 1, 2$ Hz respectively (c,d) $\gamma_c = 4\%$ and $f = 1, 2$ Hz respectively.

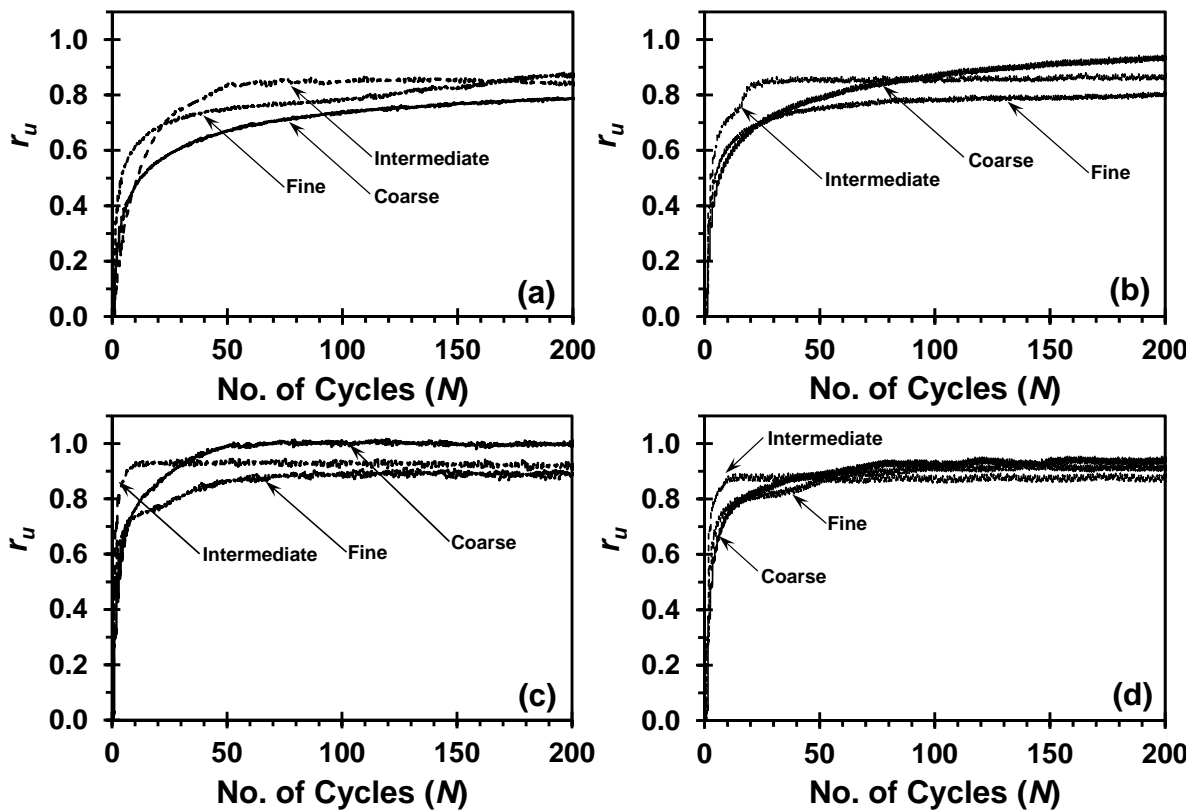


Figure 5.8: Excess pore pressure ratio versus number of cycles for specimens reconstituted to $D_r = 50$ percent: (a,b) $\gamma_c = 1.5\%$ and $f = 1, 2$ Hz respectively (c,d) $\gamma_c = 4\%$ and $f = 1, 2$ Hz respectively.

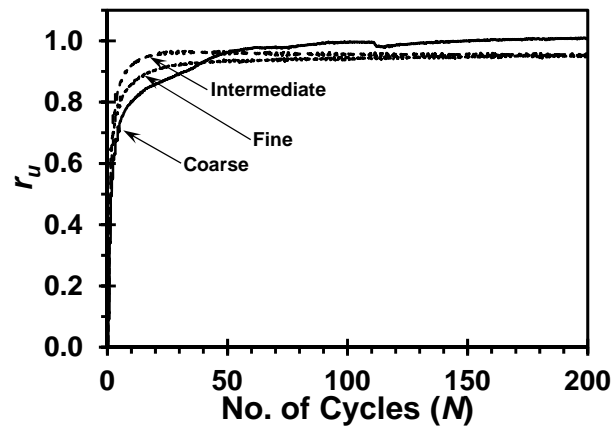


Figure 5.9: Specimens reconstituted to $D_r = 50$ percent and $\sigma'_v = 100$ kPa, excess pore pressure ratio versus number of cycles.

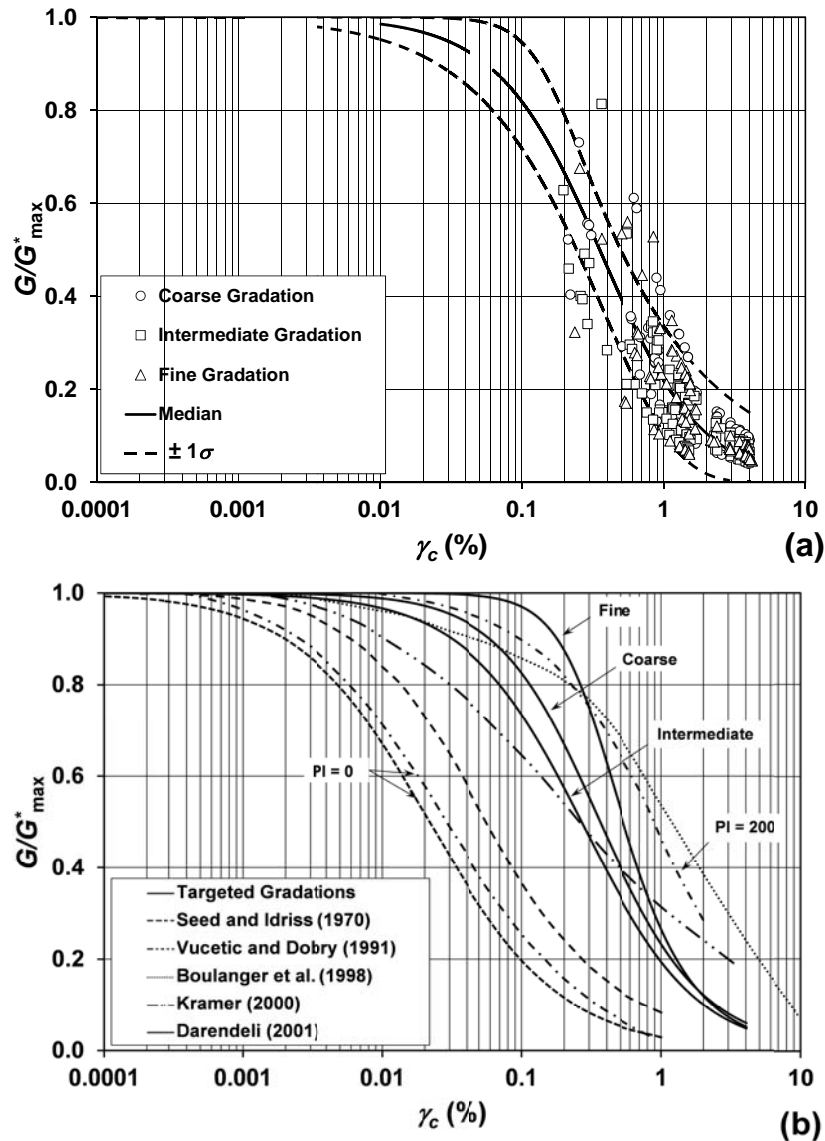


Figure 5.10: (a) Median and $\pm 1\sigma$ modulus reduction curves for all $\sigma'_v = 30$ kPa reconstituted specimens; (b) Median modulus reduction curves for the target gradations compared to the modulus reduction curves for: peat soil (Boulanger et al. 1998 and Kramer 2000-upper bound), upper bound clean sand (Seed and Idriss 1970), PI = 0 and 200 fine grained soils (Vucetic and Dobry 1991) and PI = 0 soil (Darendeli 2001).

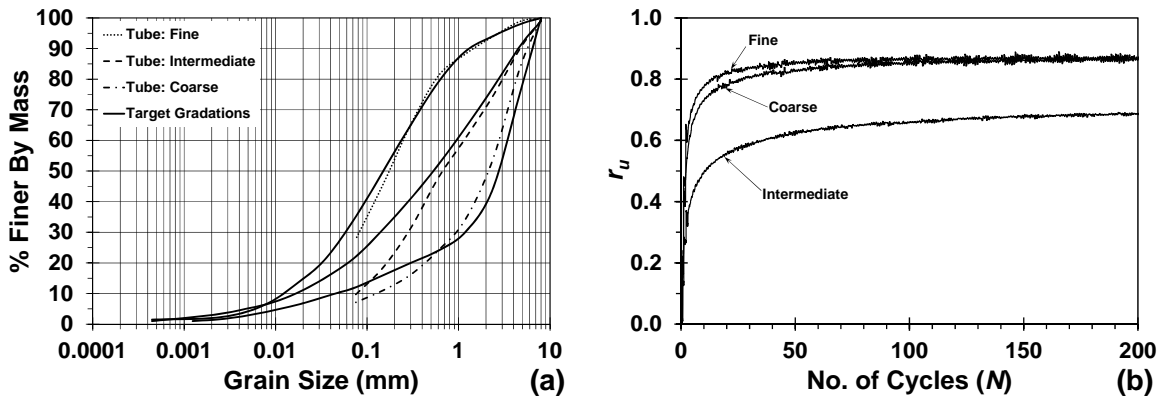


Figure 5.11: (a) Tube and targeted reconstituted specimen grain size distributions and (b) tube specimen excess pore pressure ratio versus number of cycles, with $f = 1$ Hz and $\sigma'_v = 30$ kPa.

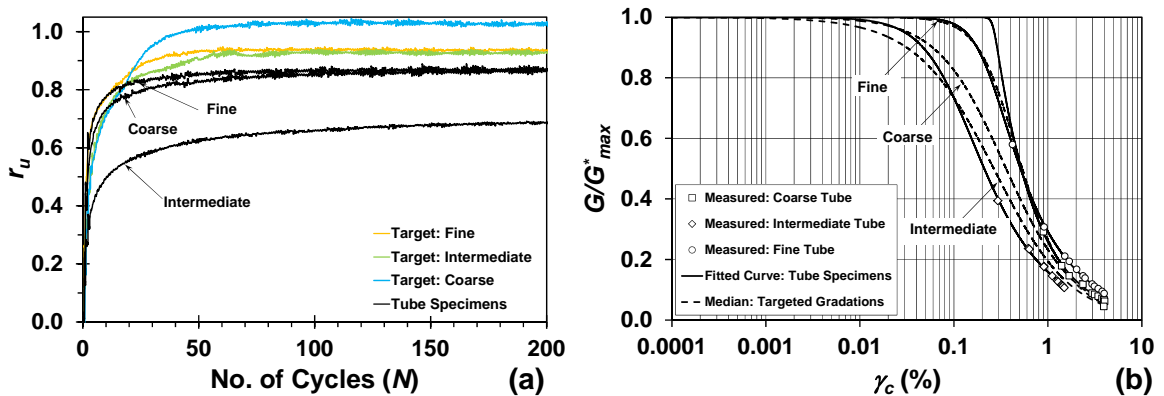


Figure 5.12: Comparison between the undisturbed tube and reconstituted specimens (a) excess pore pressure response, and (b) modulus reduction curves. The colored line types represent the associated specimen reconstituted to $D_r = 30$ percent and tested under similar parameters (i.e. γ_c, f , and σ'_v) to its respective tube specimen.

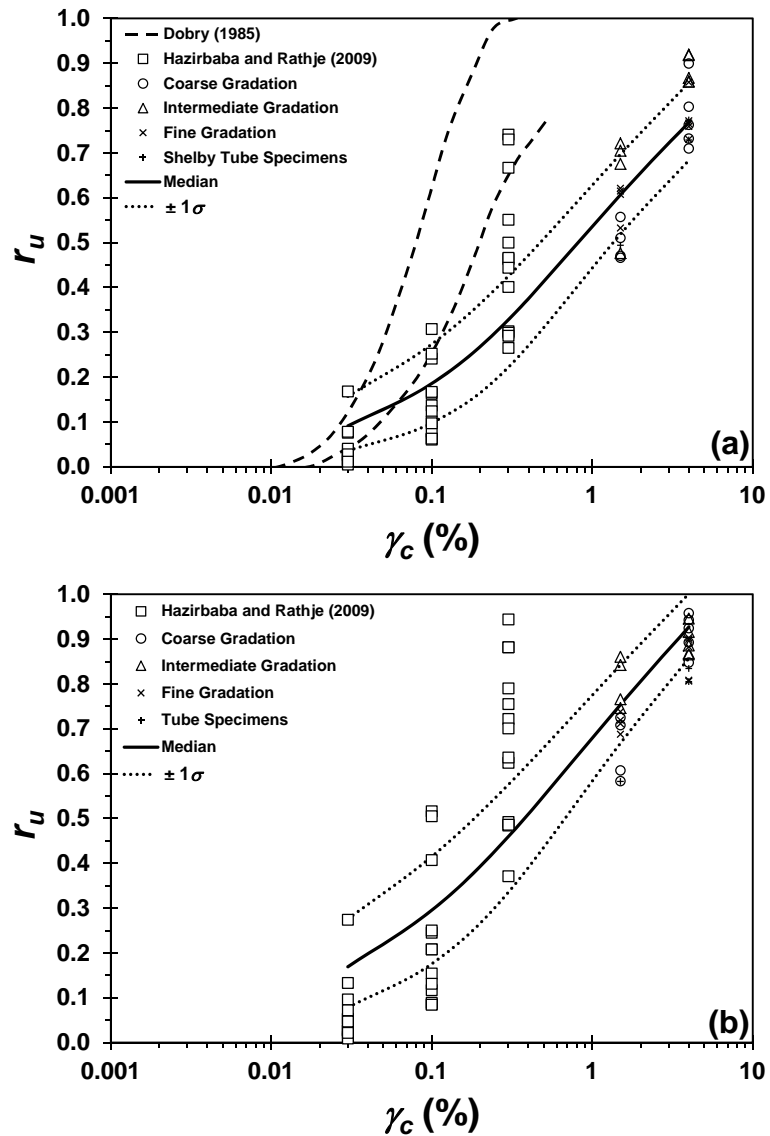


Figure 5.13: Comparison of generated excess pore pressure ratio to previous studies for all tests (a) $N=10$ cycles (b) $N=30$ cycles. Note: Roof displacement model is given by the median and plus and minus one standard deviation, and provides only an estimation for the generation of excess pore pressure.

Chapter 6: Summary and Conclusions

6.1 Summary

The recent proliferation of ecoroofs and lack of design standards in the United States has raised concerns about the engineering performance of ecoroof systems. For example, the geotechnical engineering properties of ecoroof soil have not been extensively investigated prior to this study. Accordingly, the objectives of this investigation were to develop an initial database of geotechnical index properties, and to quantify the drained static soil response and undrained dynamic soil response for targeted gradations of ecoroof soil. A field exploration provided the ecoroof soil used in this study and provided the basis for developing the database of geotechnical index properties. Three representative ecoroof soil gradations were developed and used to reconstitute strength test specimens to evaluate the drained simple shear and undrained cyclic simple shear response. Additionally, relatively undisturbed specimens were tested to understand the effect of organic content on the static and cyclic responses.

6.2 Summary and Conclusions

6.2.1 Field Exploration and Geotechnical Characterization Properties

1. The types of ecoroof systems and ecoroof construction methods encountered during the field exploration in Portland, Oregon varied significantly. Specifically, the soil depth, vegetation type, frequency of irrigation, frequency of maintenance, and drainage conditions, varied significantly between ecoroofs.

2. The variation in the geotechnical index properties of ecoroof soil was noted to be significant and was quantified using probability distribution functions and the coefficient of variation, COV . The properties that exhibited the highest level of variation were the gradational properties. The $COVs$ for the grain size thresholds corresponding to 10 and 50 percent finer, D_{10} and D_{50} , respectively, and coefficients of uniformity and curvature, C_u and C_c , respectively, were 82, 79, 94, and 119 percent, respectively.
3. The variation of D_{10} , D_{50} , C_u , and O_c were best described using the lognormal distribution.

6.2.2 Drained Static Simple Shear Response

1. Reconstituted ecoroof specimens sheared in drained simple shear appeared to yield at a shear strain of one percent. This observation was noted for each of the three target gradations and the two relative densities investigated. Therefore, the variation in the magnitude of the secant shear modulus with gradational characteristics and normal stress levels was characterized using a shear strain of one percent.
2. Dilation occurred for all of the specimens reconstituted with the coarse gradation, and for all specimens reconstituted using the intermediate gradation except one. The volumetric response of the reconstituted specimens depended directly on the ecoroof gradation.
3. The mobilized friction angle of the reconstituted specimens increased with an increase in the uniformity of the gradation. However, the mobilized friction angle

remained relatively similar for specimens with the same normal stress and relative density.

4. The reconstituted specimens exhibited strain hardening responses. Definitive peak shear strengths were not observed, and a defined critical state was not achieved. The strain hardening response was most likely observed because the magnitudes of applied normal stresses were relatively low.
5. Compared to the reconstituted specimens, the relatively undisturbed tube specimens exhibited smaller magnitudes of mobilized shear strength, and began to approach a critical state at the end of shearing. Unlike the reconstituted specimens, contractive volumetric responses were observed for all the undisturbed tube specimens. Therefore, the organic content directly influences the stress-strain and volumetric response of ecoroof soil.

6.3.3 Undrained Cyclic Simple Shear Properties

1. The pore pressure response of reconstituted ecoroof soil specimens was determined to depend mostly on the gradation.
2. Liquefaction potential for reconstituted and relatively undisturbed tube specimens was observed to be dependent on the gradation, cyclic shear strain amplitude, relative density, and organic content.
3. Specimens reconstituted using the intermediate target gradation required the lowest number of loading cycles to achieve liquefaction.

4. The modulus reduction curves for the reconstituted specimens followed relatively similar trends to modulus reduction curves developed for peats. In general, the modulus reduction response shows that more shear strain is required to induce significant softening in the ecoroof soils as compared to other sandy soils (Seed and Idriss 1970; and Darendeli 2001), and fine grained soils (Vucetic and Dobry 1991). Damping values for the first stress-strain loop were quantified and were observed to range from 29 to 40 percent, which are significantly higher than similar sandy soils (Seed and Idriss 1970; Darendeli 2001), which show damping ratios of approximately 25 percent and 20 percent for confining stresses of 143 and 101 kPa, respectively.
5. The relatively undisturbed tube specimens indicated that the presence of organic content increases the liquefaction resistance of ecoroof soil.
6. Comparison of cyclic simple shear response of ecoroof soils to silty sand soils indicated that the generation of excess pore pressure increased with an increase in shear strain amplitude and number of loading cycles. The generation of excess pore pressure in strain controlled CSS tests (e.g. Hazirbaba and Rathje 2009 and this study) were less than the response shown in relatively similar CTX strain controlled tests (Dobry 1985).

6.3 Future Work

Ecoroof sampling was limited to 18 buildings in Portland, Oregon. Portland, Oregon has its own design needs for ecoroofs, especially with regards to climate and earthquake potential. Expansion of the field exploration program to other cities across the United

States would allow for a more complete database of the geotechnical index properties and associated variability. Understanding the variation in ecoroof soils is a critical task for supporting the development of ecoroof standards in the United States.

Additional static and dynamic tests should be conducted on the target and other ecoroof soil gradations. Specifically, undrained static tests would allow for the comparison to undrained cyclic simple shear data from this study, and additional dynamic soil tests should be conducted on the target and other gradations to quantify the small-strain shear modulus and develop full modulus reduction and damping curves. Bender elements and resonant column devices would be appropriate for determination of these parameters. Additionally, surface wave testing of ecoroof soils would help further characterize the small-strain behavior.

Due to the multidisciplinary aspect of this investigation, further experimental work will be conducted, to develop appropriate recommendations for ecoroof standards; specifically, mid- and full-scale tests of ecoroof materials. The mid-scale shake table studies will allow for a full system ecoroof (i.e. all layers) to be evaluated in response to lateral loads. Additionally, the ability to test a variation in: soil depths, saturation level, gradation, and ecoroof type (i.e. layering system) with a mid-scale shake table will aid in understanding how an ecoroof system responds to lateral loading will substantially aid in the development of ecoroof design standards in the United States. The results from the mid-scale shake table tests will also inform the future investigators of proper design parameters for the full-scale load tests.

References

- Airey, D.W and Wood, D.M. (1987). "An evaluation of direct simple shear tests on clay." *Geotechnique*, 37 (1), 25-35.
- Airey, D. W., Budhu, M., and Wood, D. M. (1985). "Some Aspects of the Behavior of Soils in Simple Shear." *Developments of Soil Mechanics and Foundation Engineering*, Vol. 2, 185-213.
- Amer, M. I., Kovacs, W. D., and Aggour, M. S. (1987). "Cyclic Simple Shear Size Effects." *Journal of Geotechnical Engineering*, Vol. 113, 693-707.
- ASTM Standard D2487, (2006). "Standard Practice for Classification of Soils for Engineering Purposes (Unified Soil Classification System)." ASTM, West Conshohocken, PA.
- ASTM Standard D422, 1963 (2007). "Standard Test Method for Particle-Size Analysis of Soils." ASTM International, West Conshohocken, PA.
- ASTM Standard D2974, (2007). "Standard Test Methods for Moisture, Ash, and Organic Matter of Peat and Other Organic Soils." ASTM International, West Conshohocken, PA.
- ASTM Standard D6913, (2009). "Standard Test Methods for Particle-Size Distribution (Gradation) of Soils Using Sieve Analysis." ASTM International, West Conshohocken, PA.
- ASTM Standard D2216, (2010). "Standard Test Methods for Laboratory Determination of Water (Moisture) Content of Soil and Rock by Mass." ASTM International, West Conshohocken, PA.
- ASTM Standard D4318, (2010). "Standard Test Methods for Liquid Limit, Plastic Limit, and Plasticity Index of Soils." ASTM International, West Conshohocken, PA.
- ASTM Standard D854, (2010). "Standard Test Methods for Specific Gravity of Soil Solids by Water Pycnometer." ASTM International, West Conshohocken, PA.
- Atkinson, J. H., and Lau, W. H. W. (1991). "Measurement of soil strength in simple shear tests." *Canadian Geotechnical Journal*, Vol. 28, 255-262.
- Bardet, J. P., (1997). *Experimental Soil Mechanics*, 1st Edition, Prentice Hall, Upper Saddle River, NJ, 582pp.
- Bjerrum, L., and Landva, A. (1966). "Direct Simple-Shear Tests on A Norwegian Quick Clay." *Geotechnique*, 16 (1), 1-20.

- Borden, R. H., Shao, L., and A. Gupta, (1996). "Dynamic Properties of Piedmont Residual Soils." *Journal of Geotechnical Engineering*, Vol. 122, 813-821.
- Boulanger, R. W., Seed, R. B., Chan, C. K., Seed, H. B., and J. Sousa, (1991). "Evaluation Behavior of Saturated Sands Under Uni-directional and Bi-directional Monotonic and Cyclic Simple Shear Loading," *Report No. UCB/GT/91-08*, Berkeley, CA.
- Boulanger, R. W., Chan, C. K., Seed, H. B., Seed, R. B., and Sousa, J. B., (1993). "A low-compliance bi-directional cyclic simple shear apparatus." *ASTM Geotechnical Testing Journal*, Vol. 16, 36-45.
- Boulanger, R. W., Arulnathan, R., Harder Jr., L. F., Torres, R. A., and M. W. Driller, (1998). "Dynamic Properties of Sherman Island Peat." *Journal of Geotechnical and Geoenvironmental Engineering*, Vol. 12, 12-20.
- Boulanger, R. W. and I. M. Idriss, (2006). "Liquefaction Susceptibility Criteria for Silts and Clays." *Journal of Geotechnical and Geoenvironmental Engineering*, Vol. 132, 1413-1426.
- Bray, J. D., and R. B. Sancio, (2006). "Assessment of the Liquefaction Susceptibility of Fine-Grained Soils." *Journal of Geotechnical and Geoenvironmental Engineering*, Vol. 132, 1165-1177.
- Brennan, A.J., Thusyanthan, N. I., Madabhushi, S. P. G. (2004). "Evaluation of Shear Modulus and Damping in Dynamic Centrifuge Test." *Cambridge University Engineering Department Technical Report*, CUED/D-SOILS/TR-336: pp. 36
- Budhu, M. (1985). "Lateral stresses observed in two simple shear apparatus." *J. Geotechnical Engineering. Div., ASCE* 111 (6), 698-711.
- Budhu, M. and Britto, A. (1987). "Numerical Analysis of Soils in Simple Shear Devices." *Soils and Foundations*, 27 (2), 31-41.
- Budhu, M. (1988). "A New Simple Shear Apparatus." *Geotechnical Testing Journal*, 11 (4), 281-287.
- Darendeli, M. B., (2001). "Development of a New Family of Normalized Modulus Reduction and Material Damping Curves." *Ph.D. Dissertation*, University of Texas, Austin, Texas, 362 pp.
- De Alba, P., Seed, H. B., and C. K. Chan, (1976). "Sand Liquefaction in Large-Scale Simple Shear Tests." *Journal of the Geotechnical Engineering Division*, Vol. 102, 909-927.

- De Josselin De Jong, G. (1971). "Discussion: Session 2. Stress-strain behaviour of soil." *Proceedings Roscoe Memorial Symposium*, Parry, R. H. G., G. T. Foulis & Co. Eds., 258-261.
- Dobry, R., Ladd, R. S., Yokel, F. Y., Chung, R. M., and D. Powell, (1982). "Prediction of pore water pressure buildup and liquefaction of sands during earthquakes by the cyclic strain method." *National Bureau of Standards Building Sciences*, Rep. No. 138.
- Dobry, R. (1985). "Liquefaction of soils during earthquakes." *National Research Council*, Rep. No. CETS-EE-001.
- Doherty J.P. and Fahey M. (2011). "Three dimensional finite element analysis of the direct simple shear test." *Computers and Geotechnics*, 38, 341-346.
- Dounias, G. T. and Potts, D. M. (1993). "Numerical Analysis of Drained Direct and Simple Shear Tests." *Journal of Geotechnical Engineering*, 119, 1870-1891.
- Dunnett, N., Nagase, A., and Hallam, A. (2008a). "The dynamics of planted and colonizing species on a green roof over six growing seasons 2001–2006: influence of substrate depth" *Urban Ecosyst*, Vol. 11, 373–384.
- Figuroa, J., Saada, A., Liang, L., and N. Dahisaria, (1994). "Evaluation of Soil Liquefaction by Energy Principles." *Journal of Geotechnical Engineering*, Vol. 120, 1554–1569.
- Finn, W. D. L., Pickering, D. J., and Bransby, P. L. (1971). "Sand liquefaction in triaxial and simple shear tests." *Journal of Soil Mechanics and Foundation Engineering*, Vol. 97, 639-659.
- Forschungsgesellschaft Landschaftsentwicklung Landschaftsbau (FLL), (2008) "Guidelines for the Planning, Construction and Maintenance of Green Roofing – Green Roofing Guideline," Germany.
- Fountain, H. (2011). "Green Roof Collapses in Illinois." *The New York Times*. Accessed February 18, 2011. <http://green.blogs.nytimes.com/2011/02/18/greenroocollapsessinillinois/>
- Franke, E., Kiebusch, M., Schuppener, B. (1979). "A New Direct Simple Shear Device." *Geotechnical Testing Journal*, 2 (4), 190-199.
- Friedrich, C. (2008). "Selecting the Proper Components for a Green Roof Growing Media." 2nd National Low Impact Development Conference, Wilmington, NC, 240-251.
- Getter, K. L., and Rowe, D. B. (2006). "The Role of Extensive Green Roofs in Sustainable Development." *HORTSCIENCE*, 41 (5), 1276-1285.

- Goldfinger, C., Nelson, C. H., Morey, A., Johnson, J. E., Gutierrez-Pastor, J., Eriksson, A. T., Karabanov, E., Patton, J., Gracia, E., Enkin, R., Dallimore, A., Dunhill, G., and T. Vallier, (2012). "Turbidite Event History: Methods and Implications for Holocene Paleoseismicity of the Cascadia Subduction Zone." *USGS Professional Paper 1661-F*, Reston, VA, U.S. Geological Survey, pp. 184.
- Hazirbaba, K., and E. M. Rathje, (2009). "Pore Pressure Generation of Silty Sands due to Induced Cyclic Shear Strains." *Journal of Geotechnical and Geoenvironmental Engineering*, Vol. 135, 1892-1905.
- Holtz, R. D., Kovacs, W. D., and Sheahan, T. C. (2011). *An Introduction to Geotechnical Engineering*, Pearson Education Inc. 2nd edition, Upper Saddle River, NJ, 853 pp.
- Houlsby, G. T. (1991). "How the Dilatancy of Soils Affects Their Behavior." *Written version from invited lecture at: Tenth European Conference on Soil Mechanics and Foundation Engineering*, Florence, Italy, 1-15.
- Hutchinson, D., Abrams, P., Retzlaff, R., and Liptan, T. (2003). "STORMWATER MONITORING TWO ECOROOFs IN PORTLAND, OREGON, USA" *Greening Rooftops for Sustainable Communities*, Chicago, IL.
- Idriss, I. M., and Boulanger, R. W., (2008). "Soil Liquefaction during Earthquakes." Monograph MNO-12, Earthquake Engineering Research Institute, Oakland, CA, 261 pp.
- Jacobsen, L. S., (1930). "Steady Forced Vibrations as Influenced by Damping." *Transactions of the American Society of Mechanical Engineers*, Vol. 52, 169-181.
- Jefferies, M.G. and K. Been, (2006). *Soil Liquefaction – A critical state approach*. 1st Edition, Taylor & Francis, 478 pp.
- Jewel, R. A. and Wroth, C. P. (1987). "Direct shear tests on reinforced sand." *Geotechnique*, 31 (1), 53-68.
- Jones, A.L., Kramer, S.L., and Arduino, P. (2000) "Estimation of Uncertainty in Geotechnical Properties for Performance-Based Earthquake Engineering." Pacific Earthquake Engineering Research Center, Report PEER 2002/16, 114.
- Kikkawa, N., Orense, R. P., and M. J. Pender, (2013). "Observations on microstructure of pumice particles using computed topography." *Canadian Geotechnical Journal*, Vol. 50, 1109-1117.
- Kishida, T., Wehling, T. M., Boulanger, R. W., Driller, M. W., and Stokoe, K. H. (2009). "Dynamic properties of highly organic soils from Montezuma Slough and Clifton Court," *Journal of Geotechnical and Geoenvironmental Engineering*, Vol. 135, 525-532

- Kjellman, W. (1951). "Testing the Shear Strength of Clay in Sweden." *Geotechnique*, 2 (3), 225-232.
- Kramer, S. L., (2000). "Dynamic Response of Mercer Slough Peat." *Journal of Geotechnical and Geoenvironmental Engineering*, Vol. 126, 504-510.
- Kraupa, T. J., Mason, H. B., Stuedlein, A. W., and C. C. Higgins, (2014a). Characterization of Ecoroofs and Ecoroof Materials, *Geo-Characterization and Modeling for Sustainability, GeoCongress 2014*, ASCE, Atlanta, GA, 10 pp.
- Kraupa, T. J., Stuedlein, A. W., Mason, H. B., and Higgins, C. C. (2014b). "Geotechnical Characterization and Drained Shear Strength of Ecoroof Soil." *Journal of Geotechnical and Geoenvironmental Engineering*, submitted.
- Ladd, R. S., (1978). "Preparing Test Specimens Using Undercompaction." *Geotechnical Testing Journal*, Vol. 1, 16-23.
- Lanzo, G., Vucetic, M., and Doroudian, M. (1997). "Reduction of Shear Modulus at Small Strains in Simple Shear." *Journal of Geotechnical and Geoenvironmental Engineering*, Vol. 123, 1035-1042.
- Liptan, T., and Strecker, E. (2003) "EcoRoofs (Greenroofs)—a more sustainable infrastructure." Proceedings National Conference on Urban Stormwater: Enhancing Programs at the Local Level, Chicago, IL, 198-214.
- Lu, N., Ristow, G. H., and Likos, W. J. (2000). "The Accuracy of Hydrometer Analysis for Fine-Grained Clay Particles." *Geotechnical Testing Journal*, 23 (4), 487-495.
- Lucks, A. S., Christian, J. T., Brandow, G. E., and Høeg, K. (1972). "Stress Conditions in NGI Simple Shear Test." *Journal of Soil Mechanics Foundation Division*. 98 (1), 155-160.
- MacMullan, E., Reich, S., Puttman, T., and Rodgers, K. (2008). "Cost- Benefit Evaluation of Ecoroofs." *Proceedings of the 2008 International LID Conference (CD-ROM)*, ASCE, Seattle, WA.
- Matesic, L. and Vucetic, M. (2003). "Strain-Rate Effect on Soil Secant Shear Modulus at Small Cyclic Strains." *Journal of Geotechnical and Geoenvironmental Engineering*, Vol. 129, 536-549.
- Matthews, M. C. (1988). "The engineering application of direct and simple shear testing" *Ground Engineering*, 21(2), 13-21.
- Mazzotti, S. and J. Adams, (2004). "Variability of near-term probability for the next great earthquake on the Cascadia subduction zone." *Bulletin of the Seismological Society of America*, Vol. 94, 1954-1959.

- Monkul, M. M. and J. A. Yamamuro, (2011). "Influence of silt size and content on liquefaction behavior of sands." *Canadian Geotechnical Journal*, Vol. 48, 931-942.
- Mortezaie, A. R. and Vucetic, M. (2012). "Small-strain Cyclic Testing With Standard NGI Simple Shear Device." *Geotechnical Testing Journal*, Vol. 35, 1-14.
- Mulilis, J.P., Seed, H.B., Chan, C.K., Mitchell, J.K., and K. Arulanandan, (1977). "Effects of sample preparation on sand liquefaction." *Journal of Geotechnical Engineering*, Vol. 103, 91-108.
- Peacock, W. H. and Seed, H. B. (1968). "Sand liquefaction under cyclic loading simple shear conditions." *Journal of the Soil Mechanics and Foundation Division*, 94, 689-703.
- Polito, C. P., and J. R. Martin, (2001). "Effects of non-plastic fines on the liquefaction resistance of sands, *Journal of Geotechnical and Geoenvironmental Engineering*, Vol. 127, 408-415.
- Prevost, J.H. and Høeg, K. (1976). "Reanalysis of simple shear soil testing and Liquefaction Testing." *Canadian Geotechnical Journal*, 13, 418-429.
- Roscoe, K.H. (1953). "An apparatus for the application of simple shear to soil samples." *Proceedings of the third International Conference on Soil Mechanics and Foundation Engineering*, Zurich, 1, 186-191.
- Rossato, G., and Simonini, P. (1991). "Stress-strain behavior of sands in triaxial and direct simple shear tests." *Canadian Geotechnical Journal*, 28, 276-281.
- Rowe, P. W. (1969). "The relation between the shear strength of sands in triaxial compression, plane strain, and direct shear." *Geotechnique*, 19 (1), 75-86.
- Saada, A.S. and Townsend F.C., (1981). "State of the Art: Laboratory strength testing of soils." *Laboratory shear strength of soils, ASTM STP 740*, Young R.N. and Townsend F.C., Eds., American Society for Testing Materials: 7-77.
- Seed, H. B., and I. M. Idriss, (1967). "Analysis of Soil Liquefaction: Niigata Earthquake." *Journal of the Soil Mechanics and Foundations Division*, Vol. 93, 83-108.
- Seed, H. B., and I. M. Idriss, (1970). "Soil Moduli and Damping Factors for Dynamic Response Analyses." *Report No. EERC 70-10*, Berkeley, CA.
- Seed, H.B. and Peacock, W.H. (1971). "Test Procedures for Measuring Soil Liquefaction Characteristics." *Journal of the Soil Mechanics and Foundation Division*, 97 (8), 1099-1119.

- Seed, H. B., (1979). "Soil Liquefaction and Cyclic Mobility Evaluation for Level Ground During Earthquakes." *Journal of the Geotechnical Engineering Division*, Vol. 105, 201-255.
- Shibuya, S. and Hight, D. W. (1987). "On the stress path in simple shear." *Geotechnique*, 34 (4), 511-515.
- Silver, M.L., Tatsuoka, F., Phukunhaphan, A., and Avramidis, A.S. (1980). "Cyclic undrained strength of sand by triaxial test and simple shear test." *In Proceedings of the 7th World Conference on Earthquake Engineering*, Istanbul, 3, 281-288.
- Spolek, G. (2008). "Performance monitoring of three ecoroofs in Portland, Oregon." *Urban Ecosyst*, Vol. 11, 349-259.
- Stovin, V., Dunnett, N., and Hallam, A. (2007). "Green Roofs- Getting Sustainable Drainage off the Ground." *Proceedings of the 6th NOVATECH International Conference of Sustainable Techniques and Strategies in Urban Water Management*, Lyon, France, Vol. 1, 11-18.
- U.S. Army Corps of Engineers (1970). "Laboratory Soil Testing." Engineer Manual EM 1110-2-1906, U.S. Government Printing Office, Washington, D.C.
- U.S. Army Corps of Engineers (1972). "Soil Sampling." Engineer Manual EM 1110-2-1907, U.S. Government Printing Office, Washington, D.C.
- Vucetic, M. and Lacasse, S. (1982). "Specimen size effect in simple shear test." *Journal of the Geotechnical Engineering Division*, Vol. 108, 1567-1585.
- Vucetic, M., and R. Dobry, (1991). "Effect of Soil Plasticity on Cyclic Response." *Journal of Geotechnical Engineering*, Vol. 117, 89-107.
- Vucetic, M., Lanzo, G., and Doroudian, M. (1998). "Damping at Small Strains in Cyclic Simple Shear Test." *Journal of Geotechnical and Geoenvironmental Engineering*, Vol. 124, 585-594.
- Weiler, S. K., and Scholz-Barth, K. (2009). *Green Roof Systems; A Guide to the Planning, Design, and Construction of Landscapes over Structure*. John Wiley & Sons: Hoboken, NJ.
- Wark, C. G., and Wark, W. W. (2003). "Green Roof Specifications and Standards." *The Construction Specifier*, 56(8): 1-12
- Wood, D. M., Drescher, A., and Budhu, M. (1979). "On the Determination of Stress State in the Simple Shear Apparatus." *Geotechnical Testing Journal*, 2 (4), 211-221.
- Wehling, T. M., Boulanger, R. W., Arulnathan, R., Harder, L. F., and M. W. Driller, (2003). "Nonlinear Dynamic Properties of a Fibrous Organic Soil." *Journal of Geotechnical and Geoenvironmental Engineering*, Vol. 129, 929-939.

- Wood, D. M., Drescher, A., and Budhu, M. (1979). "On the Determination of Stress State in the Simple Shear Apparatus." *Geotechnical Testing Journal*, 2 (4), 211-221.
- Wright, D. K., Gilbert, P. A., and Saada, A. S. (1978). "Shear devices for determining dynamic soil properties." *Proceedings Specialty Conference on Earthquake Engineering and Soil Dynamics*, ASCE, 2, 1056-1075.
- Wijewickreme, D., Dabeet, A., and Byrne, P. (2013). "Some Observations on the State of Stress in the Direct Simple Shear Test Using 3D Discrete Element Analysis." *Geotechnical Testing Journal*, 36 (2), 1-8.
- Wu, P. K., Matsushima, K., and Tatsuoka, F. (2007). "Effects of specimen size and some other factors on the strength and deformation of granular soil in direct shear tests." *Geotechnical Testing Journal*, 31 (1), 1-20.
- Yamamuro J. A., and K.M. Covert, (2001). "Monotonic and cyclic liquefaction of very loose sands with high silt content." *Journal of Geotechnical and Geoenvironmental Engineering*, Vol. 127, 314-324.
- Yasuda, S., Wakamatsu, K., and H. Nagase, (1994). "Liquefaction of artificially filled silty sands." *Geotechnical Special Publication*, Vol. 44, 91-104.

Appendix A: Sampling Program and Ecoroof Soil Characterization

Table A.1: Summary Table of Ecoroof Field Exploration

	Building Name	Ecoroof Type	Ecoroof Age (Year Constructed)	Public Access	Irrigated	Ecoroof Size (m ²)	Average Depth of samples (mm)	No. of Samples
B1	Wastewater Screenhouse	Monolithic/Extensive	April 2011	No	No	576	127	3
B2	The Portland Building	Monolithic/Extensive	2006	No	Yes	279	76.2	4
B3	The Hamilton Building	Monolithic/Extensive	1999	Partial	No	543	102	4
B4	Buchman Terrace	Monolithic/Extensive	2000	No	No	139	102	3
B5	Swan Island Pump House	Monolithic/Extensive	August 2005	No	No	604	102	4
B6	Village Homes	Monolithic/Extensive	2007	No	Yes	1301	88.9	4
B7	Riva on the Park	Monolithic/Extensive	2007	No	Yes	674	76.2	4
B8	Atwater Place	Monolithic/Extensive	2005	No	Yes	2165	95.3	4
B9	The Ardea	Monolithic/Extensive Tray/Semi-Intensive	2007	No	Yes	437	Ext.= 127 Int.= 266	6
B10	UP-Fields Hall	Monolithic/Semi-Intensive	2009	No	No	167	254	3
B11	Ramona Apartments	Monolithic/Extensive	2010	No	Yes	2973	102	4
B12	Jean Vollum Nat. Center	Monolithic/Extensive	2010	No	No	557	76.2	2
B13	John Ross	Monolithic/Extensive Tray/Semi-Intensive	2004	Yes	Yes	474	Ext.= 152 Int.= 406	5
B14	International Harvester	Tray System/Extensive	2010	No	Yes	576	127	3
B15	Broadway Housing- PSU	Monolithic/Extensive	2004	No	No	1691	152	3
B16	Mult. County Building	Monolithic-Tray/Extensive	2003	Yes	Yes	1105	152	3
B17	911 Federal Building	Monolithic/Extensive	2011	No	No	1606	152	3
B18	BPA Federal Building	Intensive	2011	Yes	Yes	1226	406	4

A.1 Grain size distributions for ecoroof material retained on No. 200 sieve, prior to removal of organic matter.

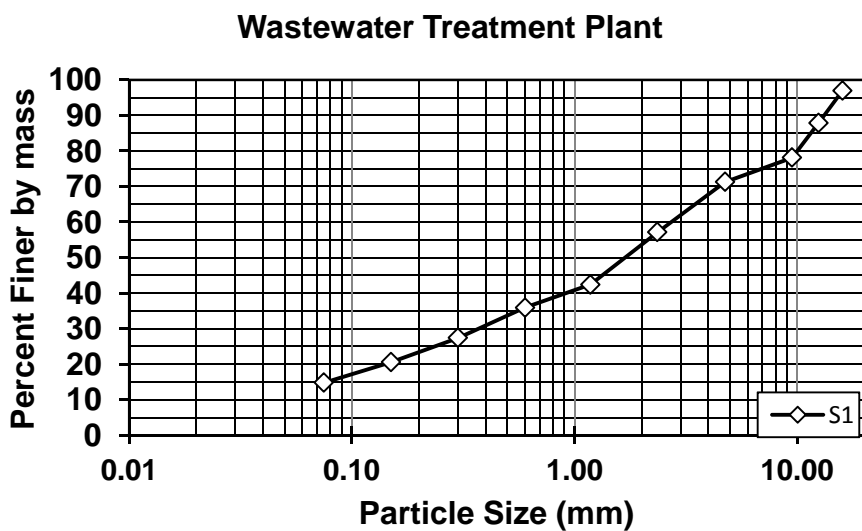


Figure A.1: Grain size distribution for Wastewater Treatment Plant-S1.

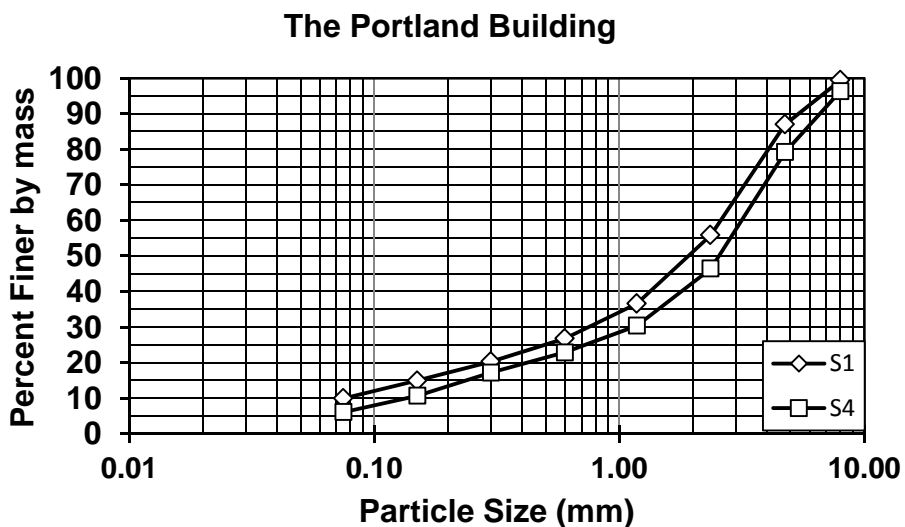


Figure A.2: Grain size distribution for the Portland Building-S1, S4.

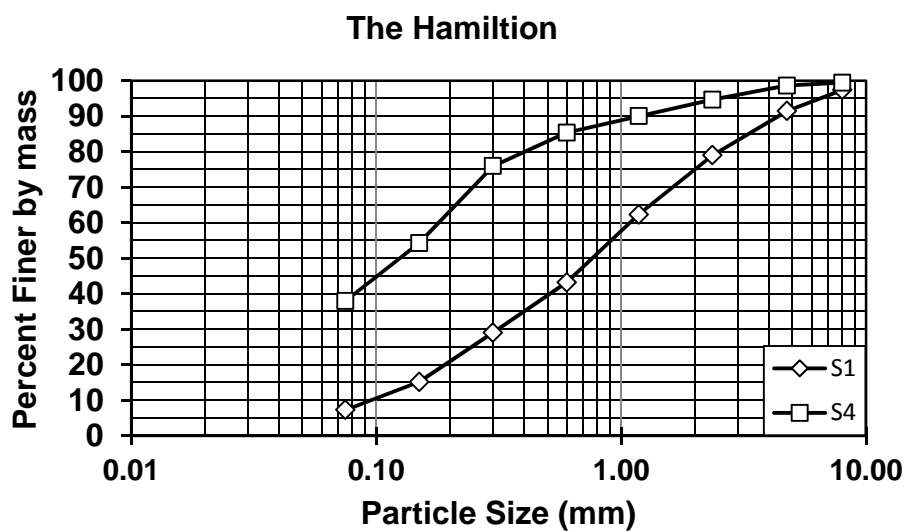


Figure A.3: Grain size distribution for the Hamilton-S1, S4.

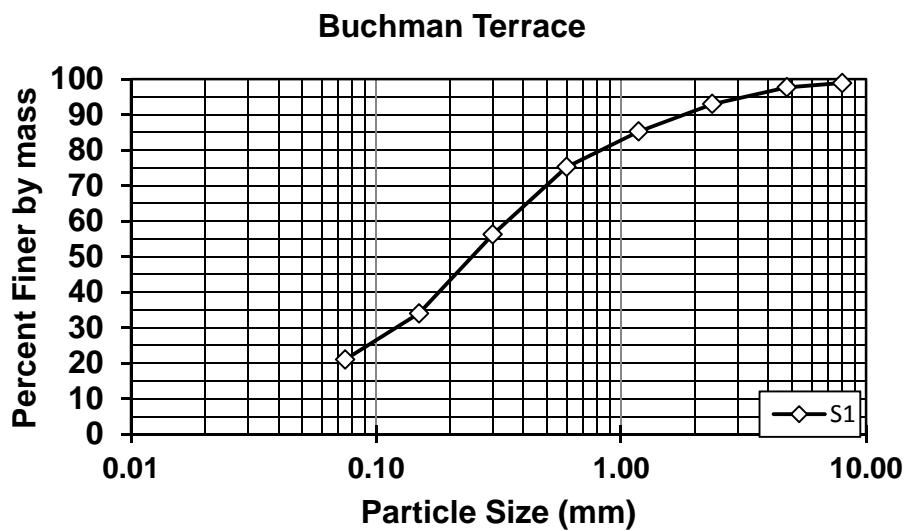


Figure A.4: Grain size distribution for the Buchman Terrace-S1.

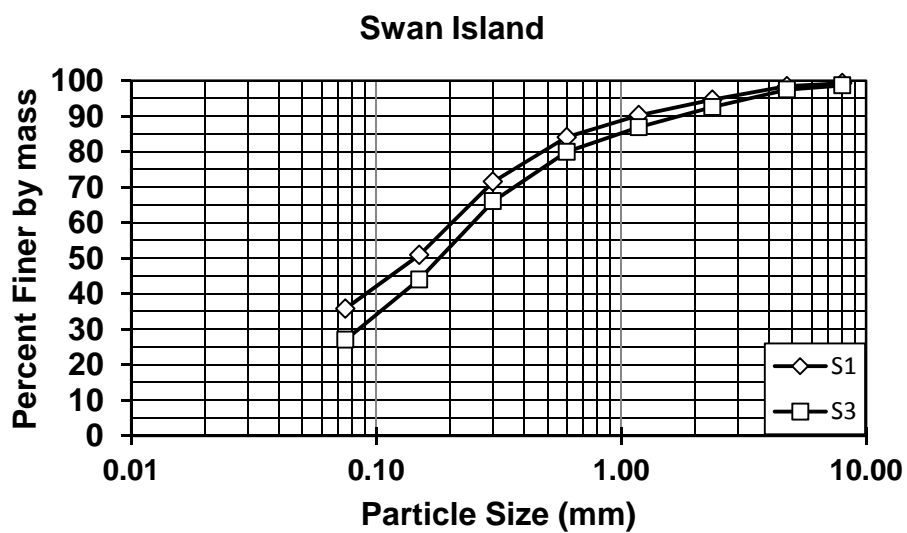


Figure A.5: Grain size distribution for Swan Island Pumphouse-S1, S3.

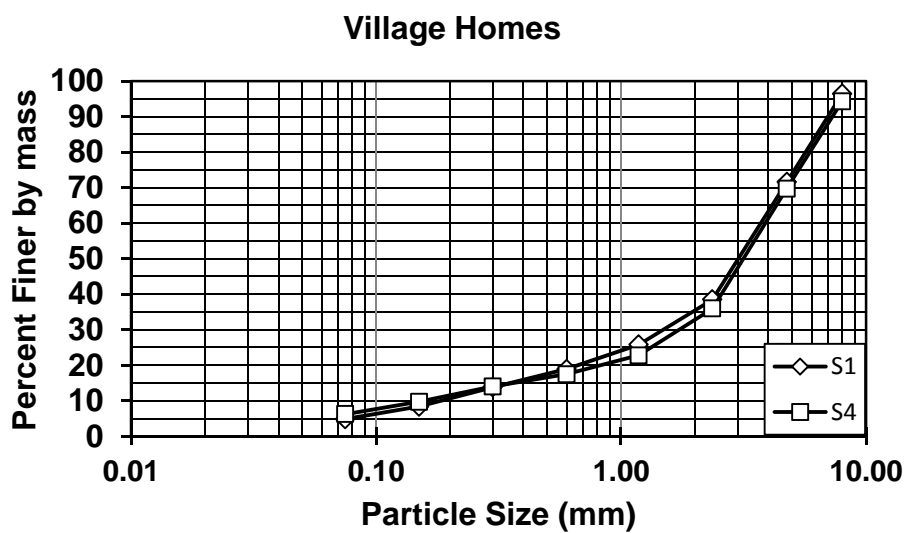


Figure A.6: Grain size distribution for the Village Home Apartments-S1, S4.

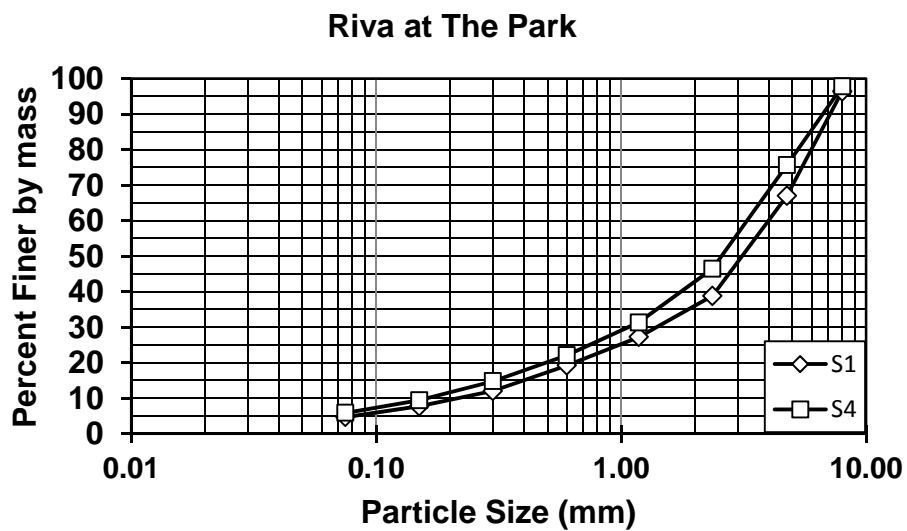


Figure A.7: Grain size distribution for Riva at the Park-S1, S4.

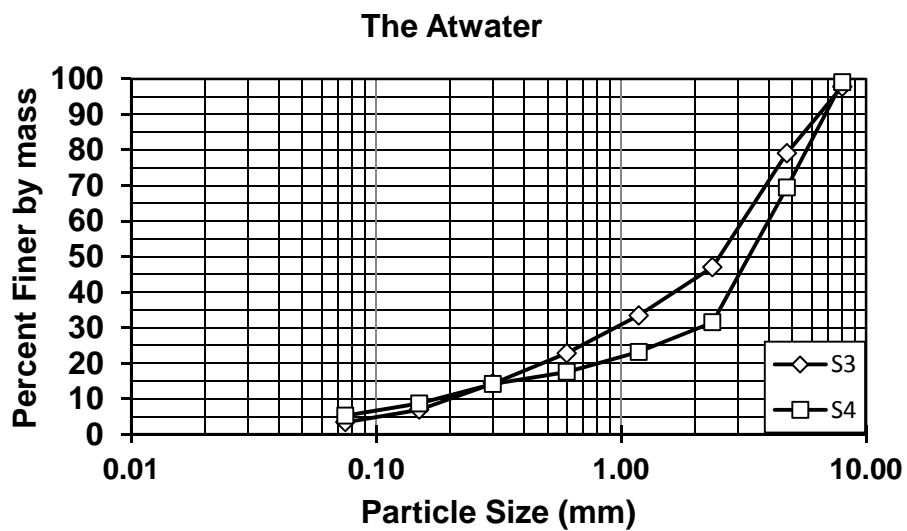


Figure A.8: Grain size distribution for the Atwater-S3, S4.

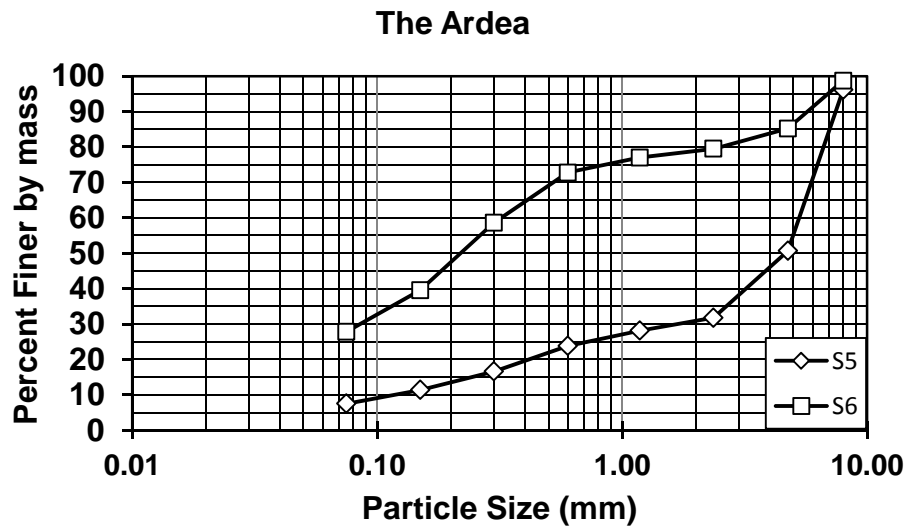


Figure A.9: Grain size distribution for Riva at the Ardea-S5, S6.

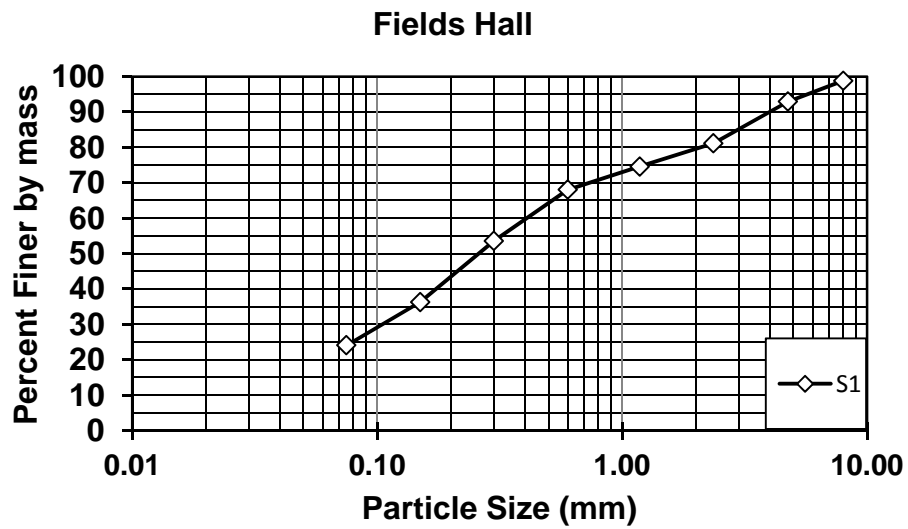


Figure A.10: Grain size distribution for Fields Hall-S1.

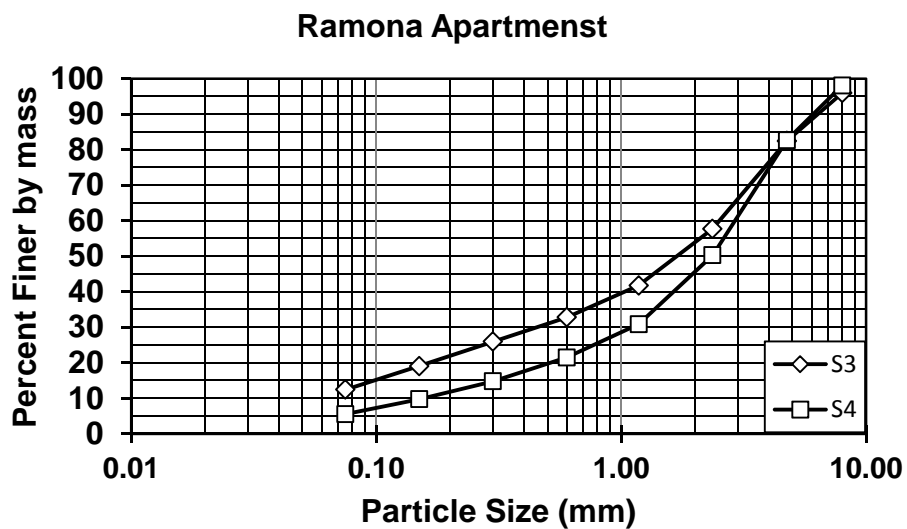


Figure A.11: Grain size distribution for Riva at Ramona Apartments-S3, S4.

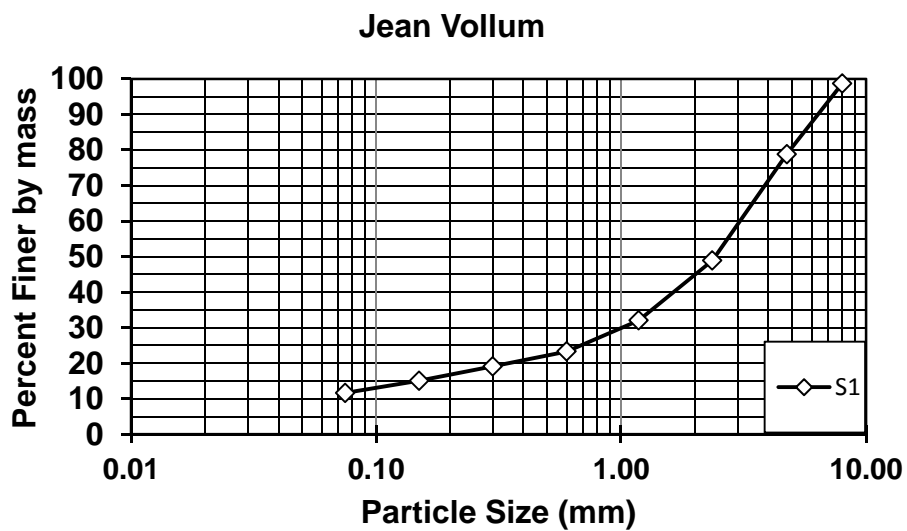


Figure A.12: Grain size distribution for Jean Vollum-S1.

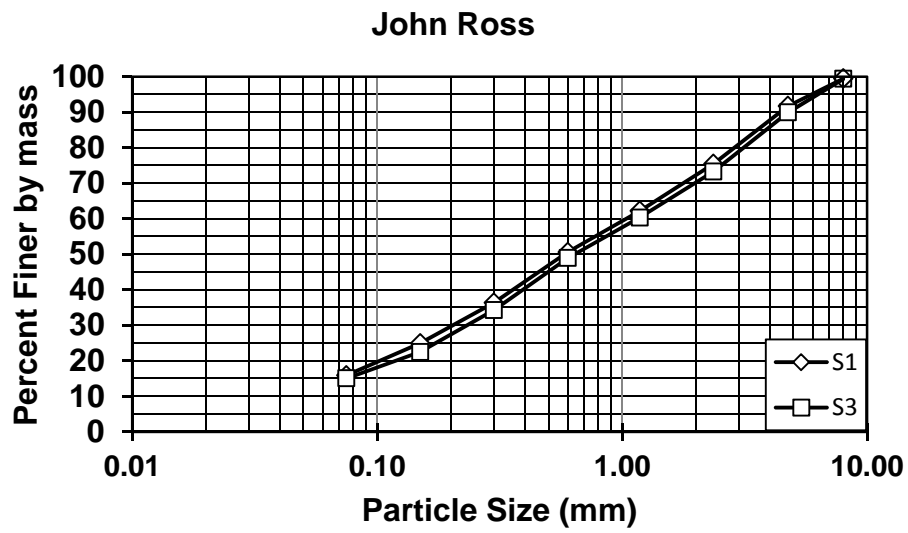


Figure A.13: Grain size distribution for John Ross-S1, S3.

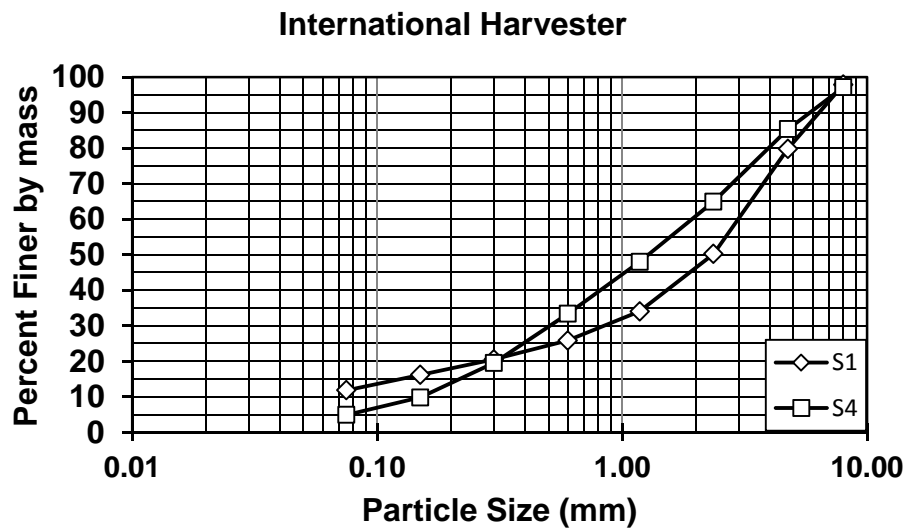


Figure A.14: Grain size distribution for International Harvester-S1, S4.

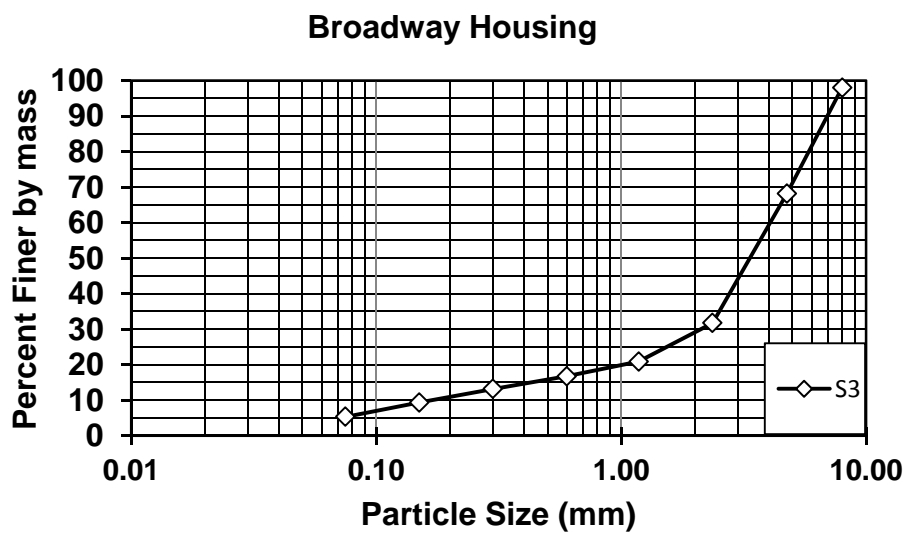


Figure A.15: Grain size distribution for Broadway Housing-S3.

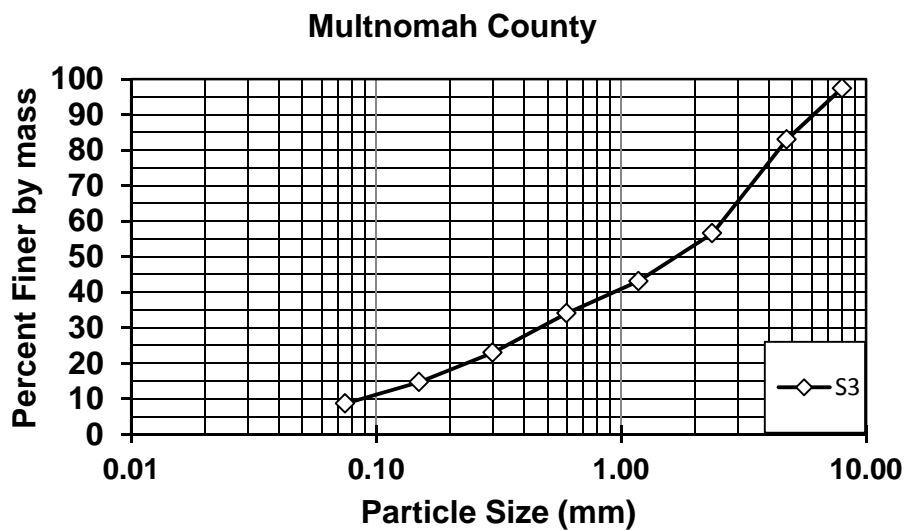


Figure A.16: Grain size distribution for Multnomah County-S3.

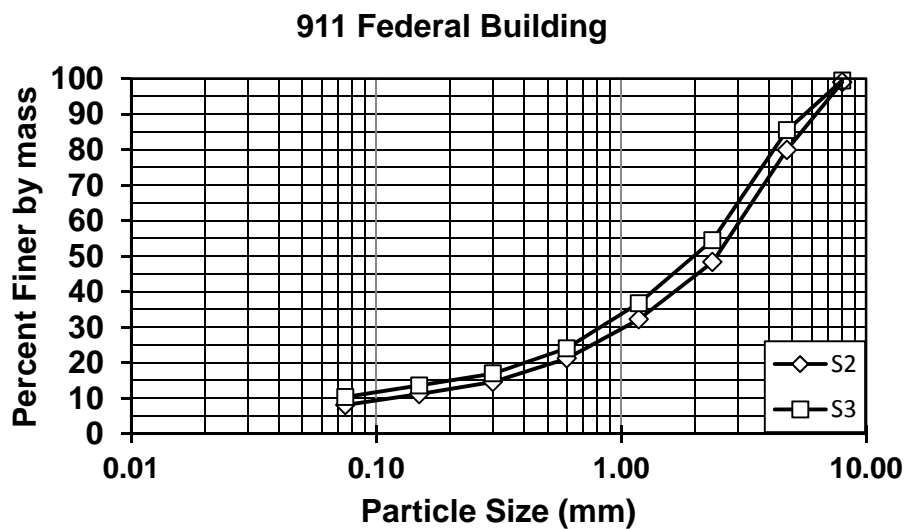


Figure A.17: Grain size distribution for 911 Federal Building-S2, S3.

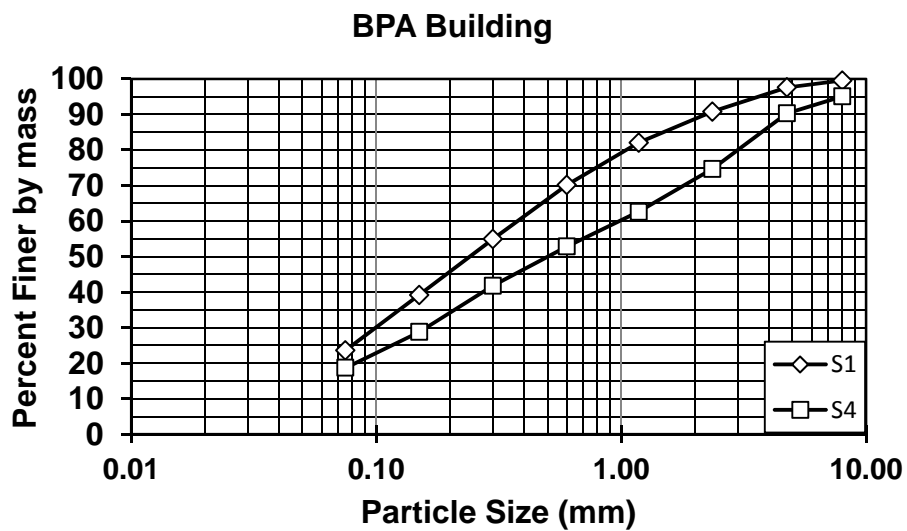


Figure A.18: Grain size distribution for BPA Building-S1, S4.

Grain size distributions for ecoroof material retained on No. 200 sieve, after removal of organic matter.

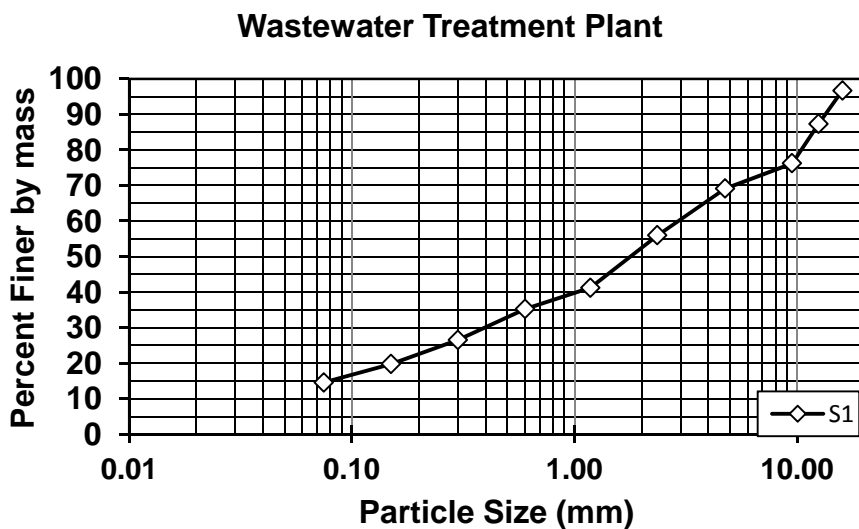


Figure A.19: Grain size distribution for Wastewater Treatment Plant-S1, no organics.

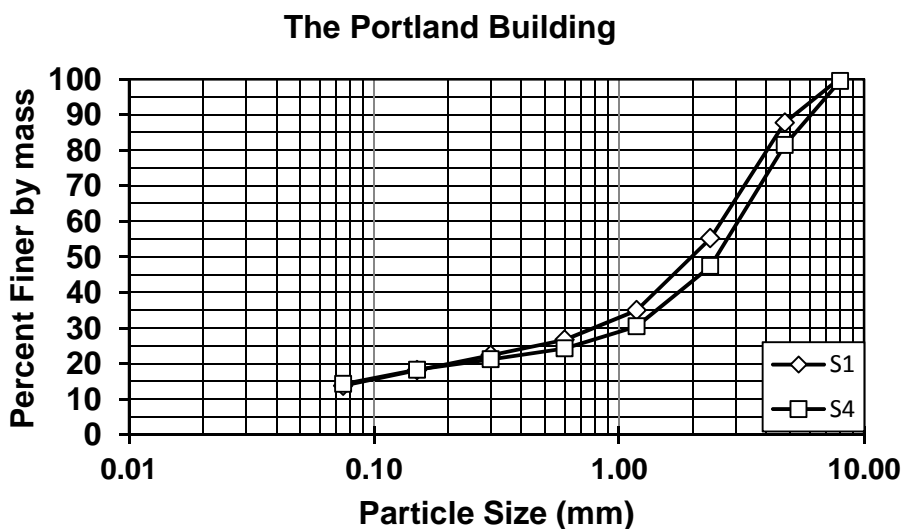


Figure A.20: Grain size distribution for the Portland Building-S1, S4, no organics.

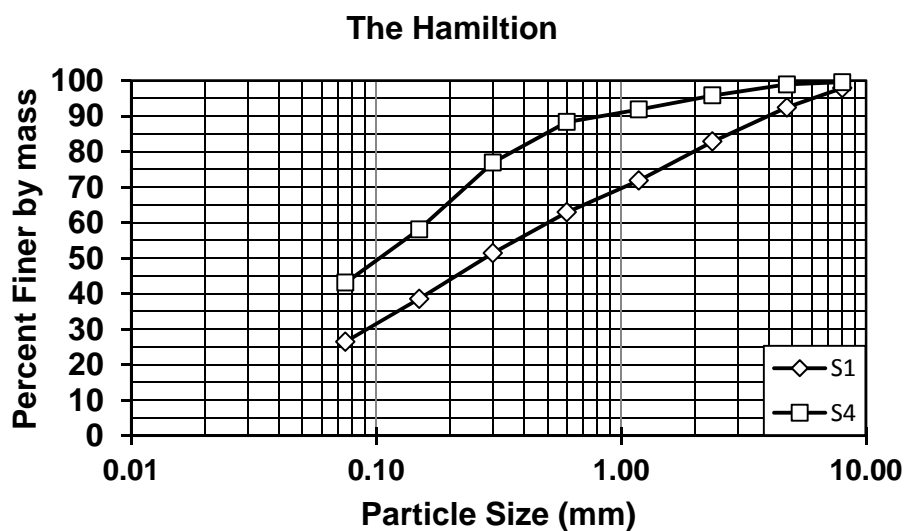


Figure A.21: Grain size distribution for the Hamilton-S1, S4, no organics.

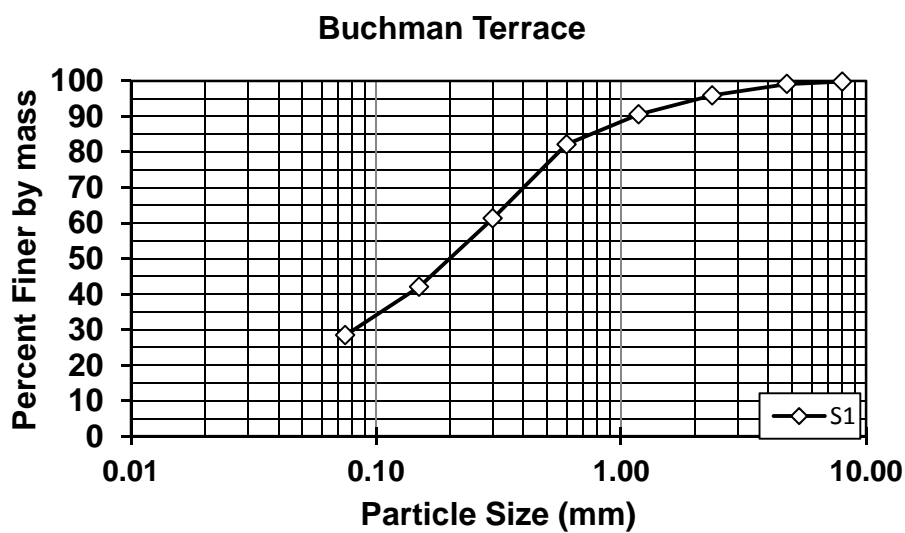


Figure A.22: Grain size distribution for the Buchman Terrace-S1, no organics.

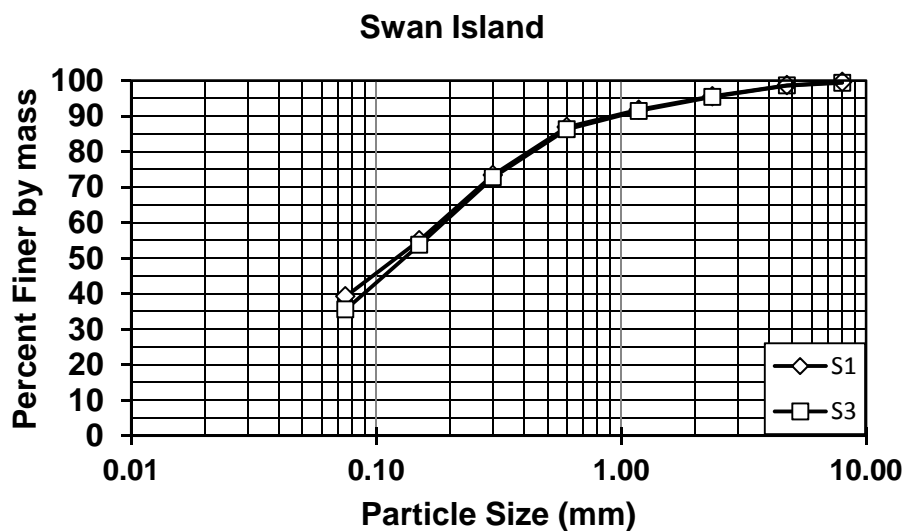


Figure A.23: Grain size distribution for Swan Island Pumphouse-S1, S3, no organics.

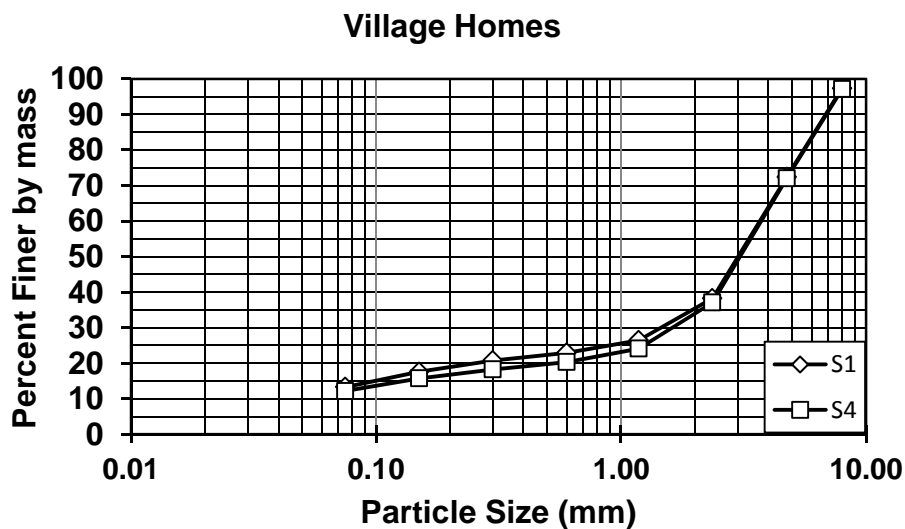


Figure A.24: Grain size distribution for the Village Home Apartments-S1, S4, no organics.

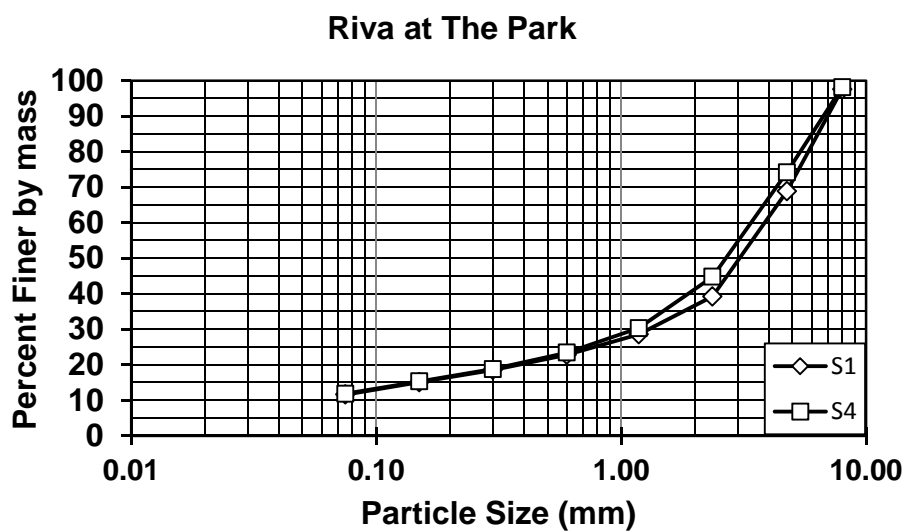


Figure A.25: Grain size distribution for Riva at the Park-S1, S4, no organics.

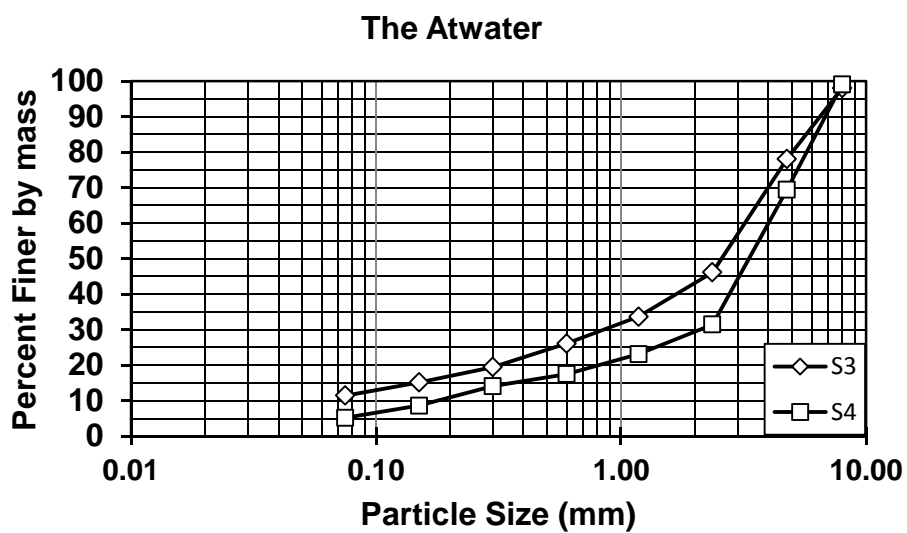


Figure A.26: Grain size distribution for the Atwater-S3, S4, no organics.

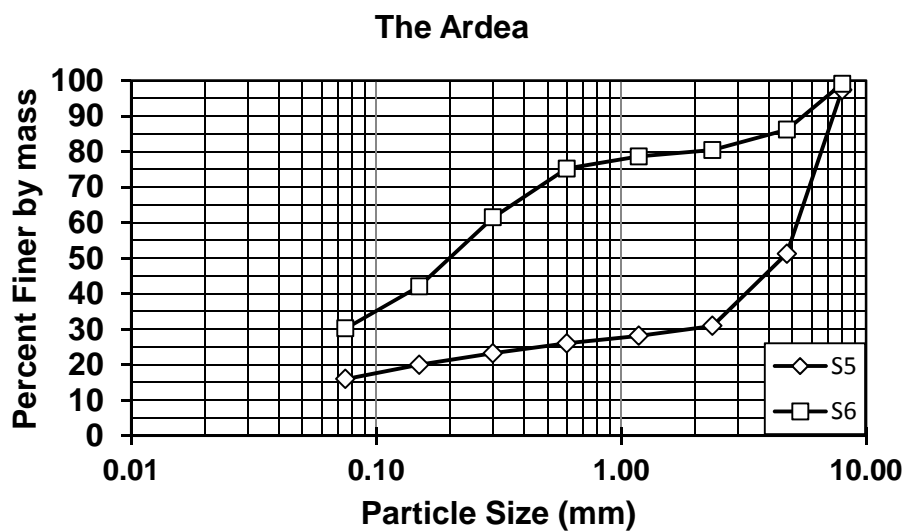


Figure A.27: Grain size distribution for Riva at the Ardea-S5, S6, no organics.

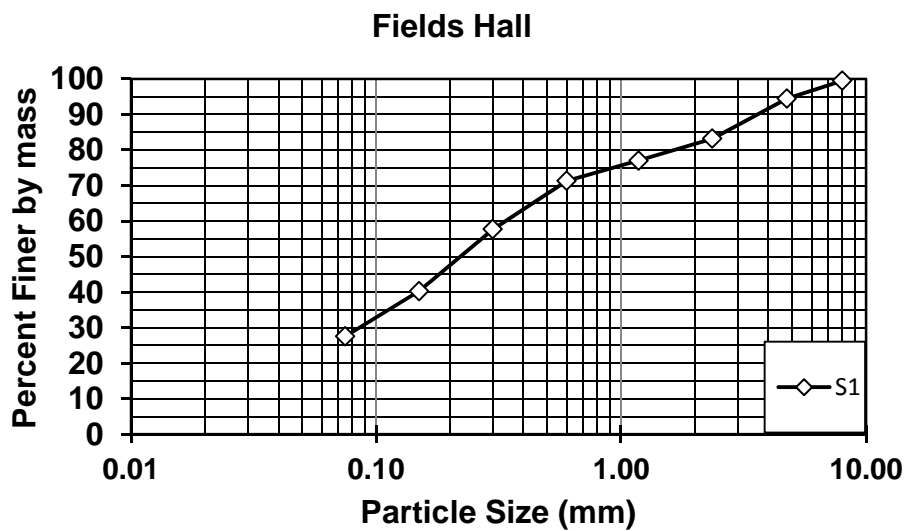


Figure A.28: Grain size distribution for Fields Hall-S1, no organics.

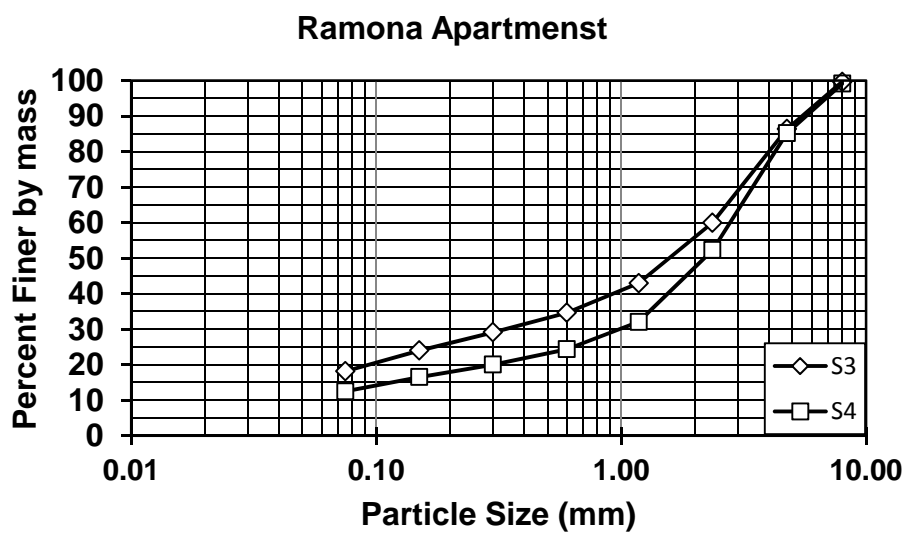


Figure A.29: Grain size distribution for Riva at Ramona Apartments-S3, S4, no organics.

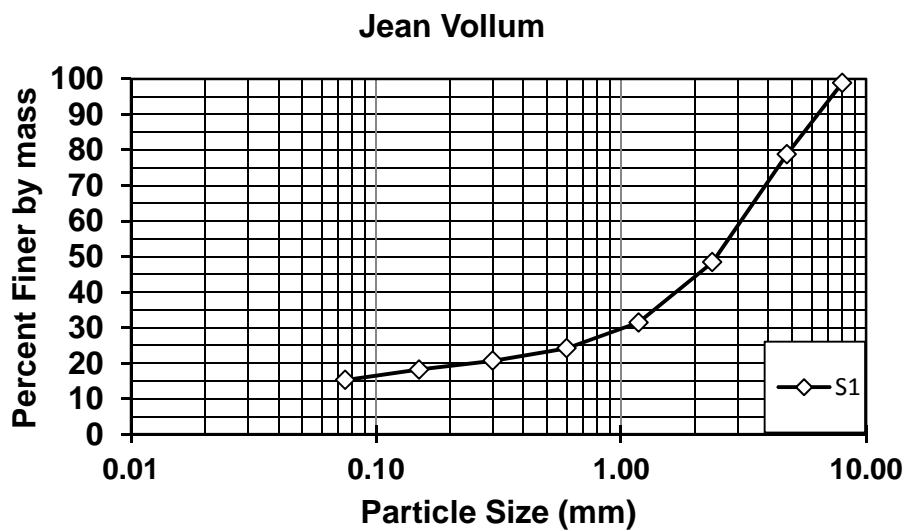


Figure A.30: Grain size distribution for Jean Vollum-S1, no organics.



Figure A.31: Grain size distribution for John Ross-S1, S3, no organics.

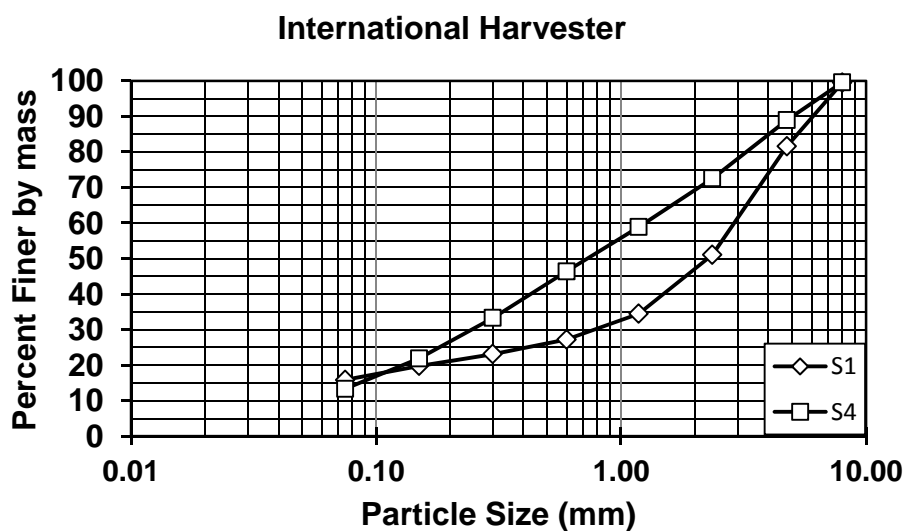


Figure A.32: Grain size distribution for International Harvester-S1, S4, no organics.

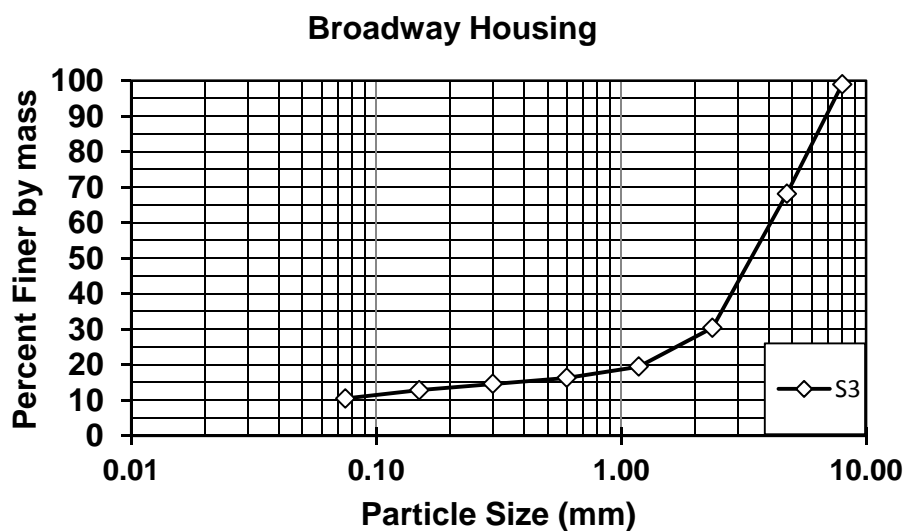


Figure A.33: Grain size distribution for Broadway Housing-S3, no organics.

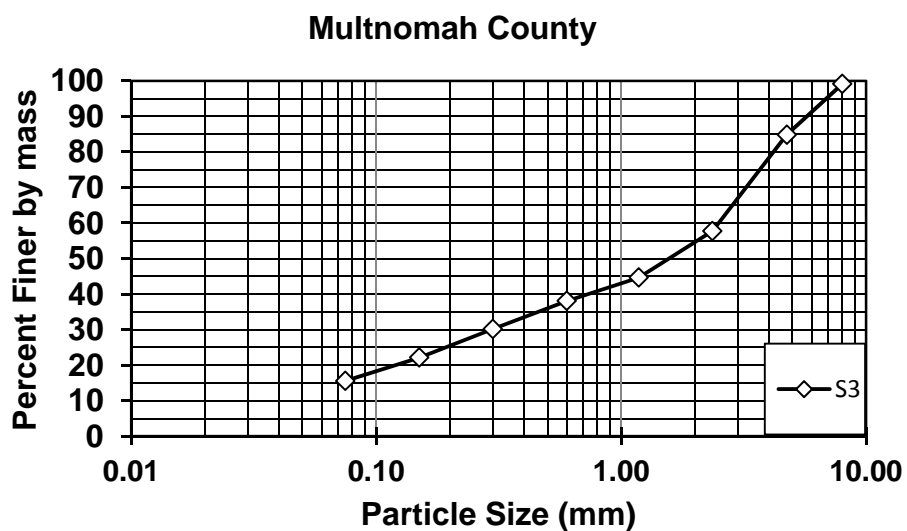


Figure A.34: Grain size distribution for Multnomah County-S3, no organics.

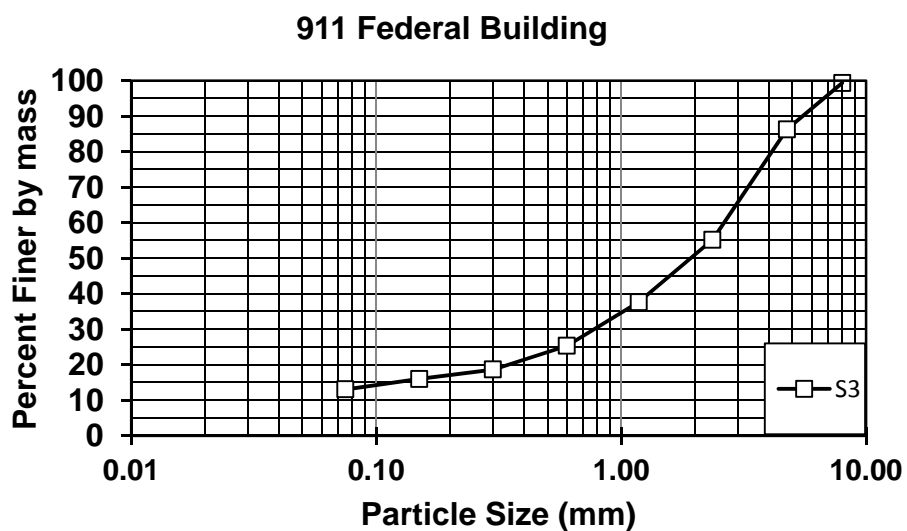


Figure A.35: Grain size distribution for 911 Federal Building-S3, no organics.

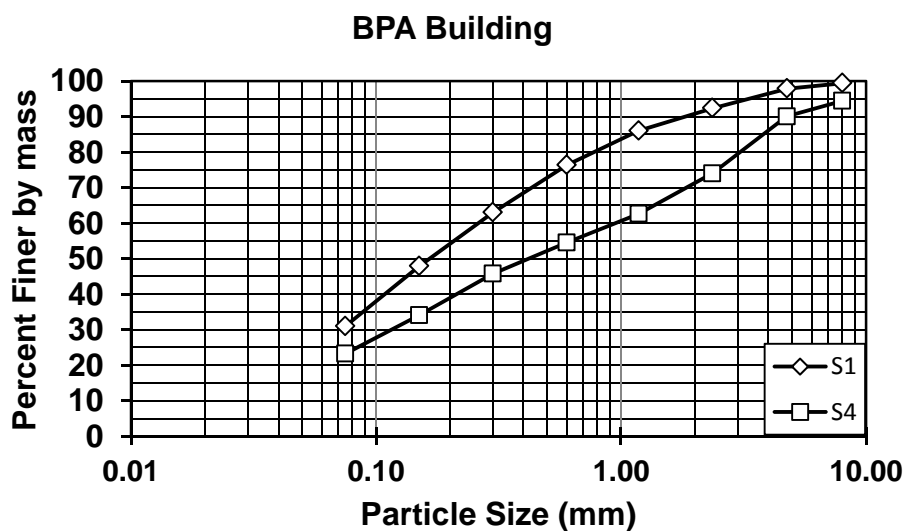


Figure A.36: Grain size distribution for BPA Building-S1, S4, no organics.

Complete grain size distributions for ecoroof material, after removal of organic matter.

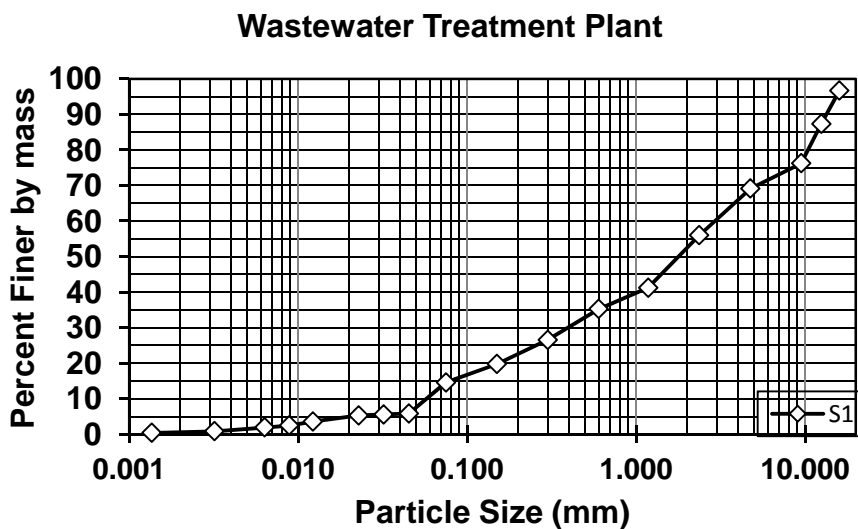


Figure A.37: Complete grain size distribution for Wastewater Treatment Plant-S1.

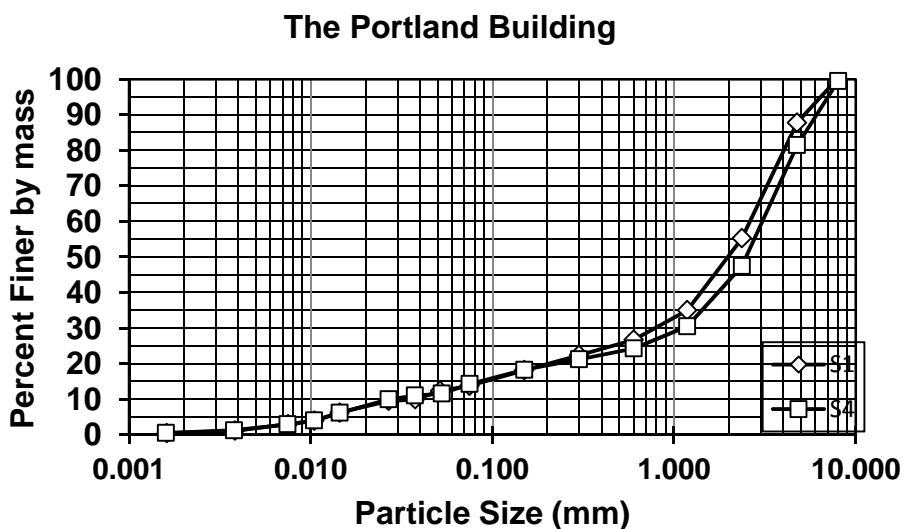


Figure A.38: Complete grain size distribution for the Portland Building-S1, S4.

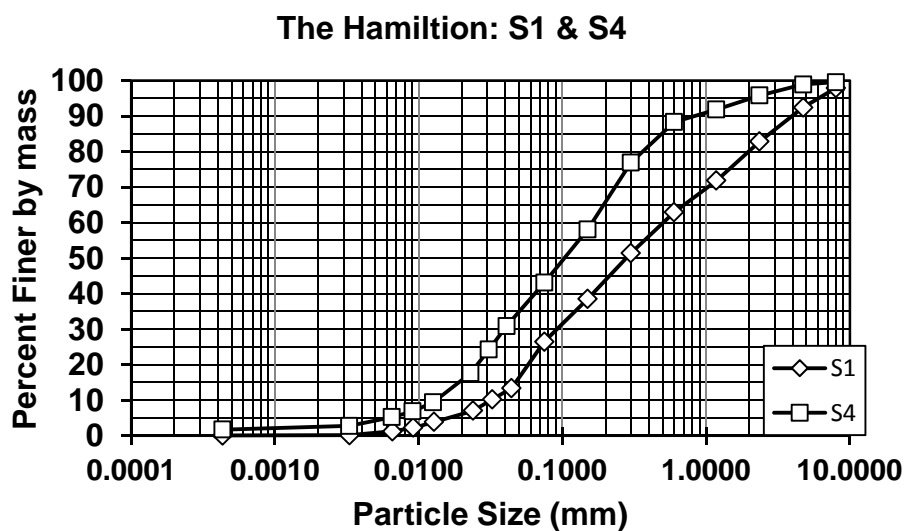


Figure A.39: Complete grain size distribution for the Hamilton-S1, S4.

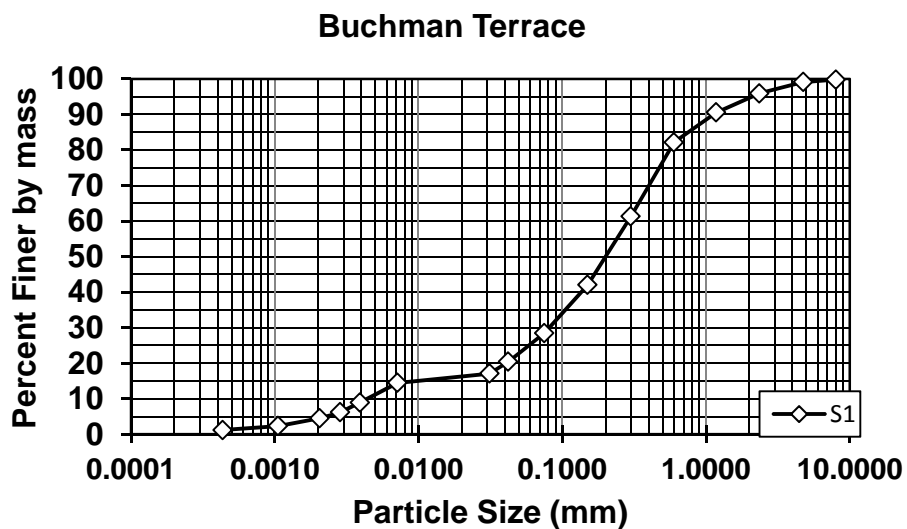


Figure A.40: Complete grain size distribution for the Buchman Terrace-S1.

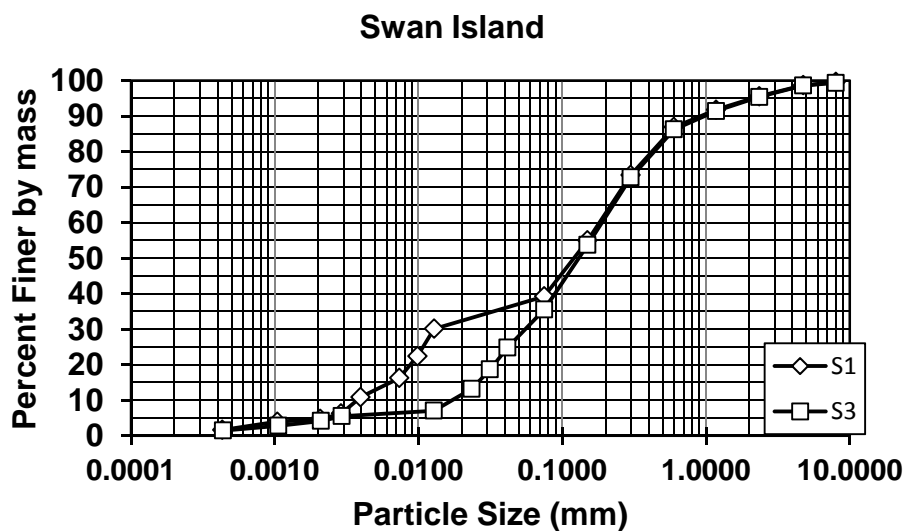


Figure A.41: Complete grain size distribution for Swan Island Pumphouse-S1, S3.

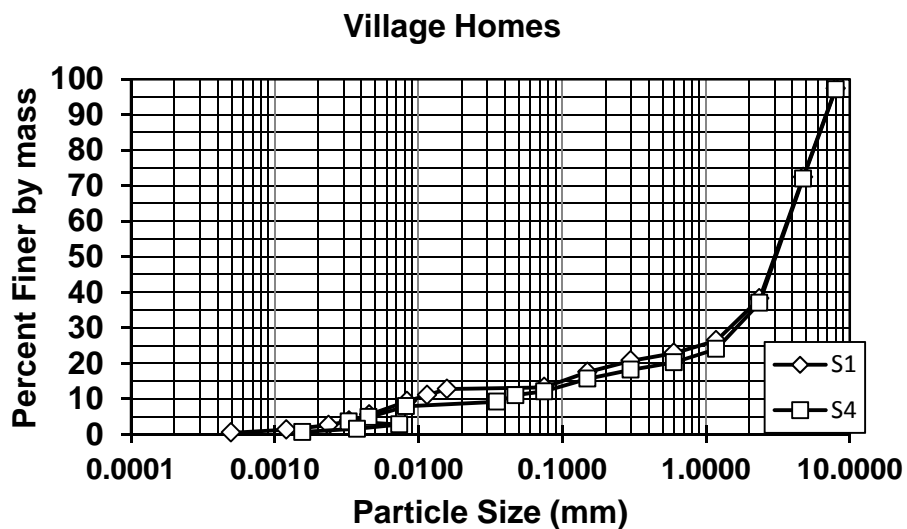


Figure A.42: Complete grain size distribution for the Village Home Apartments-S1, S4.

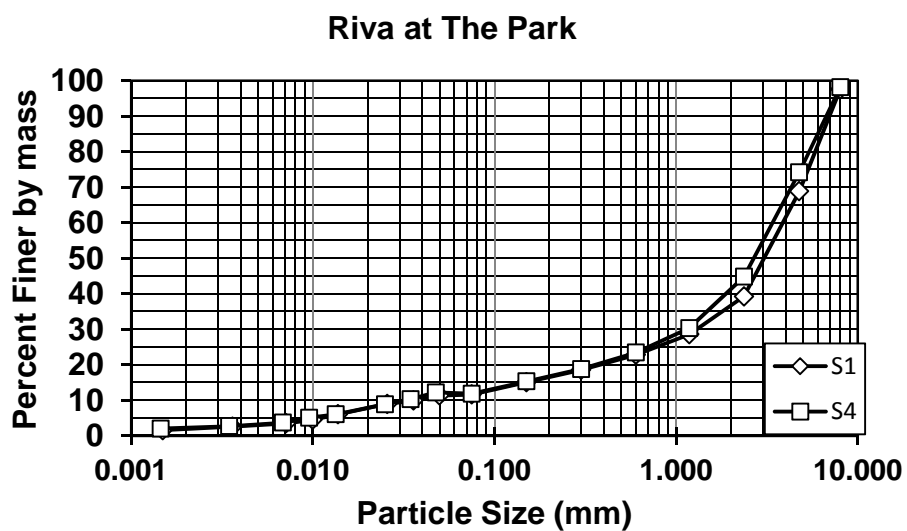


Figure A.43: Complete grain size distribution for Riva at the Park-S1, S4.

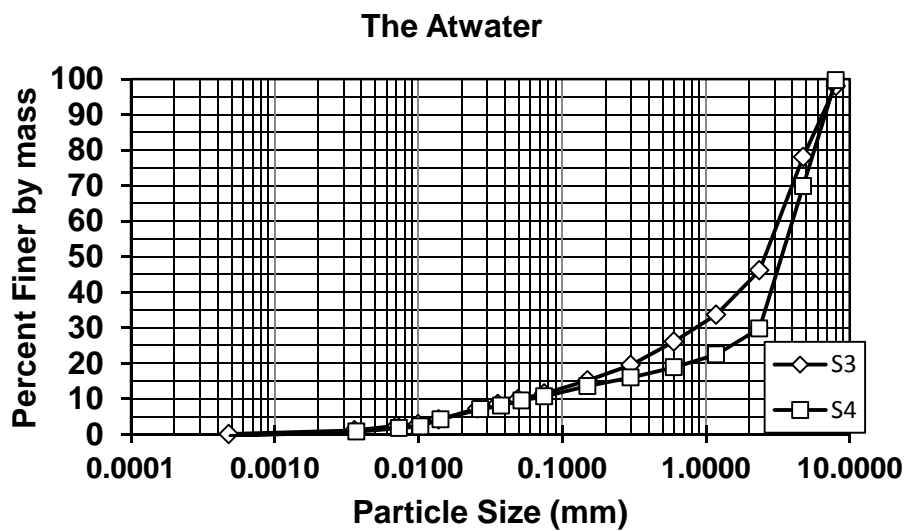


Figure A.44: Complete grain size distribution for the Atwater-S3, S4.

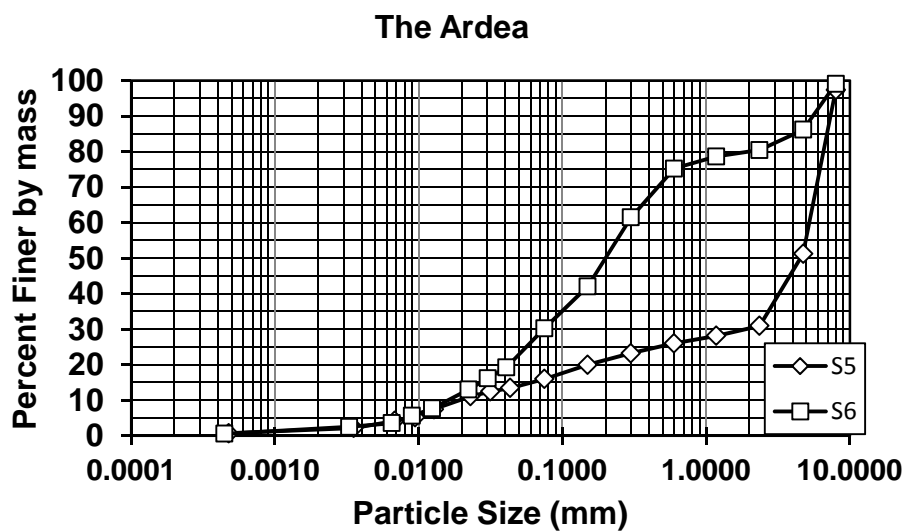


Figure A.45: Complete grain size distribution for Riva at the Ardea-S5, S6.

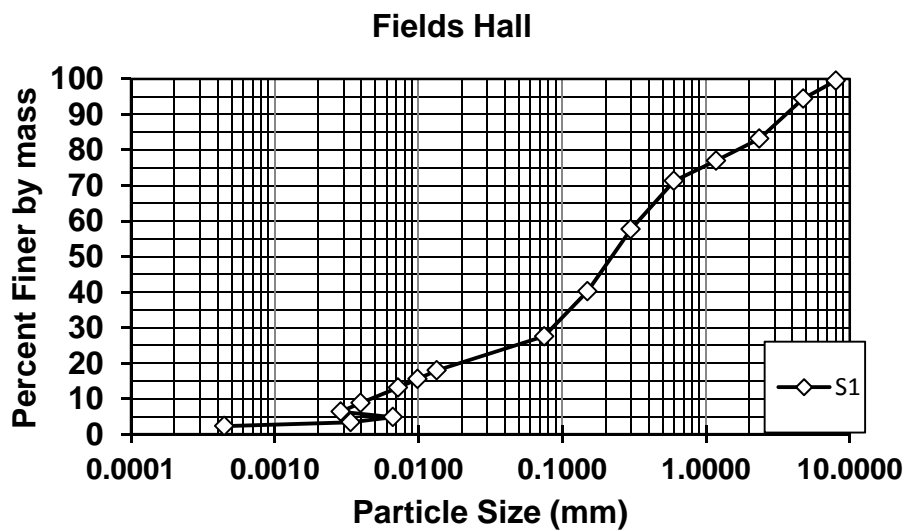


Figure A.46: Complete grain size distribution for Fields Hall-S1.

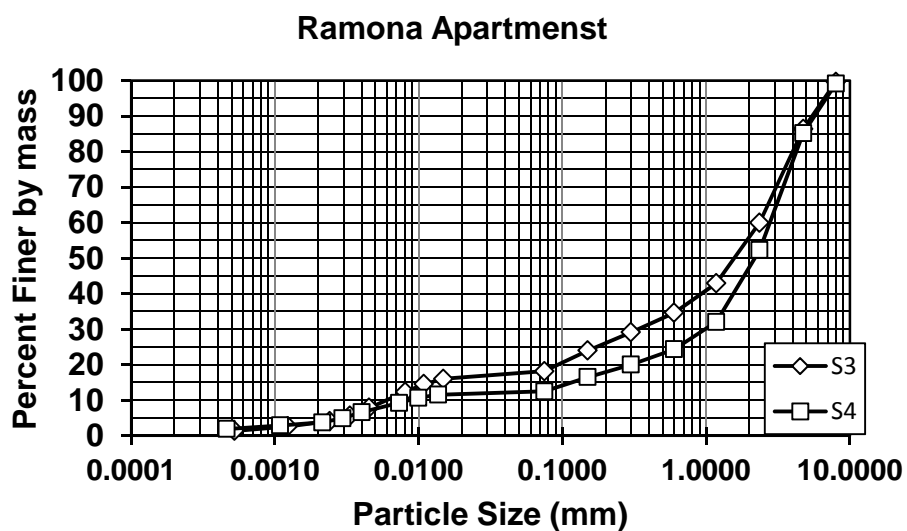


Figure A.47: Complete grain size distribution for Riva at Ramona Apartments-S3, S4.

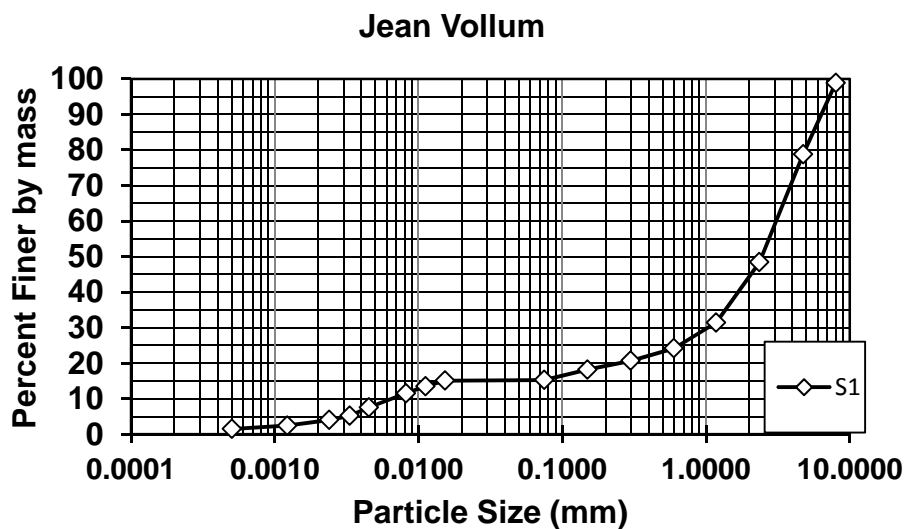


Figure A.48: Complete grain size distribution for Jean Vollum-S1.

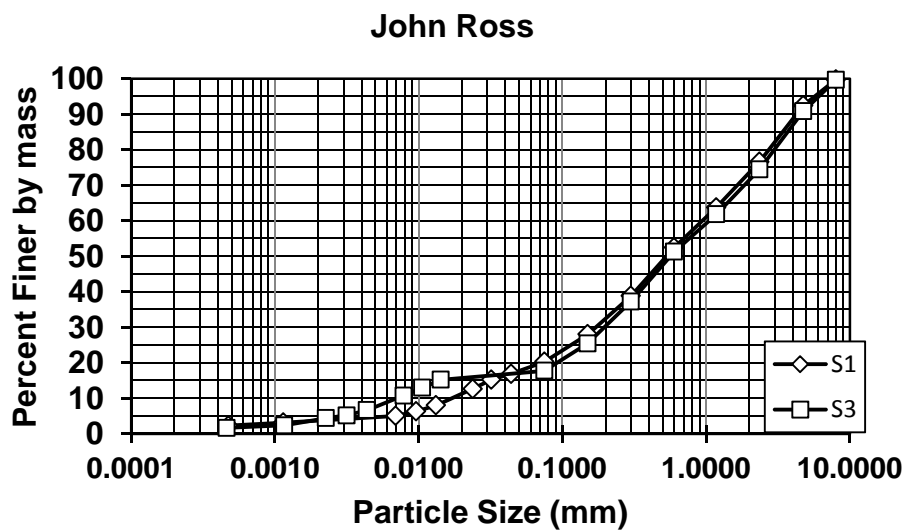


Figure A.49: Complete grain size distribution for John Ross-S1, S3.

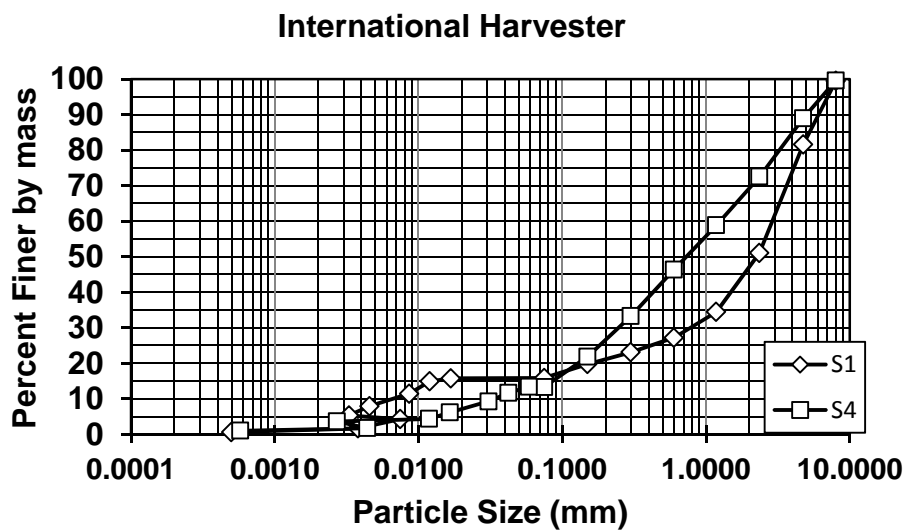


Figure A.50: Complete grain size distribution for International Harvester-S1, S4.

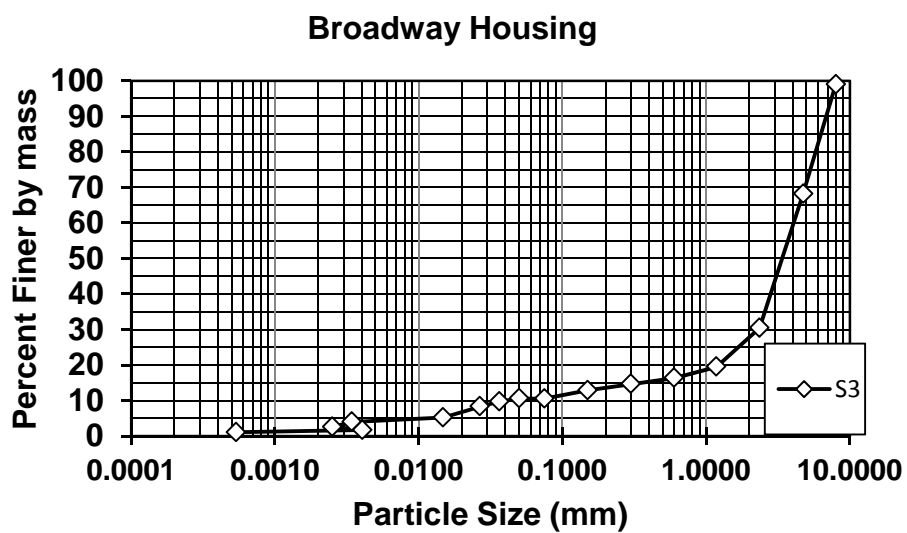


Figure A.51: Complete grain size distribution for Broadway Housing-S3.

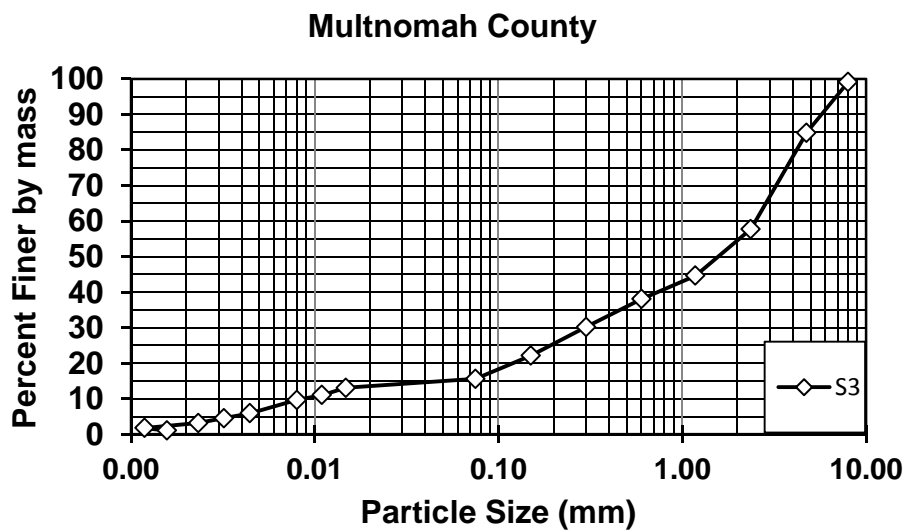


Figure A.52: Complete grain size distribution for Multnomah County-S3.

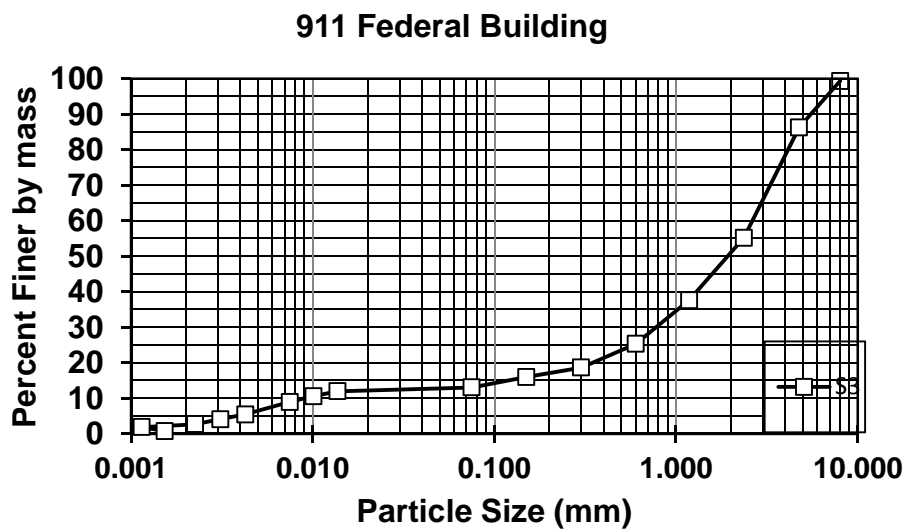


Figure A.53: Complete grain size distribution for 911 Federal Building-S3.

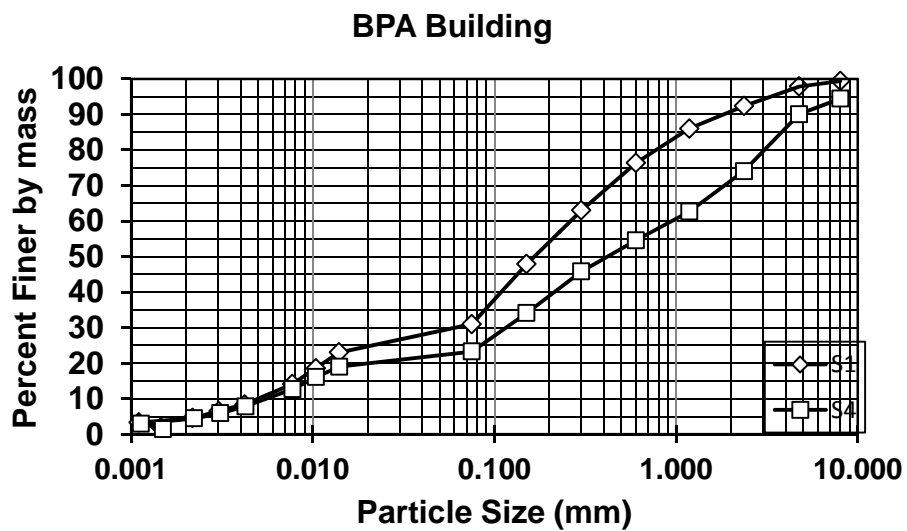


Figure A.54: Complete grain size distribution for BPA Building-S1, S4.

Flow curves for ecoroof soil prior to removal of organic matter.

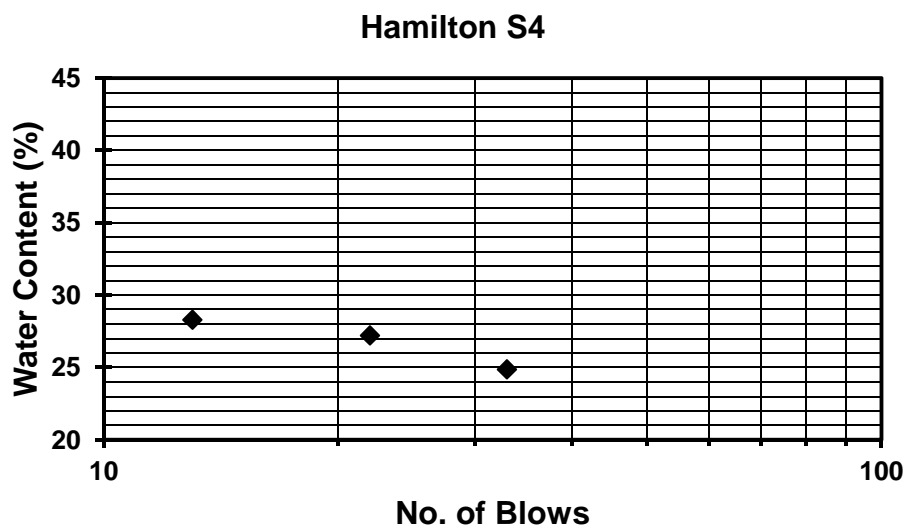


Figure A.55: Flow curve for the Hamilton-S4.

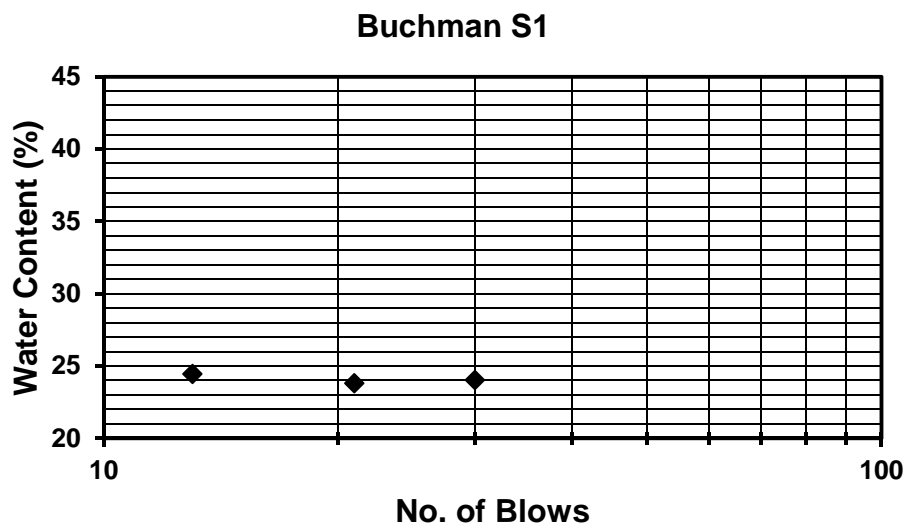


Figure A.56: Flow curve for Buchman Terrace-S1.

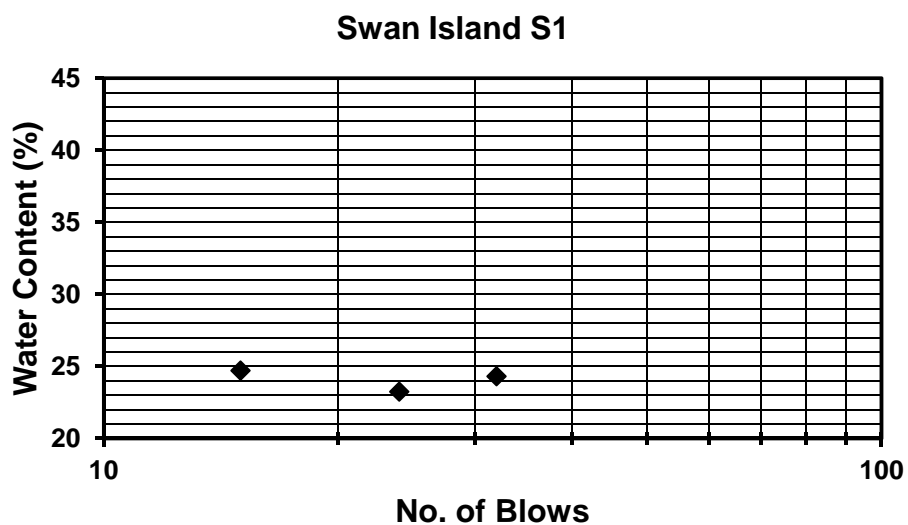


Figure A.57: Flow curve for the Swan Island-S1.

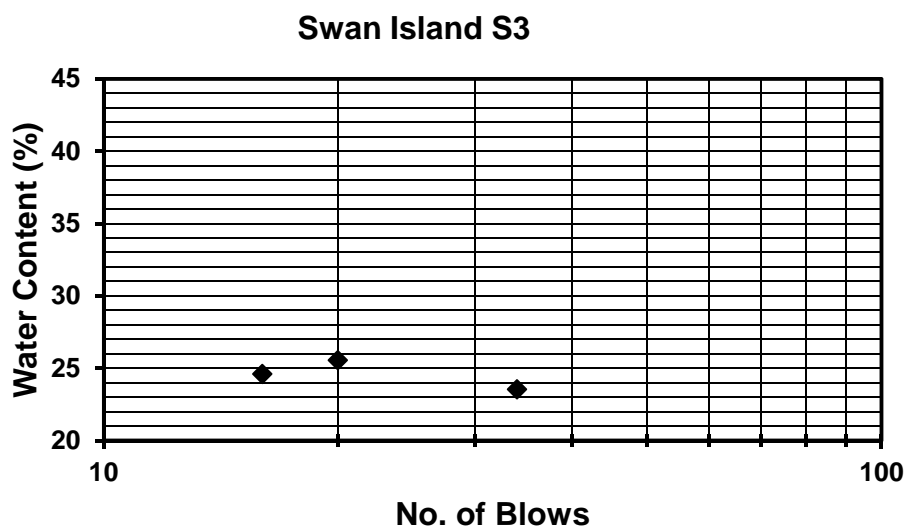


Figure A.58: Flow curve for Swan Island-S3.

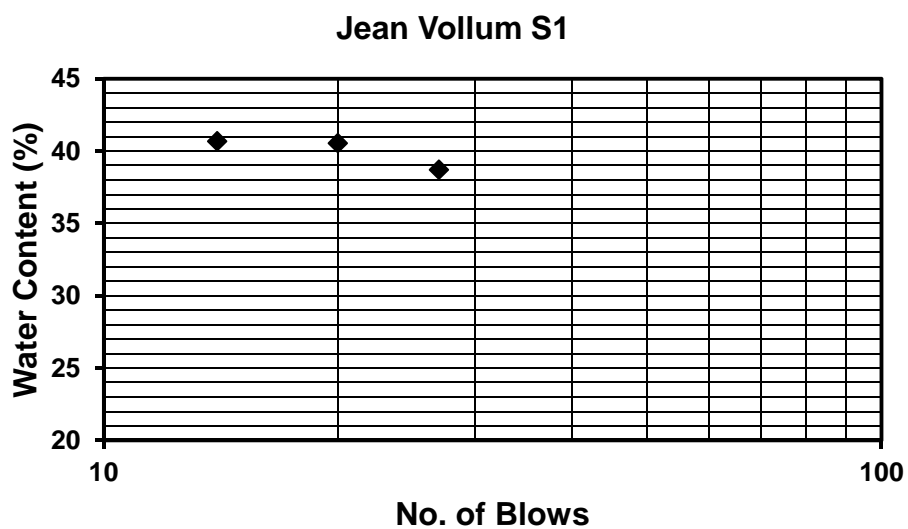


Figure A.59: Flow curve for Jean Vollum-S1.

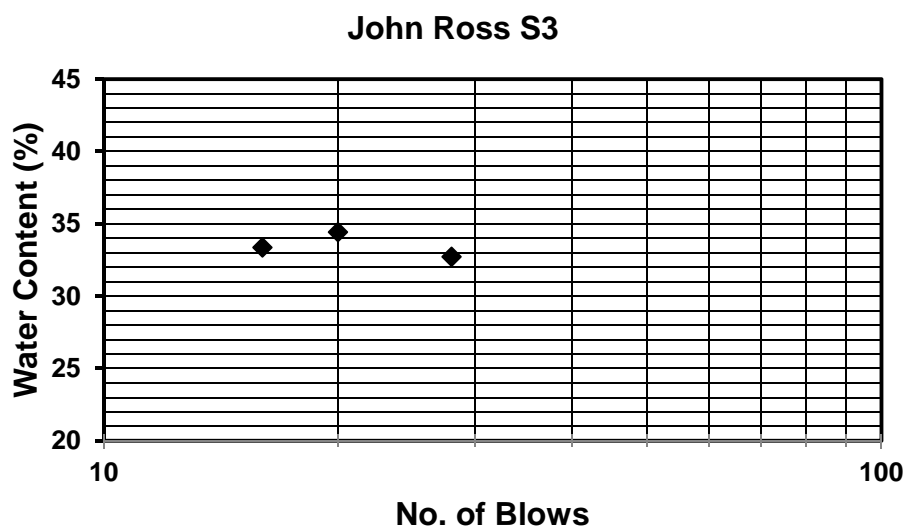


Figure A.60: Flow curve for John Ross-S3.

Target Gradations

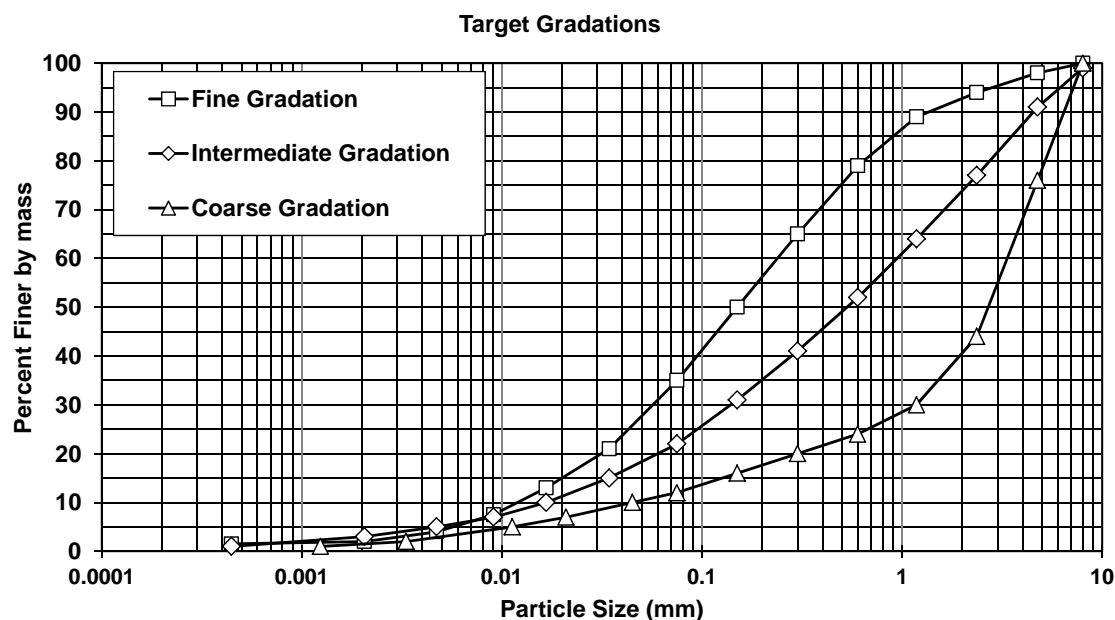


Figure A.61: Target Gradations.

Table A.2: Target Gradational Properties

	Coarse	Intermediate	Fine
D_{10}	0.04	0.017	0.012
D_{30}	1.18	0.529	0.150
D_{50}	2.69	0.139	0.060
D_{60}	3.35	0.942	0.234
Coefficient of Uniformity, C_u	74.64	56.68	19.59
Coefficient of Curvature, C_c	9.27	1.23	1.27

Table A.3: Target Gradational Reconstitution Parameters

	e_{max}	e_{min}	G_s	$\gamma_{d,min}$ (kN/m ³)	$\gamma_{d,max}$ (kN/m ³)
Fine	2.20	1.37	2.22	6.80	9.16
Intermediate	2.03	1.41	2.07	6.67	8.40
Coarse	2.54	2.09	1.90	5.27	6.05

Developed Sampling Equipment

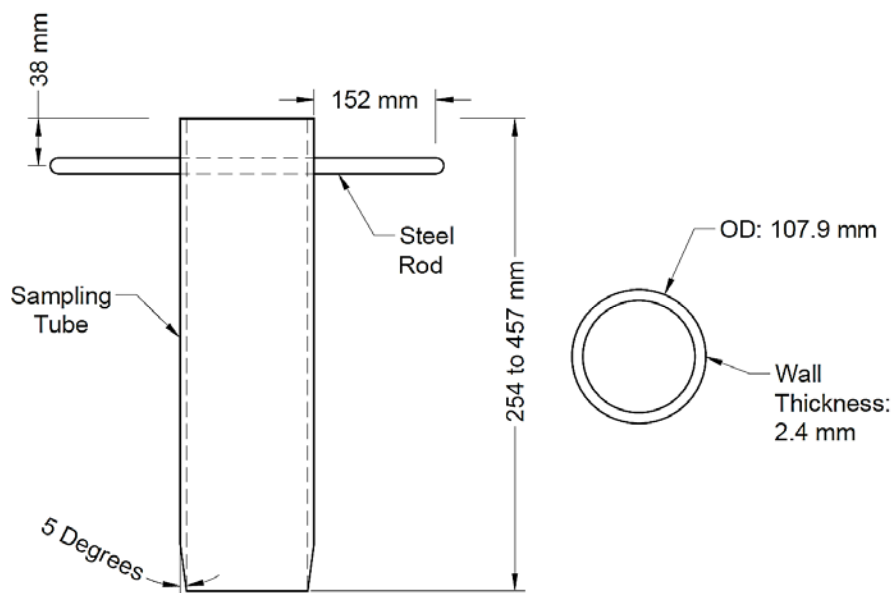


Figure A.62: Schematic of sampling tube.

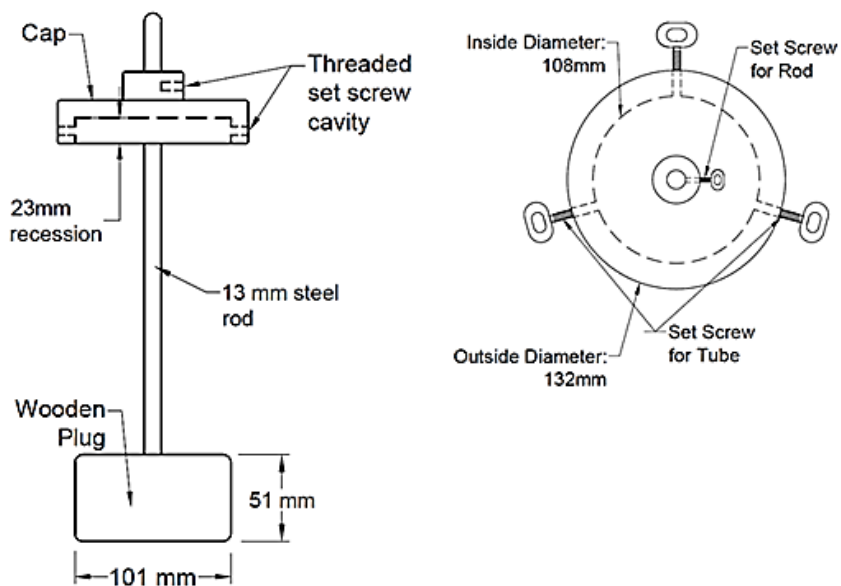


Figure A.63: Schematic of plunger and cap.

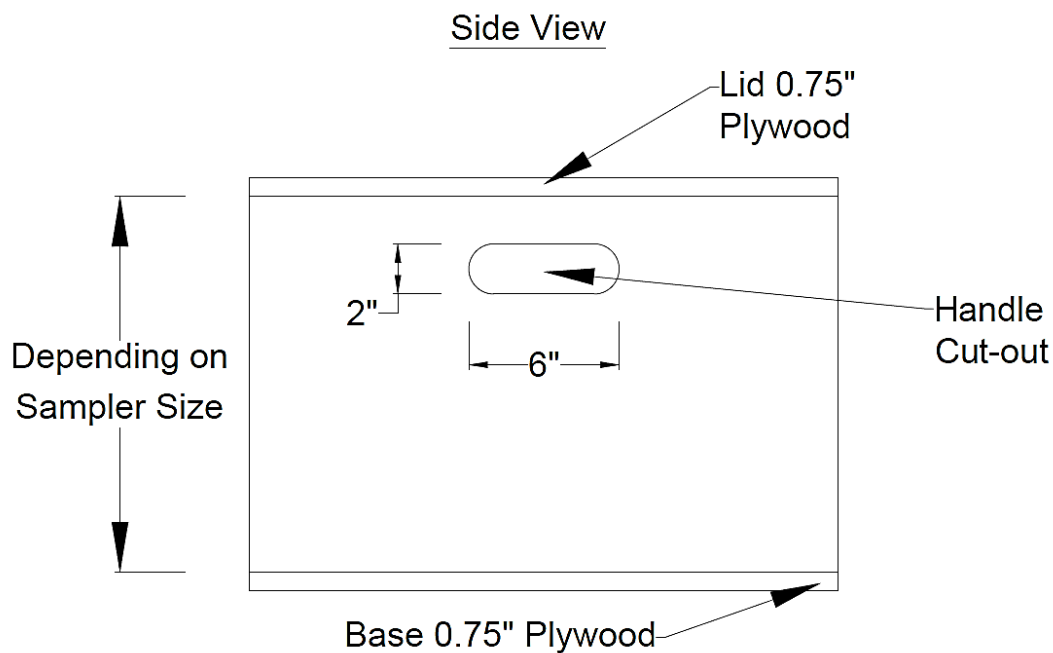


Figure A.64: Side view of transport box.

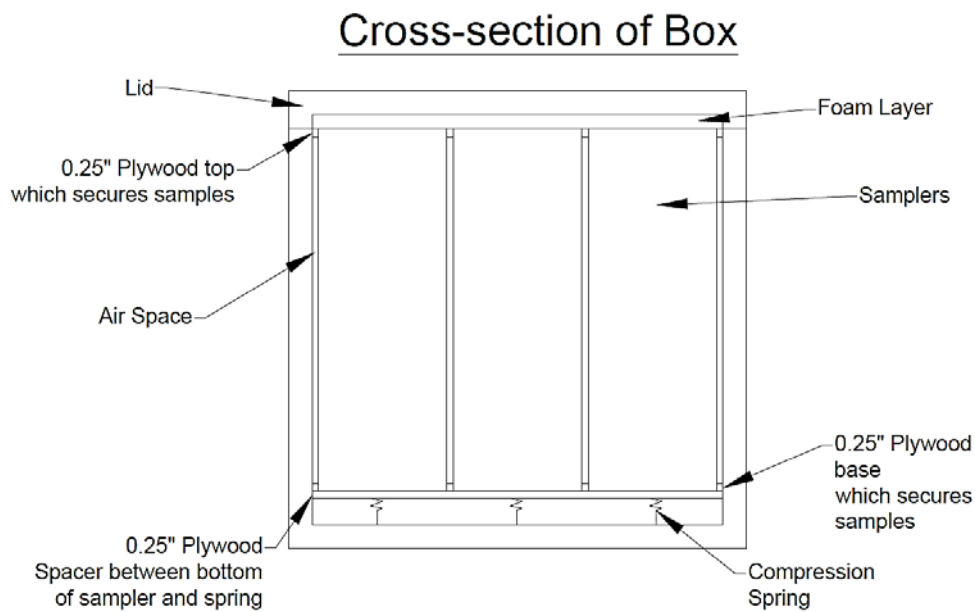


Figure A.65: Cross-section of sampler box.

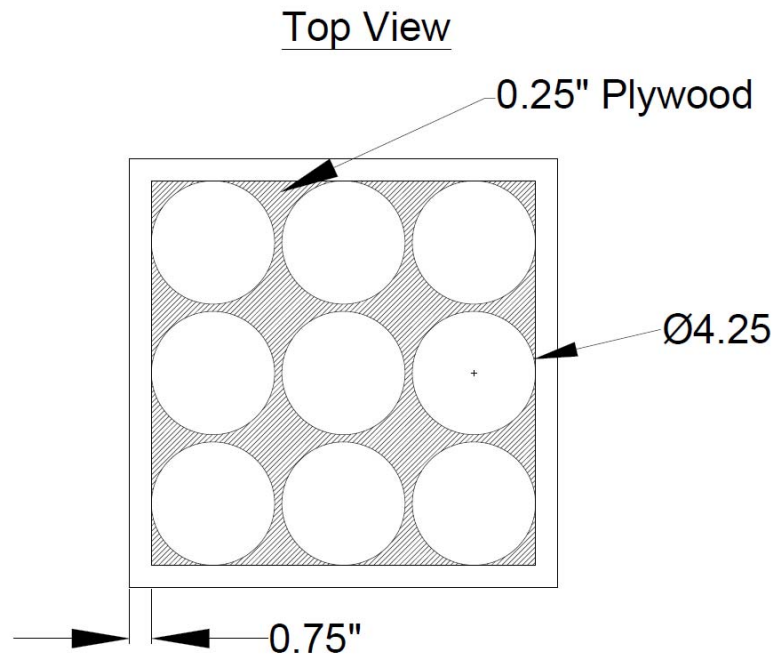


Figure A.66: Top view of sampler box.

Appendix B: Static Simple Shear Procedure

Static Simple Shear Specimen Preparation

1. Apply a small amount of vacuum grease along the circumference of the bottom platen.
2. Slide membrane over bottom platen and stretch O-rings around platen making sure that the membrane stays flush to the bottom of the platen and air does not become trapped between the membrane and platen (Figure B.1).

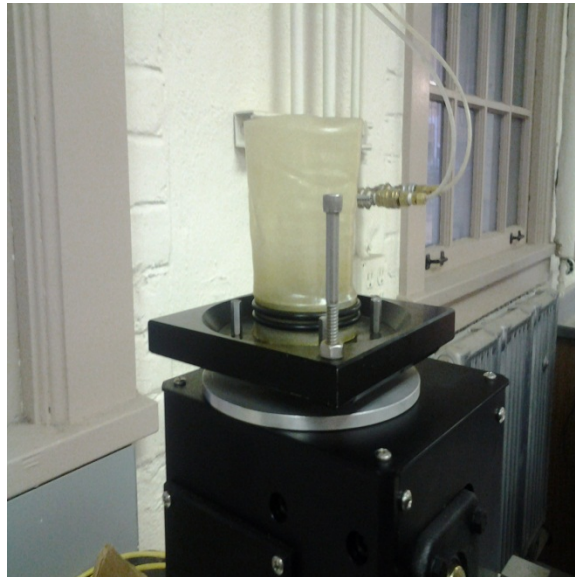


Figure B.1: Assembly of specimen membrane, O-rings, and bottom platen.

3. Inspect and clean specimen confining rings. Apply a small amount of vacuum grease to the surface of the rings and slide rings one at a time onto the steel rods (Figure B.2).



Figure B.2: Confining rings stacked onto steel rods.

4. Carefully place stacked rings centered on the bottom platen making sure that the membrane does not become pinched.
5. Remove one of the steel rods and stretch membrane around the confining rings, ensuring no air bubbles between the membrane and rings. Continue stretching membrane around the rings and remove the second steel rod accordingly (FigureB.3).

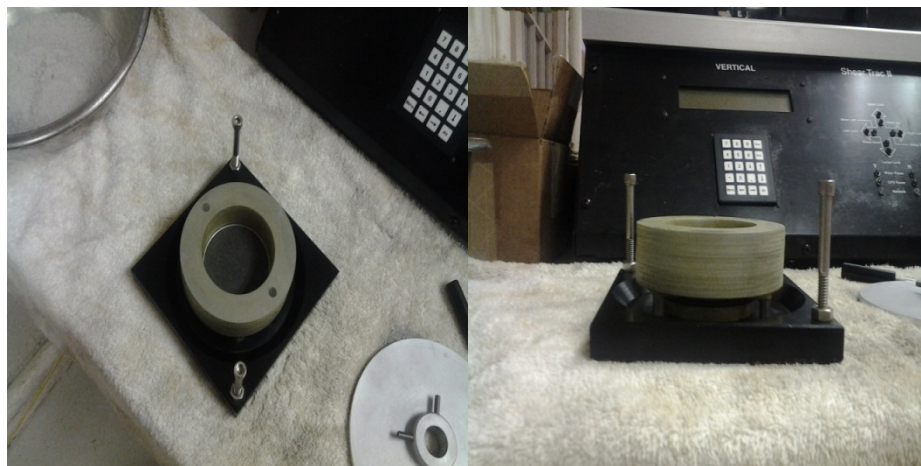


Figure B.3: Membrane stretched around confining rings.

- Using a micrometer, determine and record diameter and height of confining rings including the membrane (Figure B.4). Take a minimum of three measurements and take the average of these measurements for the volume calculation.



Figure B.4: Micrometer used to determine diameter of specimen.

- For reconstituted samples: weigh and record material mass to conform to the required testing relative density.
- Insert material into rings by air pluviation (for dry sand) vibrate accordingly to ensure all material enters the mold.
- Scrape excess material from top of specimen, ensuring a flat surface for the top platen to rest on.
- Apply a small amount of vacuum grease around the circumference of the top platen and place on top of specimen.

11. Carefully slide membrane over top platen (Figure b.5a). In addition, place one of the steel rods back through the confining rings to help stabilize the sample while the O-rings are stretched around the top platen (Figure B.5b).



(a)



(b)

Figure B.5: (a) Membrane around top platen (b) O-rings around top platen.

12. Roll membrane over the O-rings.

Static Simple Shear Equipment Set-Up

1. Insert built specimen into the shear box/water bath ensuring water channel is facing to the left (Figure B.6).

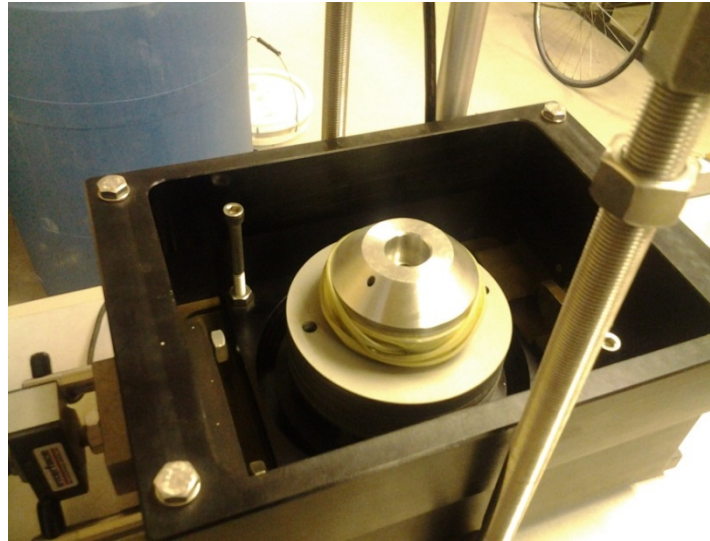


Figure B.6: Built specimen placed into shear box.

2. Tighten both set screws at base of shear box (Figure B.7).

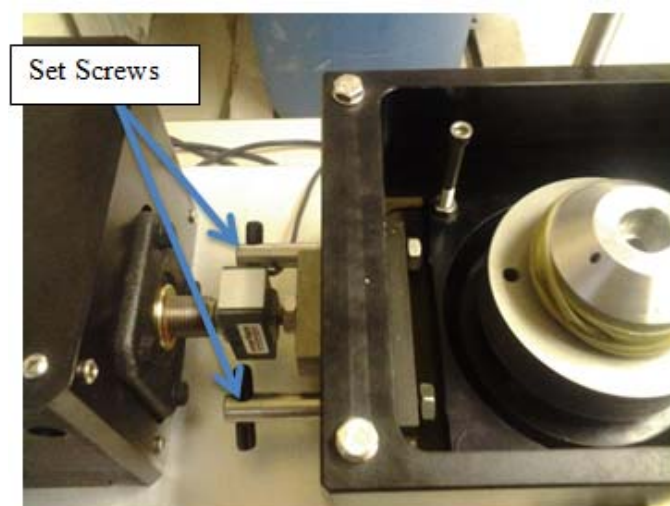


Figure B.7: Set screws on base of shear box.

3. Turn on Simple Shear unit.
4. Initialize horizontal actuator. On the right panel press: 2 → 3 → enter. The motor will automatically stop when the unit reaches the correct position.
5. Slide circular plate for vertical LVDT over the stainless steel rod leaving the setscrews loose (Figure b.8).



Figure B.8: Circular plate slid around stainless steel rod.

6. Loosen swing arm bolt and insert stainless steel rod and plate into place (Figure B.9).
Lower the swing arm and thread the rod into the top platen.

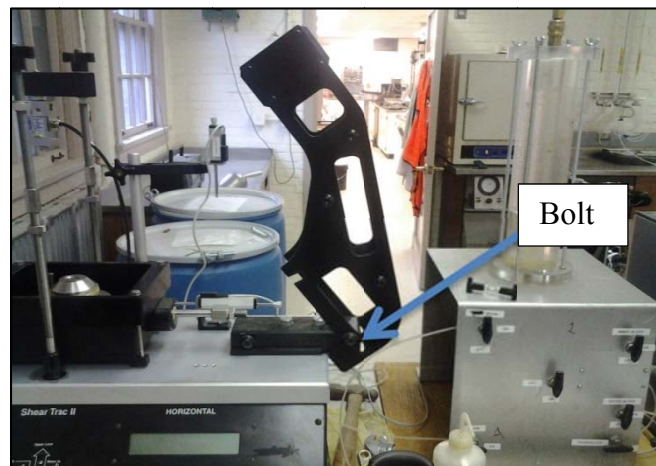


Figure B.9: Raised swing arm.

7. Slide the circular plate down until it is resting on the top platen and tighten the two set screws (Figure B.10).

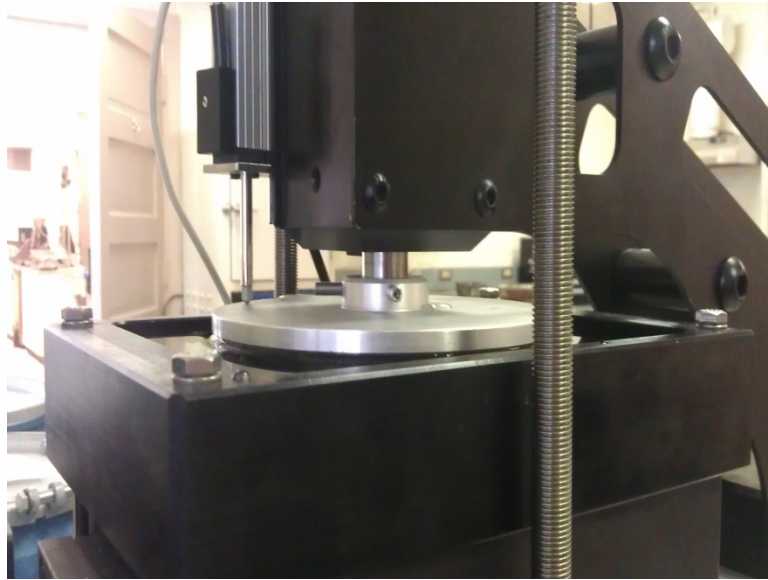


Figure B.10: Assembly of stainless steel rod and circular plate.

8. Tighten the four bolts at the base of the swing arm.
9. Swing cross-bar into place. Level the crossbar and tighten the four prong nuts.
10. Place vertical LVDT on top of circular plate, ensuring that the body of the LVDT is free from contact from the swing arm (Figure B.11).
11. Fill water bath with de-aired water.
12. Lower crossbar until the load cell slightly touches the top of the stainless steel rod.
On the left panel press: 2 → 1 → enter. Once a load is registered by the cell press any button to stop lowering the crossbar.

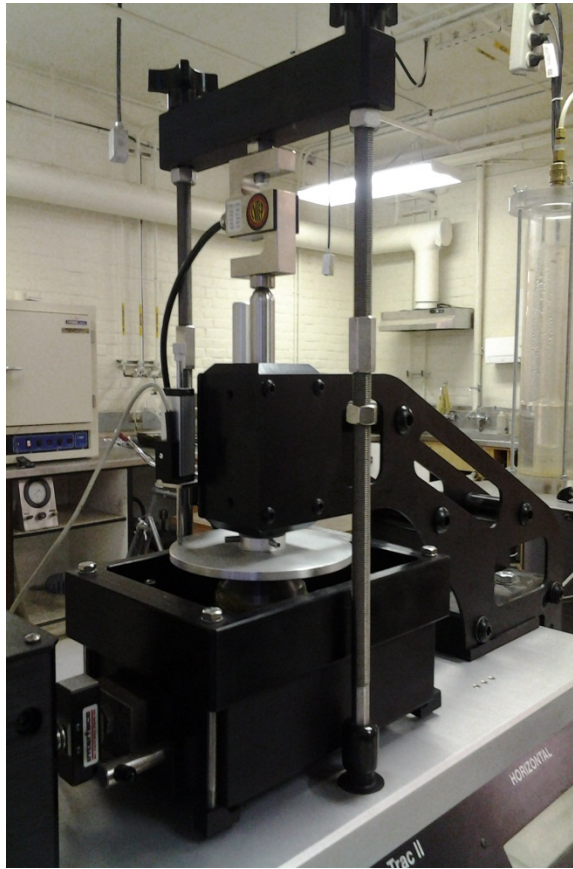


Figure B.11: Simple Shear unit and specimen fully assembled.

13. Allow specimen to self-saturate. Time required is based on the testing material.

SS Software Set-Up: Constant Vertical Stress Test “*Drained Test*”

1. Using the left panel (vertical control: ID 101) on the front of the SS unit, go to the control option (press 3) and select **apply and maintain load (press 2)**.
2. Specify the final vertical stress and loading rate.
3. Specify the final displacement; with a constant vertical stress test the max allowable vertical displacement should be large. Having too small of a predefined max displacement will abort the test before intended.
4. Specify the sampling period.
5. Using the right panel (horizontal control: ID 102) on the front of the SS unit, go to the control option (press 3) and then choose the **constant displacement rate option (press 1)**.
6. Specify the displacement rate, maximum horizontal displacement and sampling period.
7. Specify the final horizontal load, ensuring that the input value is large enough to allow the test to finish before the final load is reached. **Do not input a load higher than the load cell capacity.**
8. Zero the horizontal and vertical load cells. This can be done by navigating to: (Desktop\Shortcut to DSS\DS Testing Info\Software\DSS\shear.dss.exe) and bring down the view menu and open the system window. In addition, bring down the calibrate menu and open the summary window.
9. For both the horizontal and vertical load cells make sure that the offset values are the same in both windows. If not, change the offset value in the calibration summary

window. Once this is done, the reading from the system window for both the vertical and horizontal load cells should be zero (Figure B.12).

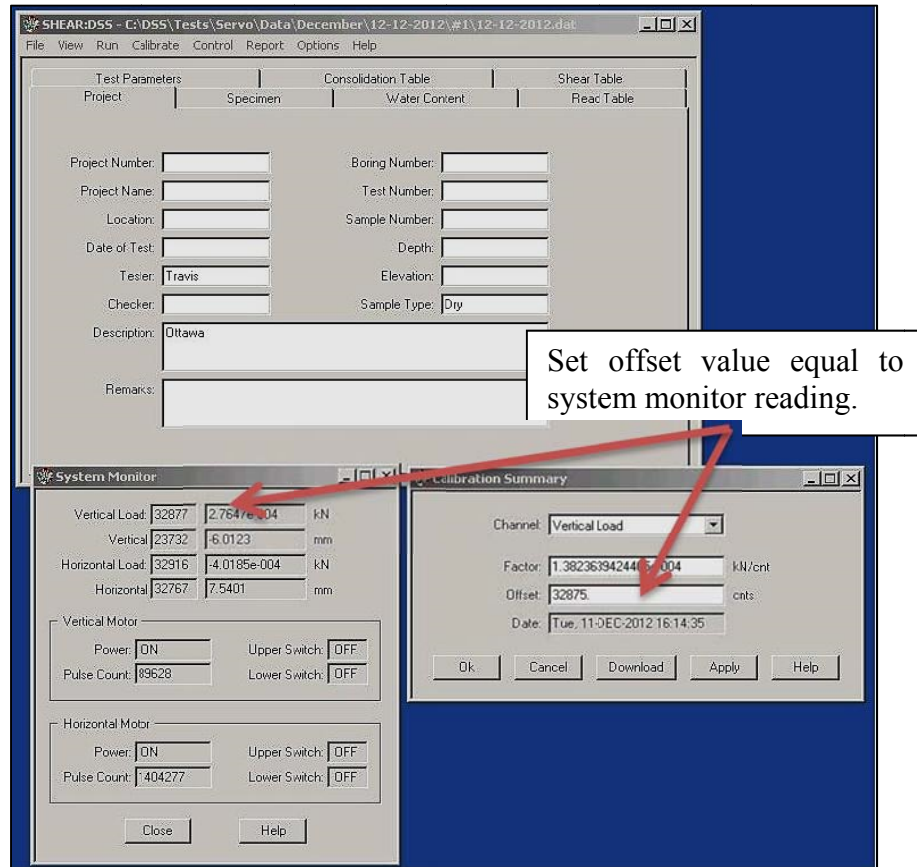


Figure B.12: Zeroing of load cells.

10. Navigate to: (Desktop\ShortcuttoDSS\DSTestingInfo\Software\diags.com20.exe).
Open this program twice.
11. Place the windows side by side and type 101 and 102 for the vertical and horizontal control ID's respectively.
12. Bring down the view menu and open the panel window. Do this for each of the control windows. The panel windows display the same information as the two panels on the front of the SS unit (Figure B.13).

13. The user can control the system from the panel windows or from the keypads on the front of the unit.
14. From the 101 control panel window start the vertical loading sequence. Click on:
3→2→6→Enter.
15. Once the system has reached the desired vertical load, allow specimen to consolidate.

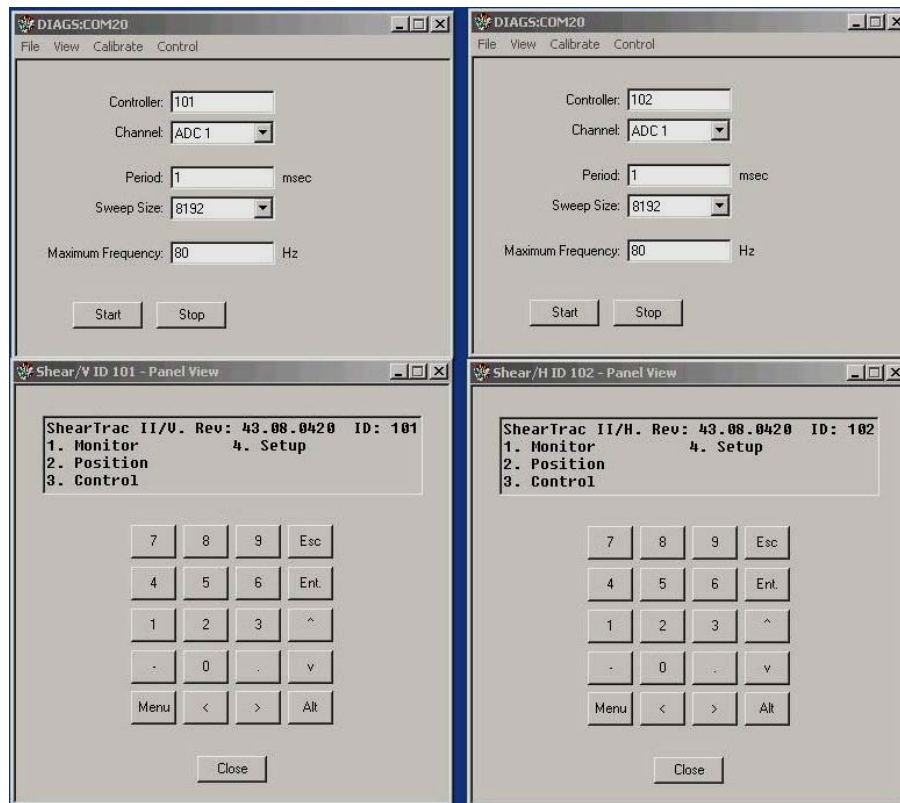


Figure B.13: Windows displaying front panel information.

16. Start the horizontal loading sequence using the 102 control panel window. Click on:
3→1→6→Enter.
17. Wait until shearing phase is complete.

Static Simple Shear Disassembly and Data Acquisition: “*Drained Test*”

1. Once test is complete: bring down the file menu and open the download window.
2. Right-click and click on select all.
3. Right-click and click copy.
4. Paste in notepad or excel.
5. Do step 2 for both controller windows.
6. Initialize shear actuator and raise crossbar.
7. Swing crossbar away from piston and remove the vertical LVDT from the circular plate.
8. Drain water bath. Use syphon hose and drain to bucket.
9. Loosen set screws holding the circular plate and unscrew piston from top platen.
10. Loosen the four bolts securing the swing arm and raise it.
11. Loosen the two set screws at the base of the shear box.
12. Remove specimen from water bath.
13. Dry and weigh specimen to obtain the actual relative density for the test.

Static Simple Shear Software Set-Up: Constant Volume “*Undrained Test*”

1. Navigate to: (Desktop\Shortcut to DSS\DS Testing Info\Software\DSS\shear.dss.exe).
2. Once open, a template file must be loaded. Use either the template file provided in the SS file or from a previous test. Click File and open download window.
3. Zero both of the load cells by: bringing down the view menu and open the system window. In addition, bring down the calibrate menu and open the summary window.
4. For both the horizontal and vertical load cells make sure that the offset values are the same in both windows. If not, change the offset value in the calibration summary window. Once this is done, the reading from the system window for both the vertical and horizontal load cells should be zero.
5. Fill in the required information into the specimen and project tabs.
6. Input the testing parameters into the water content, consolidation and shear tabs.
7. The read table tab displays how often a data point is acquired throughout the test. Input the desired sampling period.
8. Bring down the Run menu and open the Start window. Save the file to the desired location.
9. When the “position top platen” window appears click yes. Do not click OK until the crossbar has stopped moving (the green LED lights will stop flashing).
10. Click OK to start the test.
11. Monitor the test by: bring down the view menu and click on test monitor and test graph. The test graph window displays a real time image of the data collected during the test. The test monitor window allows the user to keep track of the testing process.

12. The system will automatically shut off when the test is complete, or any of the testing parameters is breached.

Static Simple Shear Disassembly and Data Acquisition: “*Undrained Test*”

1. Immediately following the completion of the test: bring down the file menu and click load. Now the data has been loaded to the template and file can be saved.
2. Bring down the file menu and under Dump click on engineering. Save file as .txt and import into spreadsheet program.
3. Initialize shear actuator and raise crossbar.
4. Swing crossbar away from piston and remove the vertical LVDT from the circular plate.
5. Drain water bath.
6. Loosen set screws holding the circular plate and unscrew piston from top platen.
7. Loosen the four bolts securing the swing arm and raise it.
8. Loosen the two set screws at the base of the shear box.
9. Remove specimen from water bath.
10. Dry and weigh specimen to obtain the actual relative density for the test.

Appendix C: Static Simple Shear Test Data

Stress-Strain Plots for Drained Static Tests Reconstituted Specimens

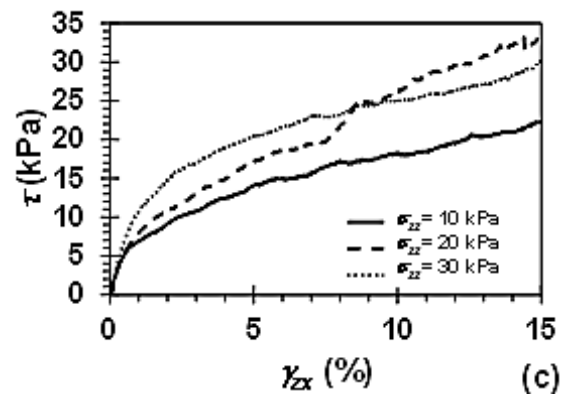
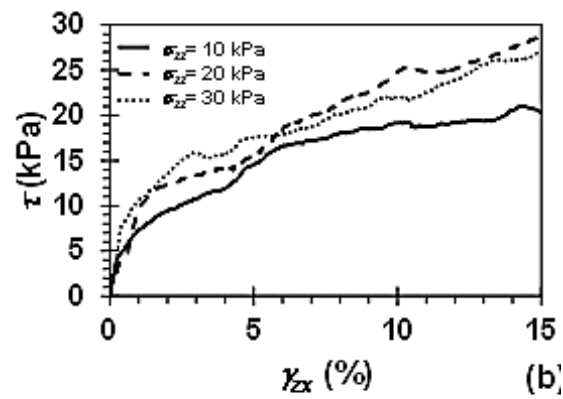
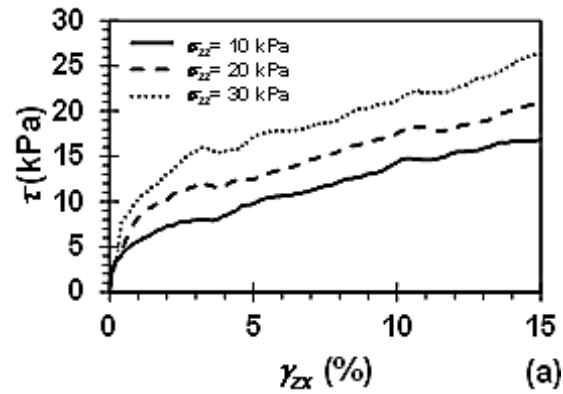


Figure C.1: Stress-strain response for specimens reconstituted to $D_r = 30\%$ for the (a) fine (b) intermediate (c) coarse gradations, respectively.

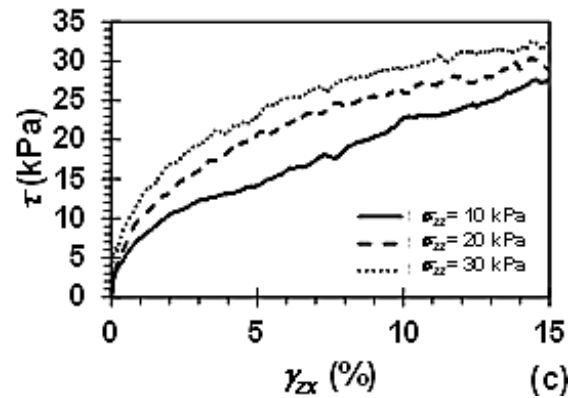
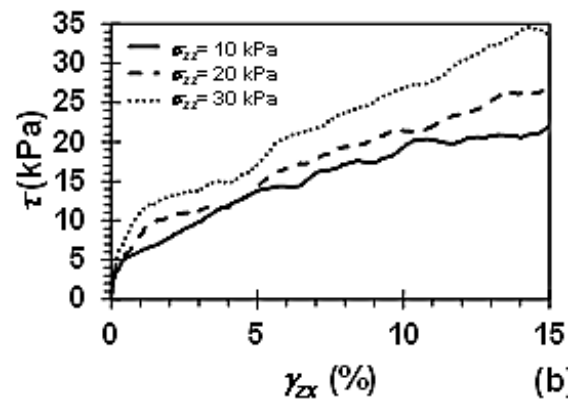
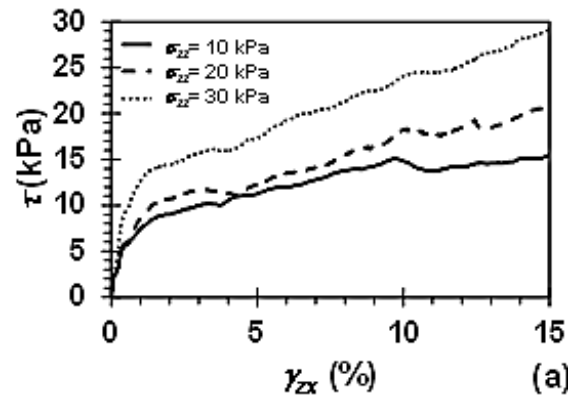


Figure C.2: Stress-strain response for specimens reconstituted to $D_r = 50\%$ for the (a) fine (b) intermediate (c) coarse gradations, respectively.

Volumetric Response Plots for Reconstituted Drained Simple Shear Tests

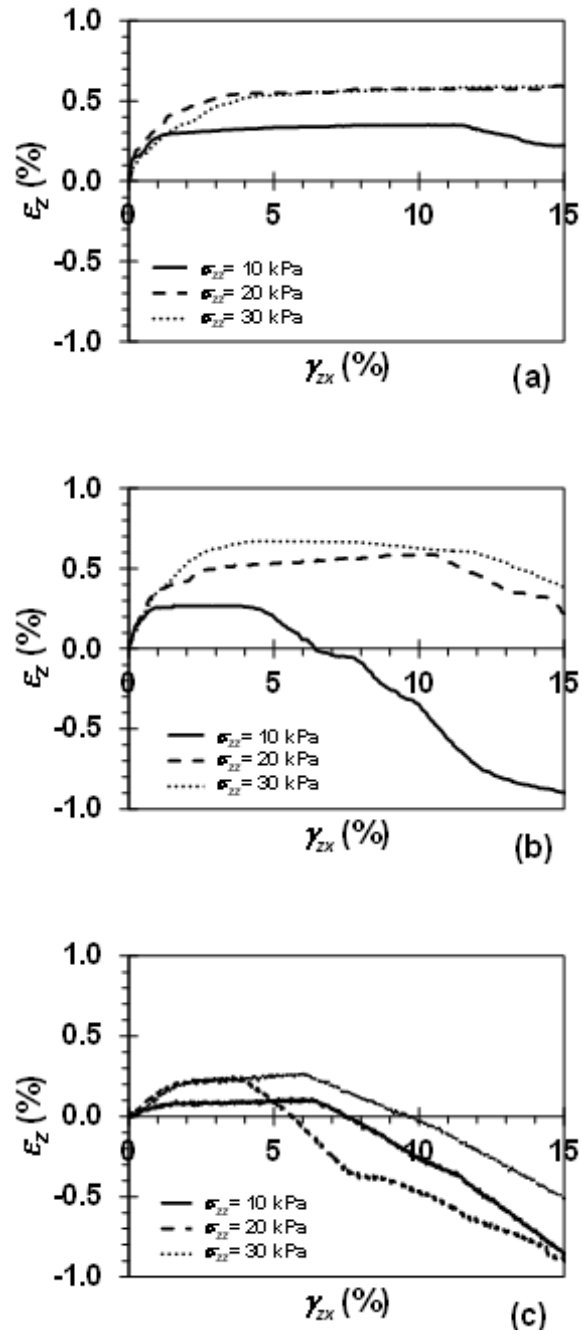


Figure C.3: Volumetric response for specimens reconstituted to $D_r = 30\%$ for the (a) fine (b) intermediate (c) coarse gradations, respectively.

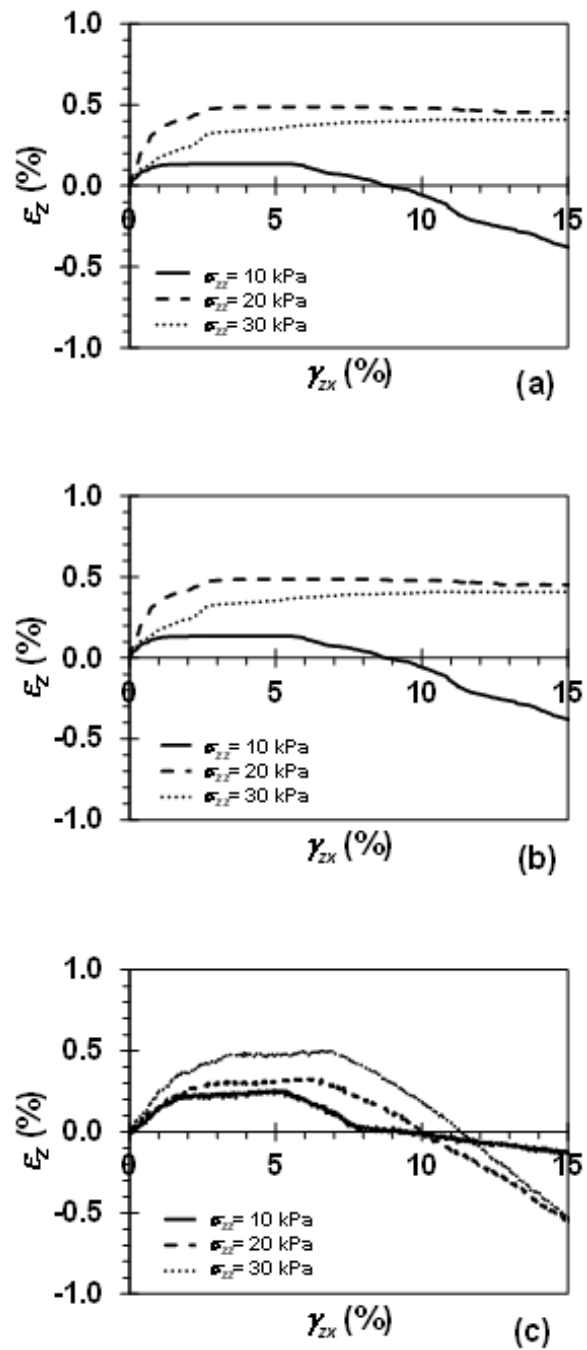


Figure C.4: Volumetric response for specimens reconstituted to $D_r = 50\%$ for the (a) fine (b) intermediate (c) coarse gradations, respectively.

Secant Shear Modulus Determination at one percent shear strain

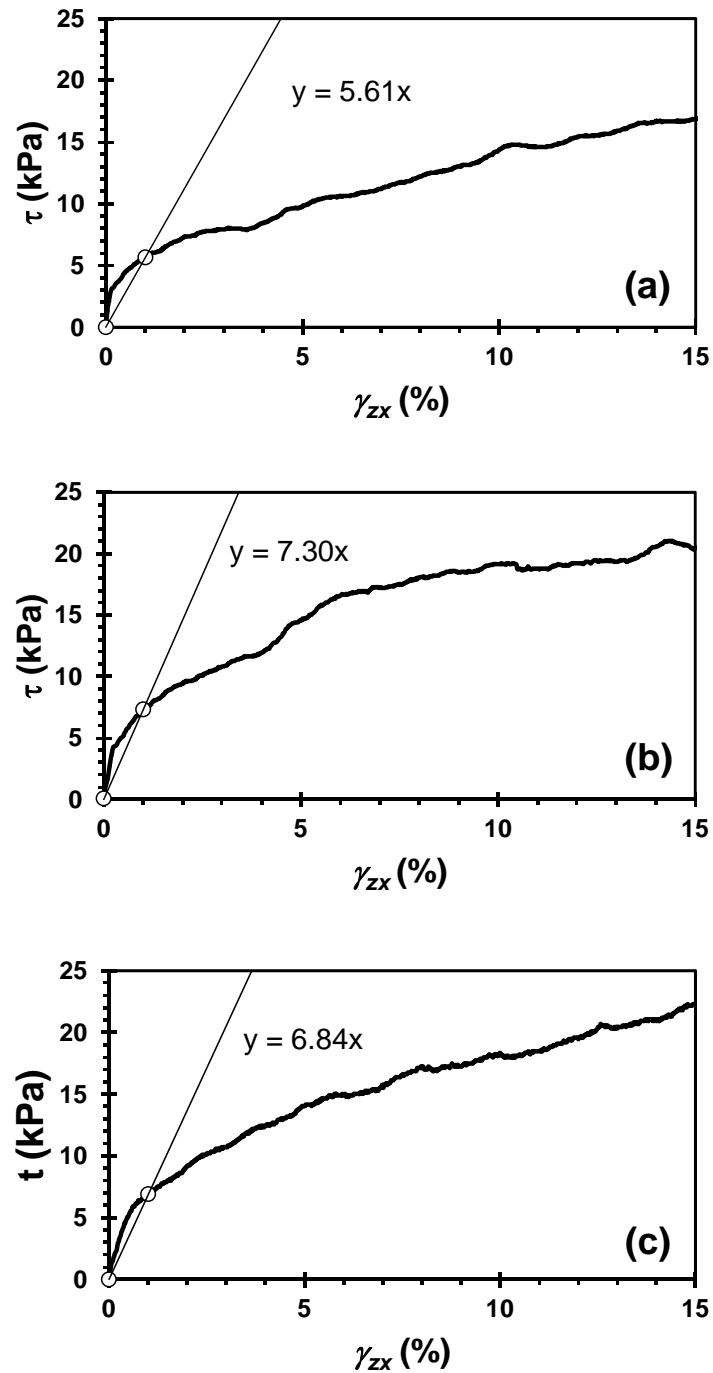


Figure C.5: Secant shear modulus at one percent shear strain with $\sigma_{zz} = 10$ kPa and $D_r = 30\%$ for: (a) fine, (b) intermediate, and (c) coarse gradations.

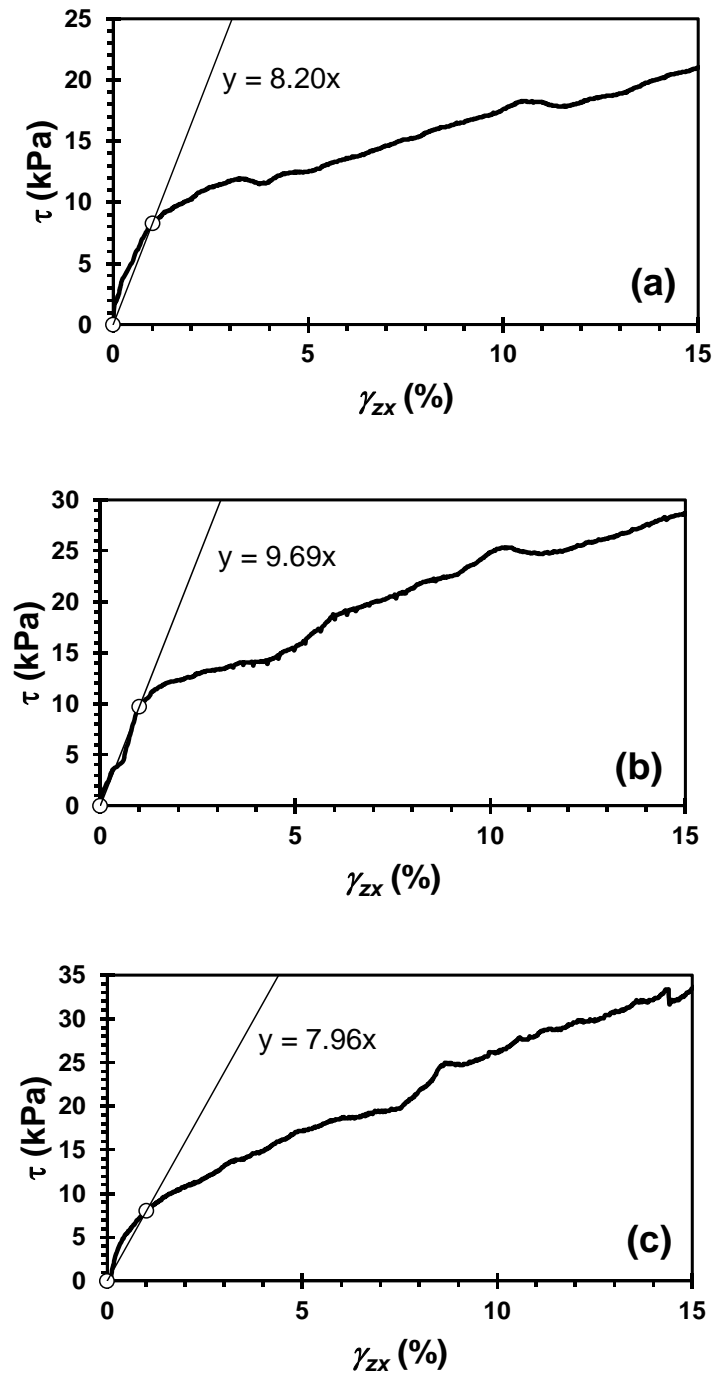


Figure C.6: Secant shear modulus at one percent shear strain with $\sigma_{zz} = 20$ kPa and $D_r = 30\%$ for: (a) fine, (b) intermediate, and (c) coarse gradations.

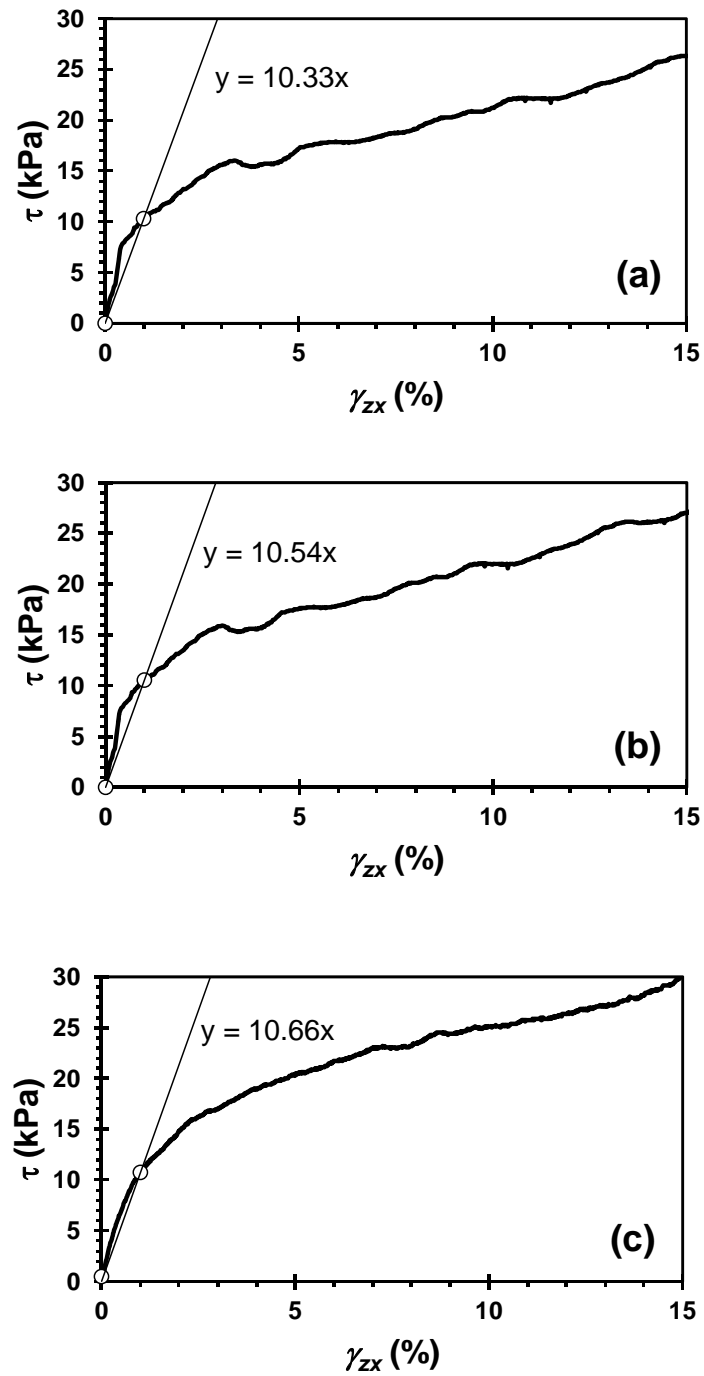


Figure C.7: Secant shear modulus at one percent shear strain with $\sigma_{zz} = 30$ kPa and $D_r = 30\%$ for: (a) fine, (b) intermediate, and (c) coarse gradations.

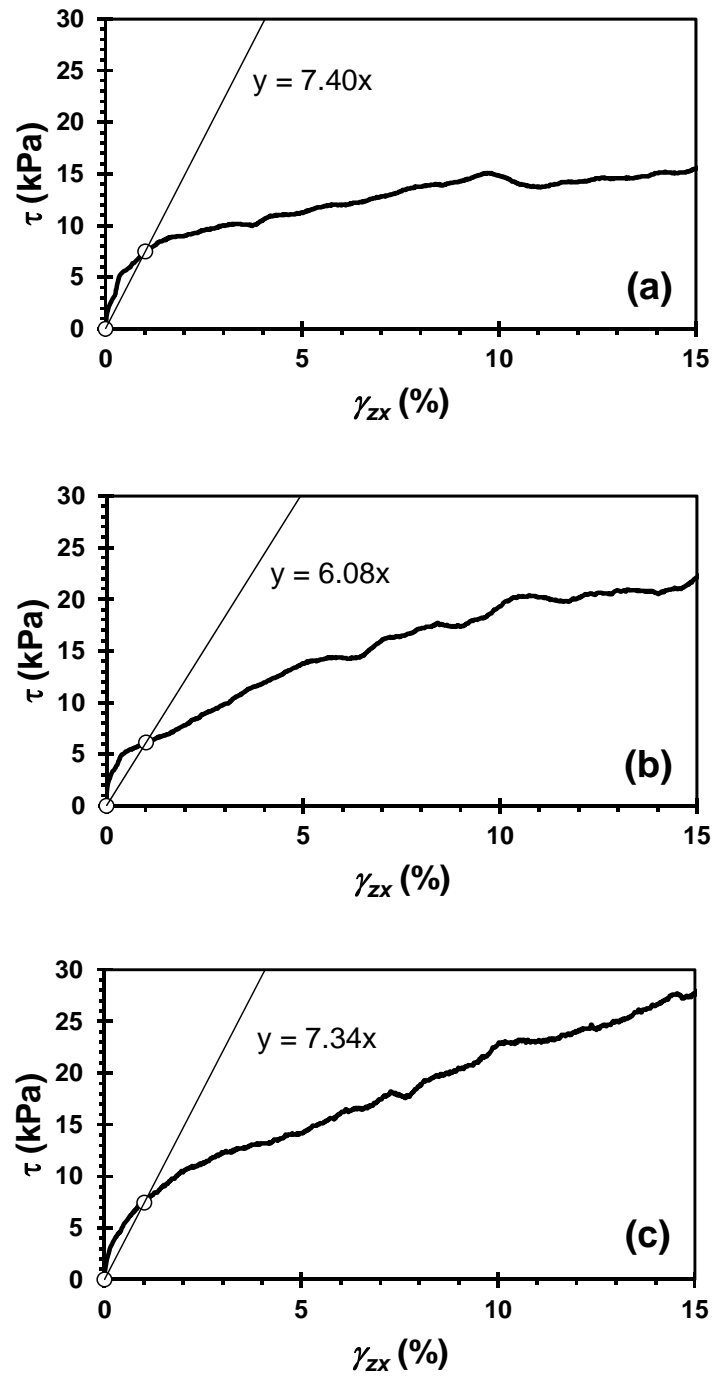


Figure C.8: Secant shear modulus at one percent shear strain with $\sigma_{zz} = 10$ kPa and $D_r = 50\%$ for: (a) fine, (b) intermediate, and (c) coarse gradations.

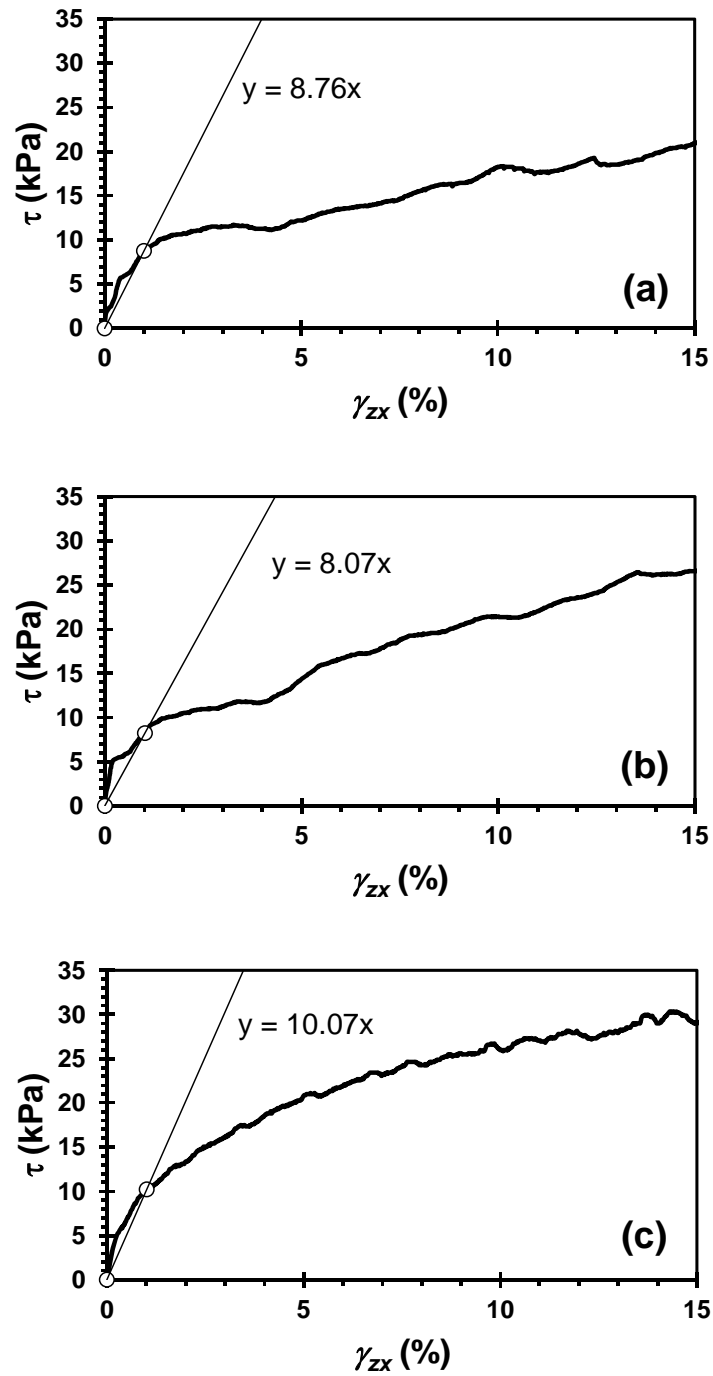


Figure C.9: Secant shear modulus at one percent shear strain with $\sigma_{zz} = 20$ kPa and $D_r = 50\%$ for: (a) fine, (b) intermediate, and (c) coarse gradations.

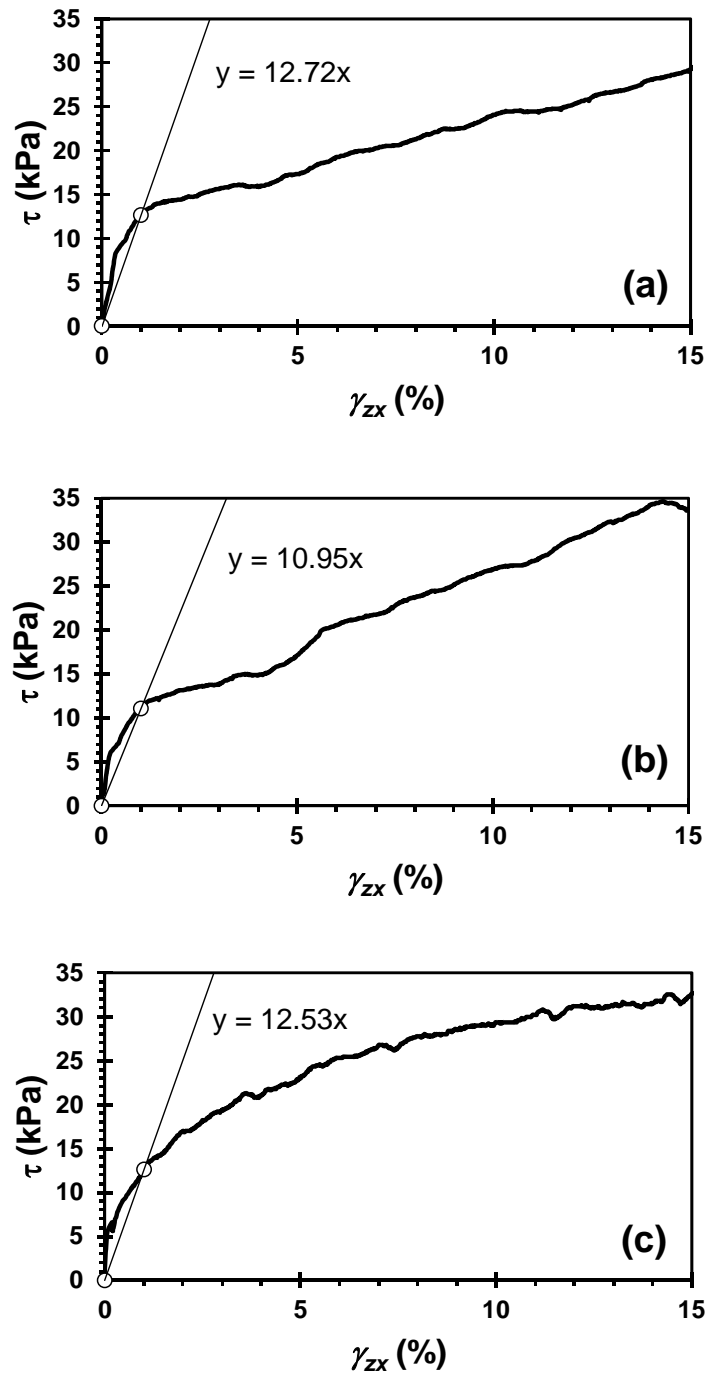


Figure C.10: Secant shear modulus at one percent shear strain with $\sigma_{zz} = 30$ kPa and $D_r = 50\%$ for: (a) fine, (b) intermediate, and (c) coarse gradations.

Appendix D: Cyclic Simple Shear Test Data

CSS results for target fine gradation specimens reconstituted to $D_r = 30\%$ and $\sigma'_v = 30\text{kPa}$. Note: One test consists of two figures (i.e. Figure D.1 and D.2 are for a single test and D.3 and D.4 are for another and so forth).

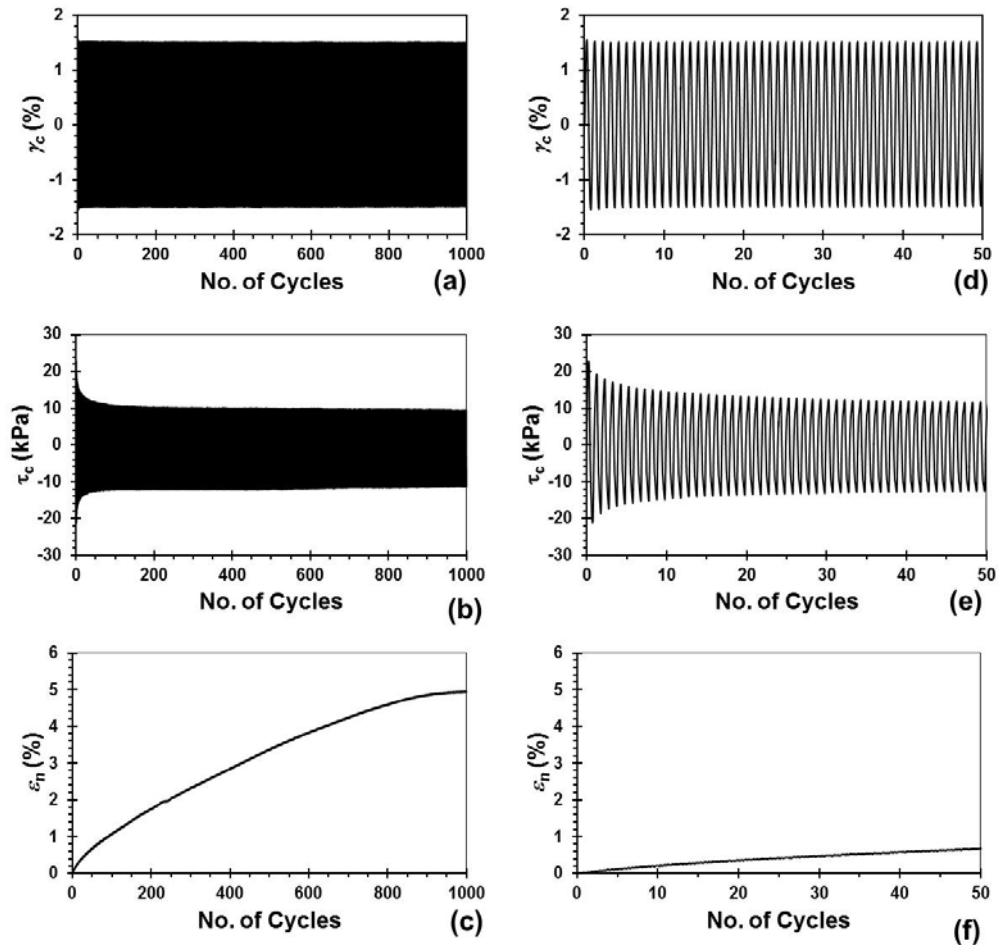


Figure D.1: Results from the fine gradation CSS test through 1000 cycles where: (a) constant magnitude sinusoidal $\gamma_c = 1.5\%$ (b) cyclic shear stress response (c) specimen normal strain. Results for the first 50 cycles: (d), (e), and (f), respectively. Note: $f = 1$ Hz.

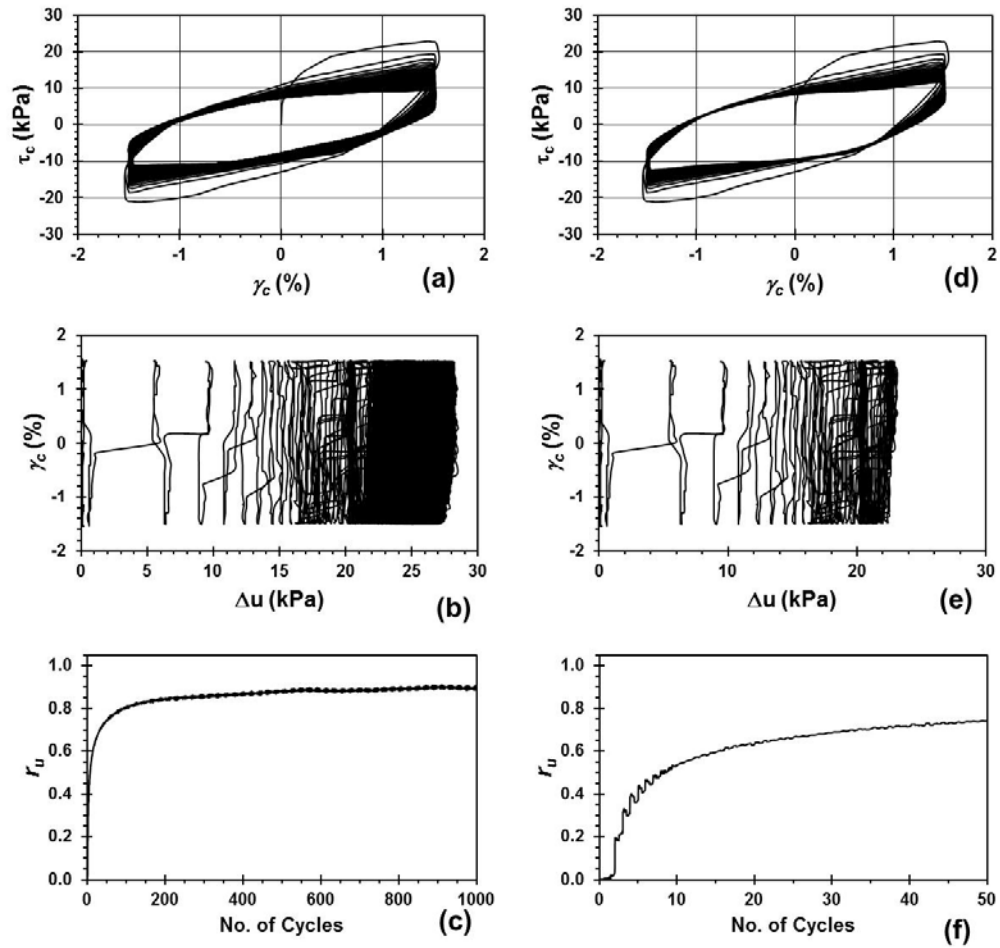


Figure D.2: Results from the fine gradation CSS test through 1000 cycles where: (a) cyclic stress-strain loops (b) cyclic shear strain induced excess pore pressure (c) excess pore pressure ratio. Results for the first 50 cycles: (d), (e), and (f), respectively. Note: $f = 1$ Hz.

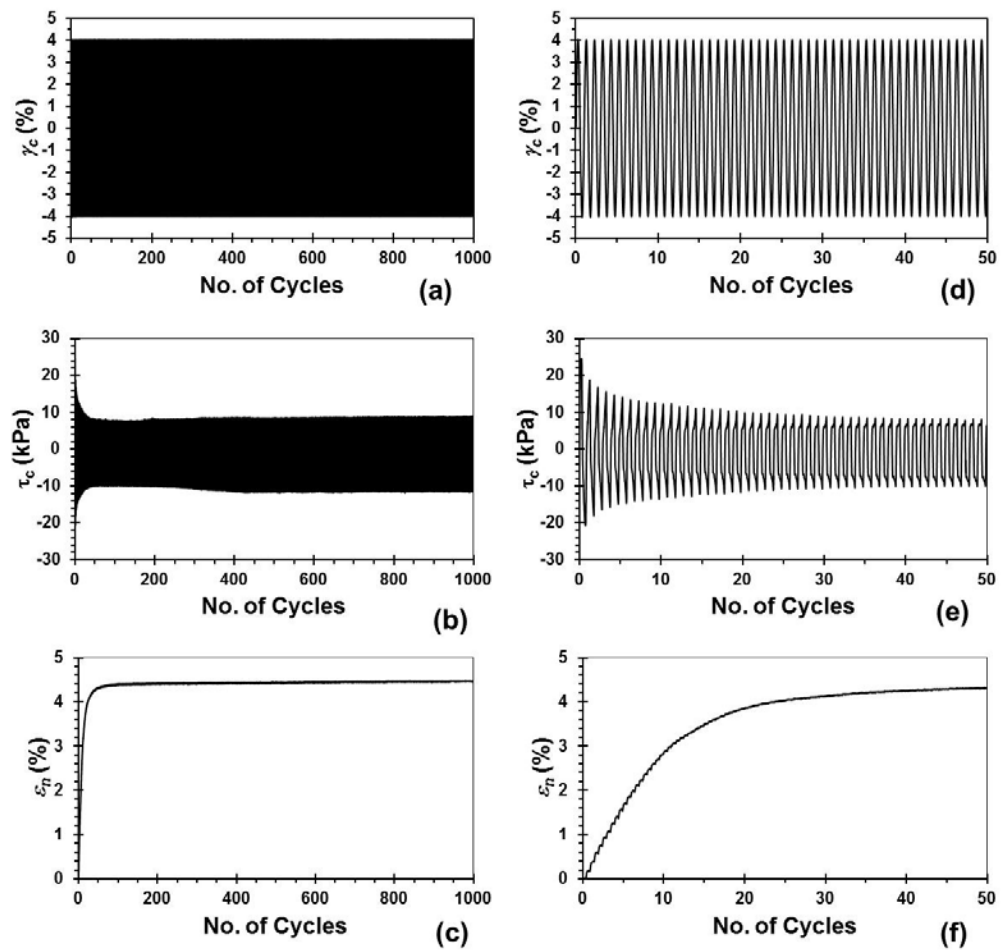


Figure D.3: Results from the fine gradation CSS test through 1000 cycles where: (a) constant magnitude sinusoidal $\gamma_c = 4\%$ (b) cyclic shear stress response (c) specimen normal strain. Results for the first 50 cycles: (d), (e), and (f), respectively. Note: $f = 1$ Hz.

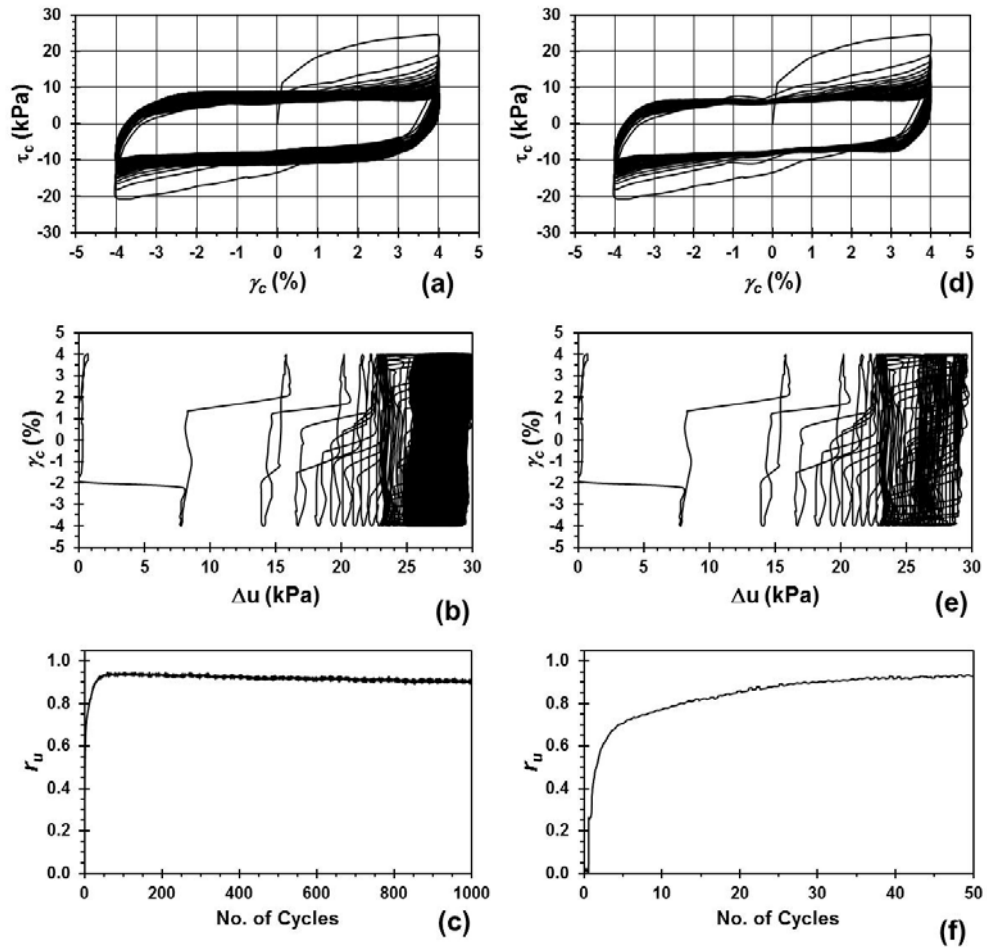


Figure D.4: Results from the fine gradation CSS test through 1000 cycles where: (a) cyclic stress-strain loops (b) cyclic shear strain induced excess pore pressure (c) excess pore pressure ratio. Results for the first 50 cycles: (d), (e), and (f), respectively. Note: $f = 1$ Hz.

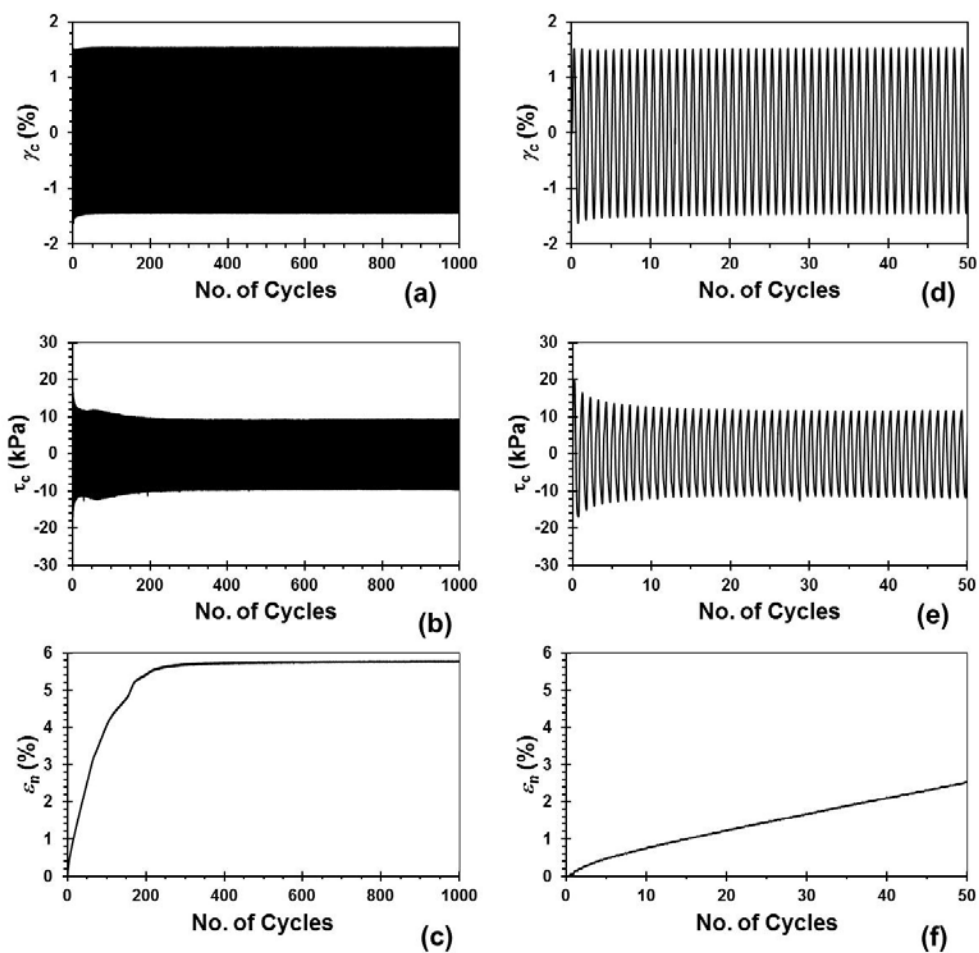


Figure D.5: Results from the fine gradation CSS test through 1000 cycles where: (a) constant magnitude sinusoidal $\gamma_c = 1.5\%$ (b) cyclic shear stress response (c) specimen normal strain. Results for the first 50 cycles: (d), (e), and (f), respectively. Note: $f = 2$ Hz.

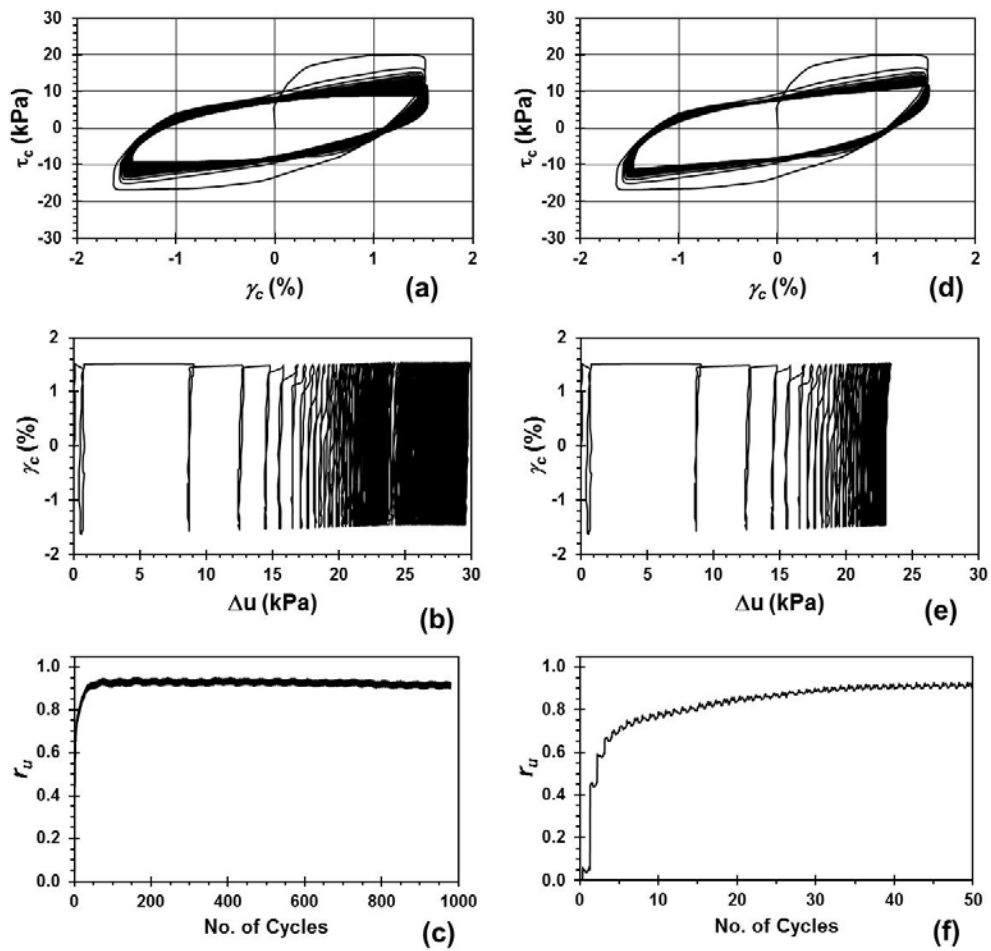


Figure D.6: Results from the fine gradation CSS test through 1000 cycles where: (a) cyclic stress-strain loops (b) cyclic shear strain induced excess pore pressure (c) excess pore pressure ratio. Results for the first 50 cycles: (d), (e), and (f), respectively. Note: $f = 2$ Hz.

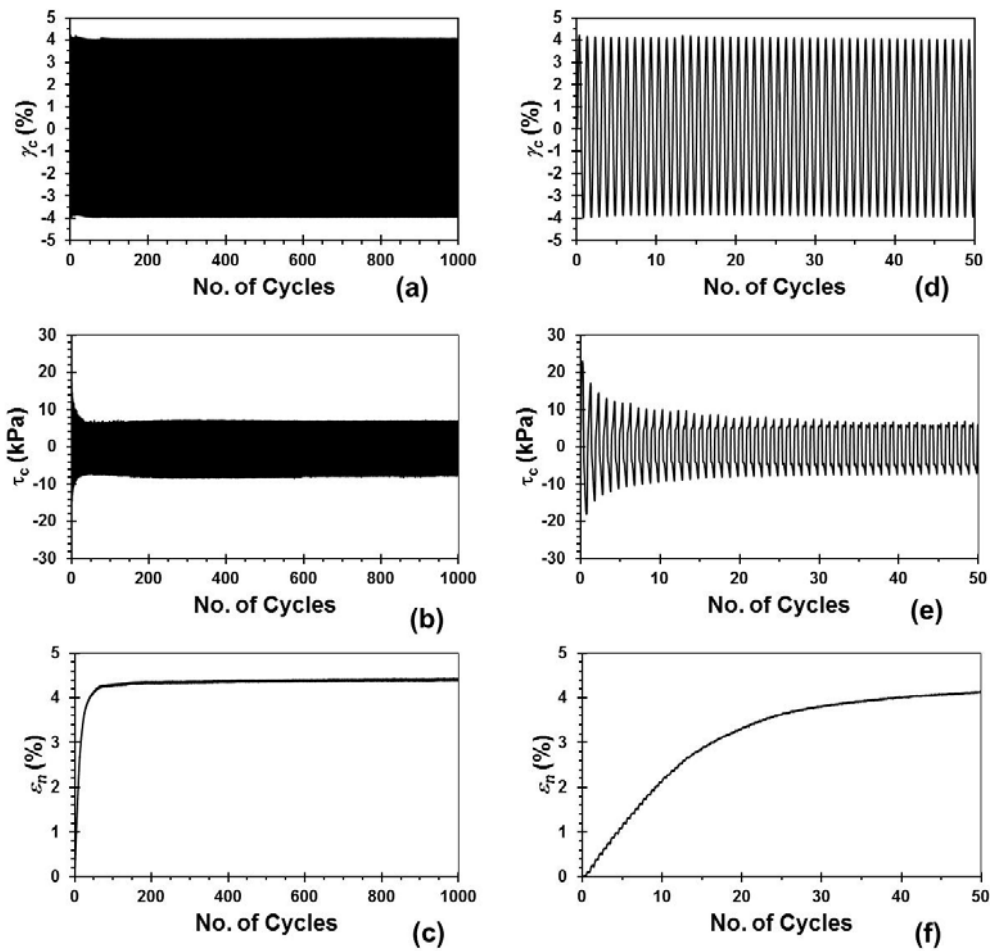


Figure D.7: Results from the fine gradation CSS test through 1000 cycles where: (a) constant magnitude sinusoidal $\gamma_c = 4\%$ (b) cyclic shear stress response (c) specimen normal strain. Results for the first 50 cycles: (d), (e), and (f), respectively. Note: $f = 2$ Hz.

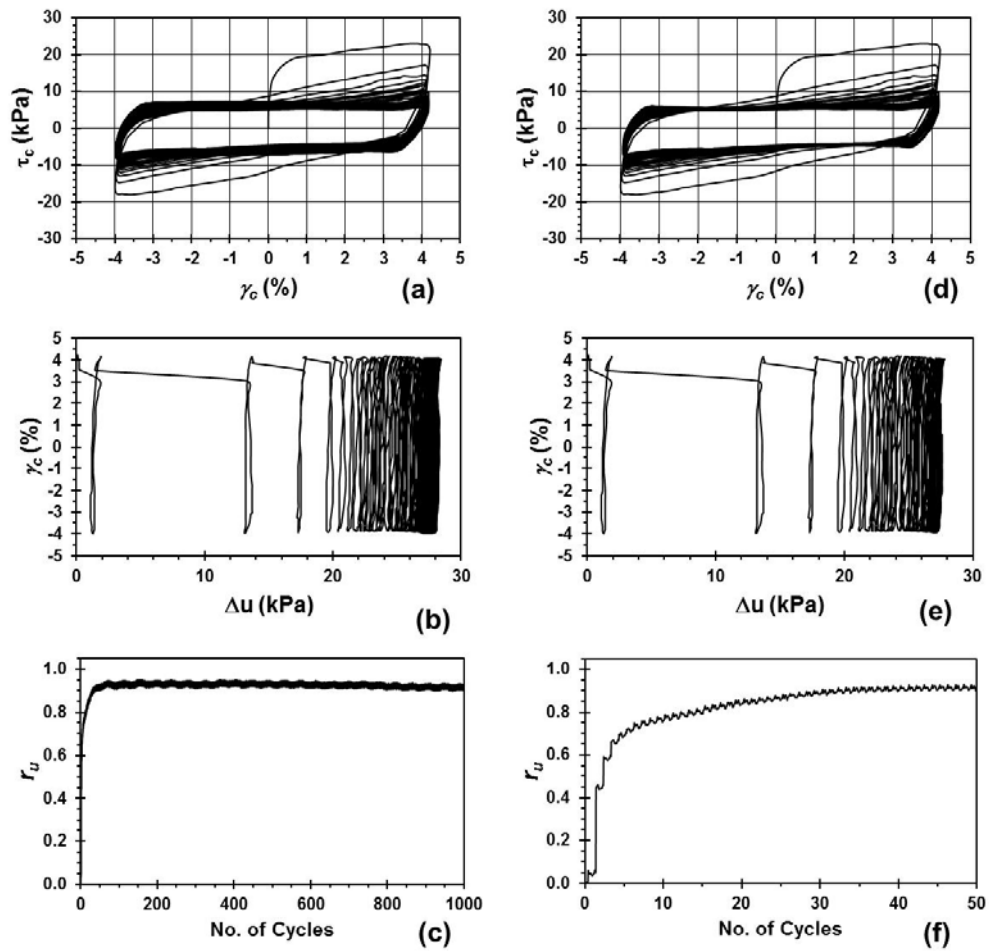


Figure D.8: Results from the fine gradation CSS test through 1000 cycles where: (a) cyclic stress-strain loops (b) cyclic shear strain induced excess pore pressure (c) excess pore pressure ratio. Results for the first 50 cycles: (d), (e), and (f), respectively. Note: $f = 2$ Hz.

CSS results for target intermediate gradation specimens reconstituted to $D_r = 30\%$ and $\sigma'_v = 30\text{kPa}$.

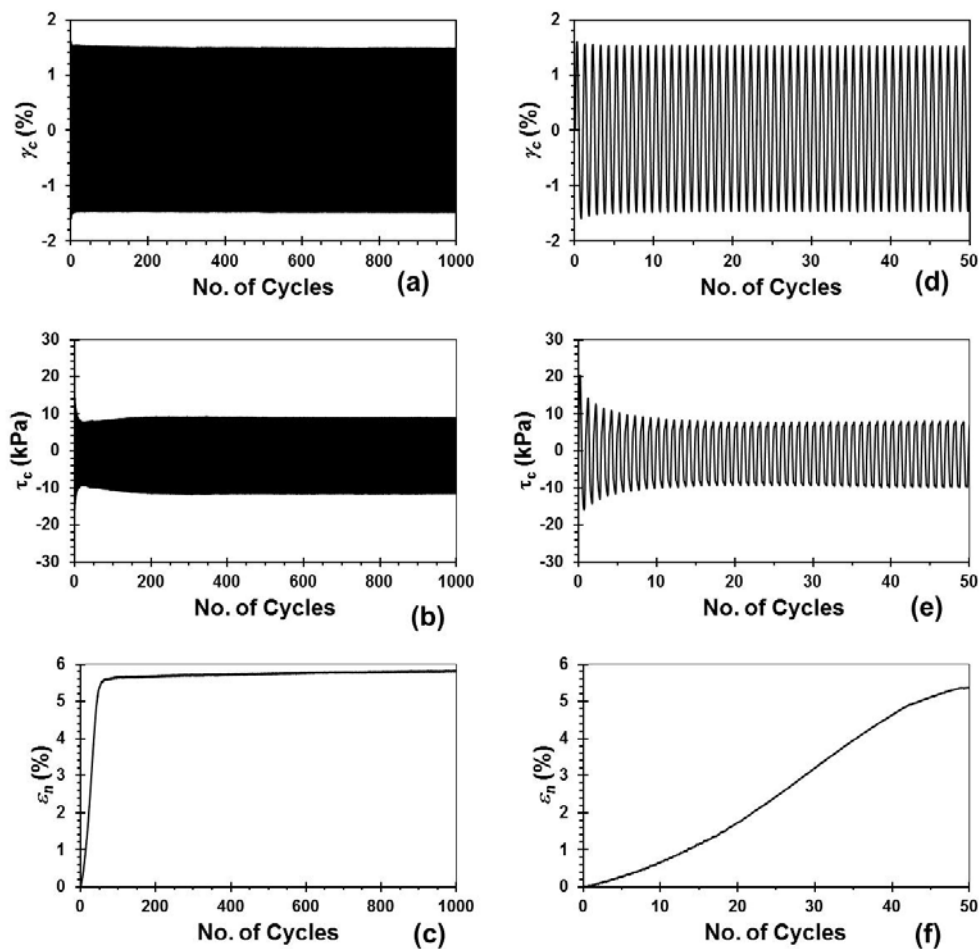


Figure D.9: Results from the intermediate gradation CSS test through 1000 cycles where: (a) constant magnitude sinusoidal $\gamma_c = 1.5\%$ (b) cyclic shear stress response (c) specimen normal strain. Results for the first 50 cycles: (d), (e), and (f), respectively. Note: $f = 1\text{ Hz}$.

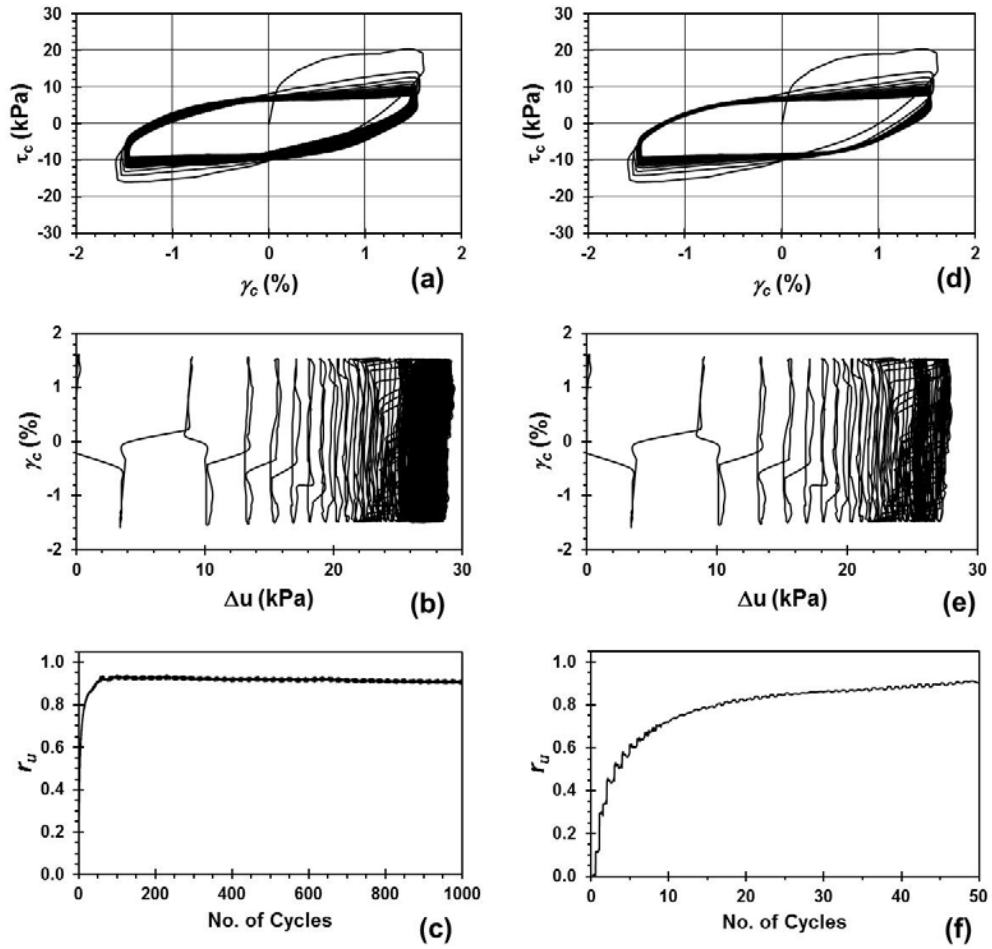


Figure D.10: Results from the intermediate gradation CSS test through 1000 cycles where: (a) cyclic stress-strain loops (b) cyclic shear strain induced excess pore pressure (c) excess pore pressure ratio. Results for the first 50 cycles: (d), (e), and (f), respectively. Note: $f = 1$ Hz.

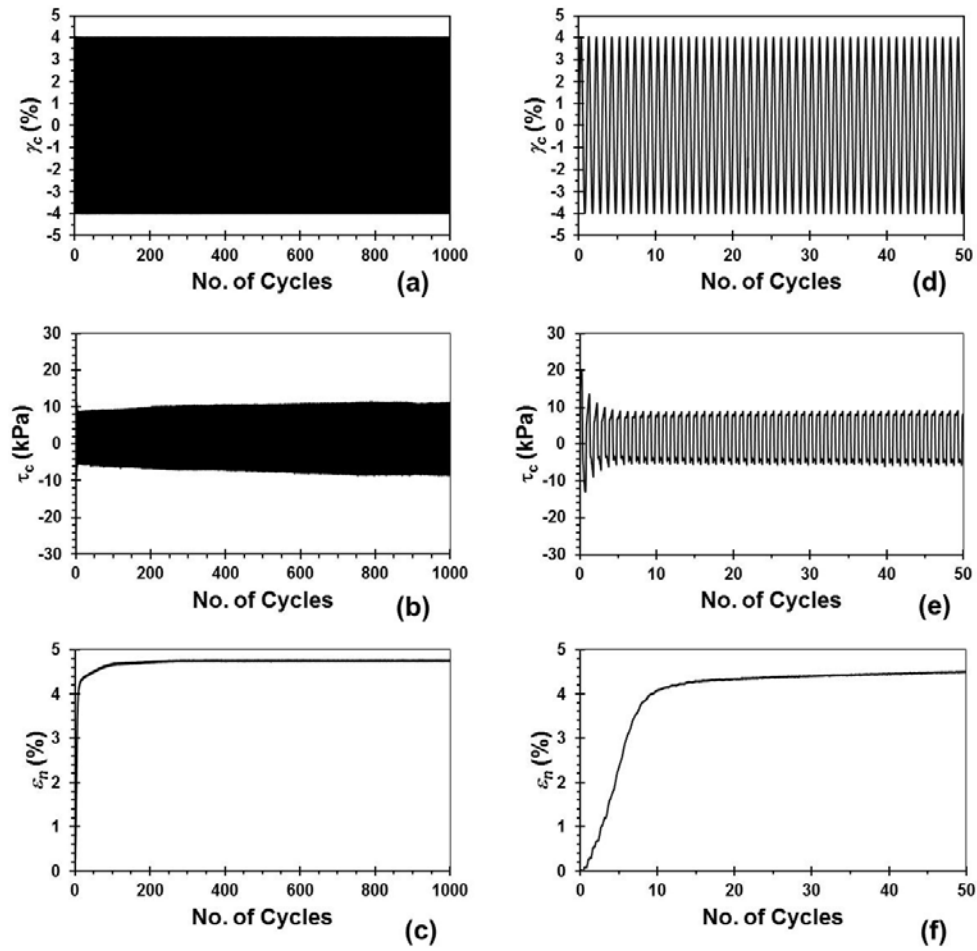


Figure D.11: Results from the intermediate gradation CSS test through 1000 cycles where: (a) constant magnitude sinusoidal $\gamma_c = 4\%$ (b) cyclic shear stress response (c) specimen normal strain. Results for the first 50 cycles: (d), (e), and (f), respectively. Note: $f = 1$ Hz.

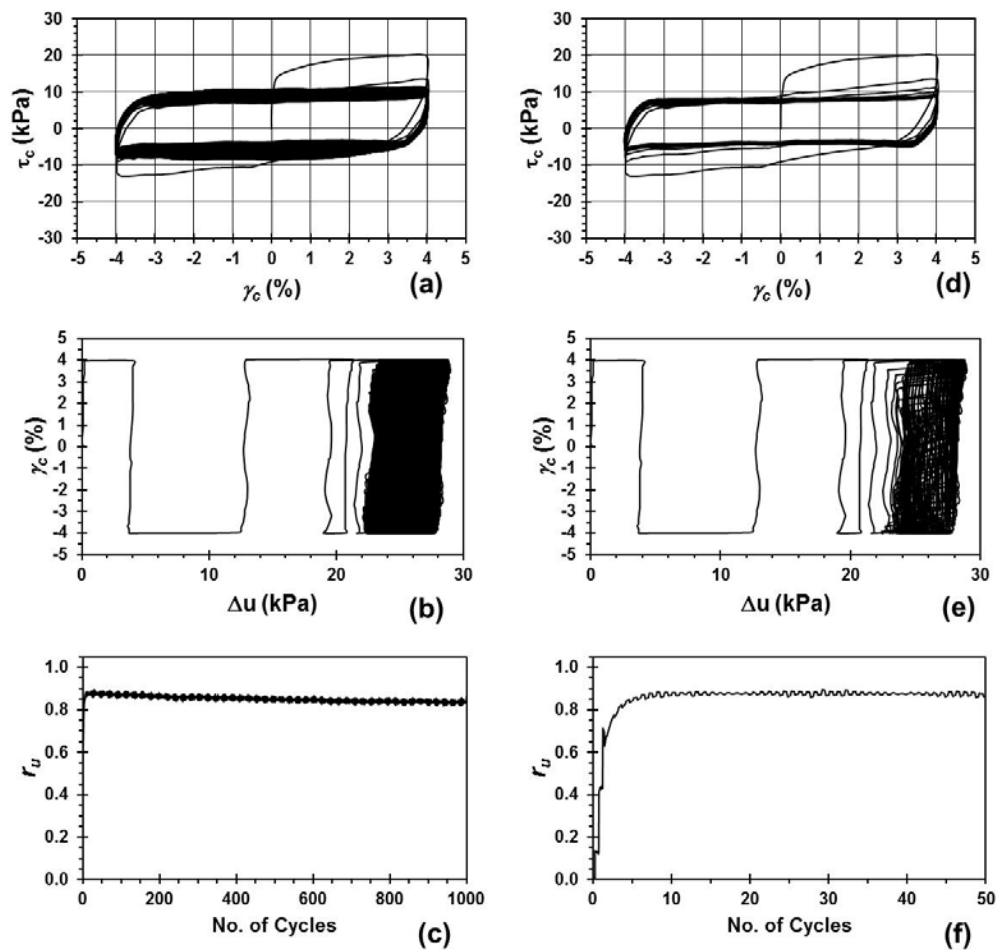


Figure D.12: Results from the intermediate gradation CSS test through 1000 cycles where: (a) cyclic stress-strain loops (b) cyclic shear strain induced excess pore pressure (c) excess pore pressure ratio. Results for the first 50 cycles: (d), (e), and (f), respectively. Note: $f = 1$ Hz.

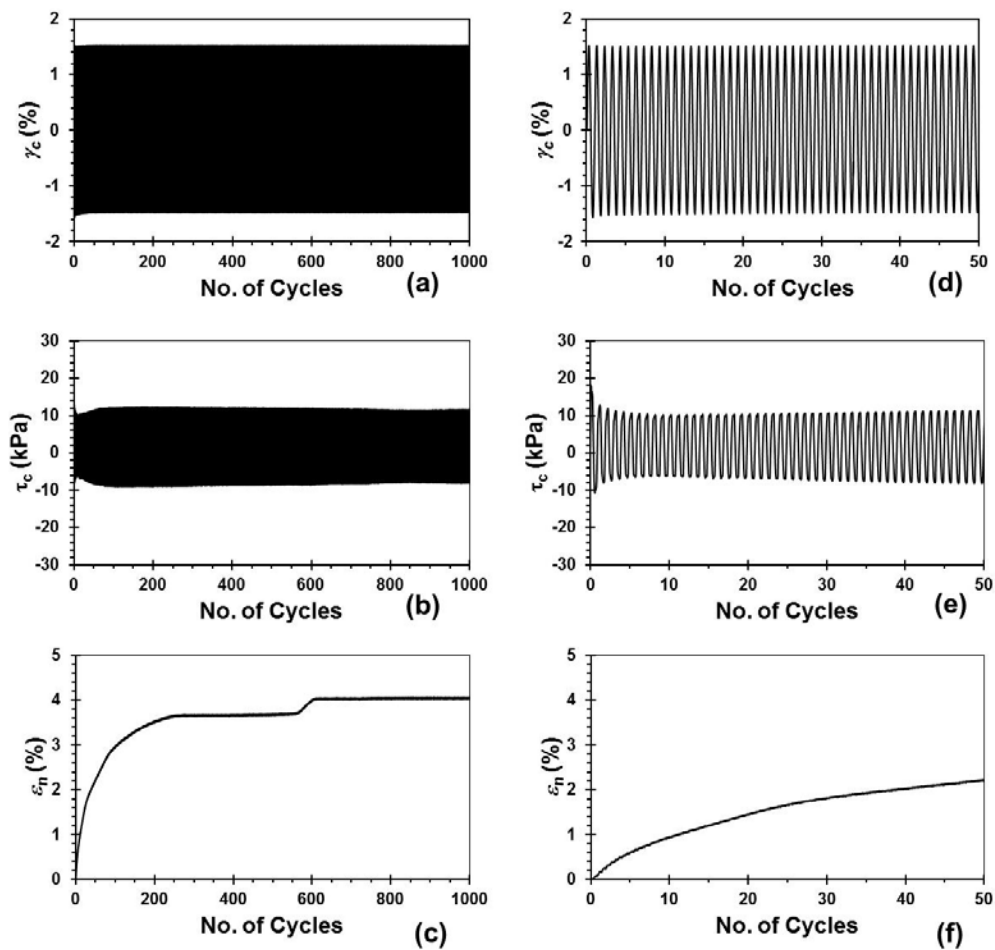


Figure D.13: Results from the intermediate gradation CSS test through 1000 cycles where: (a) constant magnitude sinusoidal $\gamma_c = 1.5\%$ (b) cyclic shear stress response (c) specimen normal strain. Results for the first 50 cycles: (d), (e), and (f), respectively. Note: $f = 2$ Hz.

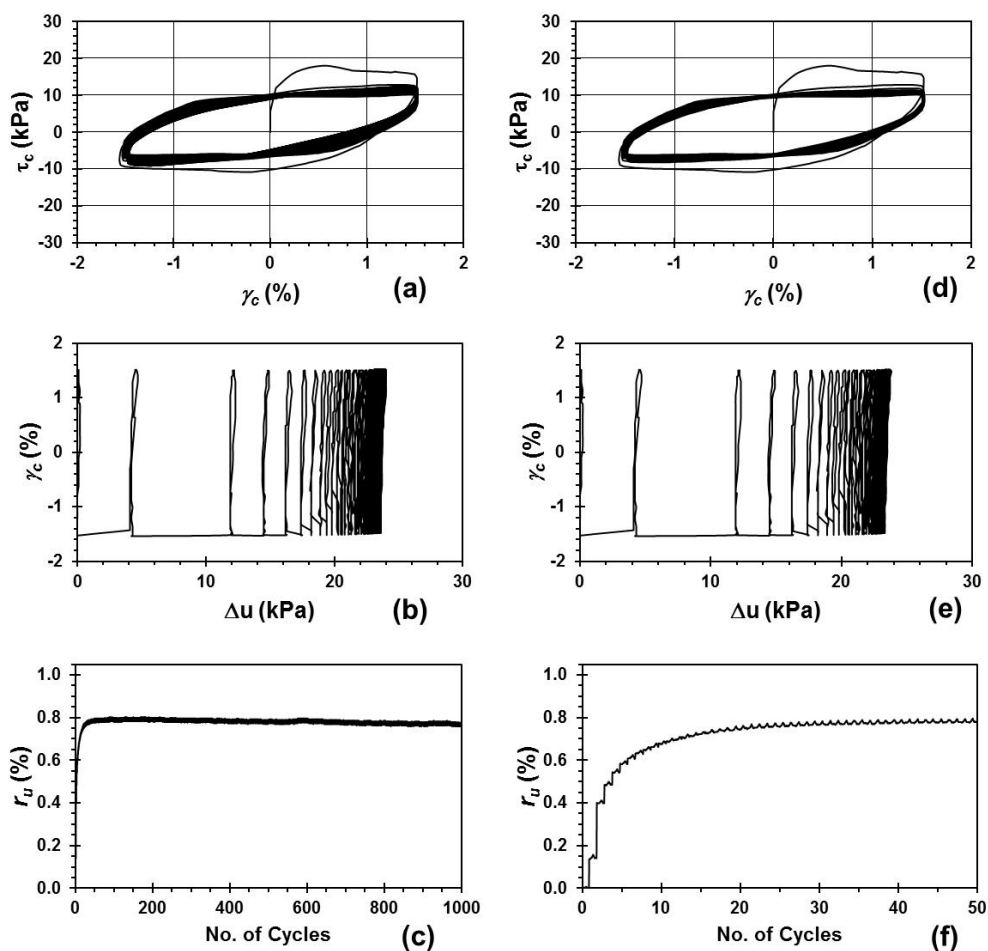


Figure D.14: Results from the intermediate gradation CSS test through 1000 cycles where: (a) cyclic stress-strain loops (b) cyclic shear strain induced excess pore pressure (c) excess pore pressure ratio. Results for the first 50 cycles: (d), (e), and (f), respectively. Note: $f = 2$ Hz.

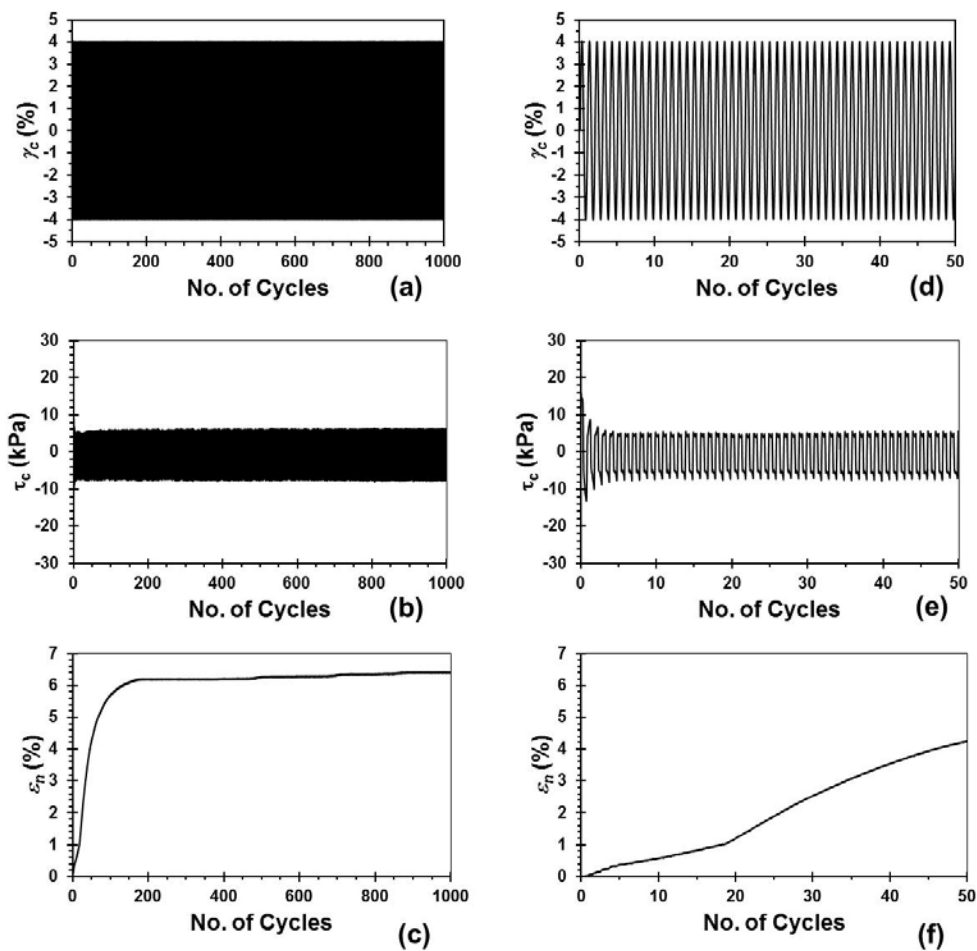


Figure D.15: Results from the intermediate gradation CSS test through 1000 cycles where: (a) constant magnitude sinusoidal $\gamma_c = 4\%$ (b) cyclic shear stress response (c) specimen normal strain. Results for the first 50 cycles: (d), (e), and (f), respectively. Note: $f = 2$ Hz.

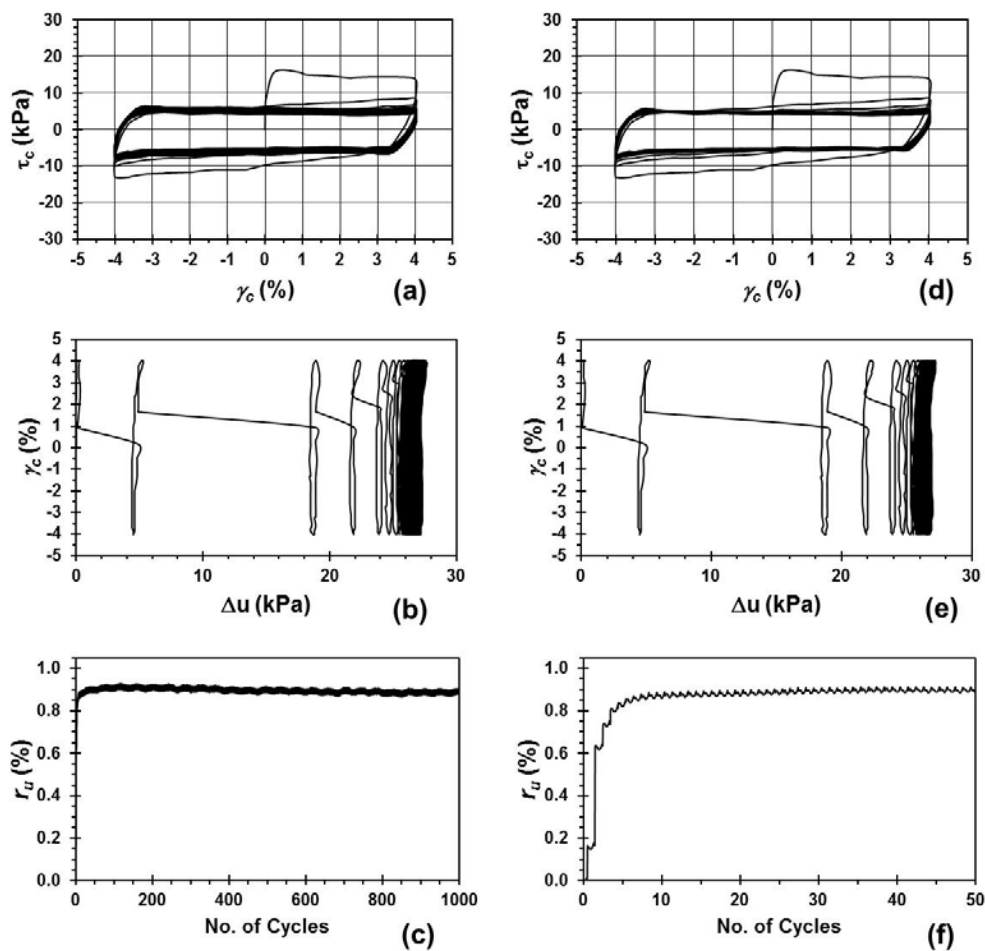


Figure D.16: Results from the intermediate gradation CSS test through 1000 cycles where: (a) cyclic stress-strain loops (b) cyclic shear strain induced excess pore pressure (c) excess pore pressure ratio. Results for the first 50 cycles: (d), (e), and (f), respectively. Note: $f = 2$ Hz.

CSS results for target coarse gradation specimens reconstituted to $D_r = 30\%$ and $\sigma'_v = 30\text{kPa}$.

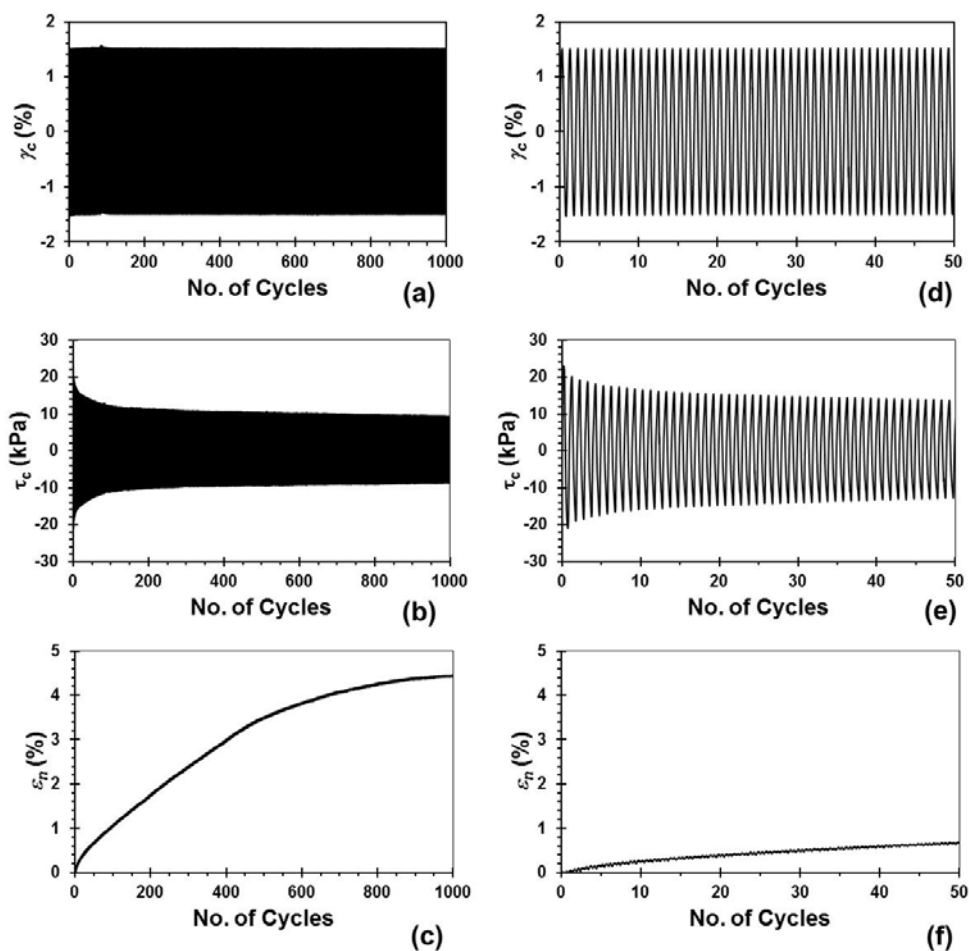


Figure D.17: Results from the coarse gradation CSS test through 1000 cycles where: (a) constant magnitude sinusoidal $\gamma_c = 1.5\%$ (b) cyclic shear stress response (c) specimen normal strain. Results for the first 50 cycles: (d), (e), and (f), respectively. Note: $f = 1$ Hz.

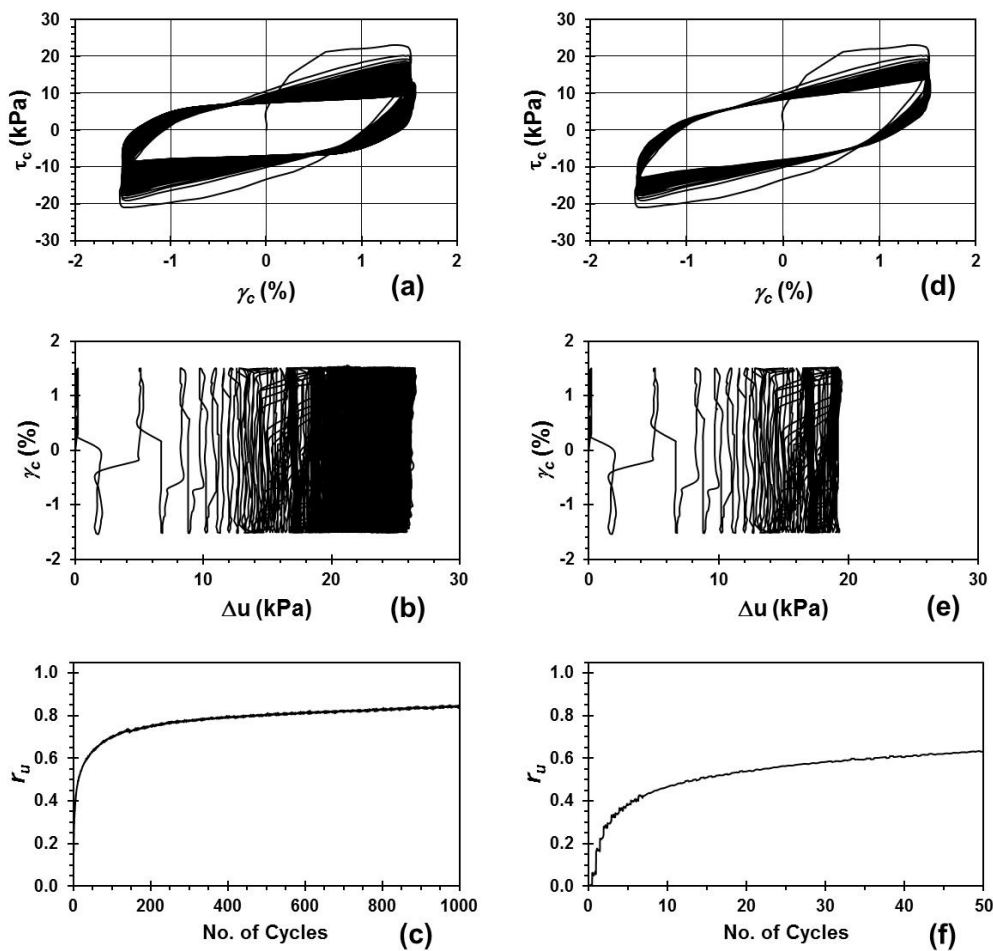


Figure D.18: Results from the coarse gradation CSS test through 1000 cycles where: (a) cyclic stress-strain loops (b) cyclic shear strain induced excess pore pressure (c) excess pore pressure ratio. Results for the first 50 cycles: (d), (e), and (f), respectively. Note: $f = 1$ Hz.

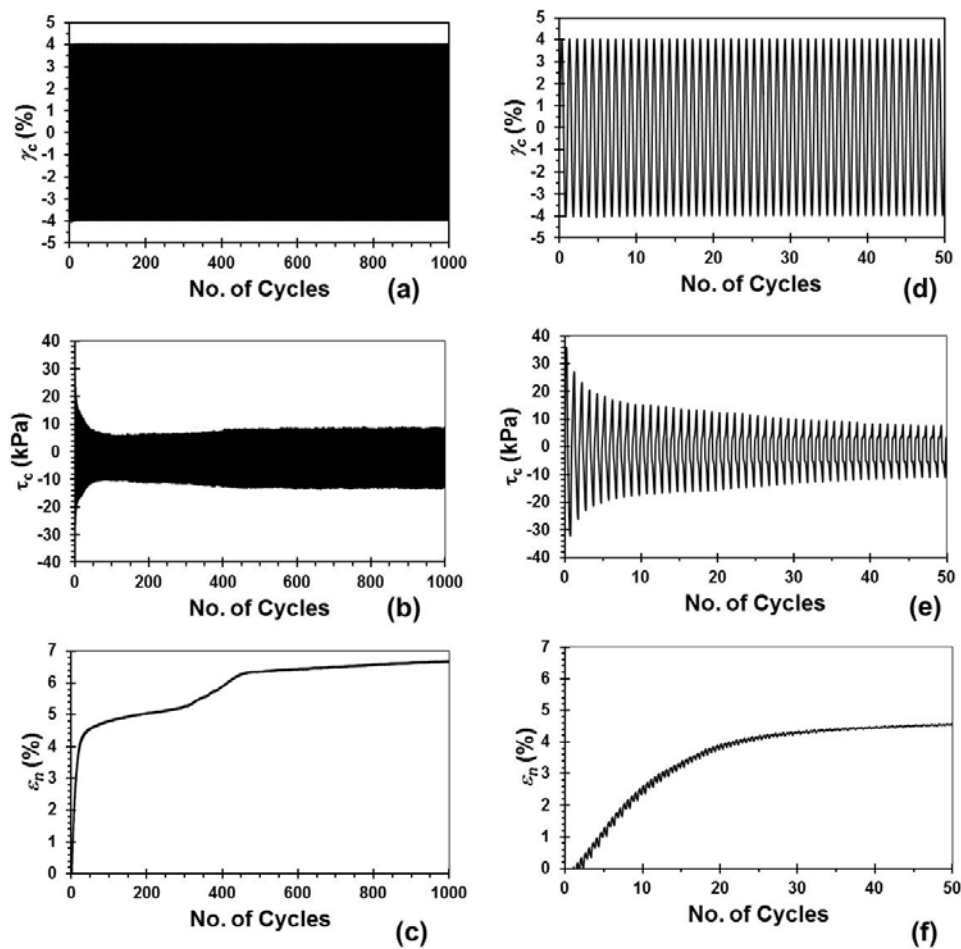


Figure D.19: Results from the coarse gradation CSS test through 1000 cycles where: (a) constant magnitude sinusoidal $\gamma_c = 4\%$ (b) cyclic shear stress response (c) specimen normal strain. Results for the first 50 cycles: (d), (e), and (f), respectively. Note: $f = 1$ Hz.

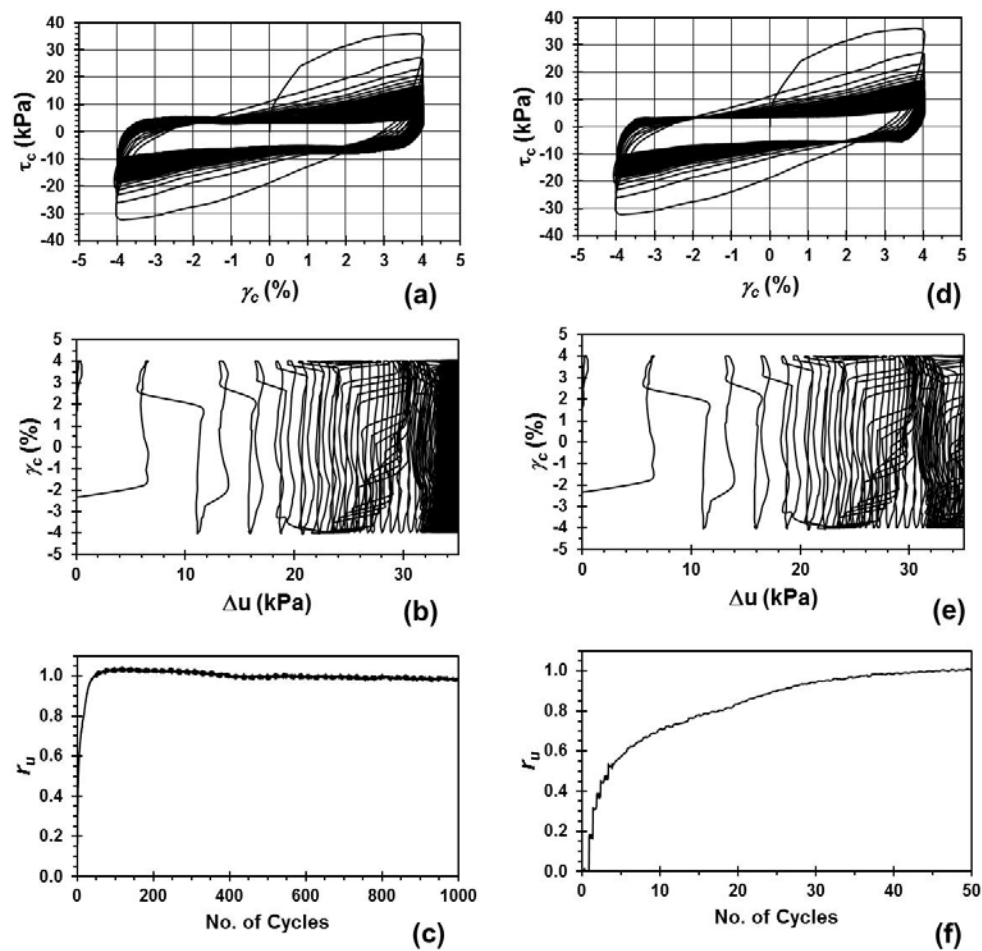


Figure D.20: Results from the coarse gradation CSS test through 1000 cycles where: (a) cyclic stress-strain loops (b) cyclic shear strain induced excess pore pressure (c) excess pore pressure ratio. Results for the first 50 cycles: (d), (e), and (f), respectively. Note: $f = 1$ Hz.

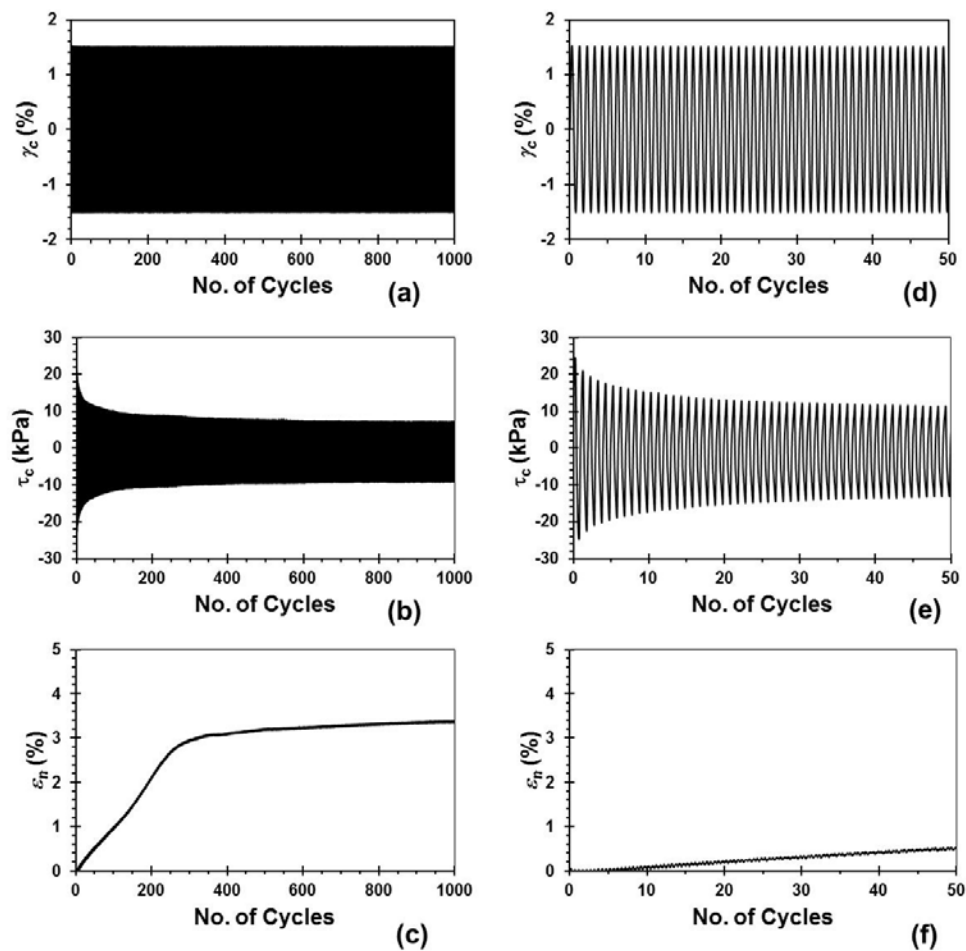


Figure D.21: Results from the coarse gradation CSS test through 1000 cycles where: (a) constant magnitude sinusoidal $\gamma_c = 1.5\%$ (b) cyclic shear stress response (c) specimen normal strain. Results for the first 50 cycles: (d), (e), and (f), respectively. Note: $f = 2$ Hz.

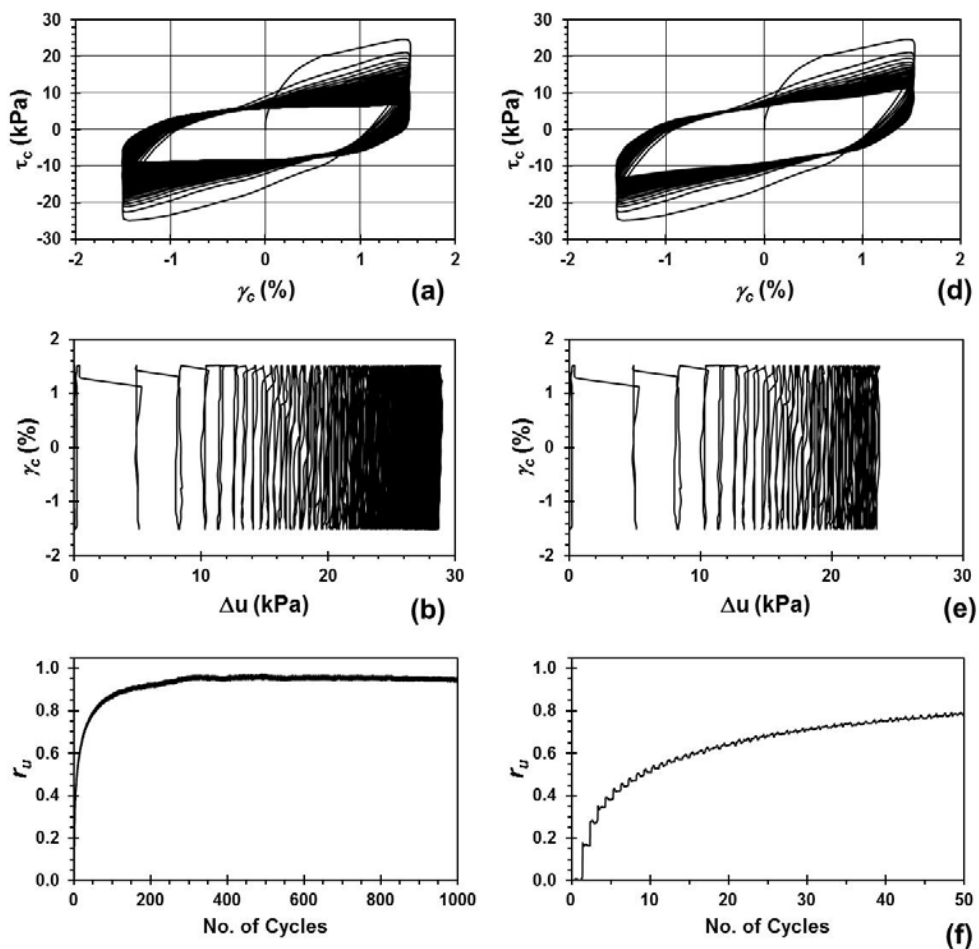


Figure D.22: Results from the coarse gradation CSS test through 1000 cycles where: (a) cyclic stress-strain loops (b) cyclic shear strain induced excess pore pressure (c) excess pore pressure ratio. Results for the first 50 cycles: (d), (e), and (f), respectively. Note: $f = 2$ Hz.

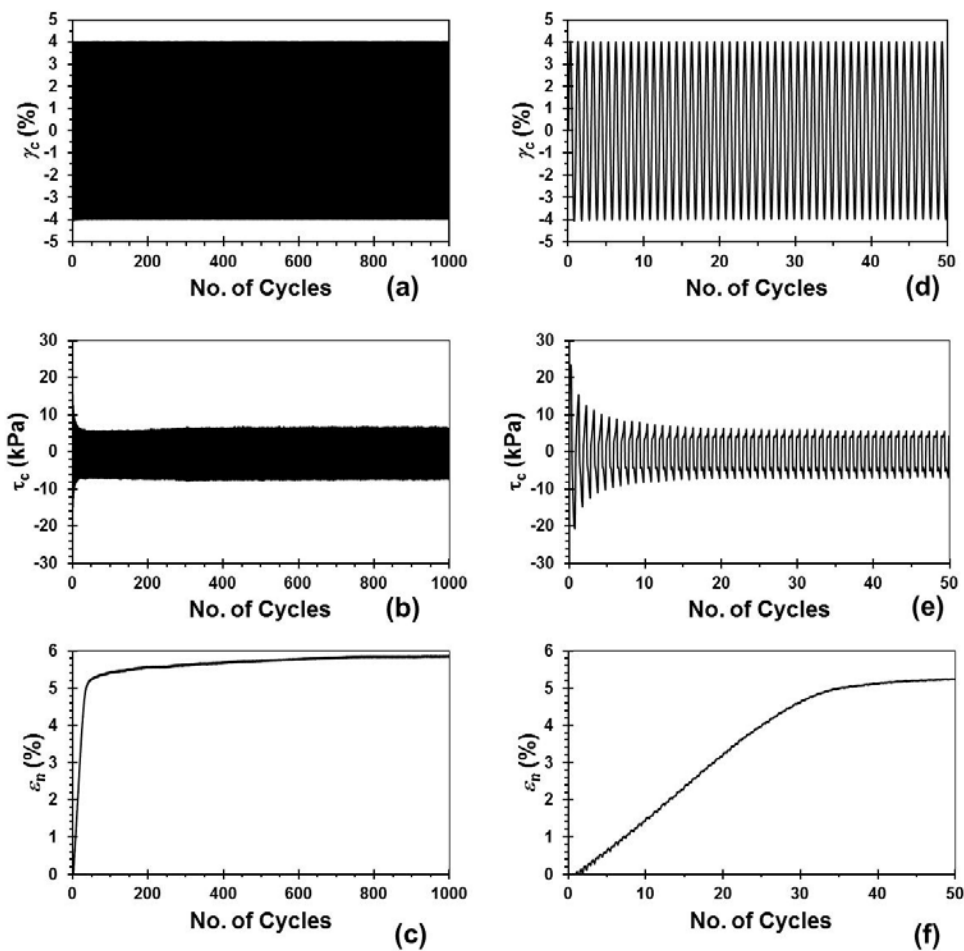


Figure D.23: Results from the coarse gradation CSS test through 1000 cycles where: (a) constant magnitude sinusoidal $\gamma_c = 4\%$ (b) cyclic shear stress response (c) specimen normal strain. Results for the first 50 cycles: (d), (e), and (f), respectively. Note: $f = 2$ Hz.

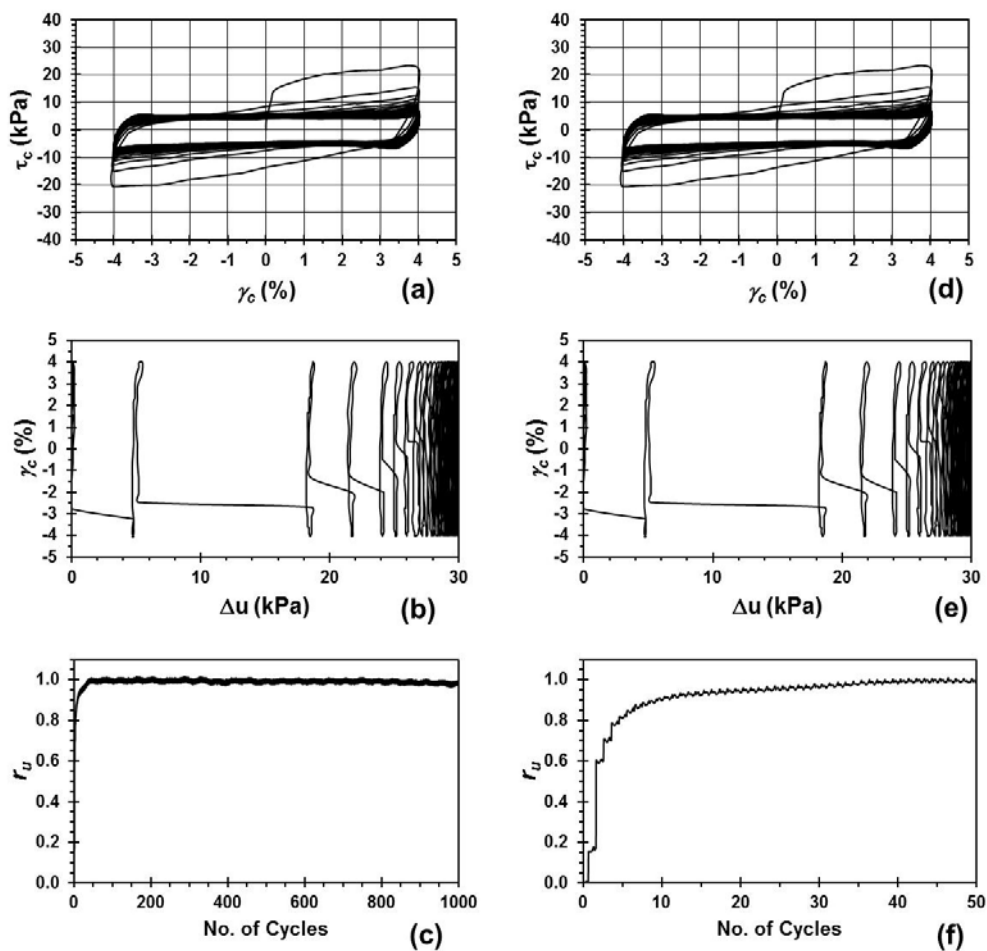


Figure D.24: Results from the coarse gradation CSS test through 1000 cycles where: (a) cyclic stress-strain loops (b) cyclic shear strain induced excess pore pressure (c) excess pore pressure ratio. Results for the first 50 cycles: (d), (e), and (f), respectively. Note: $f = 2$ Hz.

CSS results for target fine gradation specimens reconstituted to $D_r = 50\%$ and $\sigma'_v = 30\text{kPa}$.

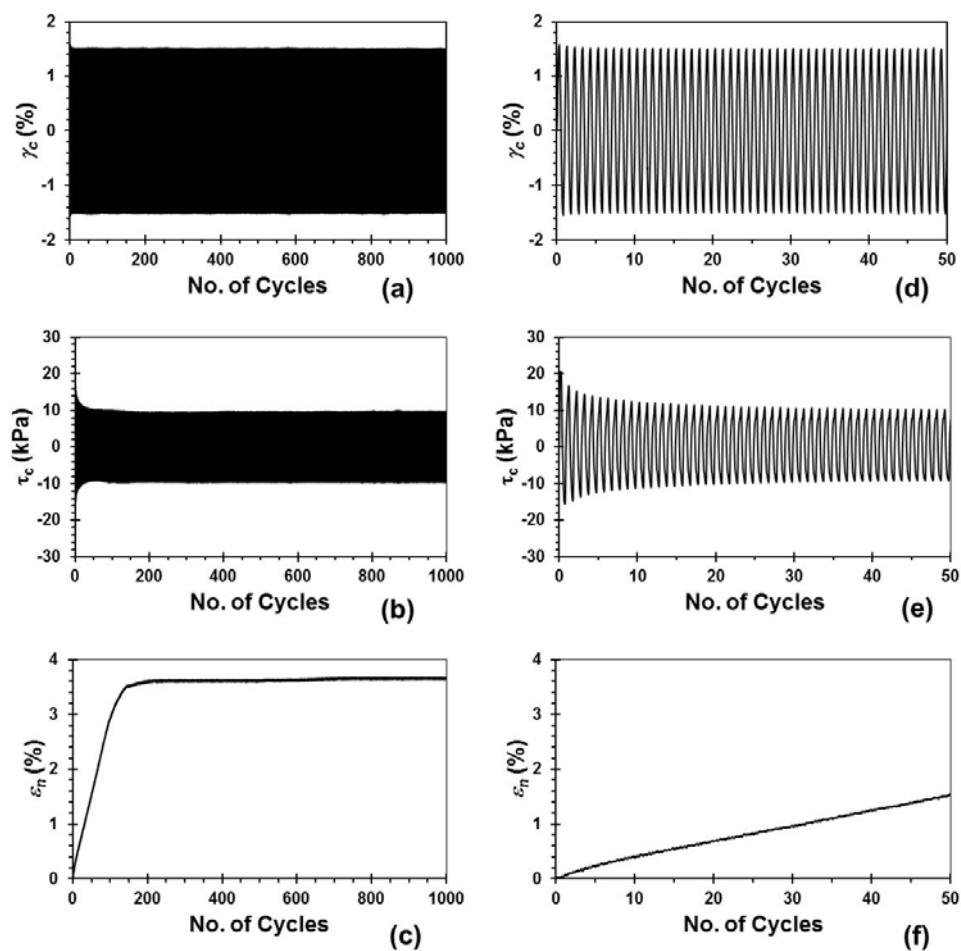


Figure D.25: Results from the fine gradation CSS test through 1000 cycles where: (a) constant magnitude sinusoidal $\gamma_c = 1.5\%$ (b) cyclic shear stress response (c) specimen normal strain. Results for the first 50 cycles: (d), (e), and (f), respectively. Note: $f = 1$ Hz.

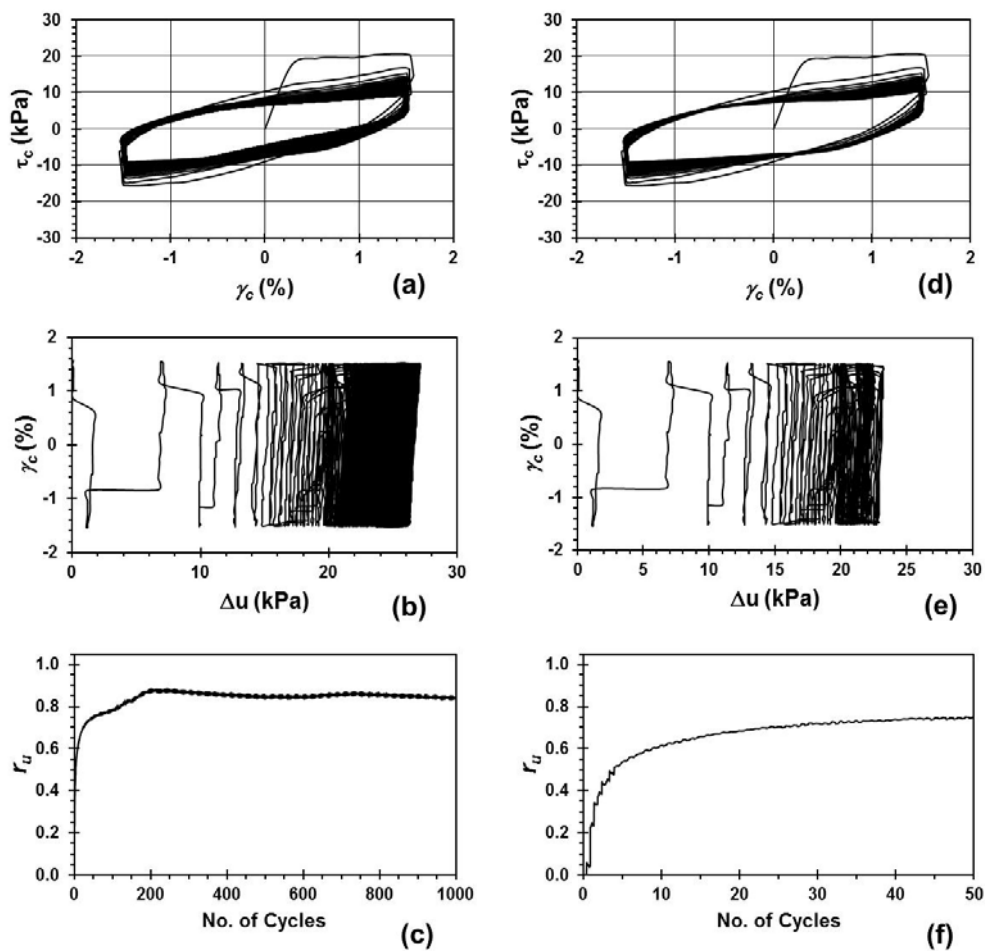


Figure D.26: Results from the fine gradation CSS test through 1000 cycles where: (a) cyclic stress-strain loops (b) cyclic shear strain induced excess pore pressure (c) excess pore pressure ratio. Results for the first 50 cycles: (d), (e), and (f), respectively. Note: $f = 1$ Hz.

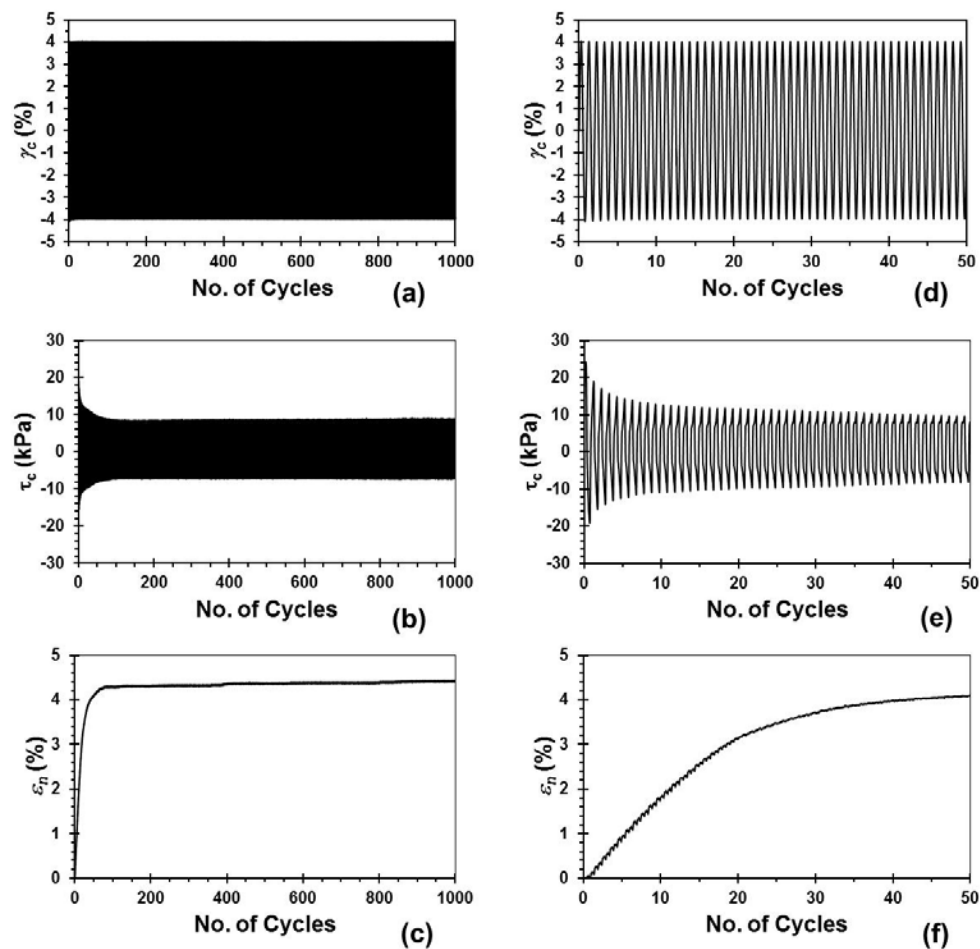


Figure D.27: Results from the fine gradation CSS test through 1000 cycles where: (a) constant magnitude sinusoidal $\gamma_c = 4\%$ (b) cyclic shear stress response (c) specimen normal strain. Results for the first 50 cycles: (d), (e), and (f), respectively. Note: $f = 1$ Hz.

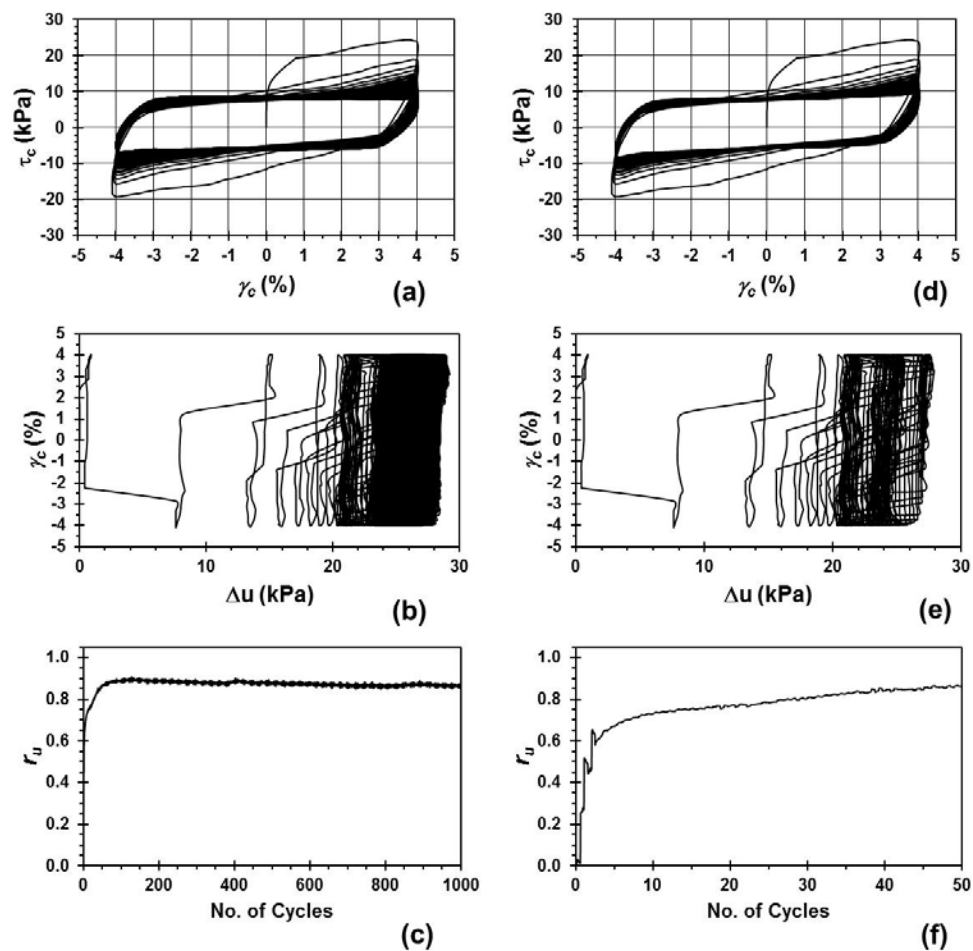


Figure D.28: Results from the fine gradation CSS test through 1000 cycles where: (a) cyclic stress-strain loops (b) cyclic shear strain induced excess pore pressure (c) excess pore pressure ratio. Results for the first 50 cycles: (d), (e), and (f), respectively. Note: $f = 1$ Hz.

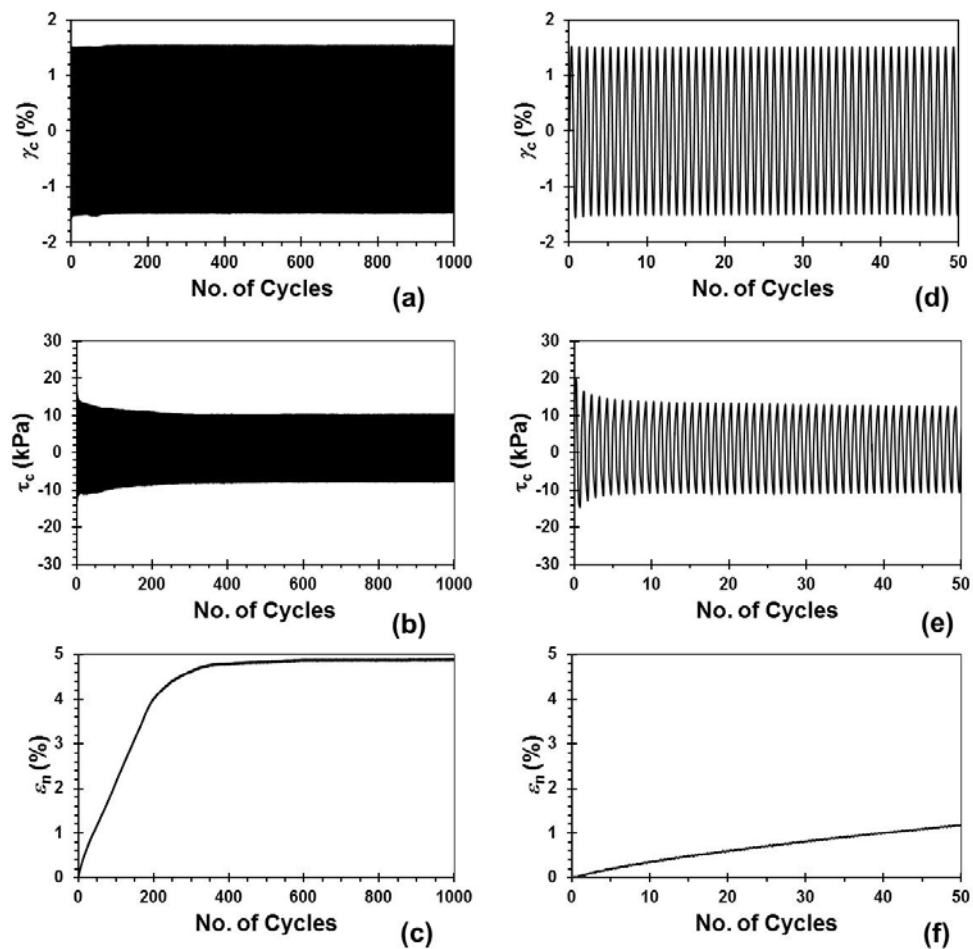


Figure D.29: Results from the fine gradation CSS test through 1000 cycles where: (a) constant magnitude sinusoidal $\gamma_c = 1.5\%$ (b) cyclic shear stress response (c) specimen normal strain. Results for the first 50 cycles: (d), (e), and (f), respectively. Note: $f = 2$ Hz.

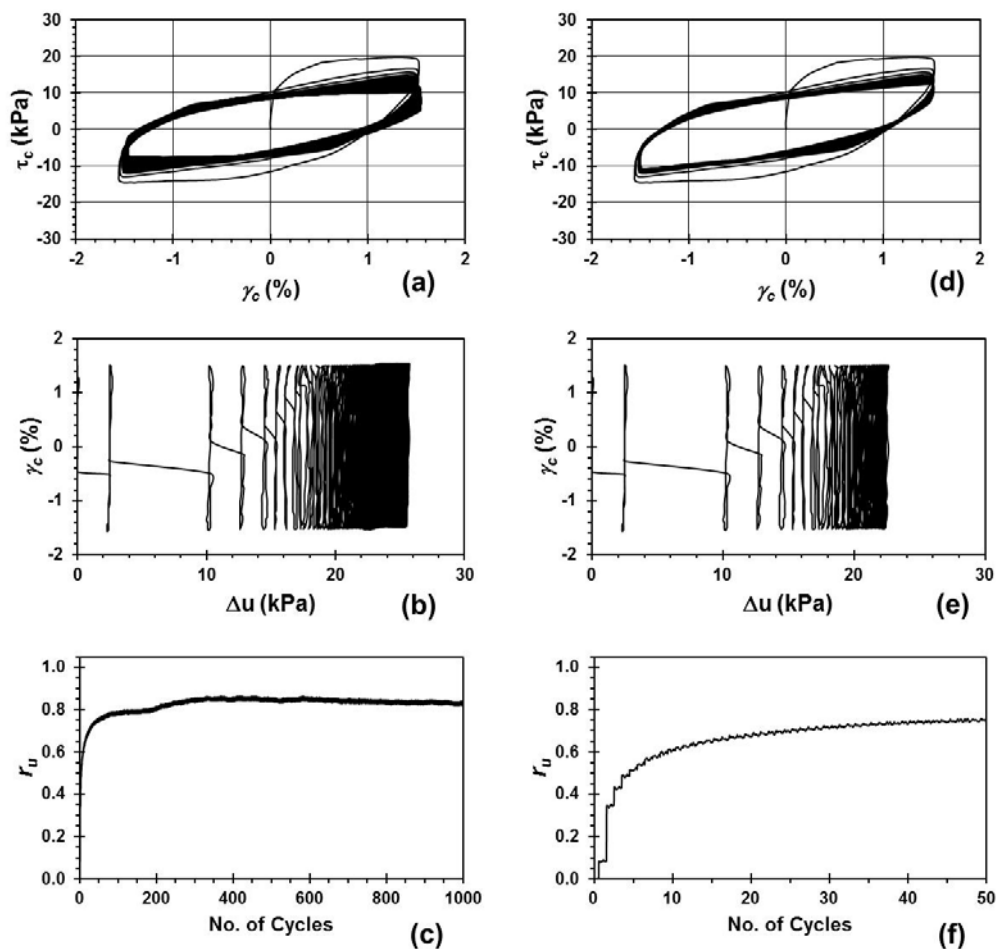


Figure D.30: Results from the fine gradation CSS test through 1000 cycles where: (a) cyclic stress-strain loops (b) cyclic shear strain induced excess pore pressure (c) excess pore pressure ratio. Results for the first 50 cycles: (d), (e), and (f), respectively. Note: $f = 2$ Hz.

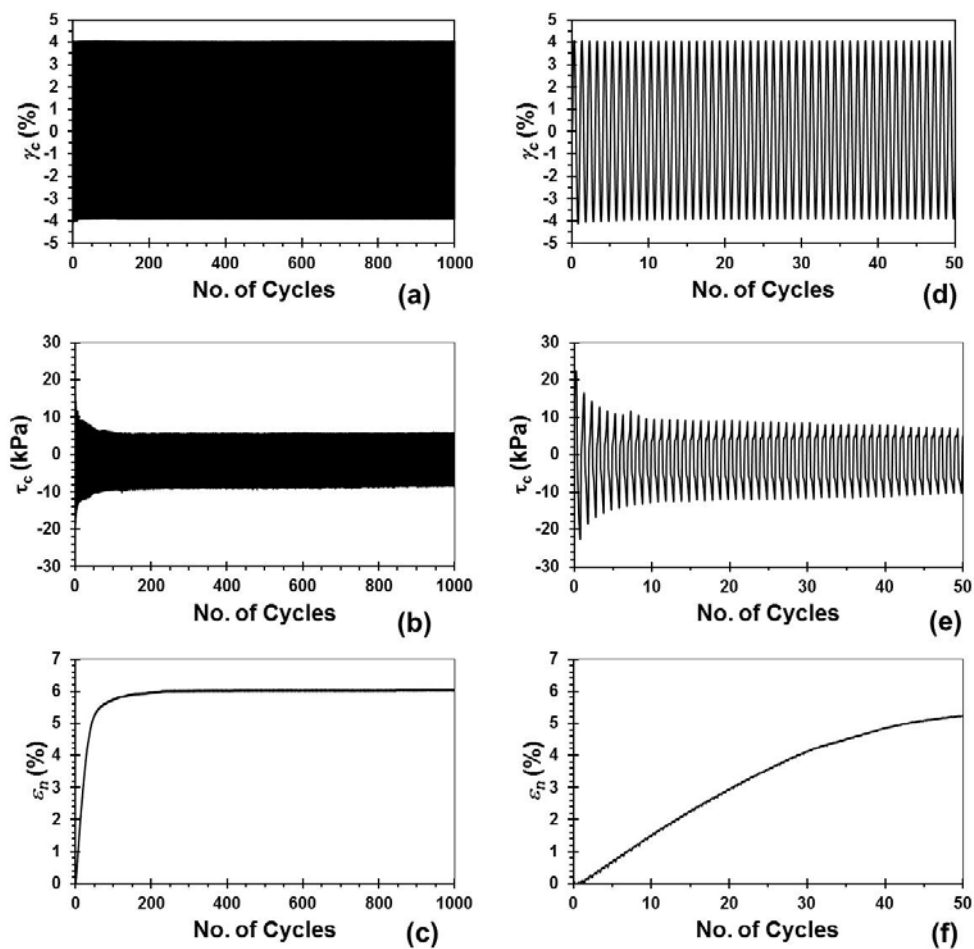


Figure D.31: Results from the fine gradation CSS test through 1000 cycles where: (a) constant magnitude sinusoidal $\gamma_c = 4\%$ (b) cyclic shear stress response (c) specimen normal strain. Results for the first 50 cycles: (d), (e), and (f), respectively. Note: $f = 2$ Hz.

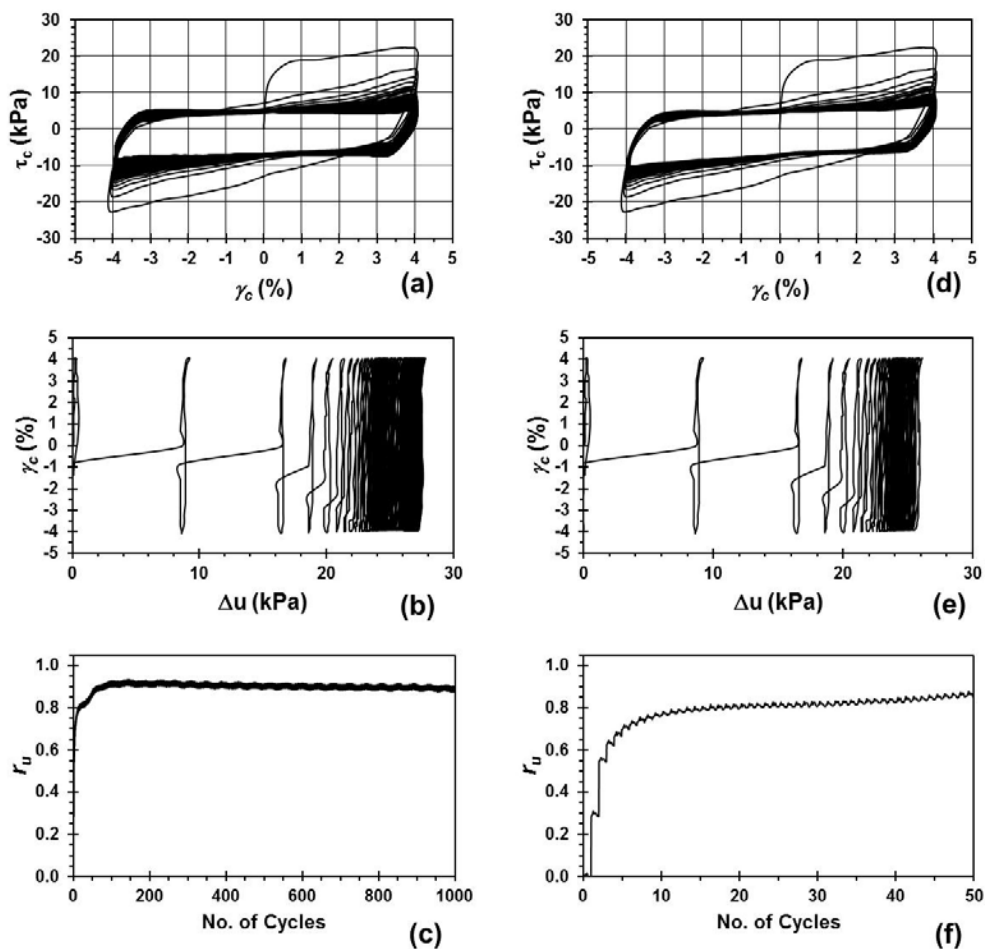


Figure D.32: Results from the fine gradation CSS test through 1000 cycles where: (a) cyclic stress-strain loops (b) cyclic shear strain induced excess pore pressure (c) excess pore pressure ratio. Results for the first 50 cycles: (d), (e), and (f), respectively. Note: $f = 2$ Hz.

CSS results for target intermediate gradation specimens reconstituted to $D_r = 50\%$ and $\sigma'_v = 30\text{kPa}$.

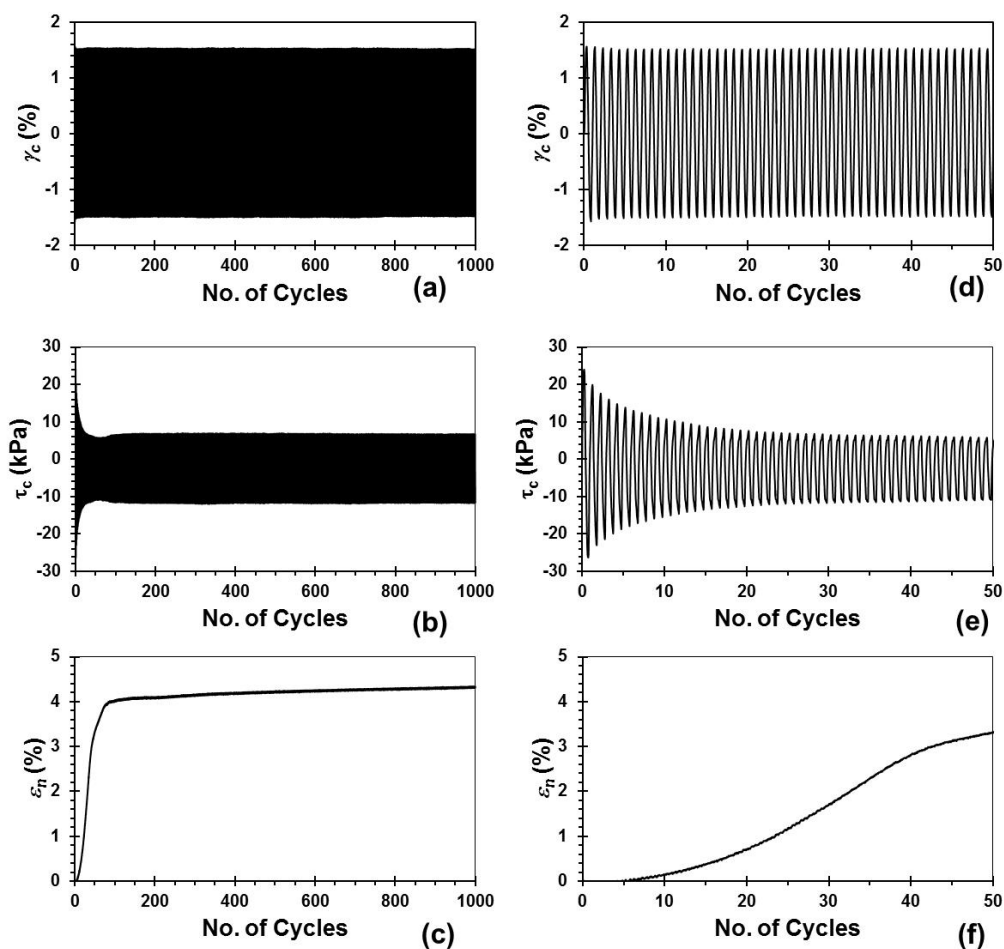


Figure D.33: Results from the intermediate gradation CSS test through 1000 cycles where: (a) constant magnitude sinusoidal $\gamma_c = 1.5\%$ (b) cyclic shear stress response (c) specimen normal strain. Results for the first 50 cycles: (d), (e), and (f), respectively. Note: $f = 1\text{ Hz}$.

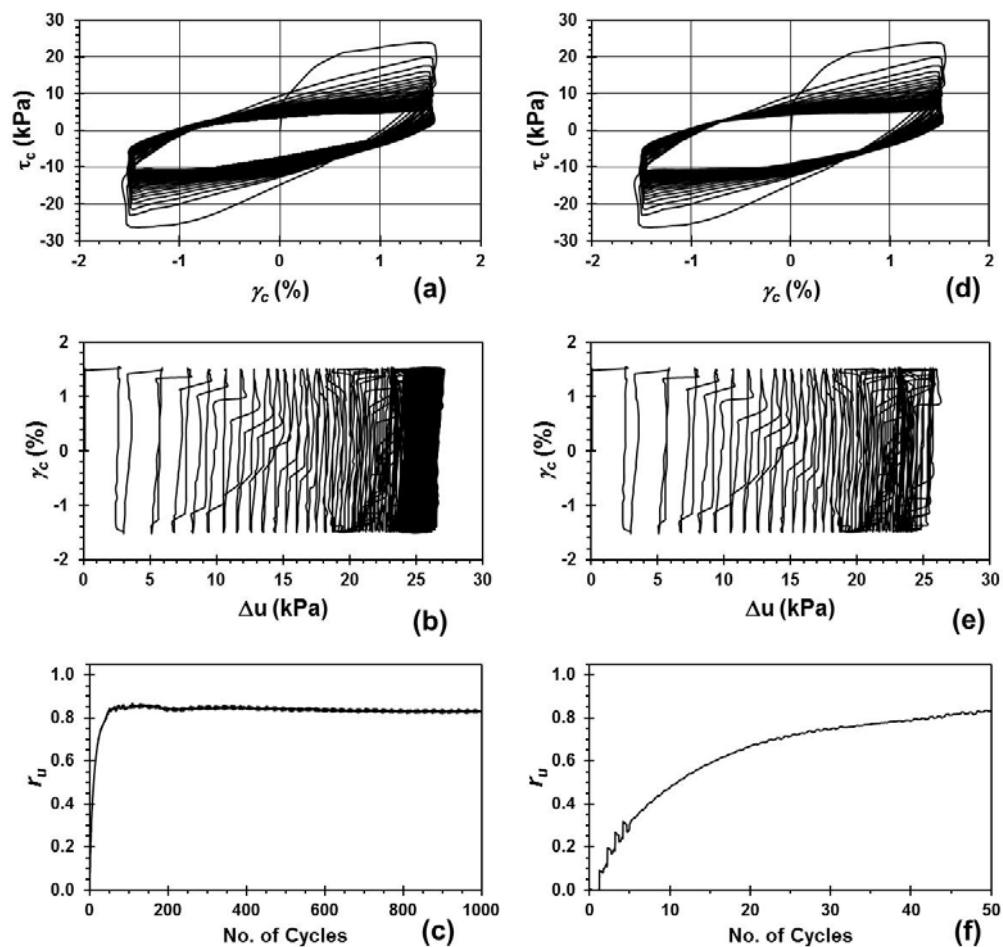


Figure D.34: Results from the intermediate gradation CSS test through 1000 cycles where: (a) cyclic stress-strain loops (b) cyclic shear strain induced excess pore pressure (c) excess pore pressure ratio. Results for the first 50 cycles: (d), (e), and (f), respectively. Note: $f = 1$ Hz.

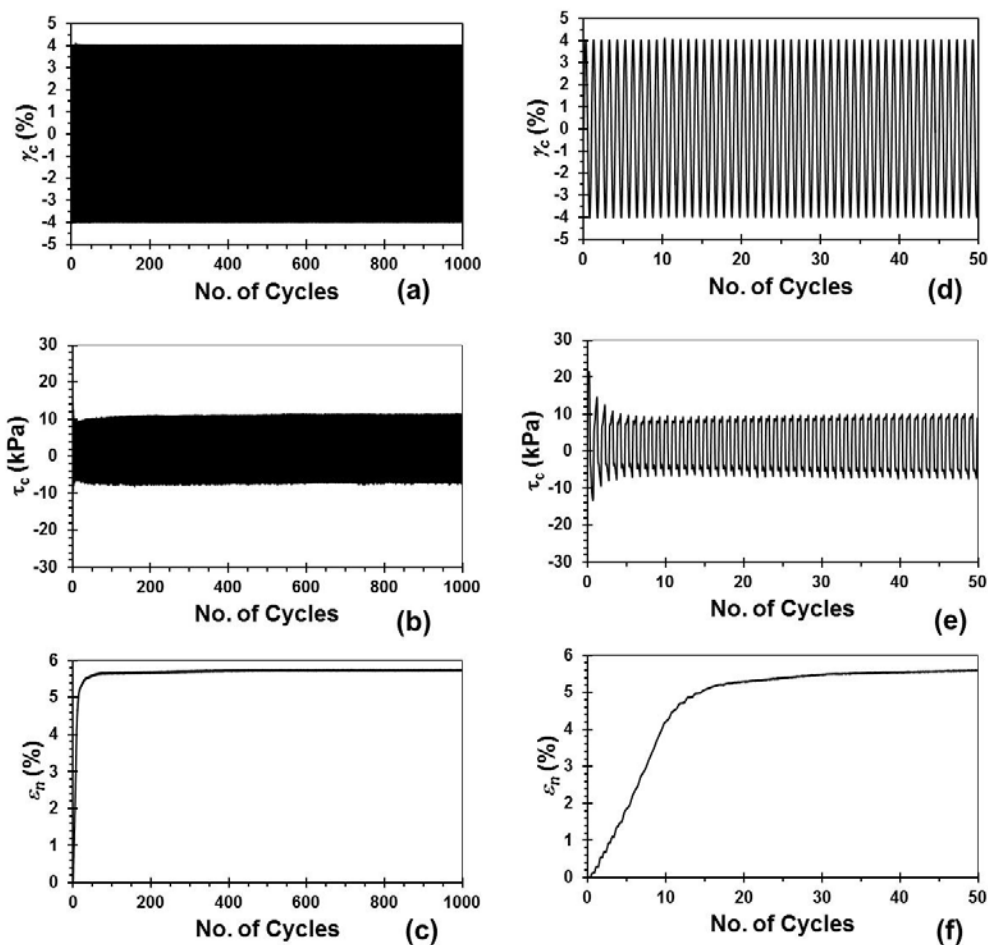


Figure D.35: Results from the intermediate gradation CSS test through 1000 cycles where: (a) constant magnitude sinusoidal $\gamma_c = 4\%$ (b) cyclic shear stress response (c) specimen normal strain. Results for the first 50 cycles: (d), (e), and (f), respectively. Note: $f = 1$ Hz.

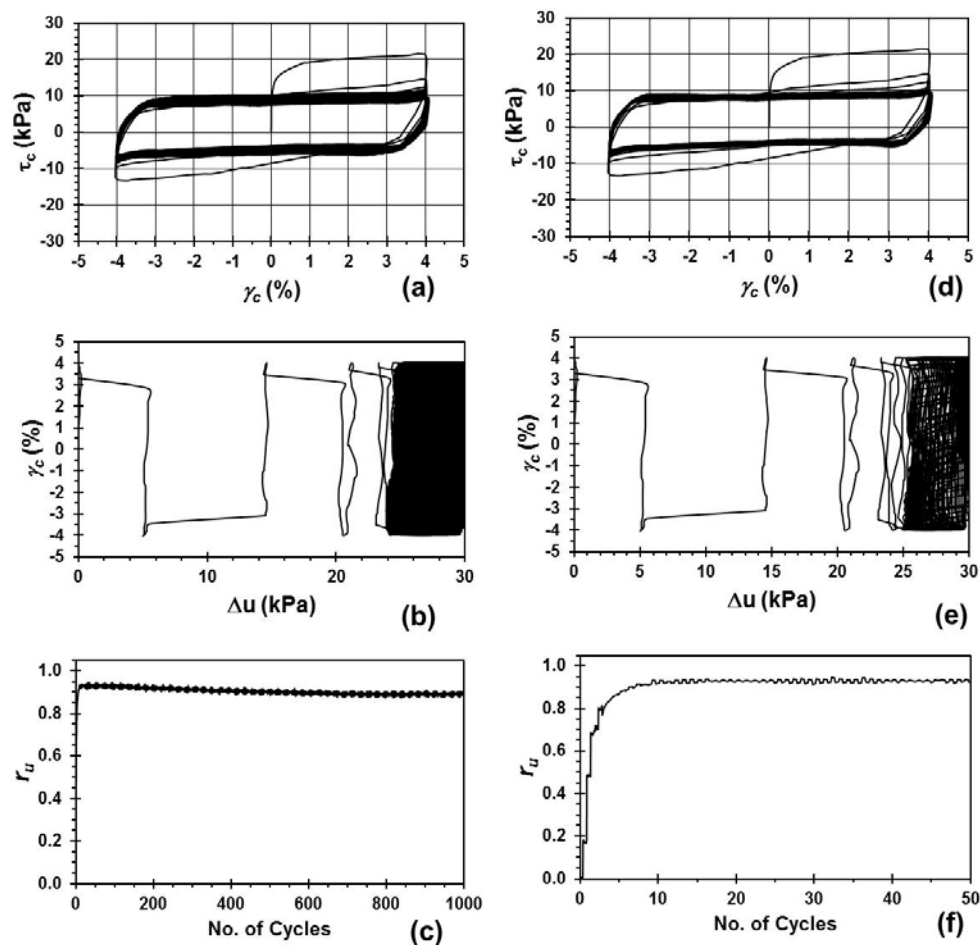


Figure D.36: Results from the intermediate gradation CSS test through 1000 cycles where: (a) cyclic stress-strain loops (b) cyclic shear strain induced excess pore pressure (c) excess pore pressure ratio. Results for the first 50 cycles: (d), (e), and (f), respectively. Note: $f = 1$ Hz.

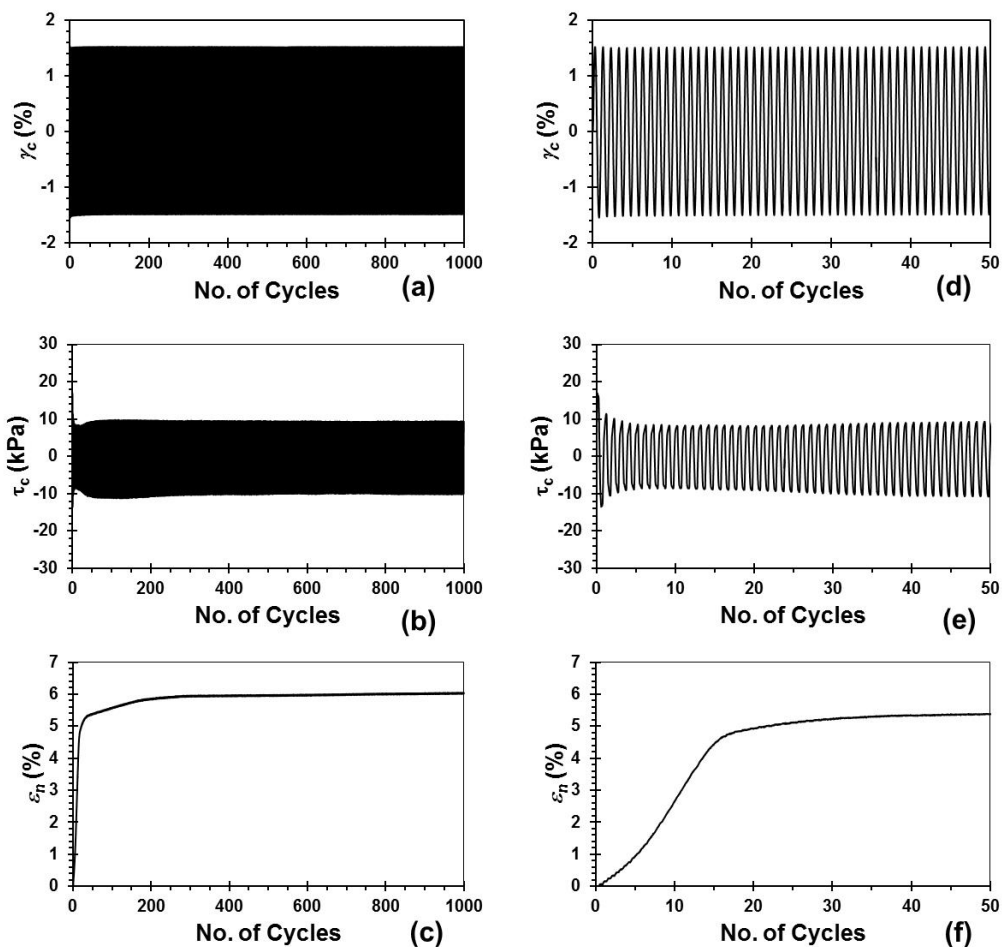


Figure D.37: Results from the intermediate gradation CSS test through 1000 cycles where: (a) constant magnitude sinusoidal $\gamma_c = 1.5\%$ (b) cyclic shear stress response (c) specimen normal strain. Results for the first 50 cycles: (d), (e), and (f), respectively. Note: $f = 2$ Hz.

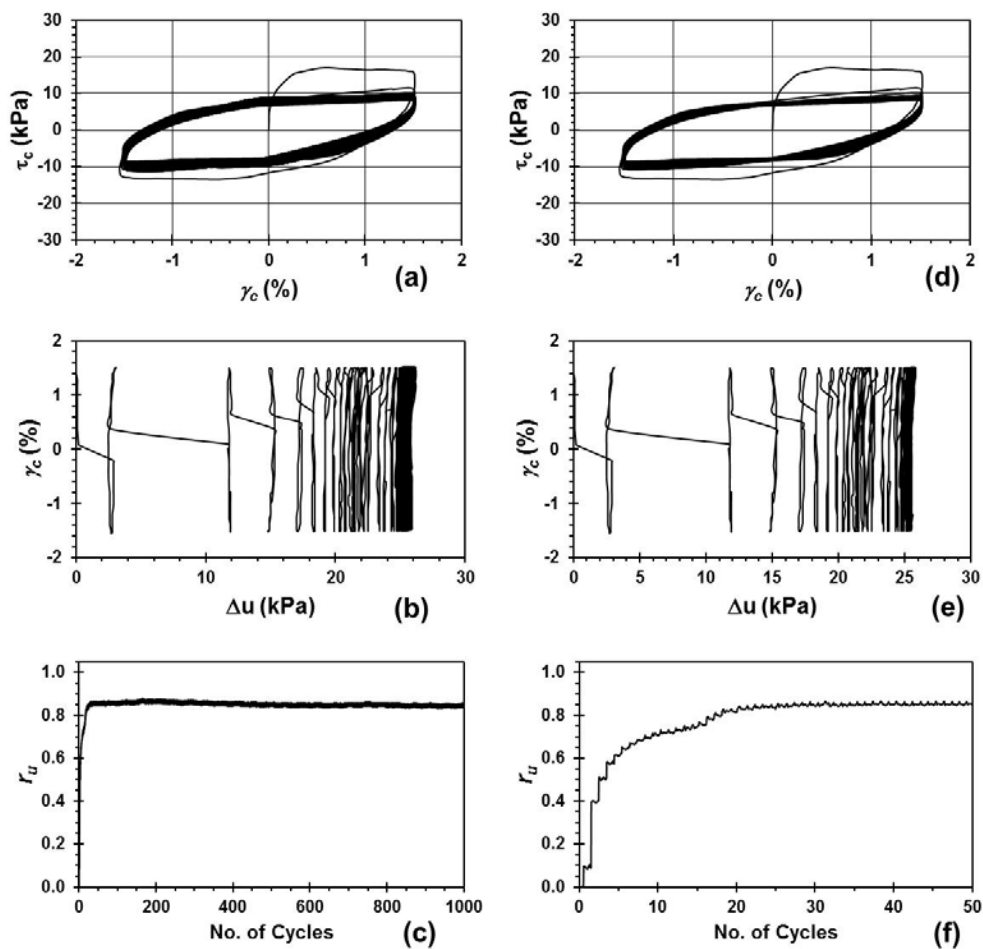


Figure D.38: Results from the intermediate gradation CSS test through 1000 cycles where: (a) cyclic stress-strain loops (b) cyclic shear strain induced excess pore pressure (c) excess pore pressure ratio. Results for the first 50 cycles: (d), (e), and (f), respectively. Note: $f = 2$ Hz.

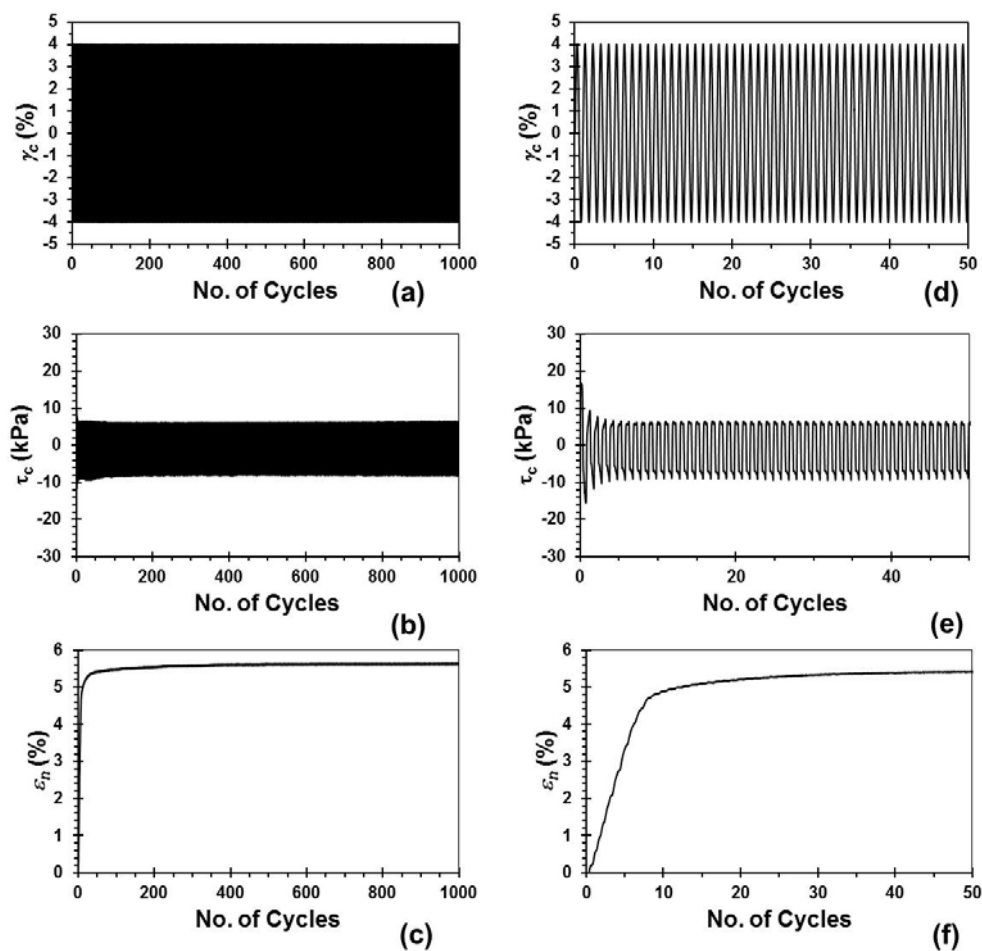


Figure D.39: Results from the intermediate gradation CSS test through 1000 cycles where: (a) constant magnitude sinusoidal $\gamma_c = 4\%$ (b) cyclic shear stress response (c) specimen normal strain. Results for the first 50 cycles: (d), (e), and (f), respectively. Note: $f = 2$ Hz.

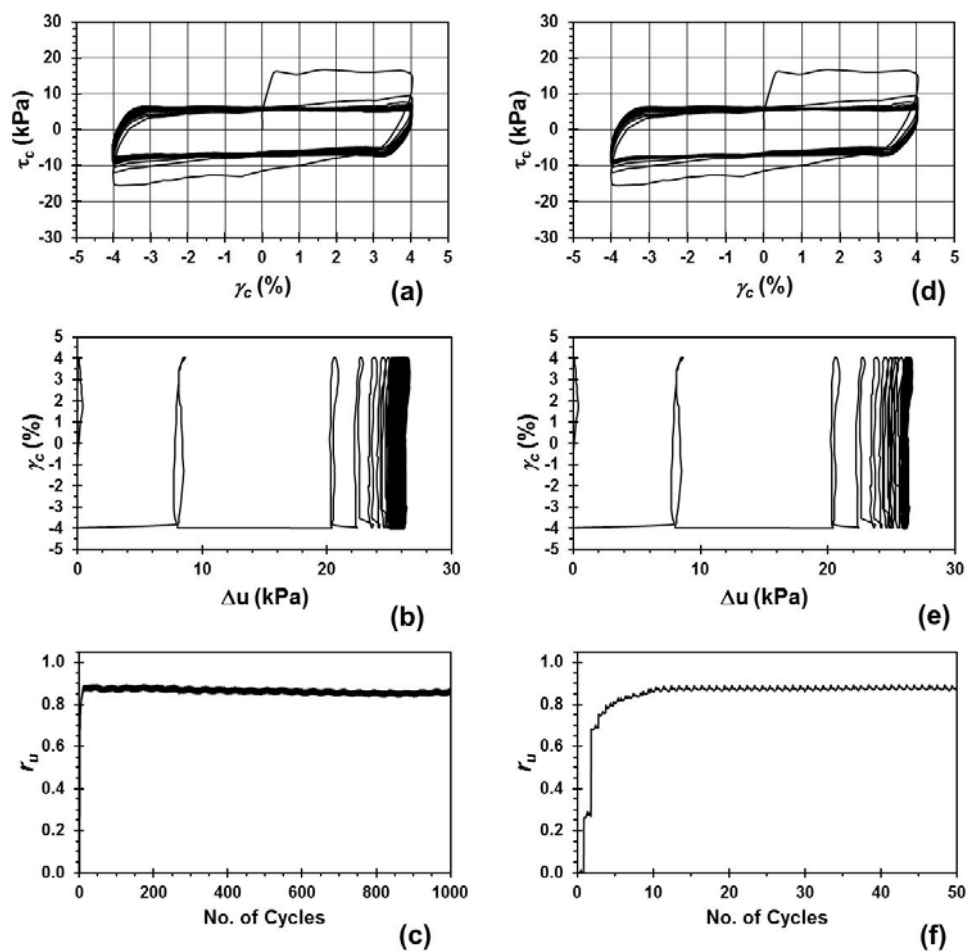


Figure D.40: Results from the intermediate gradation CSS test through 1000 cycles where: (a) cyclic stress-strain loops (b) cyclic shear strain induced excess pore pressure (c) excess pore pressure ratio. Results for the first 50 cycles: (d), (e), and (f), respectively. Note: $f = 2$ Hz.

CSS results for target coarse gradation specimens reconstituted to $D_r = 50\%$ and $\sigma'_v = 30\text{kPa}$.

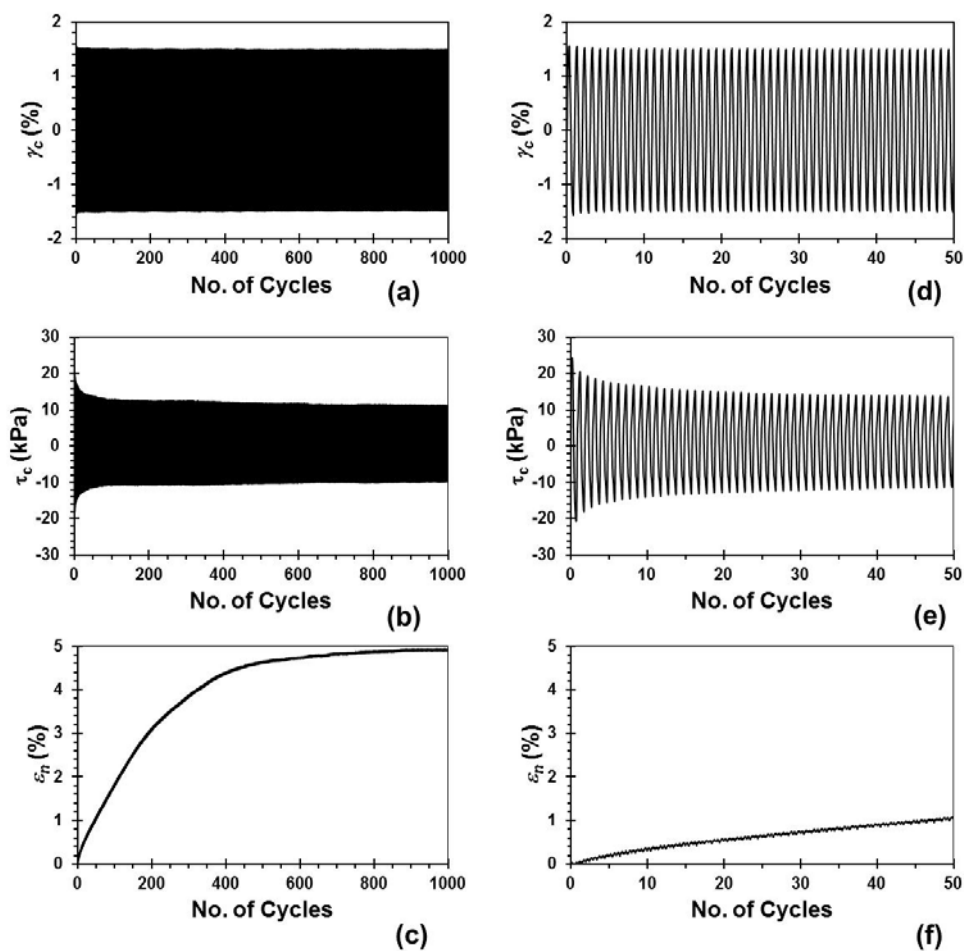


Figure D.41: Results from the coarse gradation CSS test through 1000 cycles where: (a) constant magnitude sinusoidal $\gamma_c = 1.5\%$ (b) cyclic shear stress response (c) specimen normal strain. Results for the first 50 cycles: (d), (e), and (f), respectively. Note: $f = 1$ Hz.

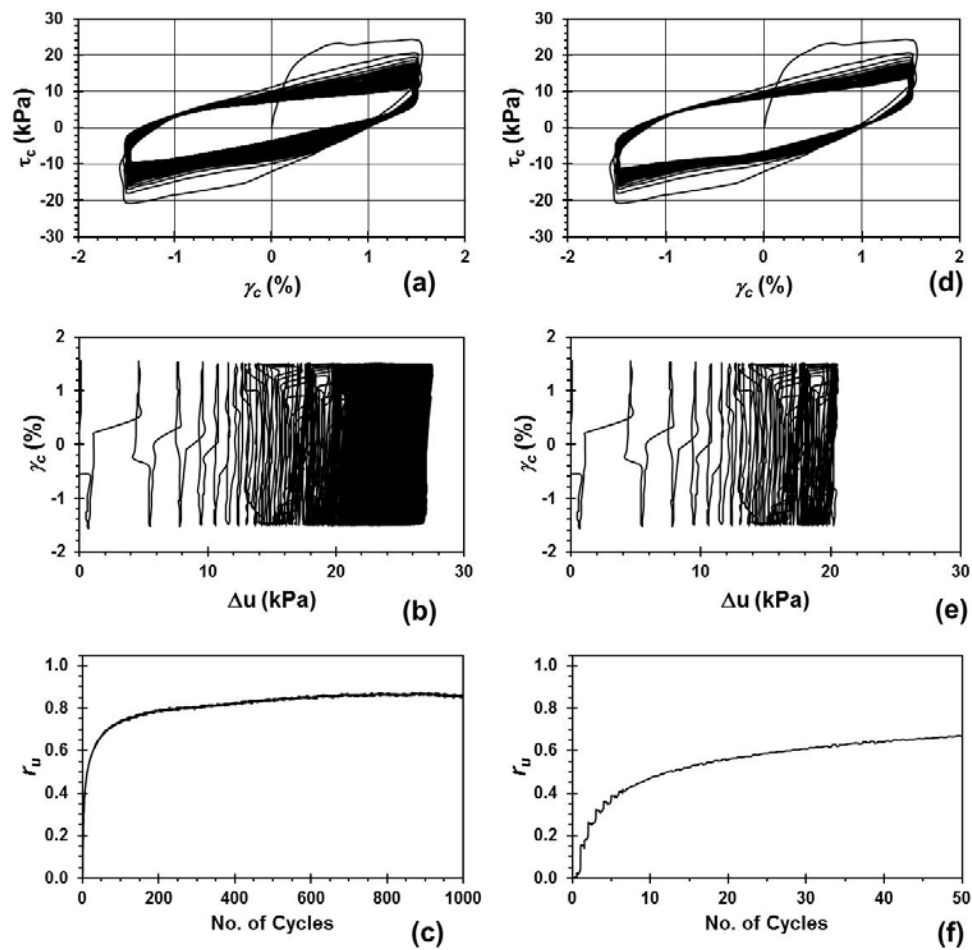


Figure D.42: Results from the coarse gradation CSS test through 1000 cycles where: (a) cyclic stress-strain loops (b) cyclic shear strain induced excess pore pressure (c) excess pore pressure ratio. Results for the first 50 cycles: (d), (e), and (f), respectively. Note: $f = 1$ Hz.

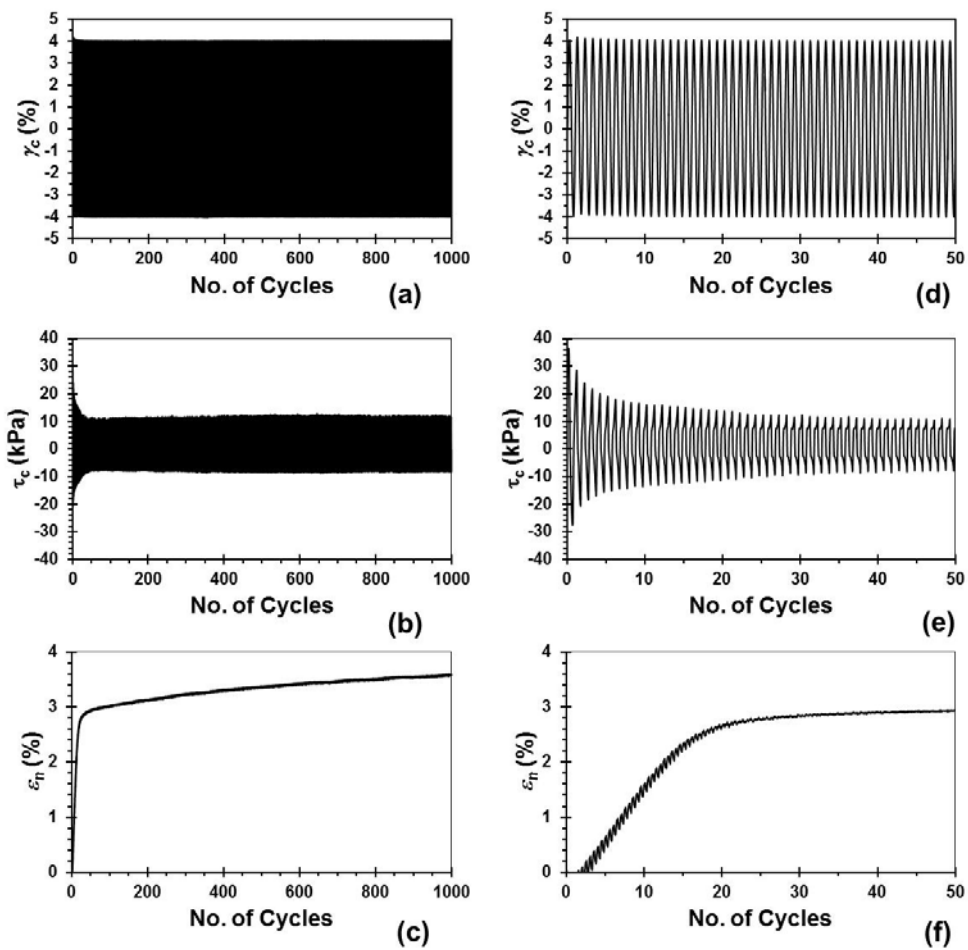


Figure D.43: Results from the coarse gradation CSS test through 1000 cycles where: (a) constant magnitude sinusoidal $\gamma_c = 4\%$ (b) cyclic shear stress response (c) specimen normal strain. Results for the first 50 cycles: (d), (e), and (f), respectively. Note: $f = 1$ Hz.

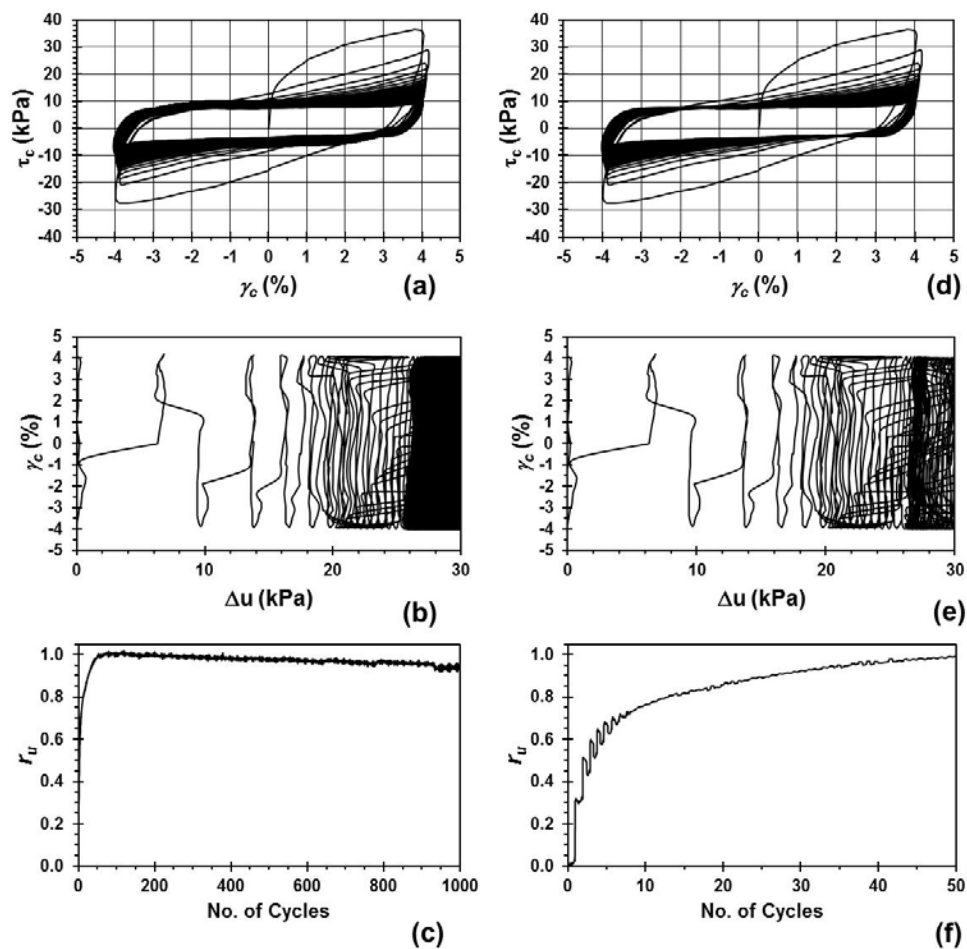


Figure D.44: Results from the coarse gradation CSS test through 1000 cycles where: (a) cyclic stress-strain loops (b) cyclic shear strain induced excess pore pressure (c) excess pore pressure ratio. Results for the first 50 cycles: (d), (e), and (f), respectively. Note: $f = 1$ Hz.

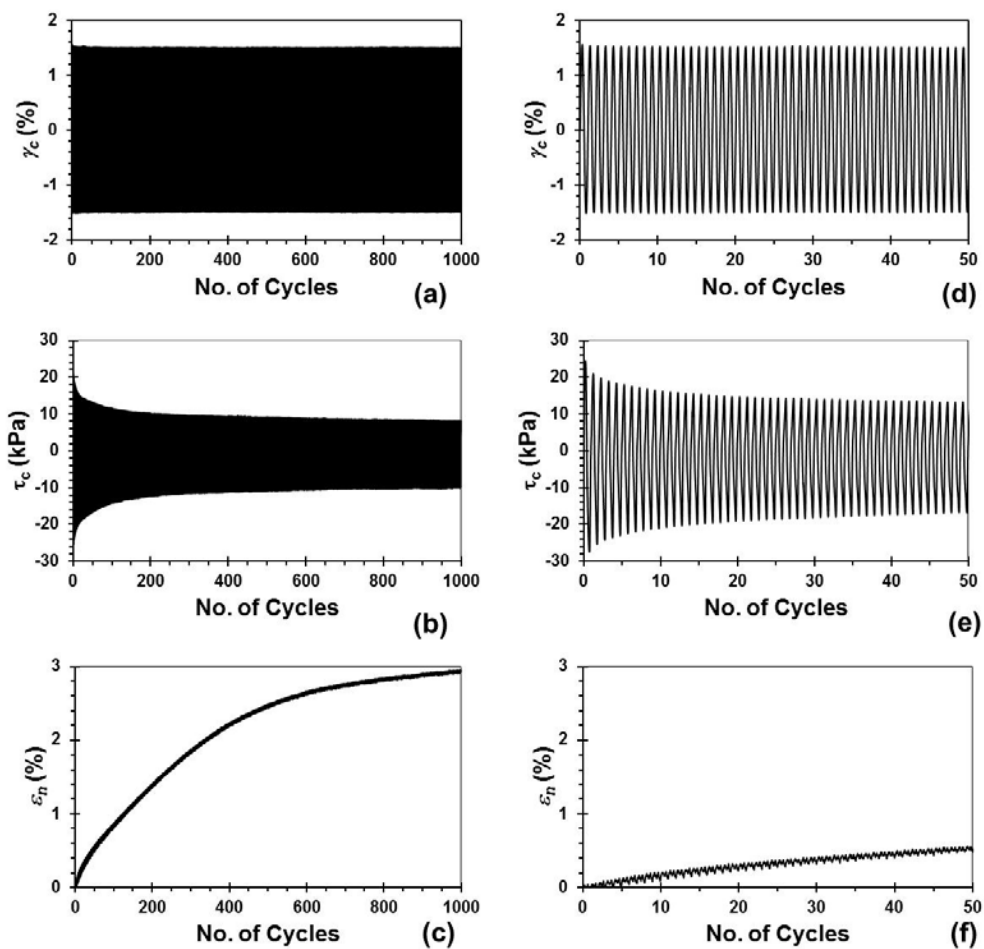


Figure D.45: Results from the coarse gradation CSS test through 1000 cycles where: (a) constant magnitude sinusoidal $\gamma_c = 1.5\%$ (b) cyclic shear stress response (c) specimen normal strain. Results for the first 50 cycles: (d), (e), and (f), respectively. Note: $f = 2$ Hz.

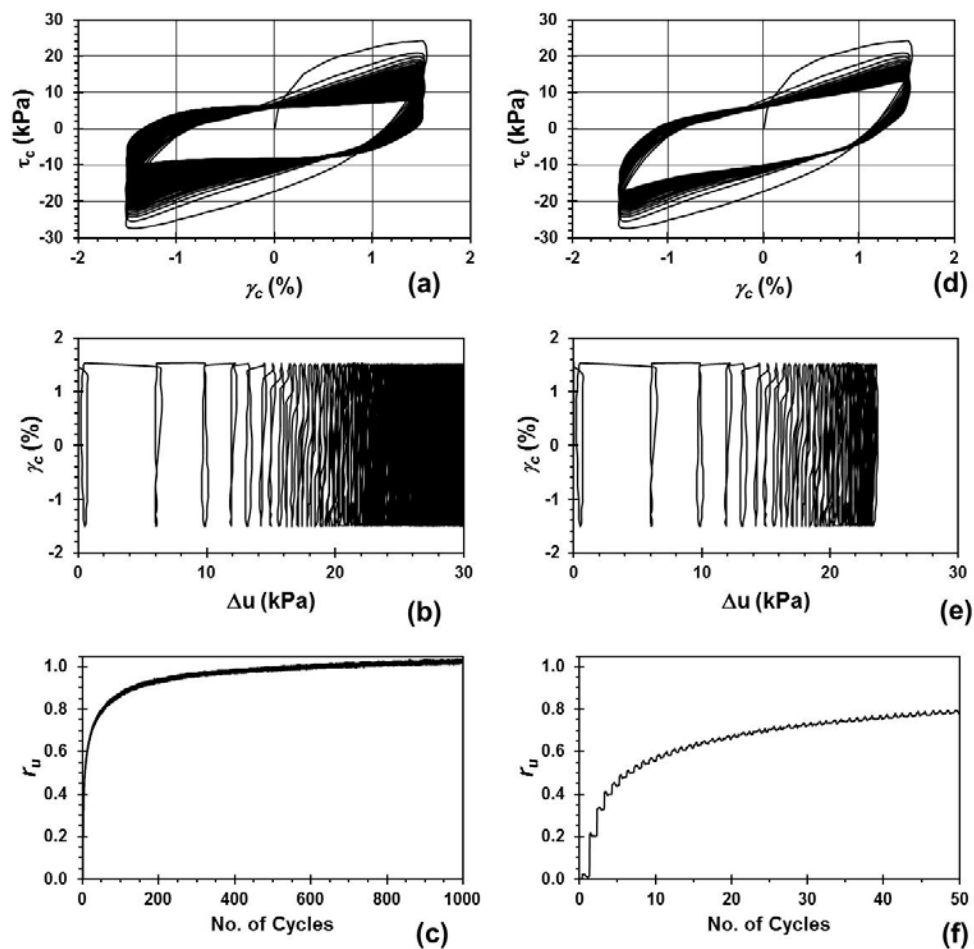


Figure D.46: Results from the coarse gradation CSS test through 1000 cycles where: (a) cyclic stress-strain loops (b) cyclic shear strain induced excess pore pressure (c) excess pore pressure ratio. Results for the first 50 cycles: (d), (e), and (f), respectively. Note: $f = 2$ Hz.

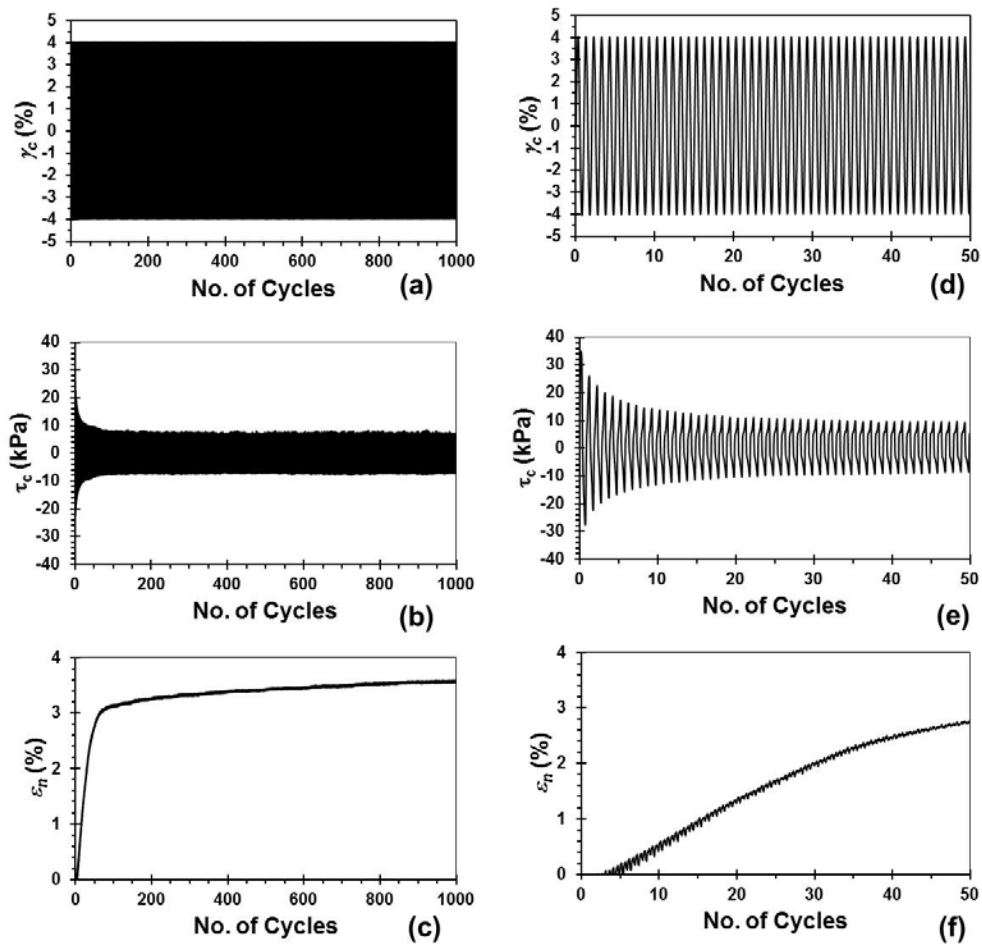


Figure D.47: Results from the coarse gradation CSS test through 1000 cycles where: (a) constant magnitude sinusoidal $\gamma_c = 4\%$ (b) cyclic shear stress response (c) specimen normal strain. Results for the first 50 cycles: (d), (e), and (f), respectively. Note: $f = 2$ Hz.

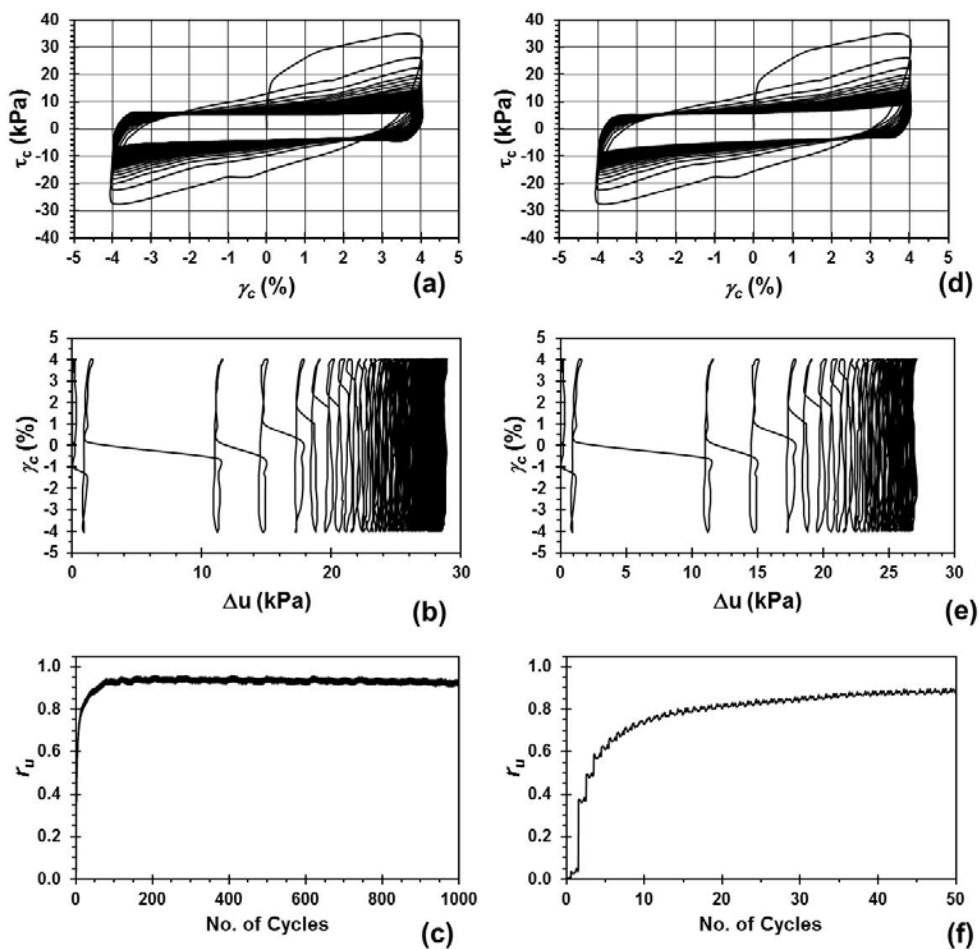


Figure D.48: Results from the coarse gradation CSS test through 1000 cycles where: (a) cyclic stress-strain loops (b) cyclic shear strain induced excess pore pressure (c) excess pore pressure ratio. Results for the first 50 cycles: (d), (e), and (f), respectively. Note: $f = 2$ Hz.

CSS results for target fine gradation specimen reconstituted to $D_r = 50\%$ and $\sigma'_v = 100\text{kPa}$.

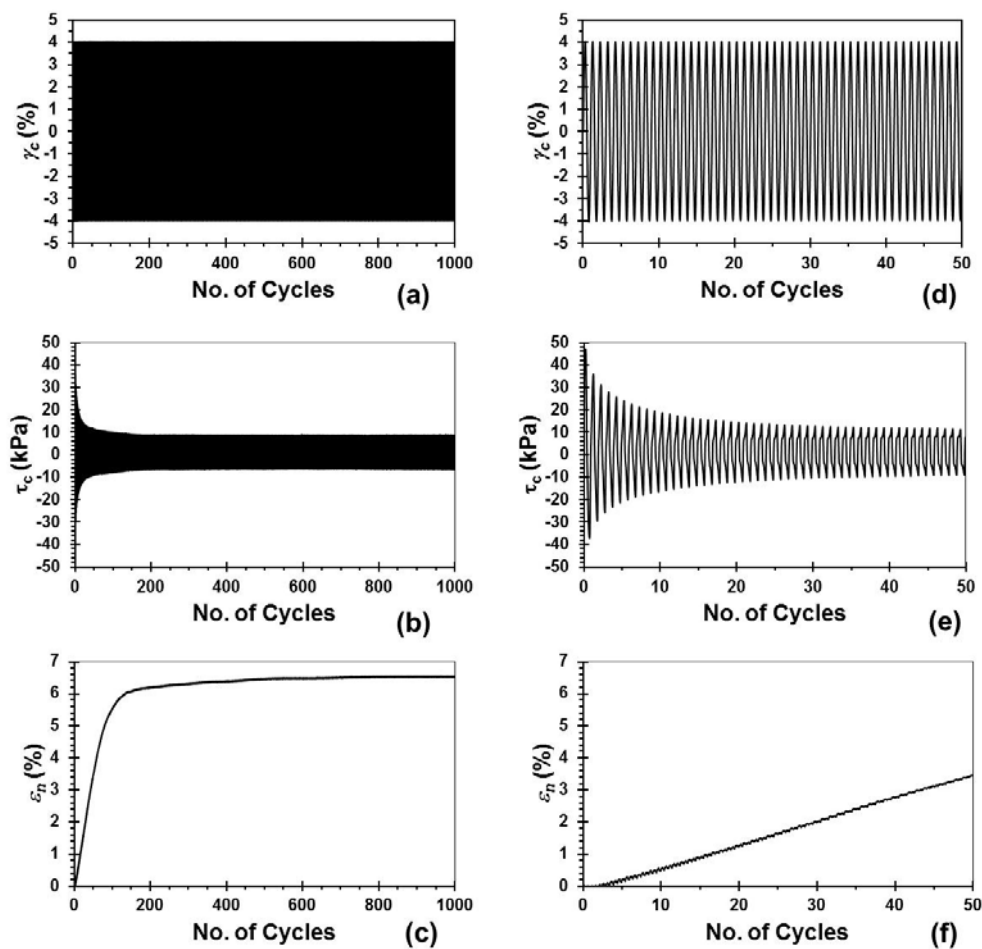


Figure D.49: Results from the fine gradation CSS test through 1000 cycles where: (a) constant magnitude sinusoidal $\gamma_c = 4\%$ (b) cyclic shear stress response (c) specimen normal strain. Results for the first 50 cycles: (d), (e), and (f), respectively. Note: $f = 1$ Hz.

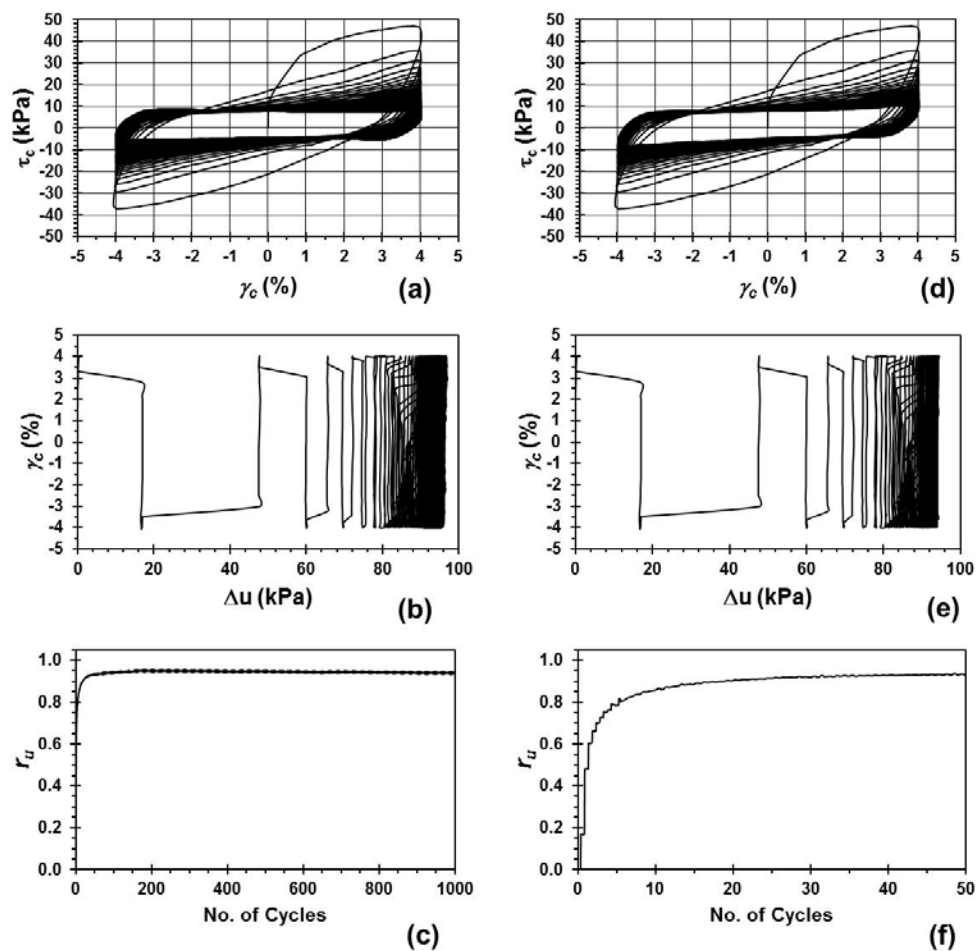


Figure D.50: Results from the fine gradation CSS test through 1000 cycles where: (a) cyclic stress-strain loops (b) cyclic shear strain induced excess pore pressure (c) excess pore pressure ratio. Results for the first 50 cycles: (d), (e), and (f), respectively. Note: $f = 1$ Hz.

CSS results for target intermediate gradation specimen reconstituted to $D_r = 50\%$ and $\sigma'_v = 100\text{kPa}$.

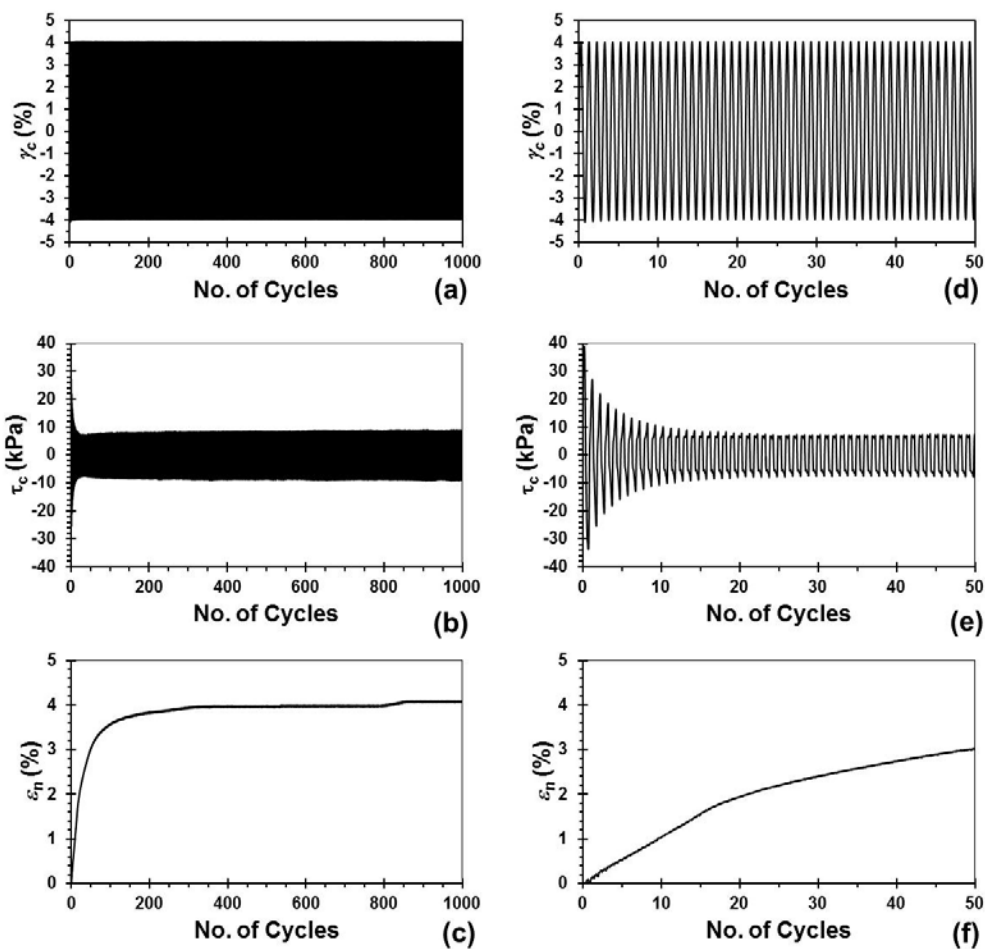


Figure D.51: Results from the intermediate gradation CSS test through 1000 cycles where: (a) constant magnitude sinusoidal $\gamma_c = 4\%$ (b) cyclic shear stress response (c) specimen normal strain. Results for the first 50 cycles: (d), (e), and (f), respectively. Note: $f = 1$ Hz.

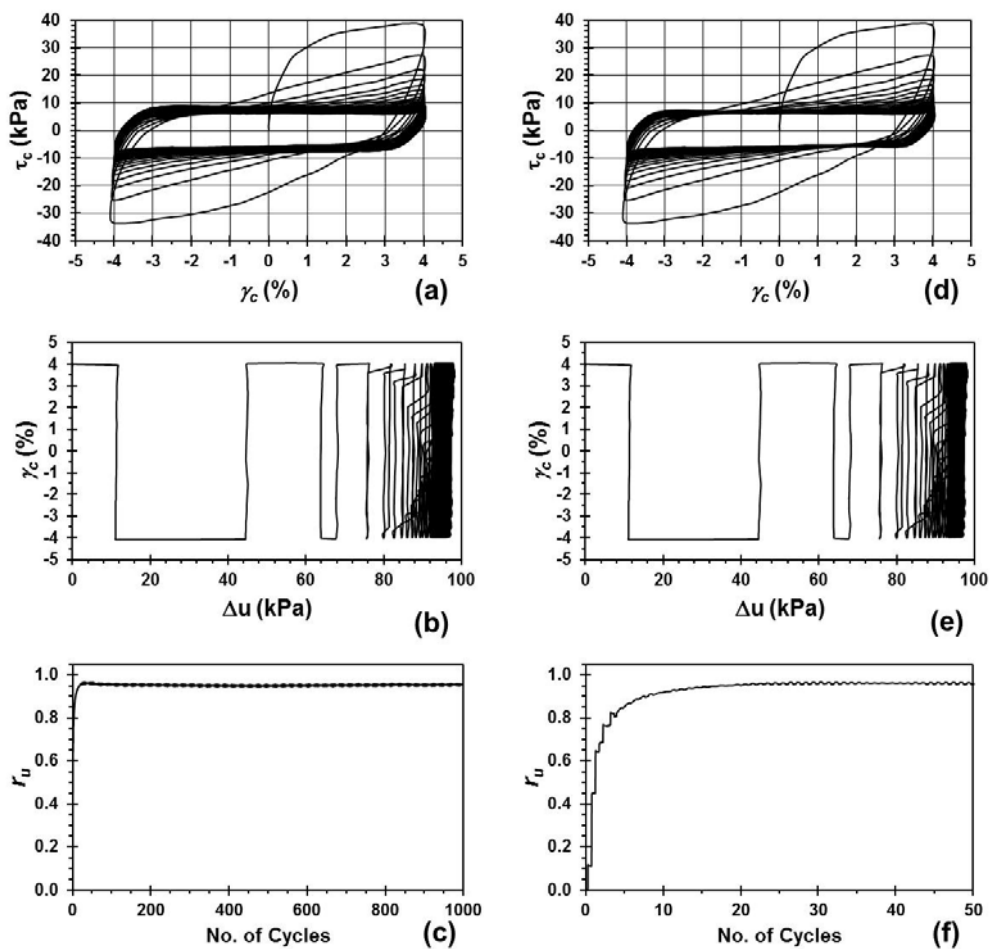


Figure D.52: Results from the intermediate gradation CSS test through 1000 cycles where: (a) cyclic stress-strain loops (b) cyclic shear strain induced excess pore pressure (c) excess pore pressure ratio. Results for the first 50 cycles: (d), (e), and (f), respectively. Note: $f = 1$ Hz.

CSS results for target coarse gradation specimen reconstituted to $D_r = 50\%$ and $\sigma'_v = 100\text{kPa}$.

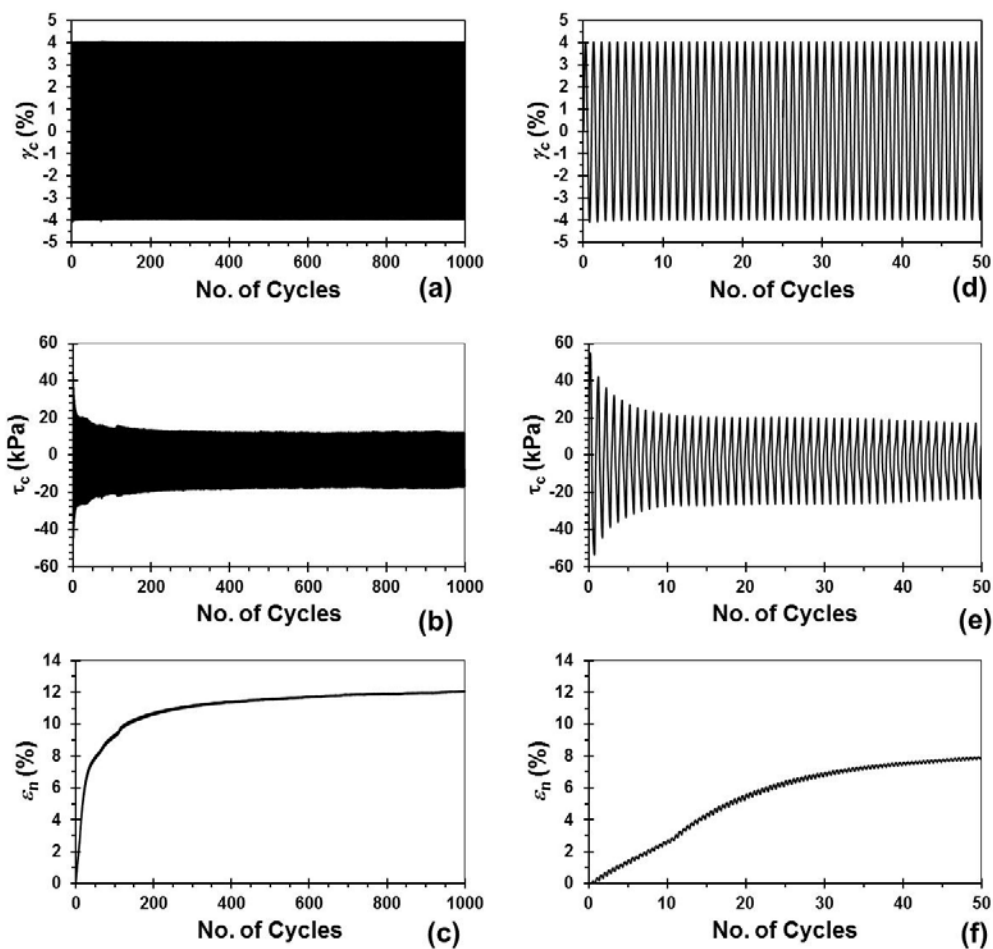


Figure D.53: Results from the intermediate gradation CSS test through 1000 cycles where: (a) constant magnitude sinusoidal $\gamma_c = 4\%$ (b) cyclic shear stress response (c) specimen normal strain. Results for the first 50 cycles: (d), (e), and (f), respectively. Note: $f = 1\text{ Hz}$.

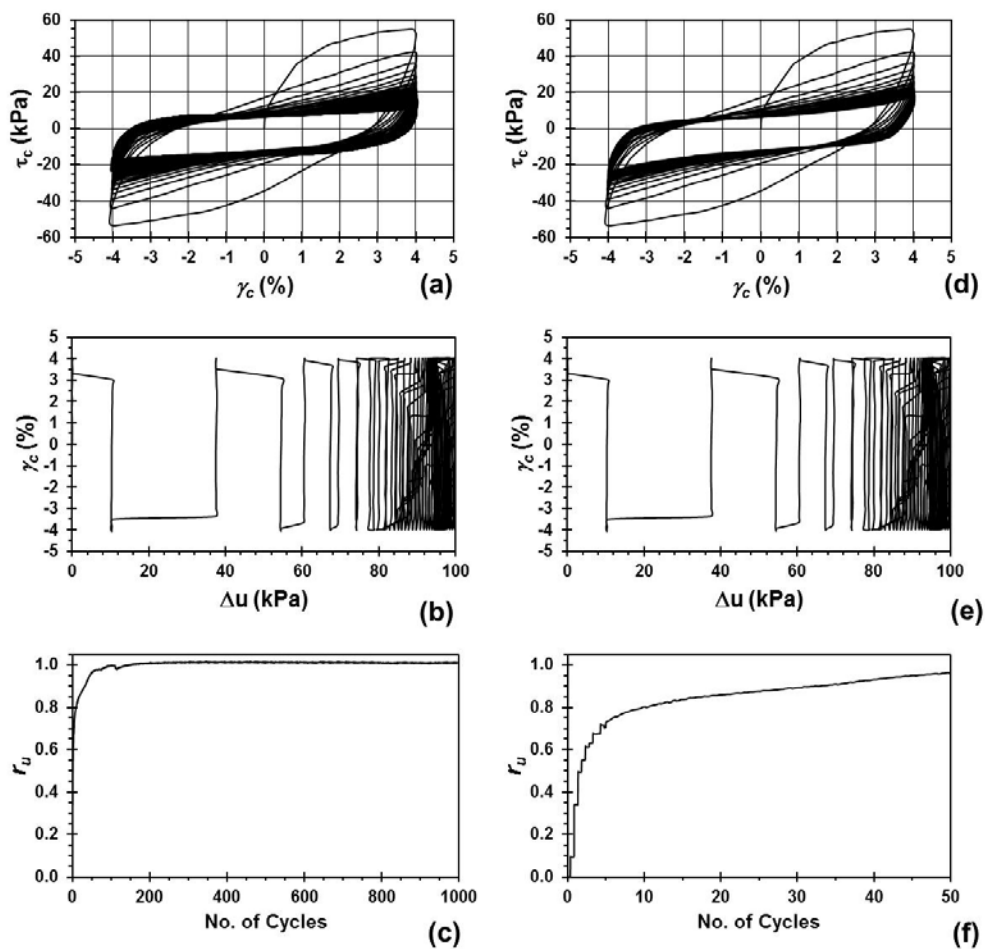


Figure D.54: Results from the intermediate gradation CSS test through 1000 cycles where: (a) cyclic stress-strain loops (b) cyclic shear strain induced excess pore pressure (c) excess pore pressure ratio. Results for the first 50 cycles: (d), (e), and (f), respectively. Note: $f = 1$ Hz.

John Ross tube specimen: $\sigma'_v = 30\text{kPa}$, intermediate gradation CSS specimen.

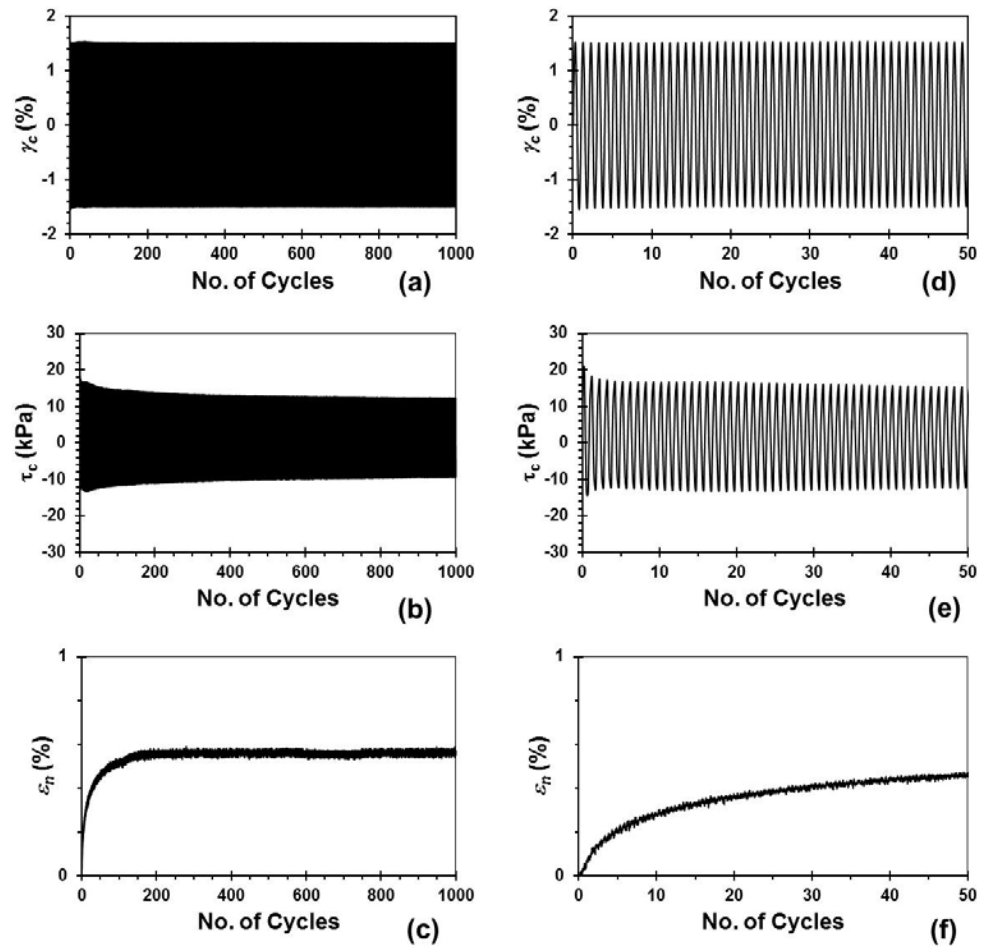


Figure D.55: Results from John Ross tube specimen CSS test with 1000 cycles where: (a) constant magnitude sinusoidal $\gamma_c = 1.5\%$ (b) cyclic shear stress response (c) specimen normal strain. Results for the first 50 cycles: (d), (e), and (f), respectively. Note: $f = 1\text{ Hz}$.

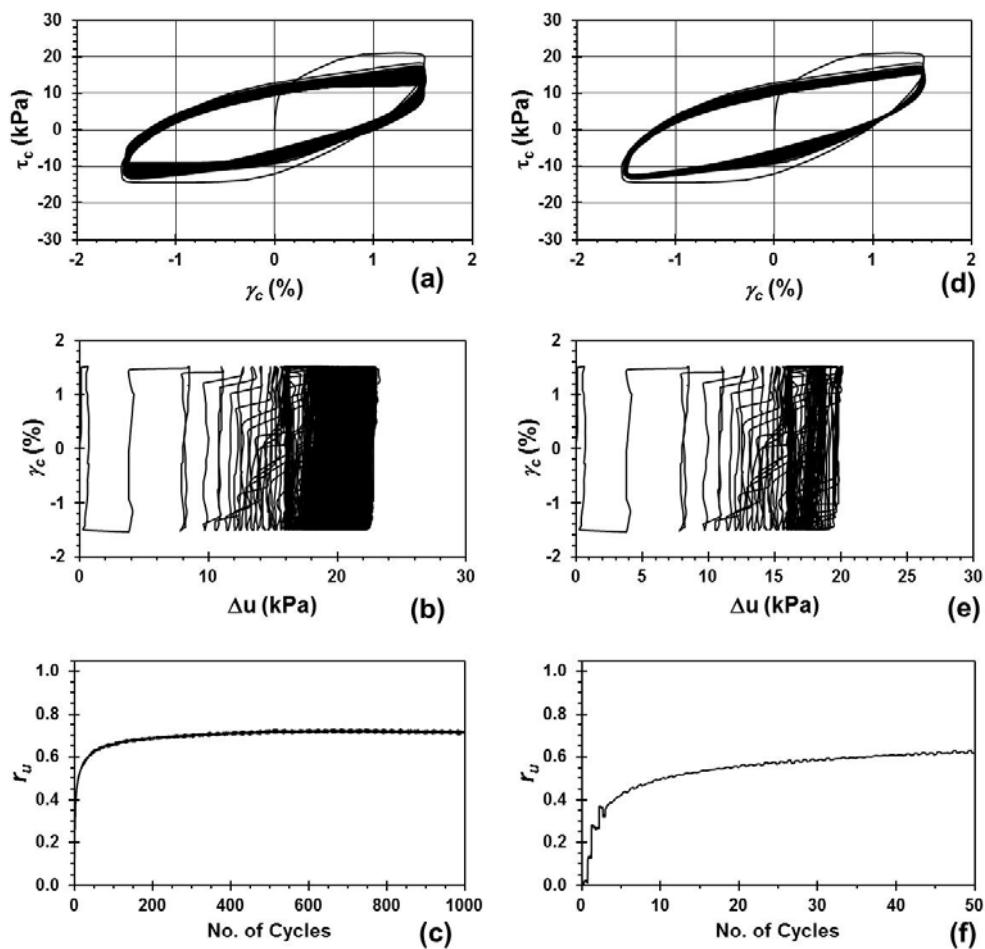


Figure D.56: Results from John Ross tube specimen CSS test with 1000 cycles where: (a) cyclic stress-strain loops (b) cyclic shear strain induced excess pore pressure (c) excess pore pressure ratio. Results for the first 50 cycles: (d), (e), and (f), respectively. Note: $f = 1$ Hz.

Portland Building tube specimen: $\sigma'_v = 30\text{kPa}$, coarse gradation CSS specimen.

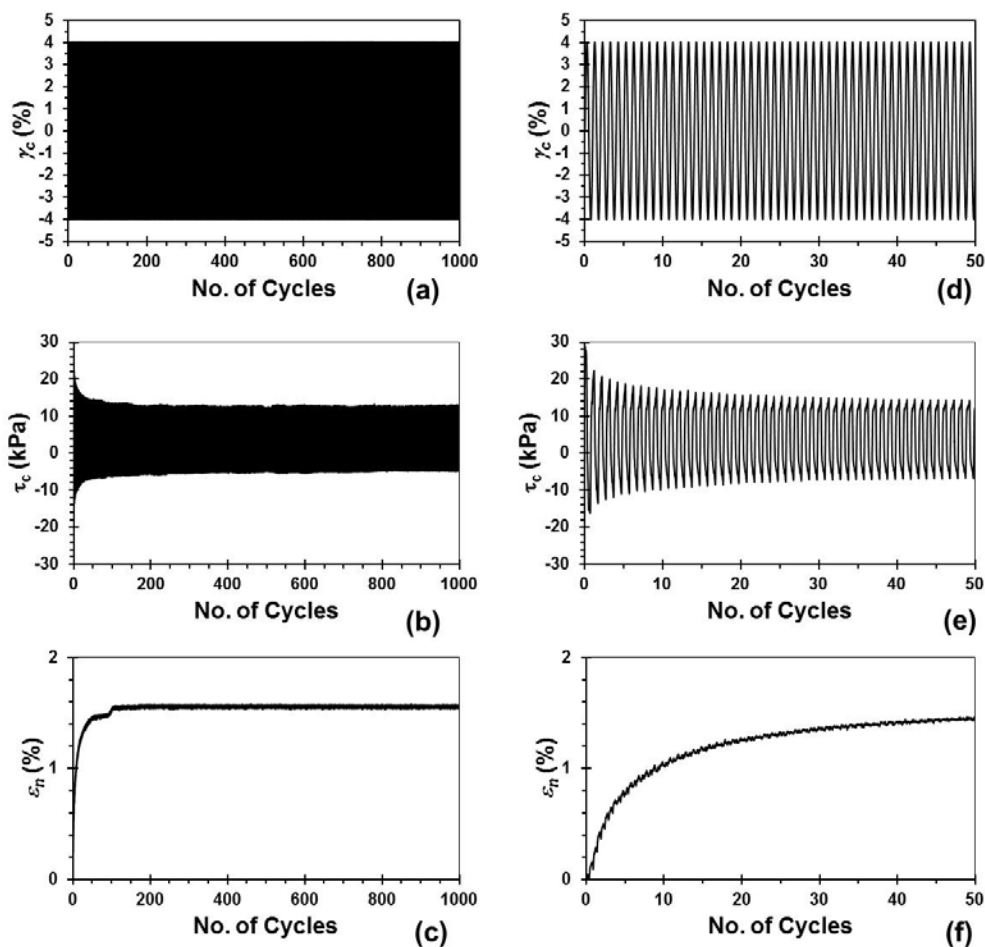


Figure D.57: Results from Portland Building tube specimen CSS test with 1000 cycles where: (a) constant magnitude sinusoidal $\gamma_c = 4\%$ (b) cyclic shear stress response (c) specimen normal strain. Results for the first 50 cycles: (d), (e), and (f), respectively. Note: $f = 1$ Hz.

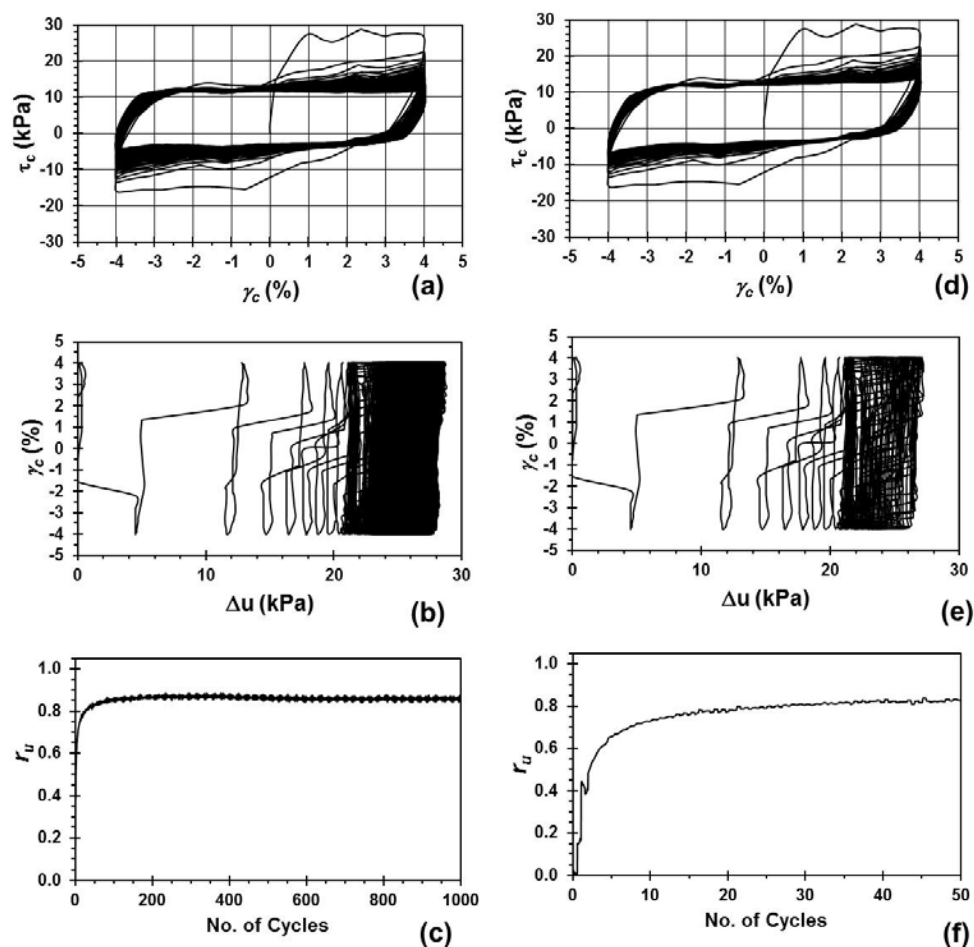


Figure D.58: Results from Portland Building tube specimen CSS test with 1000 cycles where: (a) cyclic stress-strain loops (b) cyclic shear strain induced excess pore pressure (c) excess pore pressure ratio. Results for the first 50 cycles: (d), (e), and (f), respectively. Note: $f = 1$ Hz.

Swan Island tube specimen: $\sigma'_v = 30\text{kPa}$, fine gradation CSS specimen.

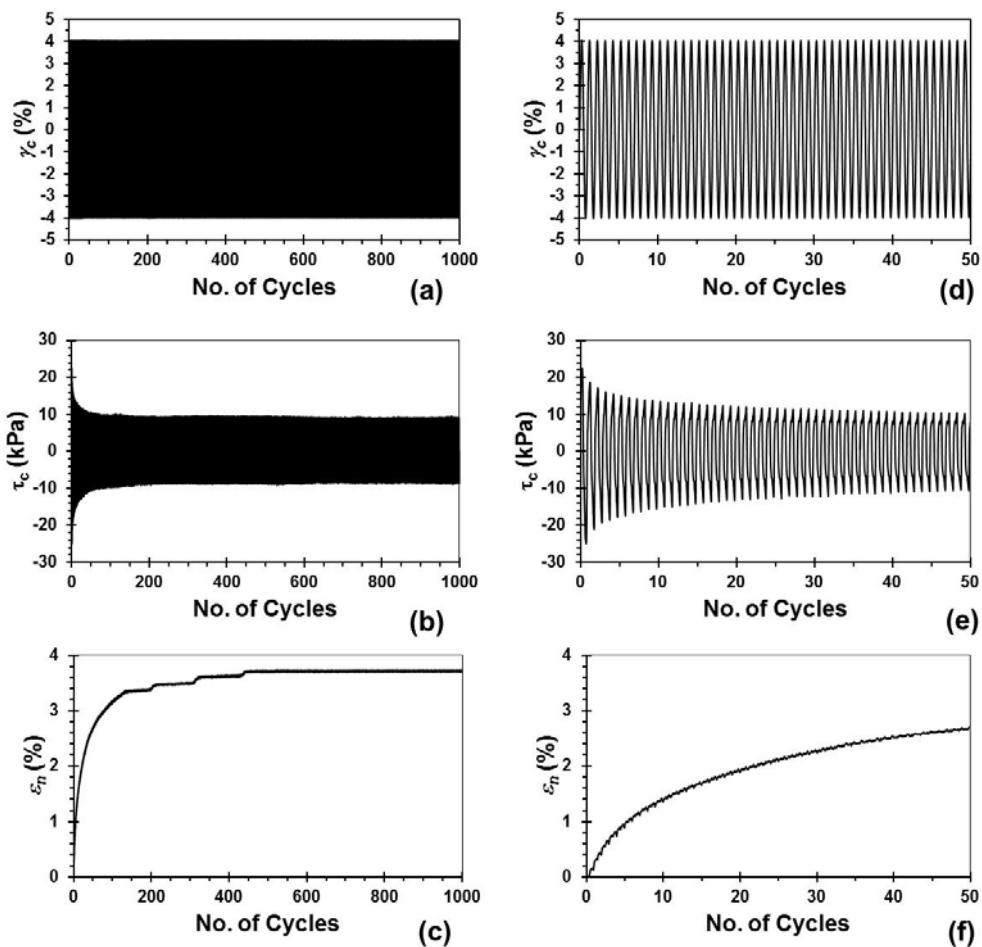


Figure D.59: Results from Swan Island tube specimen CSS test with 1000 cycles where: (a) constant magnitude sinusoidal $\gamma_c = 4\%$ (b) cyclic shear stress response (c) specimen normal strain. Results for the first 50 cycles: (d), (e), and (f), respectively. Note: $f = 1\text{ Hz}$.

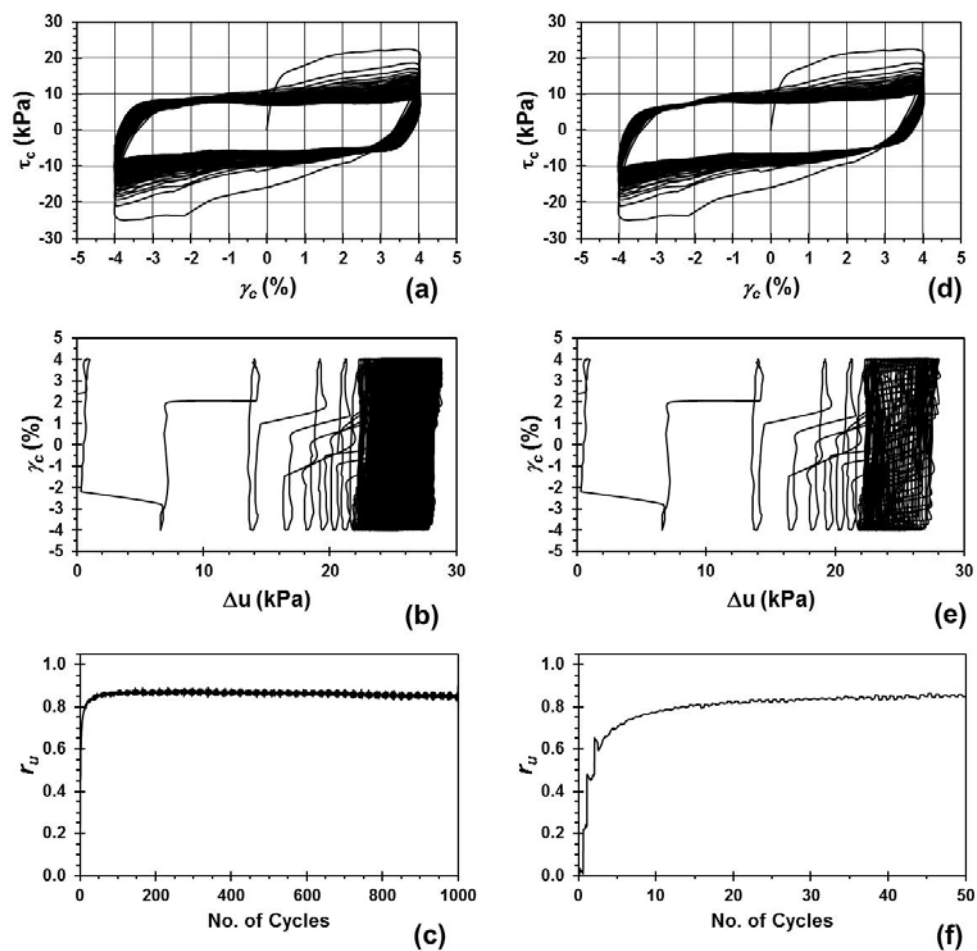


Figure D.60: Results from Swan Island tube specimen CSS test with 1000 cycles where: (a) cyclic stress-strain loops (b) cyclic shear strain induced excess pore pressure (c) excess pore pressure ratio. Results for the first 50 cycles: (d), (e), and (f), respectively. Note: $f = 1$ Hz.

Fitted modulus reduction curves for specimens reconstituted to $D_r = 30\%$ with $\sigma'_v = 30$ kPa.

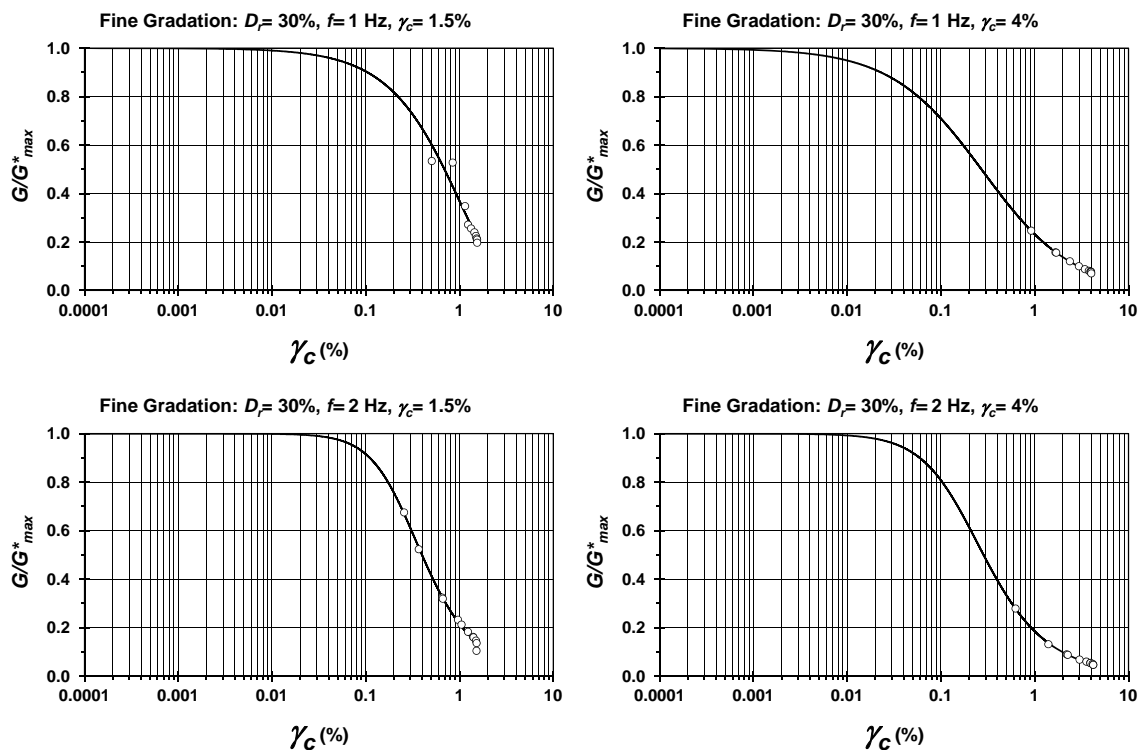


Figure D.61: Modulus reduction curves fine gradation reconstituted to $D_r = 30\%$ specimens.

Table D.1: Fitting coefficients used in Equation 5.1.

$D_r = 30\%$ Fine Gradation Specimens			
Test Parameters	Fitting Coefficients		
	a	b	c
$\gamma_c = 1.5\%$ and $f = 1$ Hz	0.058	1.005	17.810
$\gamma_c = 1.5\%$ and $f = 2$ Hz	14.436	1.929	0.562
$\gamma_c = 4\%$ and $f = 1$ Hz	2.751	0.877	1.103
$\gamma_c = 4\%$ and $f = 2$ Hz	14.199	1.538	0.620

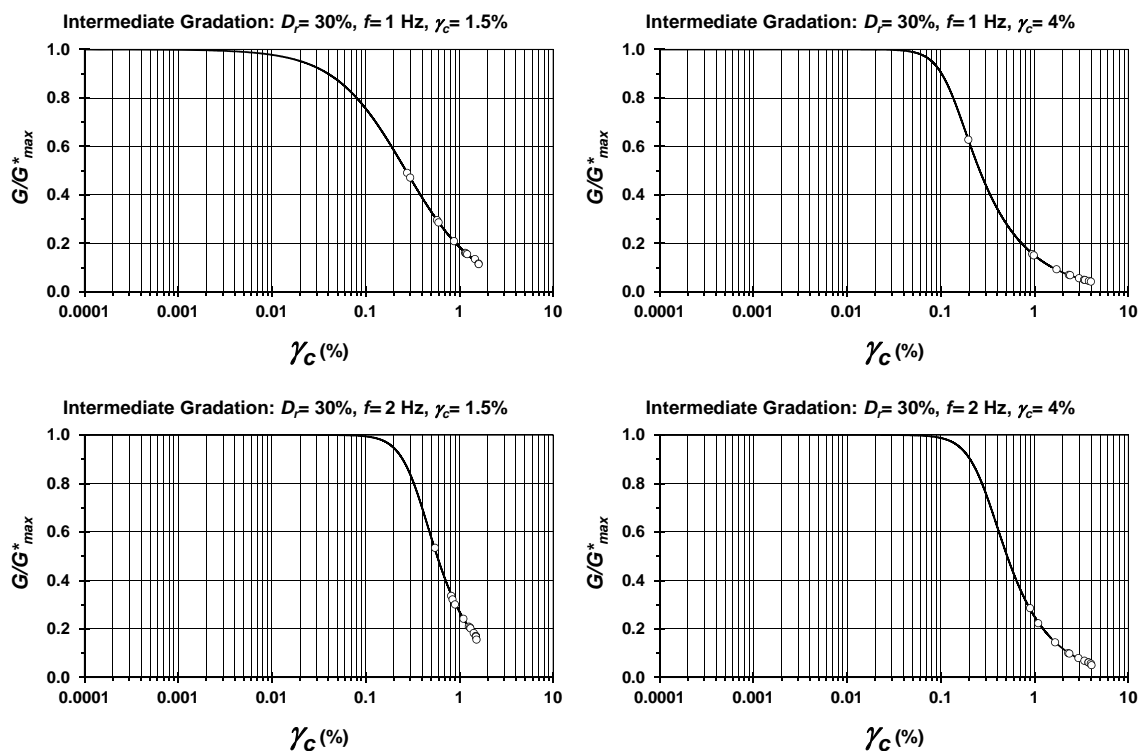


Figure D.62: Modulus reduction curves intermediate gradation reconstituted to $D_r=30\%$ specimens.

Table D.2: Fitting coefficients used in Equation 5.1.

$D_r = 30\%$ Intermediate Gradation Specimens			
	Fitting Coefficients		
Test Parameters	a	b	c
$\gamma_c = 1.5\%$ and $f = 1$ Hz	4.952	1.159	0.947
$\gamma_c = 1.5\%$ and $f = 2$ Hz	38.697	3.380	0.354
$\gamma_c = 4\%$ and $f = 1$ Hz	1608.381	3.530	0.257
$\gamma_c = 4\%$ and $f = 2$ Hz	56.841	3.189	0.341

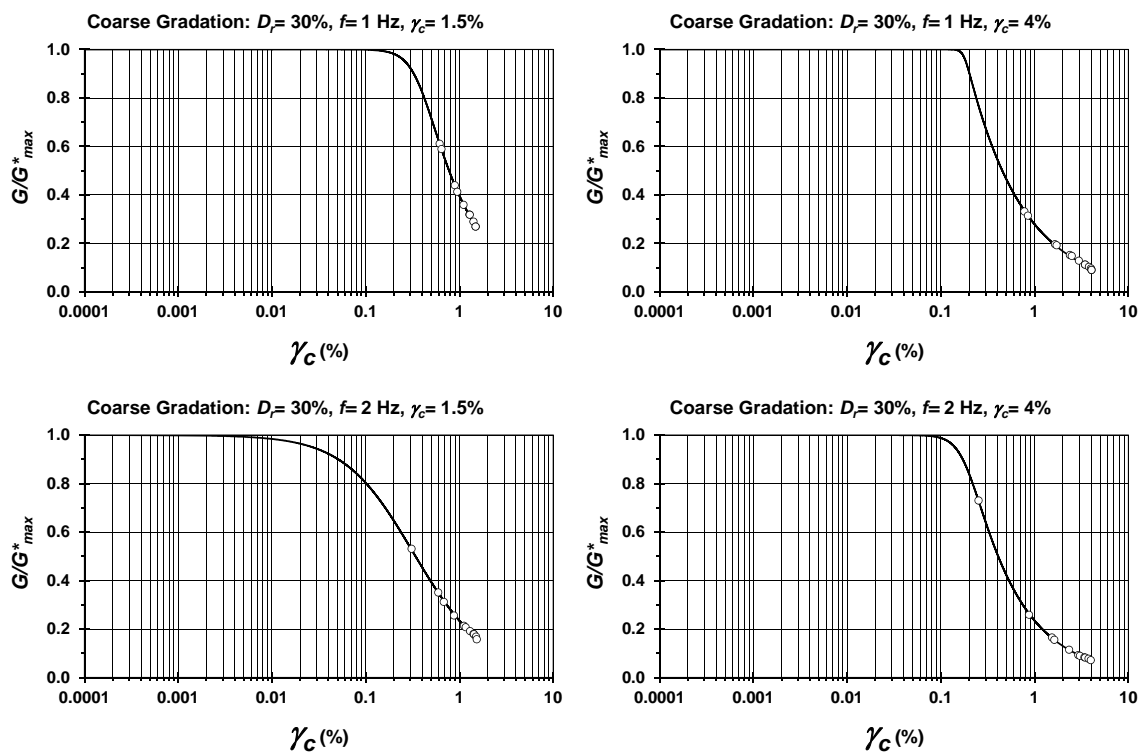


Figure D.63: Modulus reduction curves coarse gradation reconstituted to $D_r = 30\%$ specimens.

Table D.3: Fitting coefficients used in Equation 5.1.

$D_r = 30\%$ Coarse Gradation Specimens			
	Fitting Coefficients		
Test Parameters	a	b	c
$\gamma_c = 1.5\%$ and $f = 1$ Hz	47.420	3.965	0.239
$\gamma_c = 1.5\%$ and $f = 2$ Hz	4.721	1.195	0.832
$\gamma_c = 4\%$ and $f = 1$ Hz	2.011E+12	16.313	0.045
$\gamma_c = 4\%$ and $f = 2$ Hz	2314.256	4.548	0.187

Fitted modulus reduction curves for specimens reconstituted to $D_r = 50\%$ with $\sigma'_v = 30$ kPa.

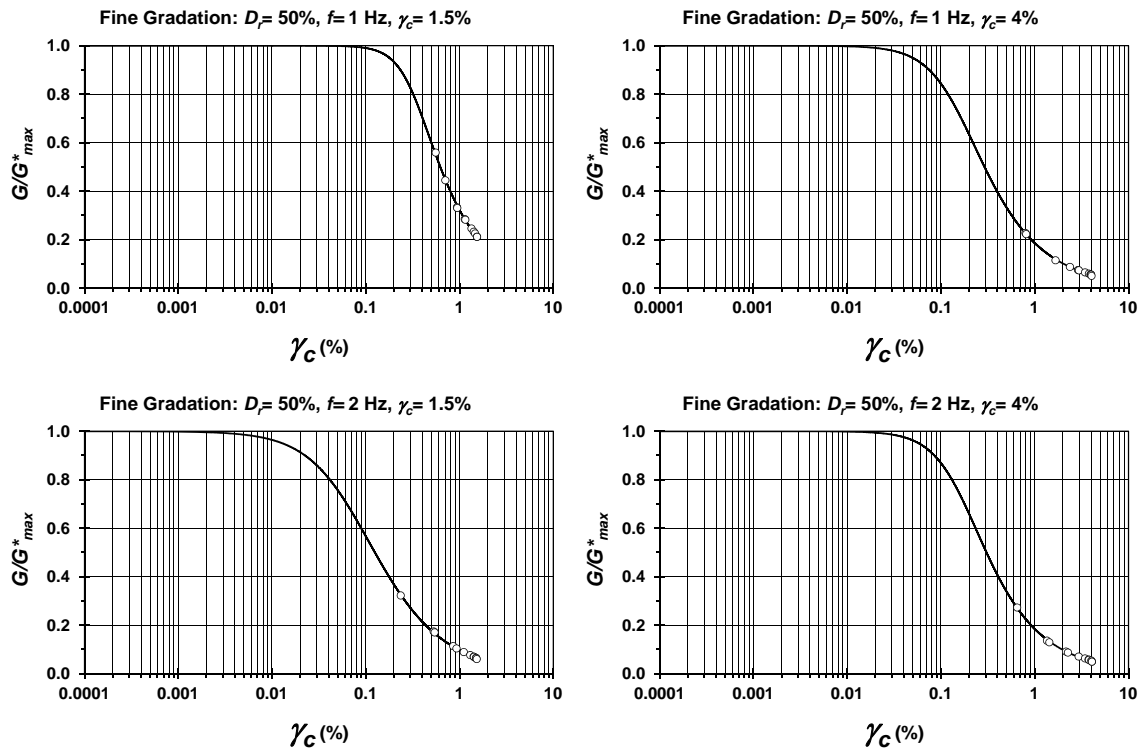


Figure D.64: Modulus reduction curves fine gradation reconstituted to $D_r = 50\%$ specimens.

Table D.4: Fitting coefficients used in Equation 5.1.

$D_r = 50\%$ Fine Gradation Specimens			
Test Parameters	Fitting Coefficients		
	a	b	c
$\gamma_c = 1.5\%$ and $f = 1$ Hz	28.815	2.998	0.333
$\gamma_c = 1.5\%$ and $f = 2$ Hz	32.889	1.384	0.661
$\gamma_c = 4\%$ and $f = 1$ Hz	37.571	1.925	0.460
$\gamma_c = 4\%$ and $f = 2$ Hz	42.264	2.060	0.448

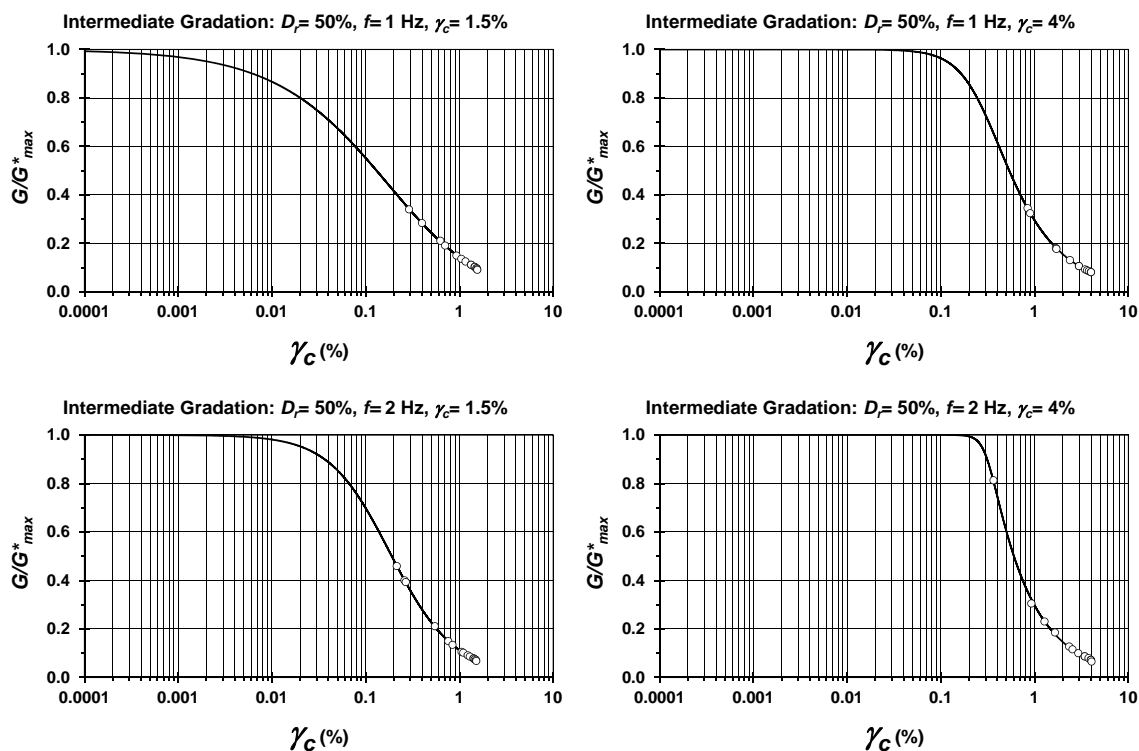


Figure D.65: Modulus reduction curves intermediate gradation reconstituted to $D_r=50\%$ specimens.

Table D.5: Fitting coefficients used in Equation 5.1.

$D_r = 50\%$ Intermediate Gradation Specimens			
	Fitting Coefficients		
Test Parameters	a	b	c
$\gamma_c = 1.5\%$ and $f = 1$ Hz	1.503	0.666	2.118
$\gamma_c = 1.5\%$ and $f = 2$ Hz	12.574	1.371	0.838
$\gamma_c = 4\%$ and $f = 1$ Hz	17.626	2.279	0.418
$\gamma_c = 4\%$ and $f = 2$ Hz	6018.048	7.355	0.140

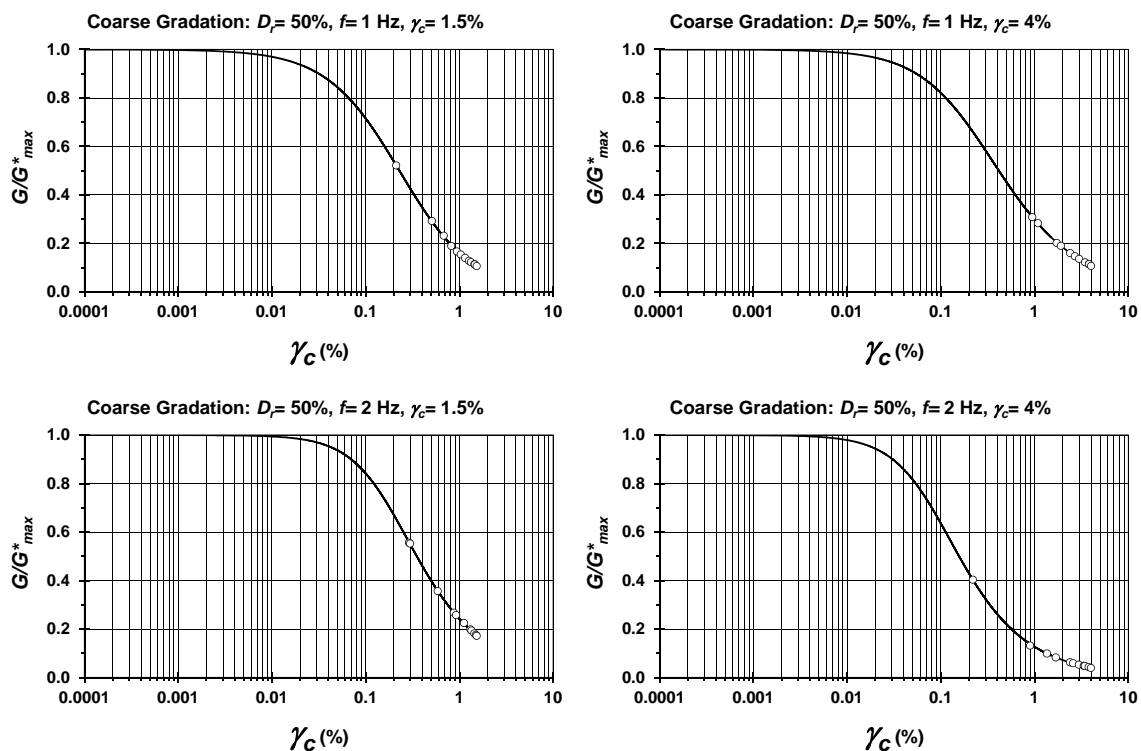


Figure D.66: Modulus reduction curves coarse gradation reconstituted to $D_r = 50\%$ specimens.

Table D.6: Fitting coefficients used in Equation 5.1.

$D_r = 50\%$ Coarse Gradation Specimens			
	Fitting Coefficients		
Test Parameters	a	b	c
$\gamma_c = 1.5\%$ and $f = 1$ Hz	4.909	1.106	1.029
$\gamma_c = 1.5\%$ and $f = 2$ Hz	14.503	1.566	0.518
$\gamma_c = 4\%$ and $f = 1$ Hz	4.835	1.162	0.687
$\gamma_c = 4\%$ and $f = 2$ Hz	43.891	1.527	0.543

Fitted modulus reduction curves for specimens reconstituted to $D_r = 50\%$ with $\sigma'_v = 100$ kPa.

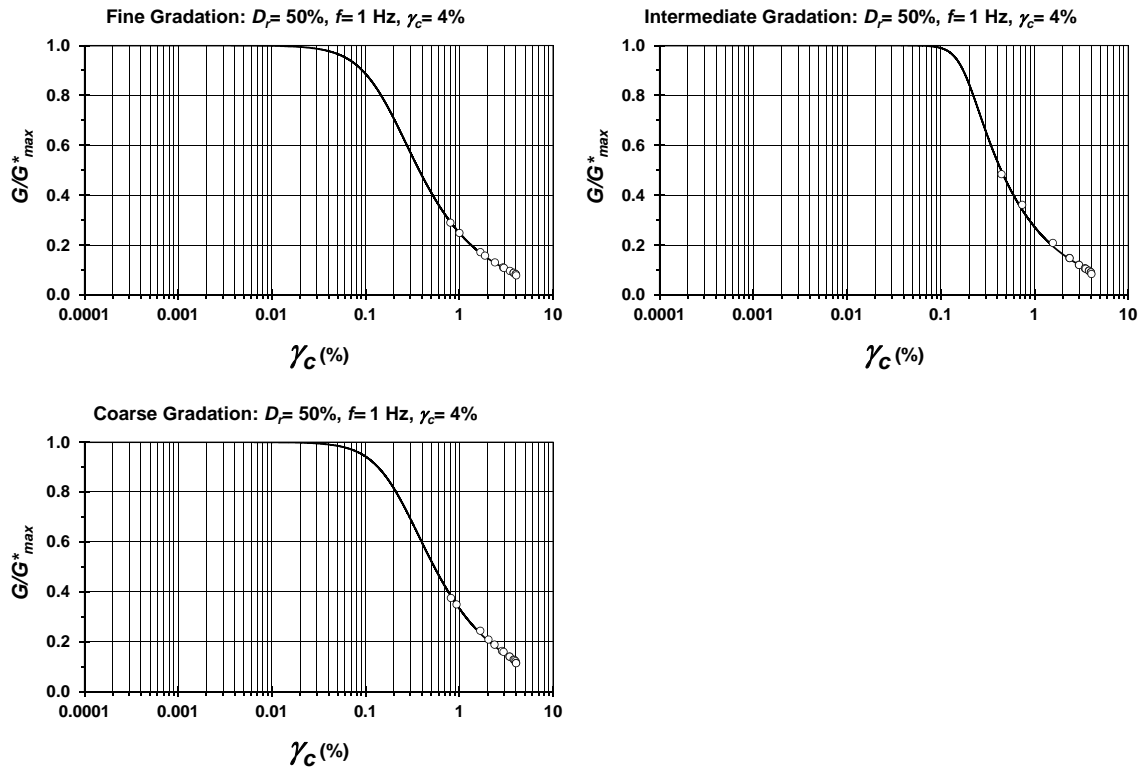


Figure D.67: Modulus reduction curves for $\sigma'_v = 100$ kPa specimens reconstituted to $D_r = 50\%$.

Table D.7: Fitting coefficients used in Equation 5.1.

Gradation	Test Parameters	$D_r = 50\%$		
		Fitting Coefficients		
		a	b	c
Fine	$\gamma_c = 4\%$ and $f = 1$ Hz	35.677	1.987	0.387
Intermediate	$\gamma_c = 4\%$ and $f = 1$ Hz	5313.760	4.894	0.151
Coarse	$\gamma_c = 4\%$ and $f = 1$ Hz	25.283	2.115	0.337

Fitted modulus reduction curves for tube specimens with $\sigma'_v = 30$ kPa.

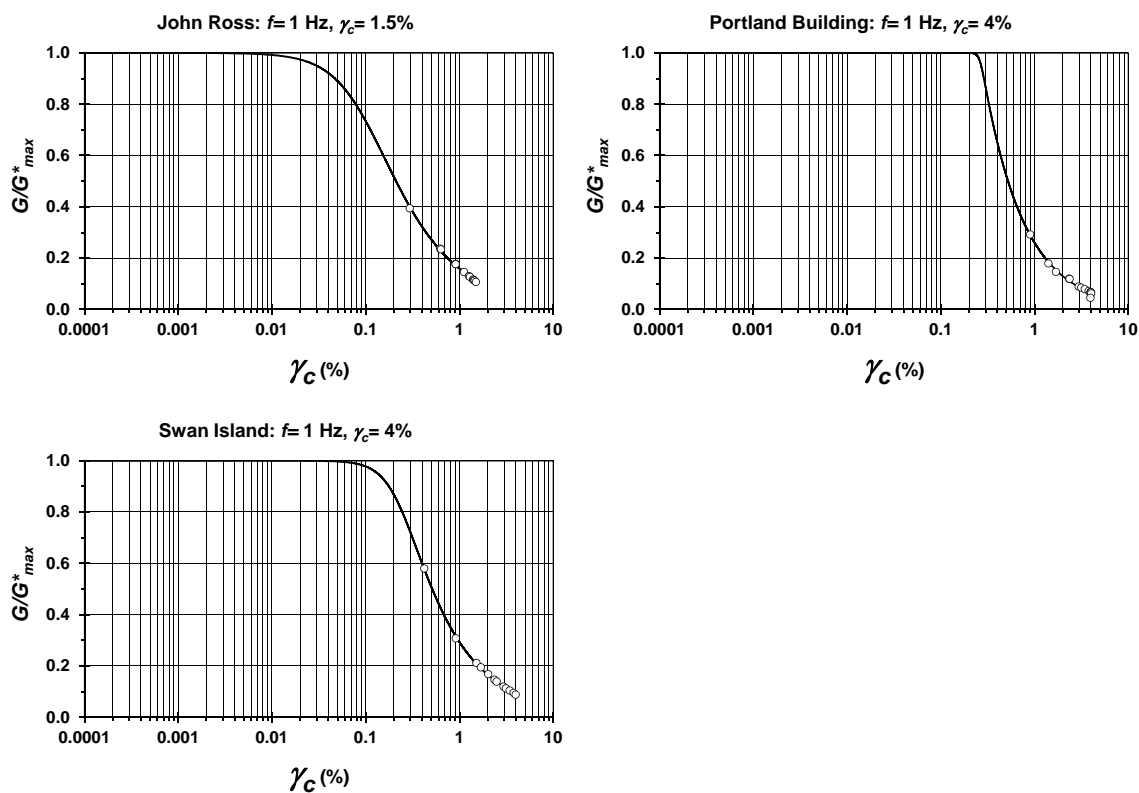


Figure D.68: Modulus reduction curves for tube specimens with $\sigma'_v = 30$ kPa.

Table D.8: Fitting coefficients used in Equation 5.1.

		$D_r = 50\%$		
		Fitting Coefficients		
Gradation	Test Parameters	a	b	c
John Ross	$\gamma_c = 1.5\%$ and $f = 1$ Hz	52.711	1.742	0.461
Portland Building	$\gamma_c = 4\%$ and $f = 1$ Hz	1.811E+12	21.014	0.048
Swan Island	$\gamma_c = 4\%$ and $f = 1$ Hz	83.557	2.996	0.277

